

## Swansea University E-Theses

---

# Experimental studies of complex fluids in complex flows.

Holder, Alexander Joseph

---

### How to cite:

Holder, Alexander Joseph (2014) *Experimental studies of complex fluids in complex flows..* thesis, Swansea University.

<http://cronfa.swan.ac.uk/Record/cronfa42995>

---

### Use policy:

This item is brought to you by Swansea University. Any person downloading material is agreeing to abide by the terms of the repository licence: copies of full text items may be used or reproduced in any format or medium, without prior permission for personal research or study, educational or non-commercial purposes only. The copyright for any work remains with the original author unless otherwise specified. The full-text must not be sold in any format or medium without the formal permission of the copyright holder. Permission for multiple reproductions should be obtained from the original author.

Authors are personally responsible for adhering to copyright and publisher restrictions when uploading content to the repository.

Please link to the metadata record in the Swansea University repository, Cronfa (link given in the citation reference above.)

<http://www.swansea.ac.uk/library/researchsupport/ris-support/>

# Experimental studies of complex liquids in complex flows

---

Alexander Joseph Holder BEng (Hons), MSc  
2014



**Prifysgol Abertawe**  
**Swansea University**

Submitted to Swansea University in the fulfilment of the  
requirements for the degree of Doctor of Philosophy



ProQuest Number: 10821385

All rights reserved

INFORMATION TO ALL USERS

The quality of this reproduction is dependent upon the quality of the copy submitted.

In the unlikely event that the author did not send a complete manuscript and there are missing pages, these will be noted. Also, if material had to be removed, a note will indicate the deletion.



ProQuest 10821385

Published by ProQuest LLC (2018). Copyright of the Dissertation is held by the Author.

All rights reserved.

This work is protected against unauthorized copying under Title 17, United States Code  
Microform Edition © ProQuest LLC.

ProQuest LLC.  
789 East Eisenhower Parkway  
P.O. Box 1346  
Ann Arbor, MI 48106 – 1346

## ***Declarations***

This work has not been previously accepted in substance for any degree and is not currently submitted in candidature for a degree in any University.

Signed

(Candidate)

Dated..10/6/2015

This thesis is the result of my own investigation except where otherwise stated. Other sources are acknowledged giving explicit references. A bibliography is appended.

Signed

(Candidate)

Dated..10/6/2015

I hereby consent for my thesis, if accepted, to be available for photocopying and for inter-library loan, and for the title and summary to be available to outside organisations.

Signed

(Candidate)

Dated..10/6/2015



## ***Certificate of Originality***

This thesis is submitted to Swansea University under the supervision of Prof. P.R. Williams in the Multidisciplinary Nanotechnology Centre in Swansea University in candidature for the degree of Doctor of Philosophy. The material in this thesis is the original work of the author except where acknowledgment to other authors is expressed.

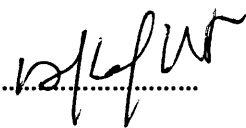
Signed

Dated...10/6/2015.....

Alexander Holder

(Candidate)

Signed ..

Dated..........

Prof. P.R. Williams

(Supervisor)

## **ABSTRACT**

Complex fluids are used in industrial manufacturing and there is a need to better understand their microstructural responses to flow. Following an introduction to Rheometry in **Chapter 1** work is reported on two techniques which enhance characterisation of complex materials, with reference to a transition from viscoelastic liquid (VEL) to viscoelastic solid (VES) states.

The first technique involves parallel superposition of a unidirectional shear flow on a small amplitude oscillatory shear (SAOS) flow. Interpretation involves the assumption that the oscillatory deformation has negligible effect on the material. This assumption is tested in **Chapter 2**. Further work based on controlled stress parallel superposition (CSPS) is reported in **Chapter 3**. CSPS is used herein to provide the first direct, real-time measurement of the thermally induced solid-to-liquid transition (SLT) in aqueous gelatine systems. Under appropriate conditions, the results of SAOS and CSPS experiments on a system undergoing transition from VEL to VES, or *vice versa* are indistinguishable. This conclusion is drawn on the basis that attainment of frequency independence of the loss tangent  $\tan\delta$  indicates the same rheological significance (in terms of the Gel Point) as frequency independence of its CSPS counterpart,  $\tan\delta//$ .

**Chapter 4** reports a second technique which is referred to as *Optimal Fourier Rheometry*, OFR. In contrast to SAOS, OFR involves a continuous modulation between two defined frequency limits, providing high densities of measurements of the complex shear modulus  $G^*(\omega)$ . An analysis of the susceptibility of OFR to rheometrical artefacts is made before its application to the study of collagen gels at different concentrations. Contrary to previous reports, the stress relaxation exponent  $\alpha$  of collagen gels is dependent on the concentration of collagen, with  $\alpha$  decreasing with increasing collagen concentration. A summary and conclusions are presented in **Chapter 5** along with recommendations for further work.

# ***Table of Contents***

<b>1</b>	<b>Introduction.....</b>	<b>1</b>
1.1	Rheology .....	1
1.2	– Rheometry for complex systems .....	3
1.2.1	- Viscoelastic responses to imposed stress .....	3
1.2.2	- Viscoelastic models (phenomenological models) .....	6
1.2.3	- Creep compliance and the Relaxation modulus.....	10
1.2.4	- Generalised models .....	14
1.2.5	- The Linear Viscoelastic Range .....	15
1.3	- Oscillatory shear .....	16
1.3.1	- Frequency based testing.....	16
1.3.2	- Small amplitude oscillatory shear .....	18
1.4	- Sol-gel transition .....	23
1.4.1	- Multi wave oscillation and the Fourier transform .....	26
1.5	- Superposition.....	33
1.5.1	- The Boltzmann superposition principle .....	33
1.6	- Relaxation Spectra .....	33
1.6.1	- Stress relaxation .....	33

1.6.2	- Discrete relaxation spectra.....	35
1.6.3	- The Continuous Relaxation Spectrum, $H(\tau)$ .....	38
2	Chapter 2 – Determination of the linear viscoelastic range: application to controlled stress parallel superposition (CSPS). .....	41
2.1	– Superposition techniques .....	41
2.1.1	– Strain and stress controlled parallel superposition.....	42
2.2	- VALIDATION OF CSPS – USING A MODEL GEL SYSTEM.....	45
2.2.1	- The Controlled Stress (CS) Rheometer .....	46
2.2.2	- Measuring Geometries .....	49
2.2.3	- Inertial Effects.....	52
2.2.4	- Gelatine .....	55
2.2.5	- Determination of the value of the relaxation exponent $\alpha$ for Gelatine gels 55	
2.2.6	- Controlled stress parallel superposition and gelling systems .....	56
2.2.7	- Linear viscoelastic range : the third harmonic criterion .....	59
2.3	- Materials and methods.....	59
2.3.1	- Gel point time determination.....	59
2.3.2	- Linearity criterion (harmonic analysis) .....	60
2.3.3	– Establishing the optimum unidirectional to oscillatory stress amplitude ratio.	61
2.3.4	- Linearity determination under parallel superposition .....	61

2.3.5	– Regions of linear response .....	62
2.4	- Results and discussion .....	62
2.4.1	- Experiment 1 – Gel point time determination of gelatine .....	62
2.4.1	- Experiment 2 – harmonic linearity criterion determination of gelatine..	66
2.4.2	- Investigation of unidirectional to oscillatory amplitude ratio .....	68
2.4.3	- Parallel superposition linearity determination .....	71
2.4.4	- Regions of linear repsonse in superposition experiments.....	73
3	- Chapter 3 – Assessment and validation of the controlled stress parallel superposition technique using the thermoreversible gelation and de-gelation characteristics of gelatine gels. ....	78
3.1	- Materials and Methods .....	80
3.1.1	- Experiment 1 – Gelation and de-gel using SAOS.....	80
3.1.2	- Experiment 2 – Gelation and de-gel during parallel superposition .....	80
3.2	– Results and Discussion .....	81
3.2.1	– Gelation and de-gelation using SAOS.....	81
3.2.2	– Gelation and melt during parallel superposition .....	86
3.2.3	- The critical gel temperature .....	128
3.2.4	- Gelation and melt using stepwise temperature increase .....	130
4	Chapter 4 - Optimal Fourier rheometry, OFR .....	135
4.1	- The OFR technique – background.....	135
4.1.1	– Collagen gels: a biopolymer test system .....	138

4.1.2	- The OFR technique - improving on FTMS .....	139
4.1.3	- The OFR waveform .....	141
4.2	- Materials and Methods .....	146
4.2.1	- Sample preparation .....	146
4.2.2	- Low frequency FTMS .....	148
4.2.3	- High Frequency FTMS.....	150
4.2.4	- Low frequency OFR.....	151
4.2.5	- High frequency OFR.....	152
4.3	- FTMS and OFR waveform analysis.....	152
4.3.1	- Gel point identification.....	154
4.4	- Results and discussion .....	157
4.4.1	- Investigation of mutation artefacts in OFR .....	157
4.4.2	- Direct comparison of OFR and FTMS techniques.....	159
4.4.3	- Application of OFR to collagen gels.....	163
5	Chapter 5 - Summary and Conclusions .....	136
5.1	Recommendations .....	171
	Nomenclature .....	173

## ***Table of Figures***

<b>Figure 1.2.1</b> - Figure showing the exemplar deformation of a fluid under stress.....	4
<b>Figure 1.2.2</b> - Figure showing the differences in shear profile for Newtonian and Non-Newtonian fluids .....	5
<b>Figure 1.2.3</b> - Figure showing a visual representation of the Maxwell model .....	7
<b>Figure 1.2.4</b> – Figure showing a visual representation of the Kelvin-Voigt model .....	8
<b>Figure 1.2.5</b> - Figure showing a visual representation of the Burgers model using springs and dashpots.....	9
<b>Figure 1.2.6</b> - Figure showing a typical creep response from a viscoelastic material .....	11
<b>Figure 1.2.7</b> - Figure showing a typical relaxation response from a viscoelastic material	12
<b>Figure 1.2.8</b> - Figure showing the Generalised Maxwell model as springs and dashpots	15
<b>Figure 1.2.9</b> - Figure showing an exemplar linear viscoelastic material under increasing shear stress .....	16
<b>Figure 1.3.1</b> - Figure showing the waveform response from an ideally viscous material.	17
<b>Figure 1.3.2</b> - Figure showing the waveform response from an ideally elastic material ..	18
<b>Figure 1.4.1</b> - Figure showing a simple applied multi-wave waveform and an appropriate viscoelastic stress 'response' .....	28
<b>Figure 1.4.2</b> - Figure showing the differences between phase optimised harmonic and anharmonic frequency peak strains .....	32
<b>Figure 1.6.1</b> - Figure showing an exemplar stress relaxation experiment on a single Maxwell model.....	34
<b>Figure 2.1.1</b> - Figure showing the process of orthogonal and parallel superposition .....	42

**Figure 2.1.2** - Figure showing the strain rate during stress operated superposition with a transient sample of building elastic strength .....43

**Figure 2.1.3** - Figure showing the strain rate during strain operated superposition with a transient sample of building elastic strength .....44

**Figure 2.2.1** - Figure showing the schematic of the TA ARG2 stress controlled rheometer .....47

**Figure 2.2.2** - Figure showing the schematic of a typical cone and plate geometry.....50

**Figure 2.2.3** - Figure showing the schematic of a typical parallel plate geometry .....52

**Figure 2.4.1** - Figure showing the sol-gel transition of gelatine at 26 °C.....63

**Figure 2.4.2** - Figure showing the sol- gel transition of gelatine at 28°C .....63

**Figure 2.4.3** - Figure showing the sol- gel transition of gelatine at 29.25°C .....64

**Figure 2.4.4** - Figure showing the relationship between gel time and temperature for 10%wt gelatine .....65

**Figure 2.4.5** - logarithmic scaled figure showing the relationship between gel time and temperature for 10%wt gelatine .....65

**Figure 2.4.6** - Figure showing an amplitude sweep carried out on 10% gelatine at the gel point .....66

**Figure 2.4.7** - Figure showing the changes in linearity for all tests with time relative to the gel point.....69

**Figure 2.4.8** - Figure showing the third harmonic linearity criterion at the gel point at varying ratios of oscillatory torque to oscillatory shear .....70

**Figure 2.4.9** - Figure showing the linearity conditions for several gel points at varying levels of oscillatory and parallel superposed shear .....72



<b>Figure 2.4.10</b> - Figure showing the region definition and non linearity in those regions for 15 $\mu$ Nm torque on 10%wt gelatine .....	73
<b>Figure 2.4.11</b> - Figure showing the Pre gel values of linearity at varying torques and frequencies .....	74
<b>Figure 2.4.12</b> - Figure showing the Gel point values of linearity at varying torques and frequencies .....	76
<b>Figure 2.4.13</b> - Figure showing the post gel values of linearity at varying torques and frequencies .....	77
<b>Figure 3.2.1</b> - Figure showing Gelation of gelatine under SAOS within the LVR. The results show the frequency dependence of $\eta'$ and $G'$ with the Gel Point marked by frequency independence of the loss tangent in accordance with the Winter-Chambon criterion. ....	82
<b>Figure 3.2.2</b> - Figure showing de-gelation of gelatine under SAOS within the LVR. The results show the frequency dependence of $\delta$ and $G'$ with the Gel Point marked by frequency independence of the loss tangent in accordance with the Winter-Chambon criterion. ....	83
<b>Figure 3.2.3</b> - Figure showing the rheological transitions (VEL to VES and VES to VEL) for gelatine samples studied under SOAS. ....	84
<b>Figure 3.2.4</b> - Figure showing the gelation and subsequent de-gelation of gelatine at zero shear under known linear conditions at seven frequencies within the range 0.2-2Hz.....	85
<b>Figure 3.2.5</b> - Figure showing the gelation and subsequent de-gelation of gelatine at zero shear under known linear conditions, for a wider frequency range (0.04 to 4 Hz) .....	86
<b>Figure 3.2.6</b> - Figure showing where the test parameters fall in terms of expected linearity – a combination of oscillatory and parallel shear of 2.4Pa in previous investigations have shown non-linear results.....	88

**Figure 3.2.7** - Figure showing the gelation and subsequent de-gelation of gelatine at 20μNm oscillatory torque and 20μNm controlled flow – this equates to an oscillatory stress and a superposed shear stress of 0.4Pa. ....89

**Figure 3.2.8** - Figure showing the gelation and subsequent de-gelation of gelatine at 40μNm oscillatory torque and 40μNm controlled flow – this equates to an oscillatory stress and a superposed shear stress of 0.8Pa. ....92

**Figure 3.2.9** - Figure showing the gelation and subsequent de-gelation of gelatine at 60μNm oscillatory torque and 60μNm controlled flow – this equates to an oscillatory stress and a superposed shear stress of 1.2Pa. ....93

**Figure 3.2.10** - Figure showing the gelation and subsequent de-gelation of gelatine at 80μNm oscillatory torque and 80μNm controlled flow – this equates to an oscillatory stress and a superposed shear stress of 1.6Pa. ....94

**Figure 3.2.11** - Figure showing the gelation and subsequent de-gelation of gelatine at 100μNm oscillatory torque and 100μNm controlled flow – this equates to an oscillatory stress and a superposed shear stress of 2Pa. ....95

**Figure 3.2.12** - Figure showing the gelation and subsequent de-gelation of gelatine at 120μNm oscillatory torque and 120μNm controlled flow – this equates to an oscillatory stress and a superposed shear stress of 2.4Pa. ....96

**Figure 3.2.13** - Figure showing the gelation of gelatine at 40μNm oscillatory torque and 40μNm controlled flow at seven known linear frequencies between 0.2-2Hz – this equates to an oscillatory stress and a superposed shear stress of 0.8Pa. ....97

**Figure 3.2.14** - Figure showing the de-gelation of gelatine at 40μNm oscillatory torque and 40μNm controlled flow at seven known linear frequencies between 0.2-2Hz – this equates to an oscillatory stress and a superposed shear stress of 0.8Pa. ....98

**Figure 3.2.15** - Figure showing the gelation and subsequent de-gelation of gelatine at 40 $\mu$ Nm oscillatory torque and 40 $\mu$ Nm controlled flow at seven known linear frequencies between 0.2-2Hz – this equates to an oscillatory stress and a superposed shear stress of 0.8Pa. ....99

**Figure 3.2.16** - Figure showing the storage and loss modulus through the pre-gel and gel point under no shear plotted against frequency at which it was measured. ....102

**Figure 3.2.17** - Figure showing the storage and loss modulus through the post-gel and pre-melt under no shear plotted against frequency at which it was measured.....103

**Figure 3.2.18** - Figure showing the storage and loss modulus through the melt point and post melt under no shear plotted against frequency at which it was measured.....104

**Figure 3.2.19** - Figure showing the storage and loss modulus for pre gel and post melt under no shear plotted against frequency at which it was measured, on the same axis.....105

**Figure 3.2.20** - Figure showing the storage and loss modulus from the gel point and through the melting of gelatine under no shear plotted against frequency at which it was measured, on the same axis. ....106

**Figure 3.2.21** - Figure showing the storage and loss modulus through the pre-gel and gel-point of gelatine under 40 $\mu$ Nm constant torque (0.8Pa shear stress) plotted against frequency at which it was measured.....108

**Figure 3.2.22** - Figure showing the storage and loss modulus through the post-gel and pre-melt of gelatine under 40 $\mu$ Nm constant torque (0.8Pa shear stress) plotted against frequency at which it was measured.....109

**Figure 3.2.23** - Figure showing the storage and loss modulus through the meltpoint and post-melt of gelatine under 40 $\mu$ Nm constant torque (0.8Pa shear stress) plotted against frequency at which it was measured.....110

**Figure 3.2.24** - Figure showing the storage and loss modulus for pre/post gel and gel/melt point of gelatine under 40 $\mu$ Nm constant torque (0.8Pa shear stress) plotted against frequency at which it was measured, on the same axis.....111

**Figure 3.2.25** - Figure showing the storage and loss modulus for the post gel and pre melting of gelatine under 40 $\mu$ Nm constant torque (0.8Pa shear stress) plotted against frequency at which it was measured, on the same axis.....112

**Figure 3.2.26** - Figure showing the storage and loss modulus through the pre-gel and gel point of gelatine under 80 $\mu$ Nm constant torque (1.6Pa shear stress) plotted against frequency at which it was measured.....113

**Figure 3.2.27** - Figure showing the storage and loss modulus through the post gel and pre melt of gelatine under 80 $\mu$ Nm constant torque (1.6Pa shear stress) plotted against frequency at which it was measured.....114

**Figure 3.2.28** - Figure showing the storage and loss modulus through the melt point and post melt of gelatine under 80 $\mu$ Nm constant torque (1.6Pa shear stress) plotted against frequency at which it was measured.....115

**Figure 3.2.29** - Figure showing the storage and loss modulus through for pre/post gel and gel/melt point of gelatine under 80 $\mu$ Nm constant torque (1.6Pa shear stress) plotted against frequency at which it was measured, on the same axis. ....116

**Figure 3.2.30** - Figure showing the storage and loss modulus through for post gel and pre melt point of gelatine under 80 $\mu$ Nm constant torque (1.6Pa shear stress) plotted against frequency at which it was measured, on the same axis.....117

**Figure 3.2.31** - Figure showing the storage and loss modulus through the pre-gel and gel point of gelatine under 120 $\mu$ Nm constant torque (2.4Pa shear stress) plotted against frequency at which it was measured.....119

**Figure 3.2.32** - Figure showing the storage and loss modulus through the post gel and pre melt of gelatine under 120µNm constant torque (2.4Pa shear stress) plotted against frequency at which it was measured.....120

**Figure 3.2.33** - Figure showing the storage and loss modulus through the melt point and post melt of gelatine under 120µNm constant torque (2.4Pa shear stress) plotted against frequency at which it was measured.....121

**Figure 3.2.34** - Figure showing the storage and loss modulus through for pre/post gel and gel/melt point of gelatine under 120µNm constant torque (2.4Pa shear stress) plotted against frequency at which it was measured, on the same axis. ....122

**Figure 3.2.35** - Figure showing the storage and loss modulus through for post gel and pre melt point of gelatine under 120µNm constant torque (2.4Pa shear stress) plotted against frequency at which it was measured, on the same axis.....123

**Figure 3.2.37** - Figure showing the gelation and subsequent de-gelation of gelatine at 20µNm oscillatory torque and zero controlled flow at five known linear frequencies between 0.04-4Hz – this equates to an oscillatory stress of 0.4Pa.....124

**Figure 3.2.38** - Figure showing the gelation and subsequent de-gelation of gelatine at 40µNm oscillatory torque and 40µNm controlled flow at five known linear frequencies between 0.04-4Hz – this equates to an oscillatory stress and a superposed shear stress of 0.8Pa. ....125

**Figure 3.2.39** - Figure showing the gelation and subsequent de-gelation of gelatine at 80µNm oscillatory torque and 80µNm controlled flow at five known linear frequencies between 0.04-4Hz – this equates to an oscillatory stress and a superposed shear stress of 1.6Pa. ....126

<b>Figure 3.2.40</b> - Figure showing the gelation and subsequent stepwise increase in temperature to 28.9°C .....	131
<b>Figure 3.2.41</b> - Figure showing the gelation and subsequent stepwise increase in temperature to 29°C .....	131
<b>Figure 3.2.42</b> - Figure showing the gelation and subsequent stepwise increase in temperature to 29.1°C .....	132
<b>Figure 3.2.43</b> - Figure showing the gelation and subsequent stepwise increase in temperature to 29.2°C .....	133
<b>Figure 3.2.44</b> - Figure showing the gelation and subsequent stepwise increase in temperature to 29.3°C .....	134
<b>Figure 3.2.45</b> - Figure showing the gelation and subsequent stepwise increase in temperature to 29.4°C .....	135
<b>Figure 3.2.46</b> - Figure showing an attempted gelation of 10%wt gelatine at 29.5°C .....	135
<b>Figure 4.1.1</b> - Figure showing a typical applied OFR strain waveform and its subsequent stress response against time .....	143
<b>Figure 4.1.2</b> – Figure showing the process of OFR analysis from experimentally gained strain/stress waveforms (top) through to storage/loss moduli calculation (middle) and finally phase angle calculation (bottom) .....	145
<b>Figure 4.2.1</b> - Figure showing the determination of the Linear viscoelastic range for molten 30%wt gelatine –It is evident that measurements deviate from the LVR after an oscillatory strain of 40%.....	149
<b>Figure 4.2.2</b> - Figure showing the determination of the Linear viscoelastic range for solid 30%wt gelatine –It is evident that measurements deviate from the LVR after an oscillatory strain of 400% .....	150

<b>Figure 4.3.1</b> – Figure showing the gel point identification process for 30wt% gelatine for data gathered through FTMS (A-C) and through OFR (D-F) .....	156
<b>Figure 4.4.1</b> – Figure showing a comparison of GP data obtained by 1) high frequency FTMS [x] 2) low frequency FTMS [o] 3) low frequency OFR [□] and 4) high frequency OFR (•). The dashed line in figure B shows Winter’s mutation criterion of $Nmu = 0.15$ .....	158
<b>Figure 4.4.2</b> - Figure showing a comparison of pre-GP, GP and post-GP rheological data for 30 wt% gelatine obtained using FTMS and OFR .....	161
<b>Figure 4.4.3</b> - Figure showing a plot of uncertainty in $\alpha$ as a function of mutation number for 1) HF-FTMS [x] 2) LF- FTMS [o] 3) LF-O FR [□] and 4) HF-OFR (•).....	162
<b>Figure 4.4.4</b> - Figure showing variation of the stress relaxation exponent for collagen gels over a range of concentration made using the HF-OFR routine at 28°C.....	164
<b>Figure 4.4.5</b> - Figure showing collagen GP data in terms of frequency independence of $\delta(t)$ for a 8 mg/ml collagen gel. Data was obtained using HF-OFR at 28°C. ....	165

## ***List of Tables***

<b>Table 2.4.1</b> –Table showing non linearity test data at the gel point.....	67
<b>Table 3.1.1</b> – Table of CSPS parameters selected for experiment 2 .....	81
<b>Table 3.2.1</b> - Table of CSPS gelation and de-gelation of 10% gelatine data between 0.2-2Hz at four known linear frequencies – values of $G'$ and $G''$ are taken at 2Hz .....	100
<b>Table 3.2.2</b> - Table of CSPS gelation and de-gelation of 10% gelatine data between 0.2-2Hz at seven known linear frequencies – values of $G'$ and $G''$ are taken at 2Hz .....	100
<b>Table 3.2.3</b> - Table of CSPS gelation and de-gelation of 10% gelatine data between 0.04-4Hz at five known linear frequencies – values of $G'$ and $G''$ are taken at 4Hz.....	127



# *Acknowledgements*

There is a vast number of people I would like to thank, however as a courtesy to anyone subjected to this foreword I will try to keep it brief. First and foremost, this thesis would never have been possible without the generous funding of Proctor and Gamble and Dr Graham Myatt, who has helped in every way, whether it be with sourcing equipment and materials or showing me the hints and tricks of formulation. Secondly – but with the highest approbation is Professor Rhodri Williams, his ability to inspire and motivate was critical to the success of both the completion of this thesis and its underlying research. It is through his radiant enthusiasm for rheological research that I found the drive to continue forward, as well as a great love for the subject itself.

I would also like to thank all the people I had the great pleasure of working with through my research, to name a few names, Dr. Daniel Curtis, Dr. Karl Hawkins, Dr. Nafiseh Badiei and soon to be Dr. Bethan Thomas - all excellent Rheologists that would always offer guidance and support no matter how trivial (or significant!) the problem.

Finally I would like to thank my family, friends and Charlotte. My mother, Caroline, and father, Simon, have always cared deeply about my education – but it is their love for each other that truly inspires. My sister, Rebecca, extended family and friends have been, as they always are, a source of limitless support in troubled times and so very much fun in the rest. To Charlotte – I cannot effectively express my thanks for the support and patience you have offered, you were – as you are, the reason for self-improvement.

# 1 Introduction

## 1.1 Rheology

*Rheology* is the science of the deformation and flow of materials (Barnes 2000). A wide range of complex fluids are used as a basis for creating products by industrial processes involving flow, e.g. in manufacture by printing or coating. In biology the physiological process of blood coagulation involves a significant element of shear flow which may influence the formation and functionality of blood clots. There is a need to better understand and characterise the rheological properties of such systems and products, in particular the evolution of their viscoelastic properties and the response of their microstructures under imposed shear flows.

In addition to the optimisation of process efficiency, consumer demands dictate that the process be designed to ensure that the industrial consumer product has the appropriate rheological properties. In the realm of personal care products hair shampoos and various skin creams need to feel sufficiently 'thick' or viscous to transfer to the hair or body without simply flowing through the fingers when poured from the bottle. Toothpastes must be sufficiently viscous to sit on the brush without sinking through the bristles, whilst being able to be squeezed out of tube with ease. Printing inks that must be easily spread during transfer to the paper, but so as to maintain a sharp edge, must not spread under the action of gravity once on the paper. Solid materials are clearly not often of great interest to the rheologist, whose work is mostly devoted to fluids.

A *fluid* can be defined as a substance in which particles (of the fluid) are free to move relative to one another. When a fluid *flows*, elements of the liquid are deforming, and

adjacent points in the liquid are moving *relative* to one another (Barnes 2000). For example, when a vessel containing liquid is carried with great care to avoid spillage, then the liquid is moving, but not flowing. However, if spillage were to occur, then the liquid leaving the glass would be flowing. Fluids may be *liquids* or *gases*, the major difference being that liquids require a *force* in order to make them flow. This force may be that induced by gravity or a manually imposed force such as stirring, squeezing, painting etc.

As well as the fluid composition, external factors such as surface geometry of the vessel, the force applied to make it flow, pressure and temperature may all affect the microstructure of the liquid in such a way that only a minor change in one of the factors dramatically affects the way in which it *flows* and *deforms*. The rheologist aims to predict behaviour of a liquid under certain conditions, and does so by attempting to quantify certain rheological properties which can be incorporated into constitutive equations for liquid behaviour.

The most widely used and most commonly measured rheological property is the shear *viscosity*, which can be thought of, in simple terms, as *a measure of a liquids ability to resist flow*. Generally though viscosity measurement is far from simple and it is necessary to be able to take real flows found in an industrial environment and simulate these on a small scale in the laboratory. External influences such as vessel geometry and applied force combine to impose *stresses* and *strains* upon the liquid. Liquids may be grouped according to the general behavioural trends that they exhibit under certain stresses and strains.

The viscosity of *Newtonian liquids* is independent of stress and strain, yet it may vary with changes in temperature and pressure. Liquids whose viscosity does vary with stress and strain may be described as *non-Newtonian*, and so naturally it is the non-Newtonian liquids

that are of greatest interest to the rheologist, as it is these that will be most affected by external influences. Some non-Newtonian liquids may exhibit *elastic* properties. In such liquids deformation from rest produces an elastic force which represents a storage of energy that will try and restore the rest state. Elastic forces differ from viscous forces in that the viscous force is an instantaneous resistance. Most concentrated structured liquids will show a combination of viscous and elastic forces when deformed and are classed as *viscoelastic liquids*. The measurement of pertinent rheological parameters which characterise a material's response to imposed stress can involve many different rheometric techniques, the most significant of which (for shear deformation and flow) are discussed below.

## ***1.2 – Rheometry for complex systems***

### ***1.2.1 - Viscoelastic responses to imposed stress***

Typically when a fluid is deformed, its response is either elastic, viscous or viscoelastic. Take a sample fluid in rest state, a time dependent force is applied and the deformation response of the fluid is measured (see figure 1.2.1). An elastic response would be a very fast recovery, losing little energy as heat during deformation and returning to its original state (Chawla 1999). A viscous response would be a response that follows Newton's Viscous Law, which states that the stress is proportional to the corresponding time derivative of strain (deformation)(Tanner 1985).

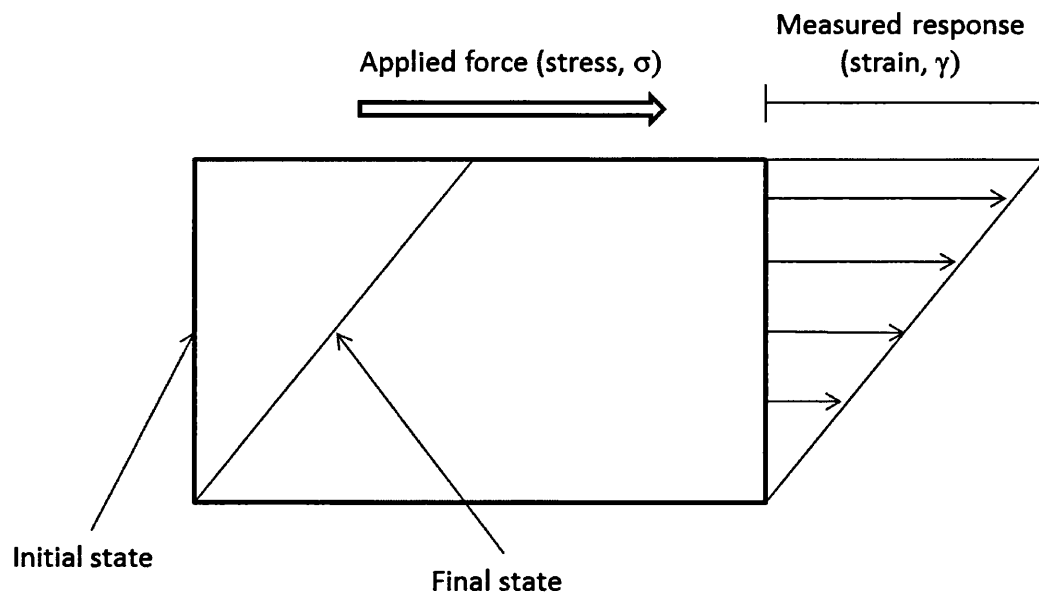


**Figure 1.2.1** - Figure showing the exemplar deformation of a fluid under stress

It follows then that a viscoelastic response is one where both viscous and elastic effects are noticeable. It is worth noting that in most materials, under appropriate circumstances, there can be found elasticity and viscosity (Tanner 1985). Most concentrated structured liquids show strong viscoelastic effects at small deformations so at these small deformations physical microstructure of a sample can be investigated. An increase, however to higher deformations, such as steady state flow typically causes a deviation from linear viscoelasticity. This can be illustrated through a seemingly dramatic loss of elastic response or through great changes in the flow pattern of the sample, such as the Weissenberg effect (Harris 1977).

Returning to Newton's viscous law, it can be deduced that if a Newtonian fluid has a proportional strain rate to the stress on the sample then all viscoelastic fluids are then non-Newtonian and behave in very different ways. As viscoelastic fluids have a stress, strain

relationship that is dependent on time some interesting phenomena can be observed, such as the stress of a sample decreasing with time at a constant strain (relaxation) and at a constant stress the strain of a sample increasing (creep)(Barnes 2000). Importantly, a viscoelastic fluid has a hysteresis (a lag) that is observable in the stress-strain curve (see figure 1.2.2). Some viscoelastic fluids exhibit thixotropic behaviour, where viscosity of a fluid decreases at a constant value of stress or strain. Other viscoelastic fluids such as dilatant and pseudoplastic fluids have an apparent viscosity that increases or decreases respectively to an increase in shear rate. They are also known as shear thinning or shear thickening fluids for this reason.

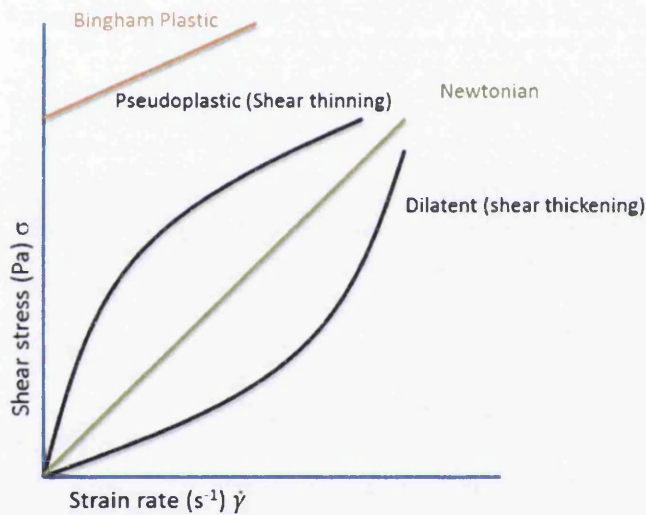


**Figure 1.2.2** - Figure showing the differences in shear profile for Newtonian and Non-Newtonian fluids

### 1.2.2 - Viscoelastic models (phenomenological models)

Simple mechanical models are useful comparatives for viscoelasticity. Consisting of linear elastic and viscous elements, when implemented properly, these models provide adequate representation of internal structure through representing relaxation. 'Springs' and 'dashpots' represent the elastic and viscous parts of a model.

The spring represents the linear elastic element of the fluid that obeys Hooke's law. Hooke's law states that the stress applied is proportional to the strain it produces within the elastic limit (Isaacs 2009). This introduces the elastic modulus,  $G$ , as the constant of proportionality between stress and strain within these 'springs' (see eq. 1.2.1 below). No time element is involved in the modelling of ideal elastic behaviour, thus the response of 'springs' are assumed to be instantaneous, representing the very fast recovery of elastic elements in a fluid.

$$\sigma = G\gamma$$

*Equation 1.2.1 – stress/strain relationship according to Hooke's law*

The representation for a viscous, Newtonian response is left then to the dashpot. This is represented through a stress and a strain rate ( $\dot{\gamma}$ ) (see eq. 1.2.2 below). It is important to note then that deformation will always be constant at any level of stress with a Newtonian sample (William N Findley 1976). The viscosity ( $\eta$ ) of the fluid being the only factor affecting the rate of deformation compared the amount of stress applied. Again it may be important to note that the rate of strain stops immediately with the ending of stress.

$$\sigma = \eta \dot{\gamma}$$

*Equation 1.2.2 – stress/strain rate relationship according to Newton's viscous law*

The spring and dashpot come together to form the Maxwell model, developed by James Clerk Maxwell, famed for the electromagnetic theory of light and the statistical theory of gasses. The spring and dashpot are placed in series and a force is applied through them (see fig 1.2.3 below).

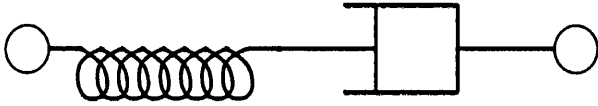


**Figure 1.2.3** - Figure showing a visual representation of the Maxwell model

This combination introduces a time dependence on the stress. Through combining all the stress and strain elements, as well taking the derivative of strain with time, an equation of stress, strain and their respective change with time can be written in the form below (eq. 1.1.3)(Roylance 2001, Harman 2003).

$$\frac{1}{G} \frac{d\sigma}{dt} + \frac{\sigma}{\eta} = \frac{d\gamma}{dt}$$

*Equation 1.2.3 – deformation rate as a function of stress and stress rate*

This can be shown as:

$$\frac{\dot{\sigma}}{G} + \frac{\sigma}{\eta} = \dot{\gamma}$$



The Maxwell model then, is a simple representation of a viscoelastic liquid. Connecting the spring and dashpot in parallel as shown in figure 1.1.4 below, a representation of a viscoelastic solid is formed. This is called the Kelvin-Voigt model after the two physicists most commonly credited with its creation.

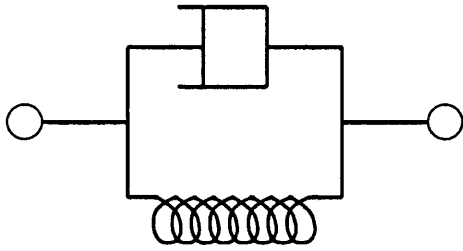


**Figure 1.2.4** – Figure showing a visual representation of the Kelvin-Voigt model

Since the two components in the model are connected in parallel then the strains on each component are equal, this leaves the Kelvin-Voigt equation with respect to time as shown below in equation 1.2.5 (M. Bulicek 2012).

$$\sigma = G\gamma + \eta\dot{\gamma}$$

This can also be expressed with a sudden application of stress  $\sigma_0$  where deformations approach the deformation of a pure elastic material and thus reach close to the deformation of a pure elastic material  $\sigma_0/G$  causing an exponential decay in the difference.

This yields equation 1.2.6 below:

$$\gamma = \frac{\sigma_0}{G} (1 - e^{-\lambda t})$$

*Equation 1.2.6 – strain at sudden application of stress*

Where  $\lambda$  is the rate of relaxation ( $G/\eta$ ) and  $t$  is time.

These two models are typically useful then as simple representations of certain kinds of viscoelastic fluids. The Maxwell and Kelvin-Voigt model may also be expanded upon though the use of multiple Maxwell components in parallel or Kelvin Voigt components in series. The desired effect is to represent the various relaxation components in the sample structure, which is covered in more detail in chapter 2.1.4.

Combining the Maxwell and Kelvin-Voigt models in series gives a new model that accounts for both viscoelastic solids and viscoelastic liquids. It is named the Burgers model (see fig 1.2.5). It is best described by the equation combination of eq.1.2.4 and 1.2.6 – rearranged and combined so that strain as a function of time over stress is on one side, giving equation 1.2.7 below (Barnes 2000).

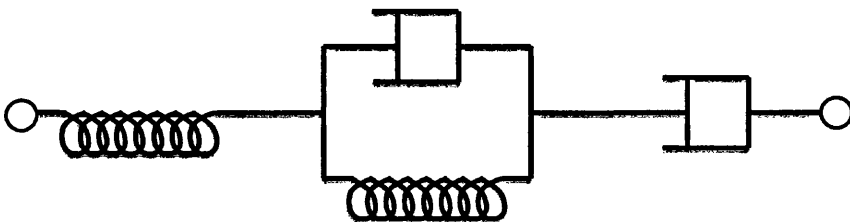


**Figure 1.2.5** - Figure showing a visual representation of the Burgers model using springs and dashpots

$$\frac{\gamma(t)}{\sigma} = \frac{1}{G_1} + \frac{1}{G_2} (1 - e^{-\lambda t}) + \frac{t}{\eta_1}$$

*Equation 1.2.7 – The burgers model in a form so as to illustrate a creep response*

Where  $G_1$  and  $G_2$  are the two elastic moduli for the two springs. It follows then from this equation that the Burgers model accounts for an immediate elastic response, followed by a delayed elastic response then finally a steady state viscous response. This is primarily useful as an indicative model for the kind of expected response from real viscoelastic samples during a creep test.

### ***1.2.3 - Creep compliance and the Relaxation modulus***

Two of the most basic rheometric methods of measuring linear viscoelasticity in materials are those of the creep and relaxation test. The creep test involves applying a constant stress and monitoring the resulting strain. A relaxation test, contrarily involves applying a constant strain and monitoring the relaxing stress.

As discussed in the explanation of the Burgers model, linear viscoelastic materials have a more complex structure than Newtonian fluids, typically with an immediate elastic response followed by an increasing response with time. This process is known as creep and it is illustrated in figure 1.2.6 below.

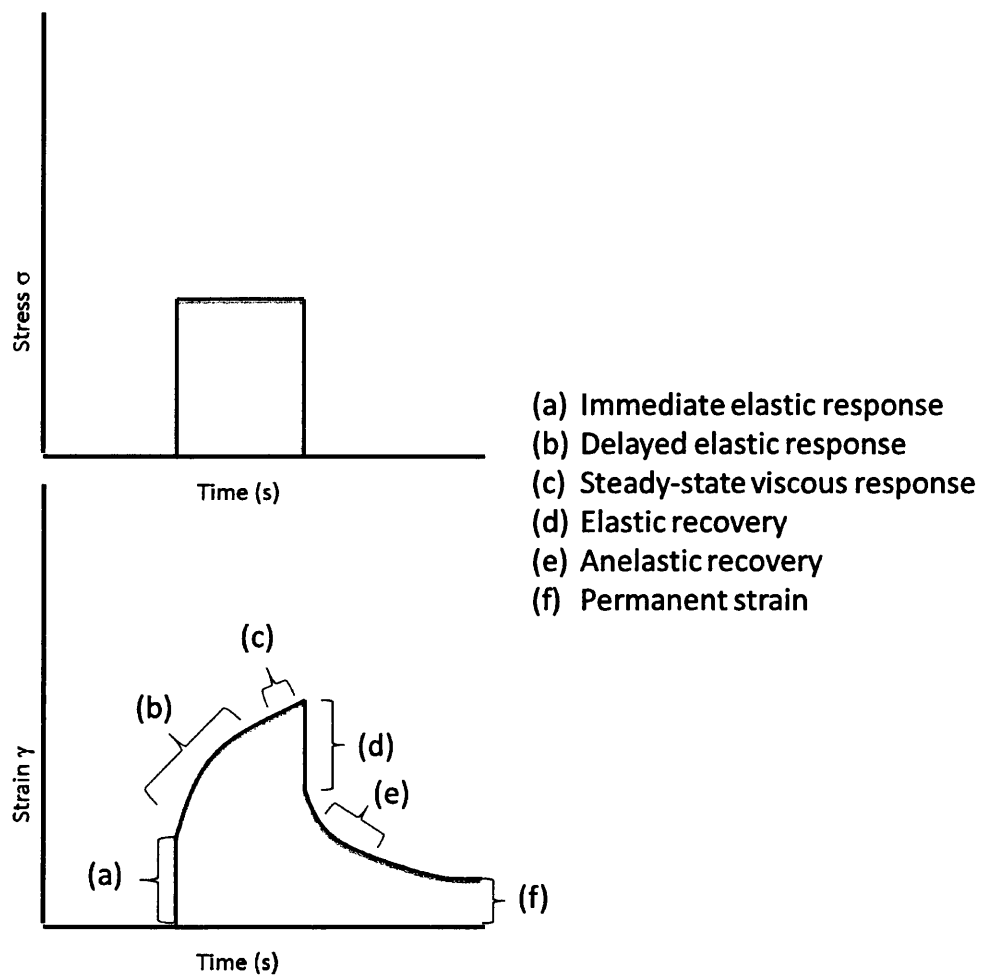


**Figure 1.2.6** - Figure showing a typical creep response from a viscoelastic material

It can be seen further from this figure that post delayed elastic response a steady state viscous response remains. Steady state in creep tests can be problematic to detect when testing viscoelastic materials.

An example of a relaxation test can be seen in figure 1.2.7 below, this is a typical response of a linear viscoelastic fluid to a steady strain.

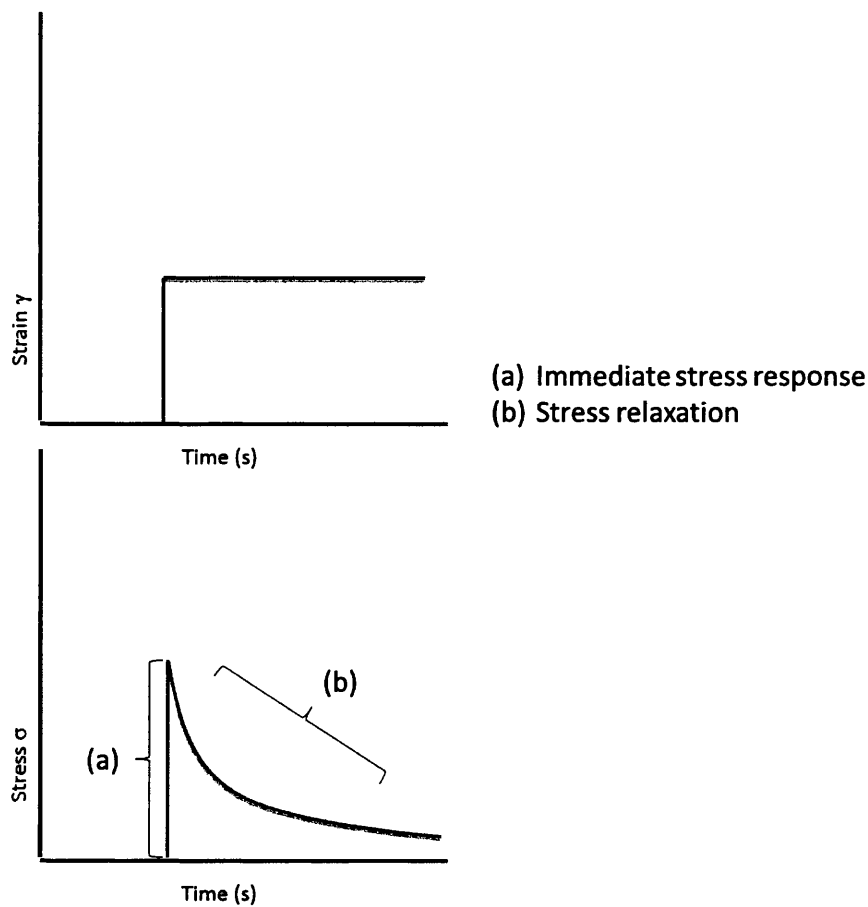


**Figure 1.2.7** - Figure showing a typical relaxation response from a viscoelastic material

Returning to the spring of our viscoelastic models, the creep compliance is the inverse of the elastic modulus and has the same value as (a) in figure 1.2.6. However If the idea of total creep compliance is implemented into a simple model, such as the Maxwell model the definition becomes more complicated. Taking the constitutive equation for the Maxwell model (equation 1.2.4) and writing it in the form:

$$\sigma + \frac{\eta}{G} \dot{\sigma} = \eta \dot{\gamma}$$

**Equation 1.2.8** – Maxwell model constitutive equation

Applying a sudden stress  $\sigma_0$  it can be deduced that after an initial elastic strain response, ( $\gamma_0 = \sigma_0 / G$ ) thereafter the dashpot takes the stress and yields a linear strain increase of slope  $\sigma_0 / \eta$ . Assuming that post the initial stress applied no further is added the rate of stress can be considered zero so the constitutive equation for the Maxwell model becomes:

$$\dot{\gamma} = \frac{\sigma_0}{\eta} \rightarrow \gamma(t) = \frac{\sigma_0}{\eta}(t) + C \rightarrow \gamma(t) = \sigma_0 \left( \frac{1}{\eta}t + \frac{1}{G} \right)$$

*Equation 1.2.9 – Maxwell model constitutive equation at  $\sigma_0$*

This is now in the form of  $\gamma = \frac{1}{G}\sigma$  thus as the inverse of the elastic modulus is the creep compliance, the creep compliance within the Maxwell model is:

$$J = \left( \frac{t}{\eta} + \frac{1}{G} \right)$$

*Equation 1.2.10 – Creep compliance equation for a Maxwell model material*

This equation produces a more accurate but far from perfect representation of creep compliance in linear viscoelastic materials.

The relaxation modulus is the inverse of viscosity similarly, returning to the dashpot. This describes the response of a material during a stress relaxation (constant strain) test. It can be evaluated in using the same method above for creep compliance. Often the relaxation modulus will contain an exponential function of the form:

$$e^{-t/\tau}$$

Where  $\tau$  is called the relaxation time and is given by a form of  $\eta/G$ . It is a measure of how quickly the material relaxes.

The greatest difficulty with using the Maxwell and other simple models is that they reveal only one relaxation time. Most real viscoelastic materials are better described using multiple relaxation times – as their relaxation behaviour changes with time.

The creep compliance also often contains exponential functions and again  $\tau$  is given in the form  $\eta/G$  however at this instance it is called a retardation time and is a measure of the amount of strain that exists i.e. at very short times the response is viscous and strain is approximately equal to  $t\sigma/\eta$ , however at  $t = \tau$  the strain has risen to approximately 63% of its final value.

#### **1.2.4 - Generalised models**

Crucially, more complicated models can be devised to apply these multiple relaxation and retardation times. Through the use of more and more elements the model becomes more complex. Typically more elements are added to the Maxwell or Kelvin-Voigt model so that the model itself contains many parameters and will exhibit an array of relaxation and retardation times.

For the purposes of brevity only the Maxwell model will be investigated as a generalised model. It consists of a set number (N) of Maxwell units in parallel each unit with different parameter values, an absence of the spring in the unit for example would indicate viscous

behaviour and the absence of the dashpot, an elastic response. This is illustrated below in figure 1.2.8.

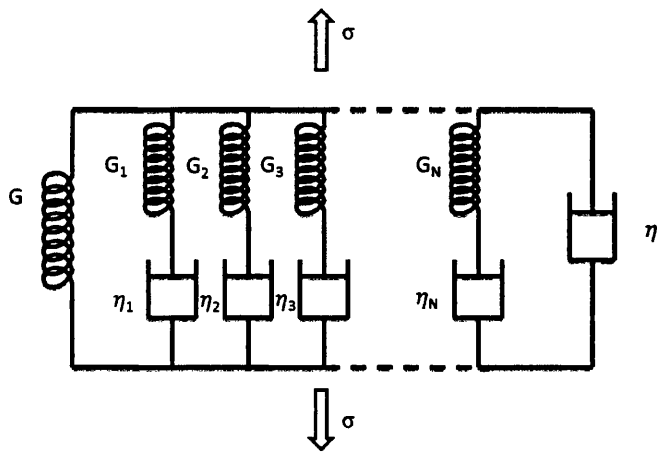


**Figure 1.2.8** - Figure showing the Generalised Maxwell model as springs and dashpots

### **1.2.5 - The Linear Viscoelastic Range**

Linear viscoelastic materials are those where the sample material has a linear relationship between stress and strain at any given time. As an example strain-time curves are shown in figure 1.2.9 below for a linear viscoelastic material. As the stresses on the material increase to three times the original amount, for a linear viscoelastic material at the same time the strain must also increase to up to three times with the stress.



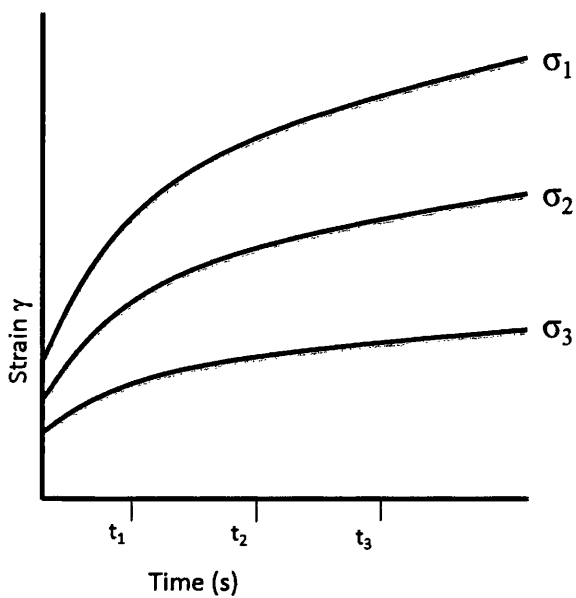


**Figure 1.2.9** - Figure showing an exemplar linear viscoelastic material under increasing shear stress

Relaxation times and retardation times as well as creep compliance and viscosity are all very useful indicators of structure and viscoelastic behaviour. However creep compliance and viscosity will become non-linear at large stresses it is important to note that to stay within a linear viscoelastic range of measurement, low stresses should be used. An important, typically low stress rheometric technique is that of oscillatory testing.

## **1.3 - Oscillatory shear**

### **1.3.1 - Frequency based testing**

As discussed above, relaxation and creep testing measure the response of a fluid over a range of time. With Oscillatory testing the sample is measures over a range of frequency. Frequencies are time related, with low frequencies taking a long time periods and high frequencies taking short periods. It follows then that more elastic responses are dominant

at high frequencies and more viscous responses are dominant at the longer time periodic low frequencies.

An oscillatory test is performed by applying a sine wave shaped stress or strain on the sample. The response of the fluid as either a stress or strain is then measured. This response yields the dynamic viscoelasticity; through the phase response of the sample, a phase angle of  $0^\circ$  means the sample exhibits ideal elastic properties. Conversely a phase angle of  $90^\circ$  illustrates the sample is an ideal viscous fluid (see figures 1.3.1-1.3.2).

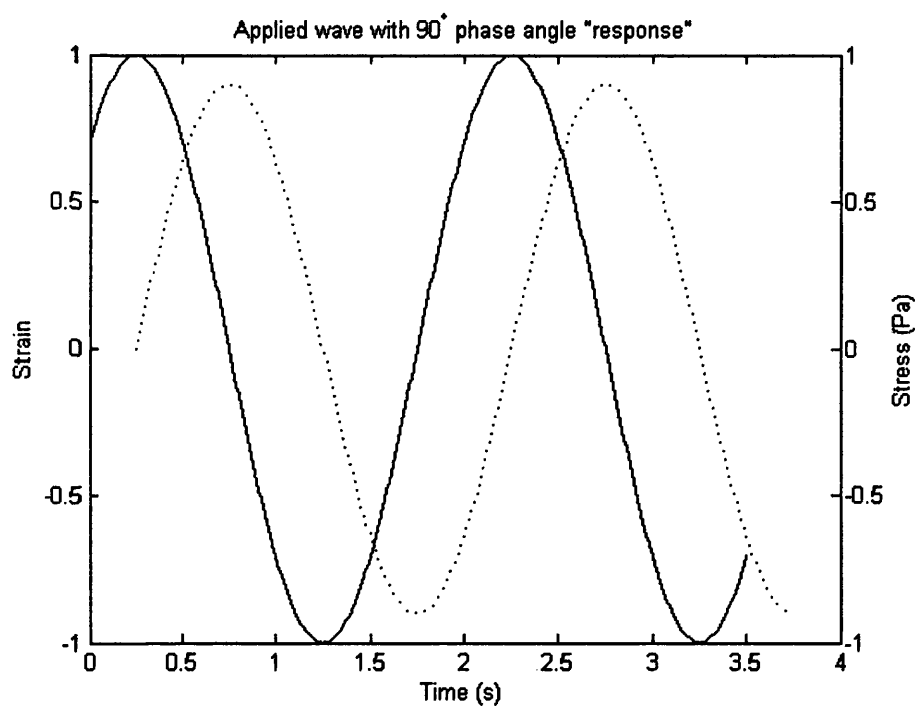


**Figure 1.3.1** - Figure showing the waveform response from an ideally viscous material

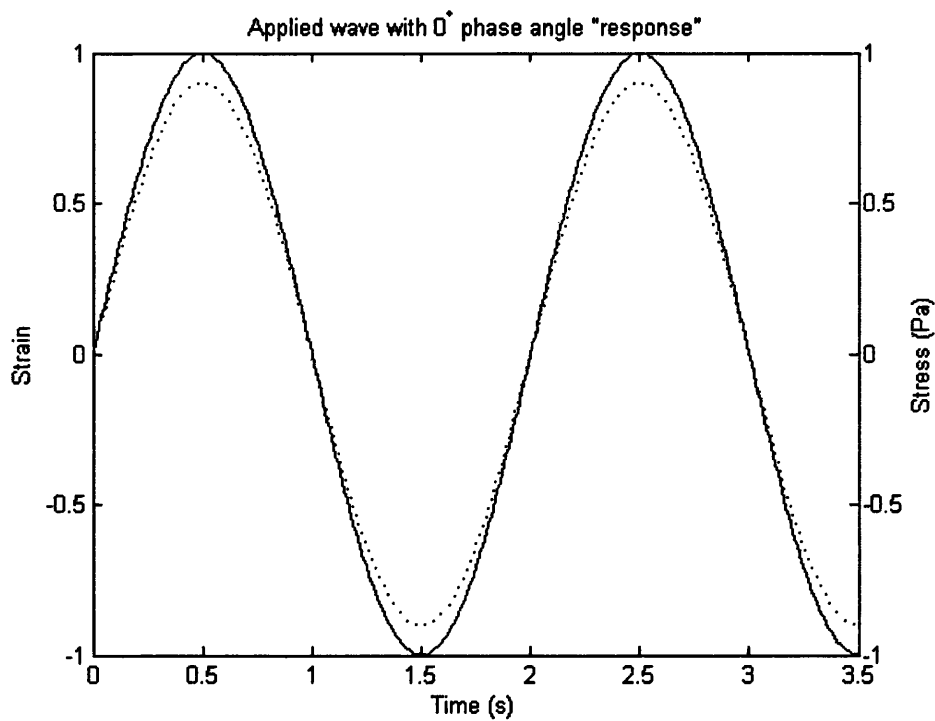


**Figure 1.3.2** - Figure showing the waveform response from an ideally elastic material

Low phase angles therefore are those where solid like properties are dominant and concurrently high phase angles are those where liquid like properties dominate. The solid like components of a sample are characterised by the storage modulus  $G'$ . The liquid like component is described by the loss modulus  $G''$ . Both of these moduli therefore vary with frequency and the calculations of them are outlined in the next section.

The most typical rheometric technique involving frequency based testing is small amplitude oscillatory shear (SAOS).

### **1.3.2 - Small amplitude oscillatory shear**

Small amplitude oscillatory shear is primarily used to perform rheological studies, this is principally because the results are very reproducible, the test is non-destructive to the sample and the assumption is made that linear viscoelastic responses are maintained

through the small deformations (Arjen Bot 1996). Simply put, deformations on the sample material are high enough for responses to be measured but not high enough to damage the sample structure or the properties of the fluid.

If a sinusoidal strain applied to a fluid is represented as figure 1.3.1 then the linear stress response can be characterised as equation 1.3.1 below:

$$\gamma = \gamma_0 \sin \omega t$$

*Equation 1.3.1 – representation of a sinusoidal strain*

$$\sigma = \sigma_0 \sin(\omega t + \delta)$$

*Equation 1.3.2 – example stress response of a sinusoidal strain with phase  $\delta$*

Where  $\delta$  is the phase lag, or phase angle in the response waveform. Typically the equations above are a fair representation of the application and response waveforms in SAOS, as the sample fluid remains linear. However at higher values of strain or stress amplitude ( $\gamma_0$  and  $\sigma_0$  respectively) a sample may become nonlinear, where slip, harmonic and other effects may be observed (J. Murali Krishnan 2010).

In SAOS the storage and loss modulus,  $G'$  and  $G''$  respectively are defined as ratios of the stress and strain amplitudes imposed on the sample.  $G'$  is based on the ratio of the amplitude of in phase stress and  $G''$  is based on the ratio of the out of phase stress. Given this, the example stress response equation 1.3.2 can be rewritten to include these moduli as shown below in equation 1.3.3.

$$\sigma = G'(\omega)\sin\omega t + G''(\omega)\cos\omega t$$

*Equation 1.3.3 – Stress based on the loss and storage moduli*

It is also possible to equate the storage and loss moduli within a simple model such as the Maxwell model. Returning to an equation for the Maxwell model:

$$\sigma + \lambda \frac{\partial \sigma}{\partial t} = \eta \dot{\gamma}$$

*Equation 1.3.4 – equation for the Maxwell model*

Where  $\lambda$  is the relaxation time and  $\eta$  is the zero shear viscosity. Long values of relaxation time signify an elastic response and low values a viscous response. Therefore the linear response of a Maxwell model in SAOS can be characterised as elastic and viscous responses, in the form of the storage and loss modulus:

$$G' = \frac{\eta \omega^2 \lambda}{1 + \omega^2 \lambda^2}$$

*Equation 1.3.5 – Storage modulus element in the Maxwell model*

$$G'' = \frac{\eta \omega}{1 + \omega^2 \lambda^2}$$

*Equation 1.3.6 – loss modulus element in the Maxwell model*

Illustrating the effective changes in  $G'$  and  $G''$  at varying frequencies as well as the existence of a crossover (occurring at the frequency  $= 1/\lambda$ ) and the existence of an elastic modulus within the model of  $\eta/\lambda$ .

The storage and loss modulus in testing are crucially calculated from the complex modulus  $G^*$  which is the vector sum of  $G'$  and  $G''$ , and is so called as it is an absolute value of a complex number in the form  $x+iy$ . For this, a mathematical proof combining the complex modulus and the storage and loss modulus is required. As explained above a sample fluid is purely viscous if it has a phase angle of  $90^\circ$  and purely elastic with a phase angle of  $0$  degrees. With the sinusoidal time variation proportional to  $e^{i\omega t}$  the size and phase relation between the stress, strain and shear rate can be described by the complex numbers shown below as equations 1.3.7-1.3.9. This is for a view to tie in the complex modulus and the storage and elastic modulus.

$$\sigma^* = \sigma e^{-i\delta}$$

*Equation 1.3.7 – Complex shear stress*

$$\gamma^* = \gamma e^{-i\frac{\pi}{2}}$$

*Equation 1.3.8 – Complex shear strain*

$$\dot{\gamma}^* = \dot{\gamma} e^{-i0}$$

*Equation 1.3.9 – Complex shear rate*

Where  $\omega = 2\pi f$ ,  $f$  is frequency in Hertz and  $\sigma$ ,  $\gamma$  and  $\dot{\gamma}$  are the peak values for the cycle of oscillation. It is important to note that for the complex shear rate the phase angle is assumed to be zero. The components of the complex shear stress (equation 2.2.7) can be re-written in component form as equation 1.3.10:

$$\sigma^* = \sigma' - i\sigma''$$

*Equation 1.3.10 – Complex shear stress as a combination of viscous and elastic stresses*

Where  $\sigma'$  is the viscous stress which also equals the stress multiplied by cosine of the phase angle  $\phi$  and  $\sigma''$  is the elastic stress, which equals the stress multiplied by the sine of the phase angle. Using these terms the complex modulus  $G^*$  can be obtained by taking the complex ratio of the shear stress to the shear strain as given in equations 1.3.7 and 1.3.8.

This is shown below in equation 1.3.11 below:

$$G^* = \frac{\sigma^*}{\gamma^*} = \left( \frac{\sigma''}{\gamma} + i \frac{\sigma'}{\gamma} \right) = G' + iG''$$

*Equation 1.3.11 – Complex modulus defined through viscoelastic stresses and strains*

The loss tangent/loss factor  $\tan \delta$  yields the relative importance of the viscous and elastic behaviours of a material, defined in equation 1.3.12 as:

$$\tan \delta = \frac{G''}{G'}$$

*Equation 1.3.12 – loss tangent expressed as loss and storage modulus*

This arrives from Maxwell's equations, a set of partial differential equations originally used to describe electromagnetic fields but since applied to many other disciplines. Given then, that peak stress over peak strain measured mechanically will yield the complex modulus  $G^*$ , a measurement of the phase angle  $\delta$  mechanically can yield the values of  $G'$  and  $G''$  through rearrangement of equation 1.3.12:

$$G' = G^* \cos \delta$$

*Equation 1.3.13 – calculation of storage modulus from  $G^*$*

$$G'' = G^* \sin \delta$$

*Equation 1.3.14 – calculation of loss modulus from  $G^*$*

## **1.4 - Sol-gel transition**

The 'Gel Point', GP (M. Muthukumar 1986, Winter HH 1986) defines the rheological transition between an elasticoviscous fluid and a viscoelastic solid. For most gelling systems the process of gelation requires the properties of a viscoelastic solid thus the GP identifies the establishment of the incipient gel, and readily identifies the point at which a viscoelastic solid forms. At the GP, the elastic and viscous components of the complex shear modulus  $G^*$  (the dynamic rigidity,  $G'$ , and loss modulus,  $G''$ , respectively) scale as power-laws in frequency,  $\omega$ , as  $G'(\omega) \sim G''(\omega) \sim \omega^\alpha$ . This feature enables the GP to be identified unambiguously by the corresponding *frequency independence* of the loss tangent,  $\tan \delta$  ( $= G''/G'$ ) (Chambon F 1987, C. Michon 1993) where  $\delta$  represents the phase angle between stress and strain waveforms in small amplitude oscillatory shear measurements and is



related to the exponent  $\alpha$  as  $\delta = \alpha\pi/2$ .

The fractal characteristics of the 3-dimensional network cluster formed at the GP have been extensively studied and are described in various theoretical treatments of polymerisation and gelation in a wide range of systems. One such treatment, known as the percolation theory, describes the GP in terms of a connectivity transition. Below the GP, isolated clusters formed from polymerised monomers represent the sol phase whereas at the GP a polymeric cluster establishes sufficient connectivity to become 'sample-spanning', thereby conferring elastic solid-like properties upon the system. The percolation theory defines the polymerising system as macroscopically homogeneous at a length-scale  $L \gg \varepsilon$  whereas for  $L \ll \varepsilon$  the sample-spanning network cluster is a 'fractal' object whose mass  $M$  scales with  $\varepsilon$  as  $M \sim \varepsilon^{D_f}$  where  $D_f$  is the fractal dimension. The value of  $D_f$  is calculated from analysis of the viscoelastic data at the GP using the established relationship (M. Muthukumar 1986)  $D_f = (D + 2)(2\alpha - D)/2(\alpha - D)$  where  $D$  is the space dimension ( $D = 3$  herein). The higher the value of  $D_f$  the more compact is the network structure, whereas low values of  $D_f$  correspond to more open/permeable networks.

Chambon and Winter (Winter HH 1986, Chambon F 1987) determined that the sol gel transition is characterised by the power laws for  $G'$  (shear storage modulus) and  $G''$  (shear loss modulus):

$$G' = G'_c \cdot \omega^n$$

$$G'' = G''_c \cdot \omega^m$$

*Equation 1.4.1/1.4.2 – power laws for  $G'$ ,  $G''$*

These equations can be introduced into the Kramers Kronig relation, designed to connect real and imaginary parts of any complex analytic function i.e. if the power law functions are positive and converge the Kramers Kronig relation can prove this mathematically (see equation 1.4.3).

$$\frac{G'}{\omega^2} = \frac{2}{\pi} \int_0^{\infty} \frac{G'' x / (x)}{\omega^2 - x^2} dx$$

*Equation 1.4.3 - power laws for  $G'$ ,  $G''$  inputted into a Kramers Kronig relation*

Equation 1.4.3 shows that m and n are essentially equal and thus during gelation the moduli and frequency are interrelated as can be shown in Equation 1.4.4 below:

$$G' \sim G'' \sim \omega^2$$

*Equation 1.4.4 – relationship between frequency and the storage and loss modulus*

Rewriting the Kramers Kronig equation with m=n yields equation 1.4.5:

$$\tan(\delta) = \frac{G''}{G'} = \tan\left(\frac{n\pi}{2}\right)$$

*Equation 1.4.5 – relationship between delta and storage and loss modulus at the gel point or sol gel transition*

At the point of gelation therefore the value of  $\tan(\delta)$  gives the value of the exponent to the power law, as well as the storage and loss modulus. Also this equation suggests that the gradients of  $G'$  and  $G''$  are the same at the sol gel transition. Crucially, while passing through this point  $\tan(\delta)$  must be frequency independent and as such becomes a useful way of

measuring the accuracy of new rheometric techniques outlined in the section below (Holly EE 1988). It has also been proposed by M.E. Rosa and H.H. Winter that a new state of the matter should be defined at the gelation threshold named the critical gel state – characterised by a power law shear stress relaxation modulus (M.E. De Rosa 1994).

#### ***1.4.1 - Multi wave oscillation and the Fourier transform***

The rheological detection of the GP involves the measurement of viscoelastic parameters ( $G'$  and  $G''$ ) over a range of frequencies ( $\omega$ ) in oscillatory shear. At the GP,  $G'$  and  $G''$  scale in oscillatory frequency,  $\omega$ , as  $G'(\omega) \sim G''(\omega) \sim \omega^\alpha$  where  $\alpha$  is the stress relaxation exponent. Thus, the GP may be identified by instant where the  $G'$  and  $G''$  scale in frequency according to identical power laws (J. Murali Krishnan 2010). Experimentally, the GP may be found by frequency sweeps, which involve repeated application of a discrete set of small amplitude oscillatory shear (SAOS) waveforms covering one or two decades of frequency, or by Fourier Transform Mechanical Spectroscopy (FTMS), which involves the simultaneous application of several harmonic frequencies and subsequent Fourier analysis. Frequency sweeps are limited to relatively slow gelation due to the presence of mutational artefacts and interpolation errors in measurement of rapidly forming gels. FTMS may overcome these limitations, but has been previously shown to be unsuitable for strain sensitive materials, such as fibrin gels, due to the application of several harmonic frequencies producing a total strain response that exceeds the linear viscoelastic range.

In FTMS the input waveform is generated by summing a sinusoidal waveform with several of its harmonics. The dynamic viscoelastic parameters at each of the discrete component frequencies are determined by comparing the Fourier Transform, FT, of the input and response waveforms. Whilst FTMS significantly reduces the time required to obtain  $G'$  and  $G''$  over a finite range of frequencies, the amplitude of the applied waveform increases as more harmonics are included. Hence, the amplitude of the applied waveform (stress or strain) may exceed the linear viscoelastic limit for strain sensitive biopolymer systems even where a modest number of harmonics are employed. Reducing the amplitude of the harmonics in an attempt to maintain linearity generally leads to a loss of resolution in the pre-GP data; thus accurate GP identification in a low initial viscosity sample is difficult.

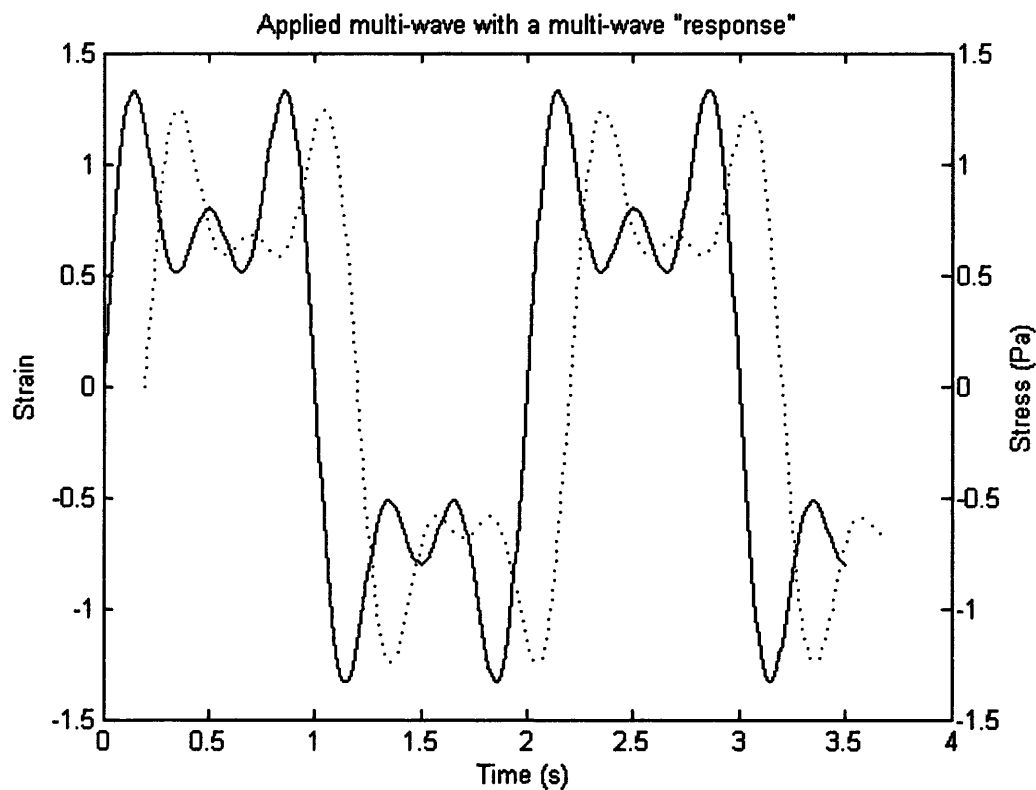


**Figure 1.4.1** - Figure showing a simple applied multi-wave waveform and an appropriate viscoelastic stress 'response'

This processes use on linear viscoelastic materials is outlined by Holly EE (Holly EE 1988) to determine the complex modulus  $G^*$  through decomposed components of a multi-wave waveform, composed of a base frequency and additive constituent harmonics.

Using a Fourier transform function with phase data the frequencies and amplitudes of both the strain and the corresponding stress waveforms are calculated along with their respective phases. By comparing these phases the phase angle at each frequency can be calculated.

Calculation of  $G'$  and  $G''$  is also possible, the methodology of this measurement through a fourier transform of a multi-wave waveform is outline by Holly EE et al (Holly EE 1988) and

is explained in brief below. Performing a fourier transform on stress waveform data for the harmonic integers (m) the resultant frequencies are illustrated in equation 1.4.1 below:

$$\sigma = \sum_{i=1}^m \sigma(\omega_i) = \sum_{i=1}^m (A_i \sin \omega_i t + B_i \cos \omega_i t)$$

*Equation 1.4.1 – Expression of component frequency and amplitude from a multi wave waveform*

Where  $A_i$  and  $B_i$  are Fourier constants. The loss tangent between the stress and strain component waveforms can then be given by equation 1.4.2 below:

$$\tan \delta(\omega_i) = \frac{B_i}{A_i}$$

*Equation 1.4.2 – An expression relating loss tangent with Fourier constants*

The storage and loss modulus are then calculated using the expressions below, which are derivations of similar equations discussed in the SOAS section above.

$$G'(\omega_i) = K_\sigma(\omega_i) \cos \delta(\omega_i) / \gamma(\omega_i)$$

*Equation 1.4.3 - Storage modulus calculation from FTMS data*

$$G''(\omega_i) = K_\sigma(\omega_i) \sin \delta(\omega_i) / \gamma(\omega_i)$$

*Equation 1.4.4 – loss modulus calculation from FTMS data*

Where the value K is a scaling factor of the geometry for the rheometer, and is calculated experimentally.

At present the system in place on most rheometers is to use the harmonics of the lowest frequency as the additional waves in a multi wave test (ie when the lowest frequency is 0.4Hz the other waves added to form the multi wave will be 0.8Hz 1.2Hz etc). This however has a number of limitations.

One primary limitation is that when trying to apply a multi-wave to a sample over a specific frequency range there is a limitation of harmonics available. As an example for a frequency range of 0.4-2Hz there are 5 available harmonics, whereas there are theoretically limitless anharmonic frequencies.

Typically the more frequencies in a multi-wave waveform the higher the peak strain, this is caused by frequencies within the waveform having a positive or negative gradient simultaneously. As the waveforms have to be harmonics there are only a few ways to optimise the system to decrease the peak strain. A high peak strain may interfere with the structure of strain sensitive samples and give an inaccurate or skewed representation of the viscoelastic properties of the sample. As this is undesirable, lowering the peak strain is critical; one method with harmonic waveforms is to alter the phase of these harmonics manually, such that their gradients do not coalesce over the time period resulting in a high peak strain.

This is still limited however, as the frequencies themselves are the biggest contributing factor to peak strain. The limitations of harmonics then are self-evident, with less choice of frequency comes less control over the peak strain. When using anharmonics the frequencies themselves can be altered such that they have a lesser effect on the peak strain.

As an example, a sample that needs to be measured over the frequency ranges 0.2-3.2Hz with five additive frequencies forming a multi-wave measurement over the time period of 300s. Using anharmonic values of 0.2, 0.4, 0.8, 1.6 and 3.2Hz, through the alteration of phase for the individual frequencies a peak strain can be optimised to 2.98 (given all frequencies have an amplitude of 1) however, through optimising the use of anharmonics and phase changes the peak strain reduces to 2.60 the deviation from the harmonics is minimal with the frequencies 0.2, 0.35, 0.75, 1.55 and 3.15Hz put into the waveform. Thus similar viscoelastic information is measured, with a 13% reduction in peak strain on the sample.

If the changes made to the original frequency are permitted to deviate further from the original harmonics, then a 17% reduction on peak strain can be found, with frequencies of 0.2, 0.3, 0.7, 1.5 and 3.1Hz

As an illustration, we can take example harmonic frequencies and alter them by no more than a set percentage value, creating anharmonic frequencies that will yield similar information for much less strain. As the number of frequencies used increases so does the difference in peak strain between anharmonic and harmonic frequencies (see figure 2).



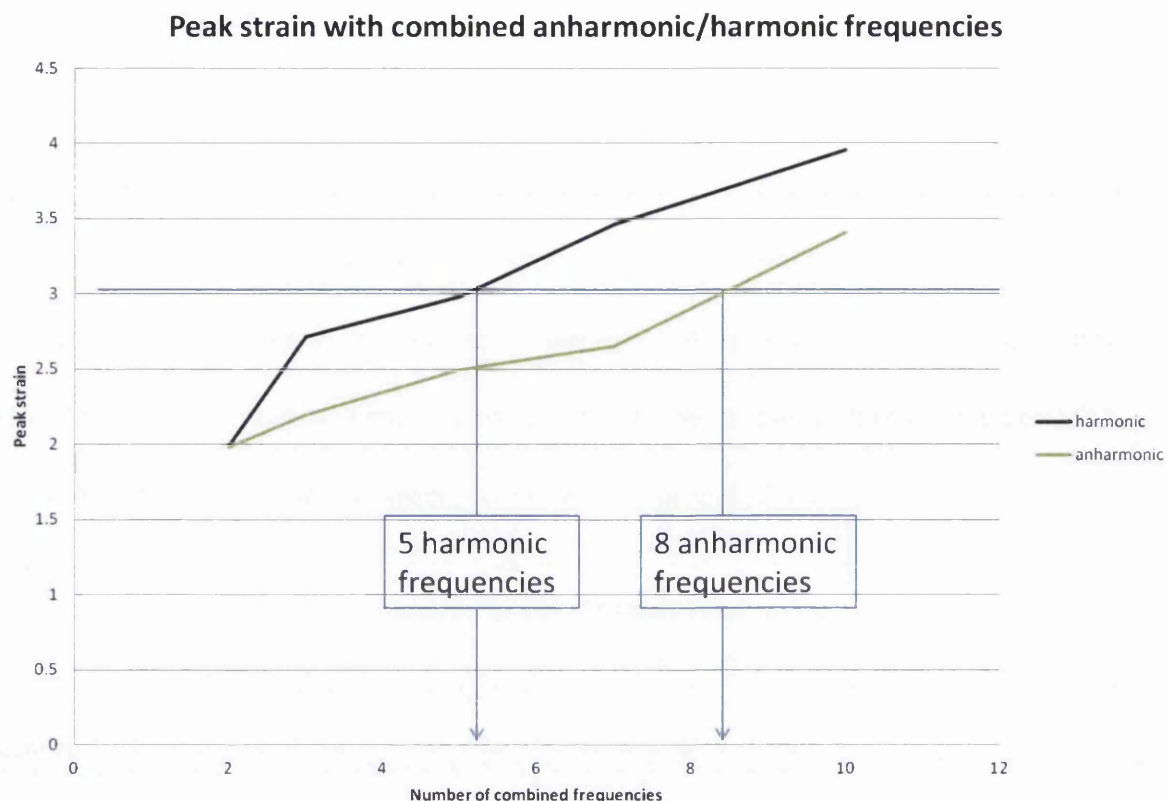


**Figure 1.4.2** - Figure showing the differences between phase optimised harmonic and anharmonic frequency peak strains

This data clearly illustrates that anharmonic waveforms can be used to increase the number of frequencies measured while keeping the peak strain low, which is critical for strain sensitive samples. As well as providing more data, a better estimation of the discrete relaxation spectra can be made as both a greater width of frequencies can be used as well as more in number, which would improve any fitting of a Maxwell model. More frequencies should also improve any estimation of the sol gel transition point.

## 1.5 - Superposition

### 1.5.1 - The Boltzmann superposition principle

The Boltzmann superposition principle is the basis of modern discrete relaxation spectra calculation as it describes the relaxation or 'stress history' of linear viscoelastic behaviour.

Named for the physicist of the same name it is perhaps best described by an example from J.D Ferry (Ferry 1980). If two stresses ( $\sigma_1$  and  $\sigma_2$ ) are applied at two different time periods  $t=0$  and  $t_1$  respectively the corresponding strain can be calculated as:

$$\gamma(t) = \sigma_1 J(t) + \sigma_2 J(t - t_1)$$

*Equation 1.5.1 – Strain calculated from two separate time dependent stresses*

This then can be generalised for a finite number of stress changes at each time  $u_i$  to give the equation:

$$\gamma(t) = \sum_{u_i=-\infty}^{u_i=t} \sigma_i J(t - u_i)$$

*Equation 1.5.2 – Strain calculated from i number of separate time dependent stresses*

## 1.6 - Relaxation Spectra

### 1.6.1 - Stress relaxation

By deforming a viscoelastic liquid rapidly to a predetermined strain will result in a stress response that decreases over time. The gradient of this decrease in stress also decreases with time until it reaches zero in the case of viscoelastic liquids or the elastic modulus ( $G_e$ ) in

the case of viscoelastic solids. If that liquid corresponds to a single Maxwell model the behaviour can be given by equation 1.6.1 below:

$$\frac{\sigma(t)}{\gamma} = G e^{\frac{-t}{\lambda}}$$

*Equation 1.6.1 – stress relaxation of a single Maxwell model*

Where the relaxation time  $\lambda$  is defined as  $\eta/G$ . Typically stress relaxation plots are shown as normalised stress ( $\sigma/G$ ) over time, see figure 1.6.1 below.

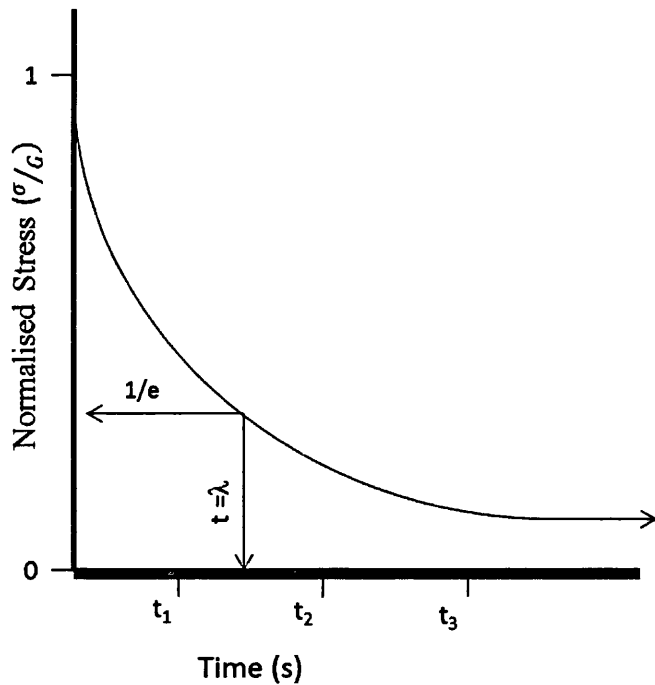


**Figure 1.6.1** - Figure showing an exemplar stress relaxation experiment on a single Maxwell model

For real viscoelastic liquids the stress relaxation curve is usually described by a series of Maxwell models in parallel, as described in section 1.1.4 – thus a generalised Maxwell model will take the form:

$$\frac{\sigma(t)}{\gamma} = G_1 e^{\frac{-t}{\lambda_1}} + G_2 e^{\frac{-t}{\lambda_2}} + G_3 e^{\frac{-t}{\lambda_3}} + G_4 e^{\frac{-t}{\lambda_4}} \dots$$

*Equation 1.6.2 – stress relaxation of multiple maxwell models*

This can also be expressed in the form:

$$G(t) = G_e + \sum_{i=1}^N g_i \exp\left(-\frac{t}{\lambda_i}\right)$$

*Equation 1.6.3 – stress relaxation of multiple maxwell models*

This is more commonly known as a relaxation spectrum of a material, as it covers the many different relaxation times within a material. They are more often obtained through non-linear curve fitting programs.

## **1.6.2 - Discrete relaxation spectra**

Typically the discrete relaxation spectra are modes that fit the generalised Maxwell model of viscoelasticity. The generalised Maxwell model is one of the most general forms of the linear viscoelastic model. Consisting of many Maxwell elements in parallel, it takes into

account that relaxation happens more over a set of times rather than a single time, with some 'modes' (Maxwell elements) affecting the relaxation more than others.

The generalised Kelvin Voigt model measures the discrete retardation spectrum ( $J_i(\tau_i)$ ) and is measured in a similar method than outlined below known as the finite element method (OC Zienkiewicz 1968, Zienkiewicz 1995). It is rheologically important however not relevant to the work carried out in this theses and will not be investigated in detail.

If the relaxation modulus  $G(t)$  is expressed as a discrete set of exponential decays (as in the Maxwell model) .

$$G(t) = G_e + \sum_{i=1}^N g_i \exp\left(-\frac{t}{\lambda_i}\right)$$

*Equation 1.6.4*

Where  $g_i$  is the strength of the component,  $\lambda_i$  is the relaxation time of that same component and  $G_e$  is the equilibrium modulus, which is a finite value for solids, but zero for liquids. The relationship between deformation and stress can be defined by the equation below (1.6.5) based on the Boltzman superposition principle for linear viscoelastic fluids. This algorithm for fitting the discrete relaxation spectra to mechanical data was proposed by Baumgaerel and Winter (Baumgaertel M. 1989, Baumgaertel M. 1992):

$$\tau(t) = \int_{-\infty}^t G(t-t') \dot{\gamma}(t') dt'$$

Equation 1.6.5

Where  $\tau$  is the stress tensor and  $\dot{\gamma}$  is the strain rate tensor

Using equation 1.6.5 in equation 1.6.4 the dynamic moduli of  $G'$  and  $G''$  become:

$$G'(\omega) = G_s + \sum_{i=1}^N g_i \left( \frac{(\omega \lambda_i)^2}{1 + (\omega \lambda_i)^2} \right)$$

Equation 1.6.6

$$G''(\omega) = G_s + \sum_{i=1}^N g_i \left( \frac{\omega \lambda_i}{1 + (\omega \lambda_i)^2} \right)$$

Equation 1.6.7

The parameters of a discrete relaxation spectrum are found by simply fitting equations 1.6.6 and 1.6.7 to  $G'$  and  $G''$  data at known frequencies. The coefficients,  $g_i$  (the strength of the component) and the relaxation times,  $\lambda_i$  are determined such that the average square deviation between predicted  $G'$  and  $G''$  values and measured  $G'$ ,  $G''$  values are at a minimum:

$$\sum_{j=1}^M \left( \left[ \frac{G'(\omega_j)}{G'_j} - 1 \right]^2 + \left[ \frac{G''(\omega_j)}{G''_j} - 1 \right]^2 \right) = \min$$

Equation 1.6.8

Where  $\dot{G}'_j$  and  $\dot{G}''_j$  are the measured data at frequencies  $M$  and  $\omega_j$ ,  $G'$  and  $G''$  are the

calculated values from equations 1.1.6-1.1.7.

This method however is most effective at calculating relaxation times the more frequencies there are available to analyse. This puts limitations measuring relaxation times for gelling solutions as they change properties with time. This change means that typically a very limited number of frequencies can be measured while operating within the mutation limits of the sample.

This is because multi-wave analysis is typically used and as such the more frequencies that are required to be measured the higher the peak strain of the measurement. This can affect the results as most structured complex fluids are compromised by high peak strains.

### ***1.6.3 - The Continuous Relaxation Spectrum, $H(\tau)$***

As the number of elements,  $N$ , in the generalised Maxwell model (as shown in Figure 2.1) tends to infinity, it is appropriate to consider a continuous spectrum of relaxation times, each with an associated infinitesimal contribution to rigidity (or spectral strength). The continuous relaxation spectrum is defined as,

$$H(\tau)d\ln(\tau)$$

*Equation 1.6.9 – a definition of the continuous relaxation spectrum*

and may be considered to be the modulus contribution associated with relaxation times which lie between  $\ln(\tau)$  and  $\ln(\tau) + d\ln(\tau)$ .  $H(\tau)$  can also be referred to as a modulus density on relaxation time (Tschoegl 1989) and replaces the discrete sum of moduli  $G_i$  in the generalised Maxwell model.

The relaxation spectrum,  $H(\tau)$ , is a fundamental quantity in the linear theory of viscoelastic fluids (Honerkamp J. 1989, I. Emri 1993). If the continuous relaxation spectrum and the associated viscoelastic constants are known, it is, in principle, possible to generate the response to *any* type of excitation. Ferry (1980) presents a comprehensive account of the interrelationships between  $H(\tau)$  and the viscoelastic functions. In response to a step excitation, the stress relaxation modulus,  $G(t)$  becomes,

$$G(t) = \{G_e\} + \int_{-\infty}^{\infty} H(\tau) \exp\left(-\frac{t}{\tau}\right) d\ln(\tau)$$

*Equation 1.6.10 – a calculation of the stress relaxation modulus*

The harmonic response functions can be derived in the same way,

$$G(\omega) = \{G_e\} + \int_{-\infty}^{\infty} \left[ \frac{H(\tau) \omega^2 \tau^2}{1 + \omega^2 \tau^2} \right] d\ln(\tau)$$

*Equation 1.6.11 – a calculation of the storage modulus*



$$G''(\omega) = \int_{-\infty}^{\infty} \left[ \frac{H(\tau)\omega\tau}{1+\omega^2\tau^2} \right] 1\tau(\tau)$$

Equation 1.6.12 – a calculation of the loss modulus

$H(\tau)$  is not directly accessible through experiments in conventional rheometry. Rather, it must be determined from readily available material functions, usually from dynamic data ( $G'(\omega)$  and  $G''(\omega)$ ). In order to obtain  $H(\tau)$  from  $G'(\omega)$  and  $G''(\omega)$ , Equations 2.12 and 2.13 (also known as Fredholm integral equations) must be inverted but a difficulty arises in that the inversion is inherently *ill-posed* due to noise amplification i.e. a small perturbation in experimentally determined data results in large errors in  $H(\tau)$  (Groetsch 1985, Groetsch 1993). The spectra obtained from such inverse solutions are an *approximation* to the unknown, true spectrum and no spectrum – produced by whatever method – is ever the *true* spectrum (Emri I. 1993).

The foregoing techniques notwithstanding there is need to better understand and characterise the rheological properties of complex fluid systems and products, in particular the evolution of their viscoelastic properties and microstructure under imposed shear flows. One rheometric response to this requirement involves the superposition of a steady (or unidirectional) shear flow on a small amplitude oscillatory shear (SAOS) flow component. This may involve parallel or orthogonal superposition of the unidirectional and oscillatory flow components, under controlled stress or controlled deformation rate conditions.

**Superposition rheometry** provides a basis for probing microstructural changes associated with a steady (or unidirectional) deformation. Interpretation of such experiments

involves the assumption that the oscillatory (or ‘probe’) deformation has negligible effect on the material and hence any apparent microstructural changes may be attributed to the steady deformation alone. Superposition rheometry is described in detail in Chapters 2 and 3 of this Thesis.

A further development in rheometry based on SAOS has recently been reported and is referred to as ***Optimal Fourier Rheometry***, OFR. In contrast to FTMS, in which the perturbation signal consists of discrete frequencies, the OFR waveform undergoes a continuous modulation between two defined frequency limits. Hence performing a Fourier analysis (using the fast Fourier transform, FFT) on an OFR waveform provides a means of identifying a number of frequency components, the number of which is limited only by the sampling rate of the raw perturbation (e.g. strain) and the corresponding response (e.g. stress waveforms). As a result, OFR offers two significant advantages over FTMS, these being a) the ability to obtain very high densities of  $G'(\omega)$  and  $G''(\omega)$  data over a finite frequency window, and b) the strain amplitude is independent of the number of component frequencies. Optimal Fourier Rheometry is described in detail in Chapter 4 of this Thesis.

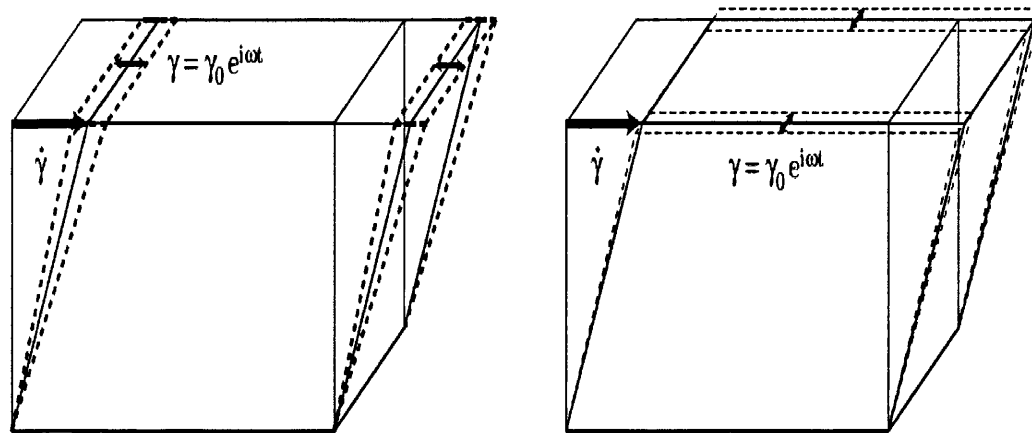


**Figure 2.1.1** - Figure showing the process of orthogonal and parallel superposition

Left: Parallel superposition; right: Orthogonal superposition on a cubical volume of sample.

The large arrows represent the direction of steady shear

The small arrows represent oscillatory shear

### **2.1.1 – Strain and stress controlled parallel superposition**

Parallel superposition involves the application of an oscillatory force in the same/direct opposite direction as that of shear flow, unlike the case of orthogonal superposition where the oscillatory stress is applied tangentially to the sample undergoing large amplitude steady deformation. Parallel superposition therefore (in principle) provides a means of measuring the viscoelastic properties of a fluid (in terms of  $G'$  and  $G''$ ) while the sample fluid is experiencing unidirectional shear flow. The microstructural response of a material can be very different in this case from that in SAOS (Booij 1966, Simmons 1968).

Parallel superposition becomes more complicated with the introduction of a transient material such as gel like gelatine. Gelatine develops substantial elastic characteristics as it gels. As a consequence the application of high stresses when in a Newtonian viscous like state would cause a non-linear response however these same stresses would be considered very low once the elastic properties of gelatine are fully developed (see figure 2.1.2).

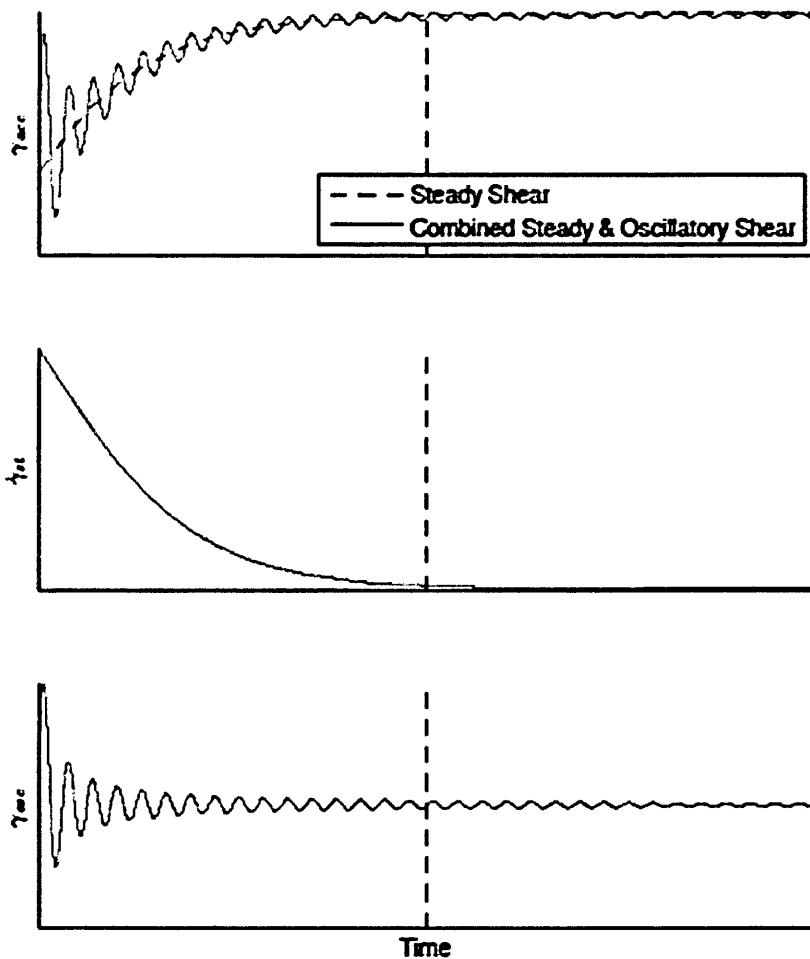


**Figure 2.1.2** - Figure showing the strain rate during stress operated superposition with a transient sample of building elastic strength

This change in strain on the fluid means that a transient sample such as gelatine becomes almost self-regulating in terms on linearity, as such very little structural damage is done through testing. This does however become a drawback as investigations into high strains become more important. A strain operated rheometer will not experience the same strain profile as can be seen below in figure

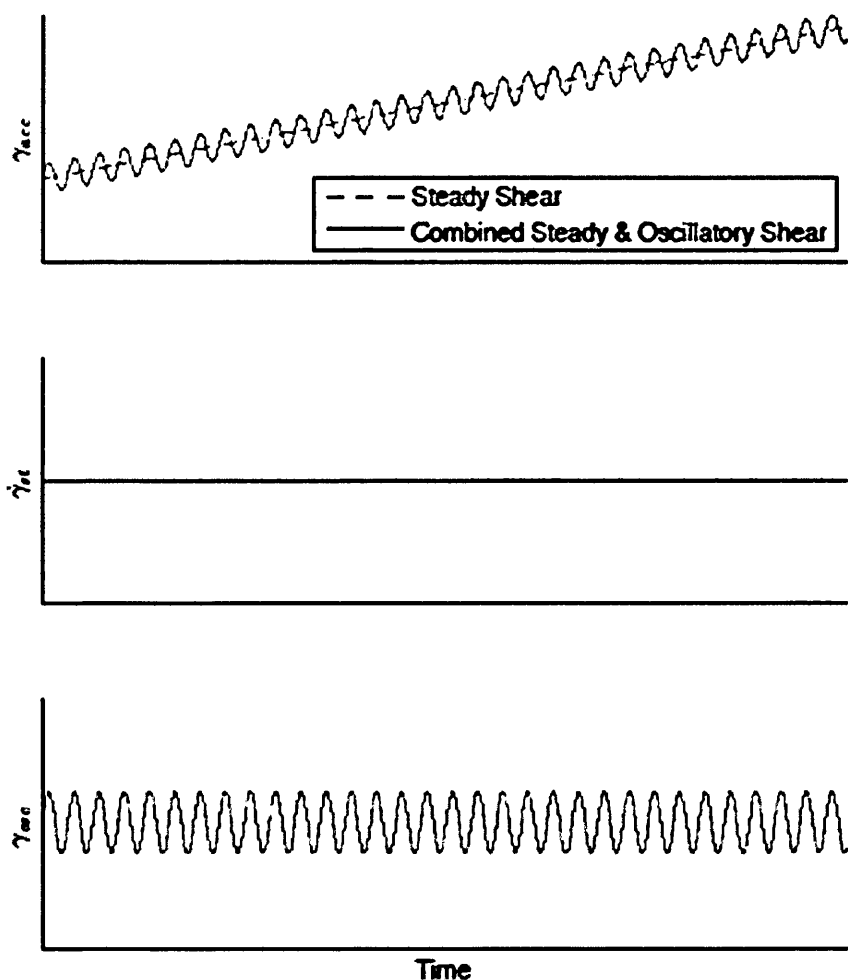


**Figure 2.1.3** - Figure showing the strain rate during strain operated superposition with a transient sample of building elastic strength

It is also important to note from these figures it is clear the oscillatory stress or strain cannot be significantly smaller than the steady stress/strain as it will get 'lost' as a signal within both the application and response. A linear range of superposition was proposed albeit briefly by Booij (Booij 1966, Booij 1968) . Where the linear range was where the amplitude of the oscillatory shear stress was proportional to the amplitude of the oscillatory shear flow.

## ***2.2 - VALIDATION OF CSPS – USING A MODEL GEL SYSTEM***

Superposition rheometry provides a basis for probing microstructural changes associated with a steady (or unidirectional) deformation. Interpretation of such experiments involves the assumption that the oscillatory (or 'probe') deformation has negligible effect on the material and hence any apparent microstructural changes may be attributed to the steady deformation alone (Ferry 1980, Dealy and Wissbrun 1990, Jomha and Woodcock 1990, Vlastos, Lerche et al. 1997, Anderson, Pearson et al. 2006, Somma, Valentino et al. 2007). Davies & Jones (Davies, Jones et al. 1987) reported the implementation of superposition experiments in a controlled stress rheometer. The ability to perform controlled stress parallel superposition (CSPS) has since been available on many commercial rheometers but its use has not been widely reported in the context of systems undergoing gelation. In this chapter work is reported which involves assessments of the validity of the superposition technique when applied to a system which displays critical-gel behaviour at the Gel Point, GP. The system chosen for study is based on gels formed from aqueous gelatine solutions whose rheological (GP) characteristics have been previously reported under SAOS/FTMS (Michon, Cuvelier et al. 1993, K. Hawkins 2008).

Determination of SWHS for ... Chapter 2

The rheometer chosen for this study was the TA Instruments AR G2 controlled stress instrument whose principal features and operation are now described below.

### **2.2.1 - The Controlled Stress (CS) Rheometer**

All rheological measurements reported in this chapter were carried out using a controlled stress rheometer (AR-G2, TA Instruments, Uk). The AR-G2 imposes a sinusoidal stress through the upper measuring geometry and measures the resulting strain at the same geometry (the lower portion of the geometry remains static at all times). In this instrument the shear stress and shear strain are not directly measured but the angular displacement,  $\Delta$ , is measured as a result of applied torque,  $T_Q$ . These parameters are then multiplied by stress and strain factors in order to evaluate the shear stress and shear strain values, respectively. Controlling the torque and measuring the resulting displacement is one of the earliest rotational rheometerical techniques for investigating a material's steady shear properties (J.R. Van Wazer 1963), however, in order to provide a comprehensive characterisation of viscoelastic properties, it is generally necessary to operate in dynamic or oscillatory mode.

Jones *et al.* (T.E.R. Jones 1984) reported that the CS rheometer principle can operate in oscillatory mode. CS based oscillation has been used to study a wide range of systems such as oils (H. Conrad 1995), emulsions (Pal 1997, A. Guerrero 1998), inks (E. Fernandez-Cara 1998) and gels (Carnali 1992, C.J. Rueb 1997, A. Rodd 2001).

A schematic of the rheometer is shown in figure 2.2.1. The instrument consists of the following six main components.

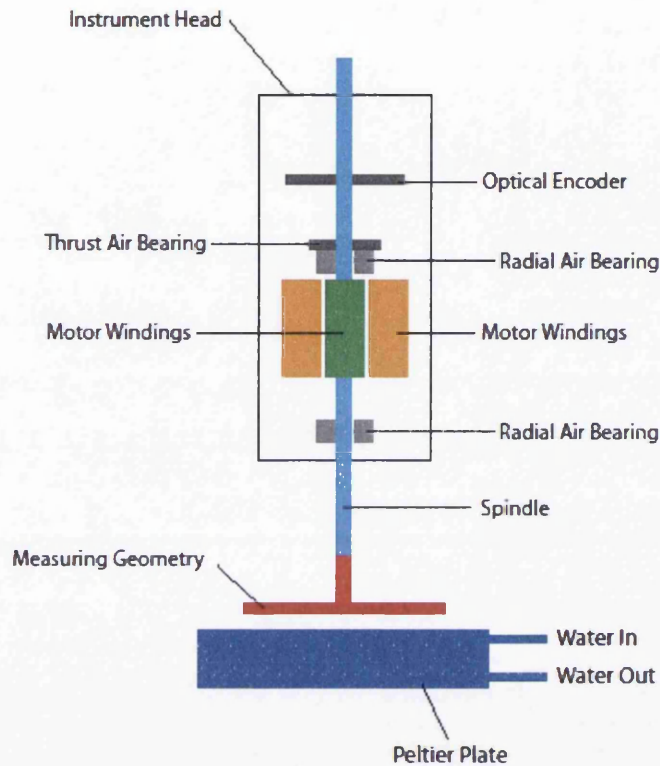


**Figure 2.2.1** - Figure showing the schematic of the TA ARG2 stress controlled rheometer

### ***(i) The drag cup motor***

A drag cup motor is used to apply stress to the sample, the drag cup motor assembly consists of a cup shaped rotor (conducting material) wrapped around a magnetic stator.

### ***(ii) The air-bearing***

The bearing is a key element in all rheometers and several types are available. The ARG2 utilises a magnetic bearing in which magnets are used to suspend the spindle.



***(iii) The Peltier plate***

A Peltier plate was used in order to maintain a constant temperature during experiments. Peltier plates exploit the thermoelectric effect which converts an applied voltage to a temperature difference. The Peltier plate is attached to a water bath, operating at room temperature, which acts as a heat sink. A cylindrical version of the Peltier plate was used in tests in which concentric cylinder geometry was employed.

***(iv) The normal force transducer***

The instrument allows normal forces to be measured through the lower component of the measuring geometry. This feature was used in the rheometer “gap setting” routines.

***(v) The optical encoder***

The optical encoder is used for measuring angular displacement. It consists of a patterned disk connected to the spindle, and a similar disk held stationary. Both disks are positioned between a non-contacting light source and a photodetector. The patterned disk acts as a diffraction grating and hence by analysing the diffraction pattern the angular displacement of the spindle can be assessed. The measurement of angular displacement is converted to strain and strain rate using geometry specific equations, some of which are described overleaf.

## 2.2.2 - Measuring Geometries

### 2.2.2.1 The Cone and Plate Geometries

A cone and plate geometry consists of a truncated cone (upper geometry) and a flat plate (lower geometry) as shown in Figure 2.2.1. Cone and plate geometries are commonly used for single phase homogenous samples and are unsuitable for samples containing large particulates. In order to calculate stress and strain and strain-rate from the applied torque (M) and measured displacement (d) and angular velocity (W), geometry specific equations are used in the instruments software, these equations can be expressed as:

$$\tau = F_{\tau} M$$

Equation 2.2.1 – calculation of shear stress

$$\gamma = F_{\gamma} d$$

Equation 2.2.2 – calculation of shear strain

$$\dot{\gamma} = F_{\dot{\gamma}} W$$

Equation 2.2.3 – calculation of shear strain rate

Where  $F_{\tau}$  and  $F_{\dot{\gamma}}$  are termed the stress and rate factors respectively and are calculated as

$$F_{\tau} = \frac{3}{2\tau R^3}$$

Equation 2.2.4 – calculation of the stress factor for a cone and plate geometry

$$F_{\square} = \frac{1}{\tan \square}$$

Equation 2.2.5 – calculation of the rate factor for a cone and plate geometry

Cone and plate geometries are available in various diameters (20 mm, 40 mm, 60 mm), cone angles (0.5° to 4.0°) and materials (stainless steel, aluminium, acrylic). The choice of geometry depends on the material under investigation; generally, less viscous fluids require larger plates with lighter geometries (in order to minimise inertial effects) than more viscous fluids. Cone and plate geometries have a cone angle and truncation gap such that the strain rate is constant across the entire diameter of the geometry.

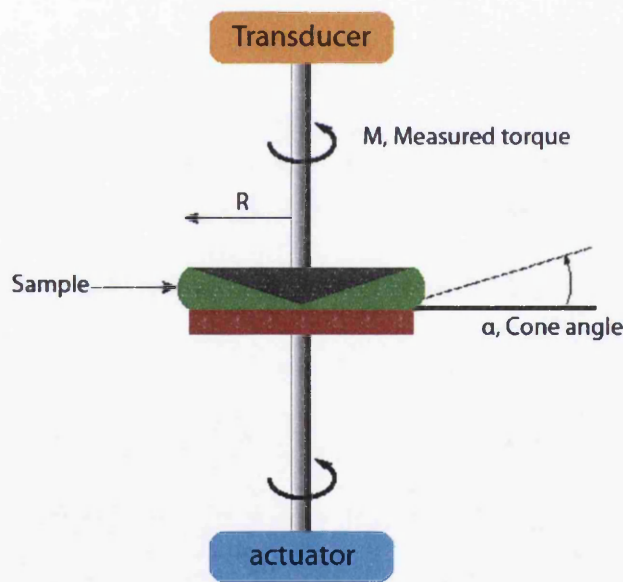


**Figure 2.2.2** - Figure showing the schematic of a typical cone and plate geometry

### 2.2.2.2- The Parallel Plate Geometries

Parallel plate geometries are commonly used for materials containing large particulates that may be trapped in the truncated region of cone and plate geometry. Such geometry consists of two flat plates of radius R separated by a gap distance D. The upper plate is made of different types of materials such as stainless steel, aluminium, acrylic or titanium. For accurate operation of the rheometer the gap should be at least ten times the diameter of the largest particle. A parallel plate geometry is shown in figure 2.2.1 and stress, strain and strain rates are calculated using equations 2.2.1-2.2.3 but with the stress and strain factors below.

$$F_{\square} = \frac{2}{\square R^3}$$

*Equation 2.2.6 – calculation of the stress factor for a parallel plate geometry*

$$F_{\circ} = \frac{R}{D}$$

*Equation 2.2.7 – calculation of the stress factor for a parallel plate geometry*

It is important to note that the stress is not uniform over the entire diameter of the measuring geometry in a parallel plate system and that the stress factors of equations 2.2.6 and 2.2.7 refer to the rim of the geometry (and therefore its maximum value). The instrument software is able to compensate for this during internal calculations. This effect can be considered of negligible significant in small amplitude measurements within the linear viscoelastic range LVR (Mezger 2006).

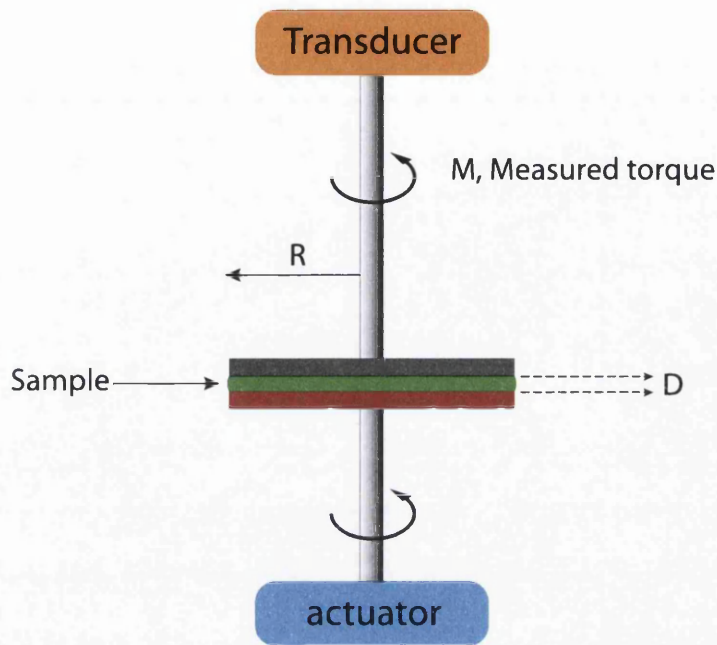


**Figure 2.2.3** - Figure showing the schematic of a typical parallel plate geometry

### 2.2.3 - Inertial Effects

#### 2.2.3.1- Instrument Inertia

In a rotational rheometer, it is important to take into account the motion of the apparatus when the force and the displacements are measured with the same surfaces. In a controlled stress rheometer, where measurements are performed at the surface, it is convenient to discuss the mechanical impedance,  $Z_M^*$ , or the complex ratio of force to velocity of a moving element. This includes contributions from the surface in contact with the sample, the inertia elastance, and the friction of the moving element itself (Ferry 1980). Neglecting sample inertia, analysis of the equation of motion for driving with a sinusoidal force gives a simple expression for the mechanical impedance ( $Z_M^*$ ) of the moving element:

$$Z_M^* = \frac{F^*}{v} = R_M + iX_M = R_M + i\left(\omega M - \frac{S_M}{\omega} - \frac{S_M^0}{\omega}\right)$$

*Equation 2.2.8 – calculation of the mechanical impedance neglecting sample inertia*

Where

$F^*$  is the complex force (N)

$v$  is the velocity of the moving part ( $\text{m s}^{-1}$ )

$R_M$  is the frictance of the sample ( $\text{kg s}^{-1}$ )

$X_M$  is the mechanical resistance ( $\text{kg s}^{-1}$ )

$M$  is the mass of the moving element (kg)

$S_M$  is the elastance of the sample ( $\text{N m}^{-1}$ )

$S_M^0$  is the elastance in the axial direction of the mechanism, which supports and centres the moving element ( $\text{N m}^{-1}$ )

Whence

$$G' = \frac{(-\omega X_M + \omega^2 M - S_M^0)}{b}$$

*Equation 2.2.9 – mechanical calculation of the storage modulus*

$$G = \frac{aR_M}{b}$$

Equation 2.2.10 – mechanical calculation of the loss modulus

where

$b$  is a geometrical form factor (m)

There are certain limitations for the above equations. First,  $S_M^0$  should be small compared to  $S_M$  and second, sets a low frequency limit. At high frequencies the  $\omega^2 M$  term in equation 2.2.9 may become dominant and only inertia of the element will be measured. This sets a high frequency limit for the rheometer as resonant frequency is approached. The instrumental inertial forces are calibrated prior to experiments, which introduce a correction factor, by the rheometer software to correct the applied torque.

### 2.2.3.2 - Sample Inertia

Sample inertia forces are deemed to be very small for low density samples compared to the quantity of  $\frac{G'}{h^2 \cdot f^2}$  where  $h$  is the gap size between the parallel plates and  $f$  is the frequency of the oscillation. This condition is based on the assumption that the strain or stress is constant throughout the shearing gap (Ferry 1980). In general, the inertia correction in cone and plate geometry is very small and much smaller in parallel plate geometry so that the inertia contribution is insignificant and can be ignored

#### **2.2.4 - Gelatine**

Gelatine is derived through the thermal deanturation of collagen, a common structural protein in animal tissues. It has a wide range of uses, typically as a gelling agent for foodstuffs as well as cosmetics and pharmaceuticals as upon cooling it forms elastic thermoreversible gels. The typical composition of gelatine is that of many glycine, proline and 4-hydroxyproline residues, similar to that of collagen (A.G Ward 1977).

As for its structure, gelatine is much the same as collagen, however during the process of hydrolysis the natural molecular bonds between polypeptide bands are broken down into a form that rearranges more easily. Gelatine consists of single and multiple polypeptide bands that can contain up to 1000 amino acids the have broken down from collagen chains as well as intact collagen chains and their oligomers (K. Okuyama 2006). These chains form helices that form the main structure of the gel as they cool.

#### **2.2.5 - Determination of the value of the relaxation exponent $\alpha$ for Gelatine gels**

The relaxation exponent  $\alpha$  provides a rheological measure of gel microstructural response to imposed stress. It is obtained during the transition from sol to gel (i.e. at the Gel Point) and is defined as (Winter HH 1986, Chambon F 1987).

$$G(t) = St^{-\alpha}$$

*Equation 2.2.11*



Where  $S$  is the relaxation modulus at the gel point, and can be re-written as:

$$G^*(\omega) \sim \omega^\alpha$$

*Equation 2.2.11*

Therefore the frequency independent point of gelling systems not only allows calculation of  $t_{gel}$  but also  $\alpha$ .

The relaxation exponent of gels is inherently tied to the microstructure within the gel (S.Z. Ren 1993). For gelatine this relates to the lengths of the helical coils formed within the gel. It has been argued that the rate of cooling affects how these helical structures form (Liang Guo 2003) and therefore the relaxation exponent should change with time. Further investigation has shown that the relaxation exponent  $\alpha$  remains constant regardless of the rate of cooling as well as concentration (K. Hawkins 2008).

For gelatine the value of  $\alpha \sim 0.69$  is reportedly independent of concentration and gelation rate promotes. Gelatine gels thus provide a useful model test reference for viscoelastic tests.

### ***2.2.6 - Controlled stress parallel superposition and gelling systems***

In parallel superposition an oscillatory deformation of amplitude  $\gamma_0$  and frequency  $\omega$  are superimposed upon a steady strain rate, with both deformations occurring in the same direction. The resulting equation for the total applied strain rate is (Booij 1966, Walters 1975, J. Dealy 1990):

$$\dot{\gamma}(t) = \dot{\gamma}_s + \gamma_0 \cos(\omega t)$$

*Equation 2.2.12 – calculation of the total applied strain rate for CSPS*

Booij (Booij 1966) suggested that if the oscillatory deformation was carried out within the linear viscoelastic range (LVR) then the resulting stress waveform would take the form:

$$\sigma(t) = \sigma_s + |G^*| \gamma_0 \sin(\omega t + \delta)$$

*Equation 2.2.13 – calculation of the total resultant stress for CSPS*

Thus  $G^*$  (and hence  $G'$  and  $G''$ ) can be defined for systems undergoing parallel steady and oscillatory shear, provided that the oscillatory deformation has negligible effect on the material (i.e. occurs within the LVR). The suffix '\*' is used to differentiate these parameters from their counterparts determined under quiescent conditions (Dealy 1984). Alternatively, an oscillatory stress,  $\sigma_0$ , may be superimposed on a steady stress,  $\sigma_s$ , resulting in a similar pair of equations. In parallel superposition the effect of the oscillatory perturbation on  $\dot{\gamma}_s$  can be assessed using:

$$\gamma_0 \ll \frac{\dot{\gamma}_s}{\omega}$$

*Equation 2.2.14 – calculation of the total resultant stress for CSPS*

Satisfying this inequality (in conjunction with the usual LVR considerations) confirms that the effect of the oscillatory deformation on the steady deformation will be minimal (Somma 2007) (as shown in figure 2.1.2). Hence the molecular rearrangements and disentanglements can be assumed to be solely to the steady deformation.

Prior to the present work no study of combined oscillation and steady shear has yet been carried out on gelling systems. Carvalho and Djabourov (W. Carvalho 1997) studied gelatine gelation under shear by applying alternating oscillation and steady shear. Steady shear was realised by applying both controlled shear stresses and controlled shear rates. Under controlled stress conditions a critical strain rate of  $3 \text{ s}^{-1}$  was observed at which a sudden increase in viscosity was observed; such behaviour suggests that the gel point may only occur where the steady strain rate is below this critical value (at higher strain rates the kinematics cause significant cluster disruption), indeed Carvalho and Djabourov observed no gelation transition where the shear rate was controlled greater than  $50 \text{ s}^{-1}$  but the transition was observed upon cessation of steady shear. Interestingly the ratio of  $G'-G''$  reached an equilibrium value dependent on the steady shear history indicating that gel microstructure can be controlled by preshearing at high shear rates. They also note that gels formed under constant stress exhibit a yield stress behaviour and will flow at large applied stresses, thus they conclude that the gels formed under constant stress have a particulate nature where stress is supported due to adhesion between micro-gel particles. Such behaviour was not observed in gels formed under quiescent conditions.

The effects of shear upon globular proteins such as gelatine has been carried out (M. Joly 1949), however the focus was on denaturation of proteins under shear and was investigated at concentrations of gelatine that did not induce gelation. Synthetic polymeric solutions that are stable within a solvent have also been thoroughly investigated, noting a phase separation with shear (Wolf 1984). It follows then that further work should continue on CSPS of polymeric and globular proteins through the gelation process, investigating any effects that the procedure may have on the relaxation exponent.

### ***2.2.7 - Linear viscoelastic range : the third harmonic criterion***

An initial assessment of the linear viscoelastic range (LVR) for the materials studied herein was made by performing amplitude sweeps in the pre and post gel regions. Clearly, assessment of linearity at the GP is difficult to achieve using the conventional amplitude sweep approach due to the transient nature of the gelation process. Hawkins et al (K. Hawkins 2008) employed the relative amplitude of the 3rd harmonic and fundamental frequency components of the displacement signal (i.e.  $H_3/H_1$ ) at the gel point as a measure of deviation from linearity. In the present study, where the presence of a unidirectional stress component further complicates the analysis of linearity,  $H_3/H_1$  was used to assess linearity over a range of unidirectional stress levels with a ratio ( $H_3/H_1$ ) greater than 0.001 indicating the onset of non-linearity, the threshold value being obtained by monitoring  $H_3/H_1$  during a traditional stress amplitude sweep on a slow gelling gelatine sample. The absence of mutation artefacts was ensured by excluding data associated with rapid gelation where the mutation number ( $N_{mu}$ ) exceeded 0.15 as proposed by Winter (M.E. De Rosa 1997).

## ***2.3 - Materials and methods***

### ***2.3.1 - Gel point time determination***

An AR-G2 stress controlled rheometer was used to measure the sol gel transition of 10wt% general purpose grade gelatine. The 10wt% gelatine was made as a 100g solution with 10g general purpose gelatine and 90g purified water. The gelatine/water solution was heated in a water bath at 60°C for forty-five minutes, with intermittent agitation of the solution. After such time passed the gelatine had formed a homogeneous solution. It was then separated into 20, 5ml aliquots and refrigerated at 4°C for at least 24 hours.

The 10wt% gelatine solution was then loaded onto the rheometer, which had been outfitted with aluminium cone and plate geometry. The cone had an angle of approximately 2 degrees, and was 60mm in diameter yielding a truncation gap of 57 $\mu$ m and a sample size of 1.96ml. All appropriate preliminary calibrations had been performed prior to the experiment. For loading the 10% gelatine solution it was required to break down its structure and micropipette 1.96ml of molten gelatine onto the lower plate of the rheometer before lowering the cone. This was performed by placing a 5ml aliquot of gelatine in a water bath set at 60°C for 40 minutes, again with intermittent agitation.

For a simple determination of the sol-gel transition at different temperatures in Gelatine the AR-G2 was set to oscillate over four frequencies in sequence repeatedly at an oscillation torque of 10 $\mu$ Nm. The four frequencies chosen were 0.2, 0.43, 0.93 and 2Hz so as to cover a decade of frequencies while maintaining a relatively fast sweep through the frequency cycle. The temperatures chosen were 26, 27, 28, 29 and 29.25°C. Which were maintained on the sample gelatine until such time as it was clear the sol gel transition had been surpassed.

### **2.3.2 - Linearity criterion (*harmonic analysis*)**

10wt% gelatine was loaded onto the rheometer as in experiment 1. A temperature for the gelatine of 28°C was used because the gel time at this temperature is approximately 5000 seconds, providing a suitable mutation number (over 200 seconds) of 0.07. The rheometer was set to perform 5000 seconds of oscillatory measurement and then start a 200 second experiment where oscillatory torque was ramped up from 0.5 $\mu$ Nm to 11300 $\mu$ Nm at a single frequency of 1Hz.

This oscillatory ramp at the gel point is designed to investigate the boundaries of the harmonic linearity criterion for gelatine so care was taken such that the third and fifth harmonic displacement values were measured during the test.

### ***2.3.3 - Establishing the optimum unidirectional to oscillatory stress amplitude ratio.***

As an investigation into the ratio at which shear and oscillatory stress yield the best results, a series of gel point tests were carried out and the third harmonic ratio was analysed. The gelatine sample was loaded as before on an AR-G2 stress controlled rheometer. The oscillatory torques employed were 5, 10, 15, 20, 30 and 40 $\mu$ Nm, while the unidirectional flow torque was maintained constant (at 10 $\mu$ Nm). The ratio of the third harmonic to total deformation was measured throughout the gelation, over a time period of 1000 seconds. The frequencies chosen for analysis were again, 0.2, 0.43, 0.93 and 2Hz. The third harmonic ratio was analysed at 0.93 Hz as it is the closest value to the frequency at which linearity was determined.

### ***2.3.4 - Linearity determination under parallel superposition***

To conclusively determine a region in which superposition could be linearly operated at the gel point, 166 runs of gelatine gel points were ran at varying degrees of oscillation and shear ranging from 0-300 $\mu$ Nm of each which equates to 0-7.12Pa. The point mutation number and harmonic ratio was measured at the gel point for every test and its linearity condition was noted as linear, nonlinear through harmonic analysis or nonlinear through harmonic analysis and mutation.

The set up for the sol gel transition was the same as in experiment three with frequencies selected as 0.2, 0.63, 0.93 and 2Hz. The time of each experiment was set to 1000 seconds.

### ***2.3.5 - Regions of linear response***

The linearity investigations for the experiments up to this point were conducted at the gel point. Supplementary experiments were conducted to assess linearity of response in the pre and post gel regions. In these experiments gelatine was loaded on the rheometer as in the prior experiments; a test length of 1200 seconds was set, with frequencies of 0.5, 1, 1.5, 2 and 5 Hz and a temperature of 26°C.

The oscillatory torque was changed so as to illustrate a change in linearity with increasing torques through these regions. The torques selected were 15, 25, 35, 45, 55, 65, 75 and 85μNm. Regions were divided into pre gel (0-500 seconds), gel point (500-700 seconds) and post gel (700-1200 seconds). The peak linearity criterion value during these regions were taken.

## ***2.4 - Results and discussion***

### ***2.4.1 - Experiment 1 – Gel point time determination of gelatine***

Results for the temperatures 26, 28 and 19.25°C are shown overleaf in figures 2.4.1-

2.4.3:

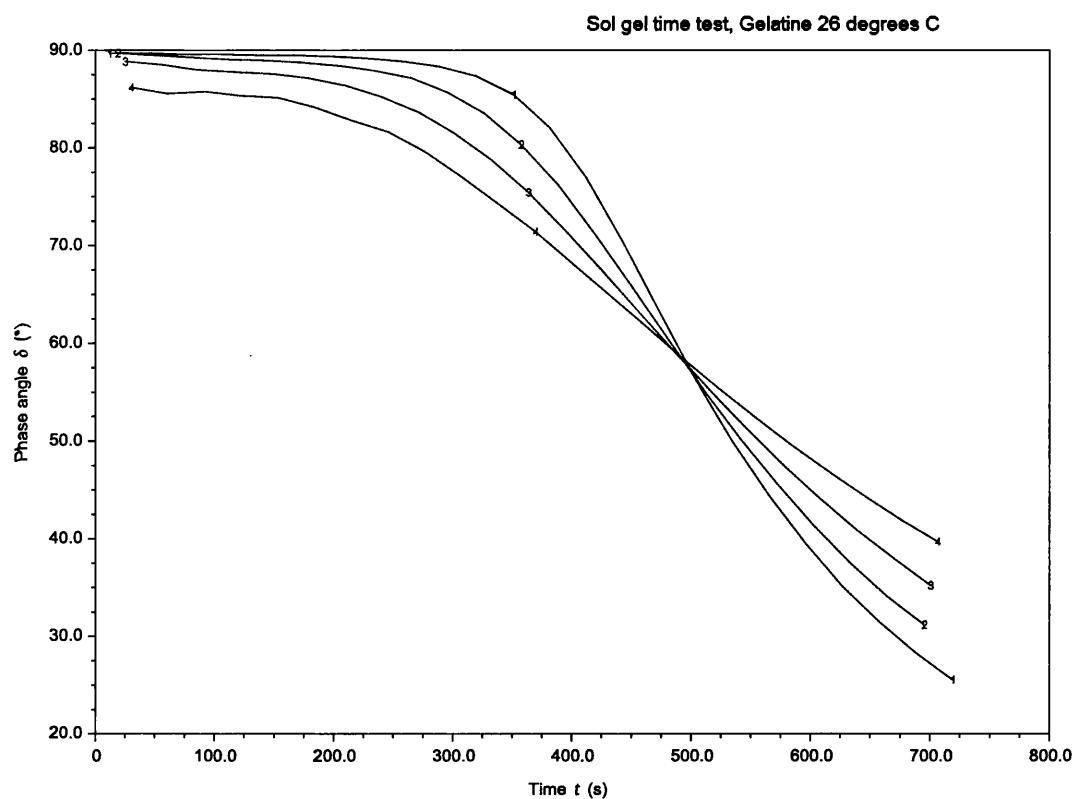


**Figure 2.4.1** - Figure showing the sol-gel transition of gelatine at 26°C

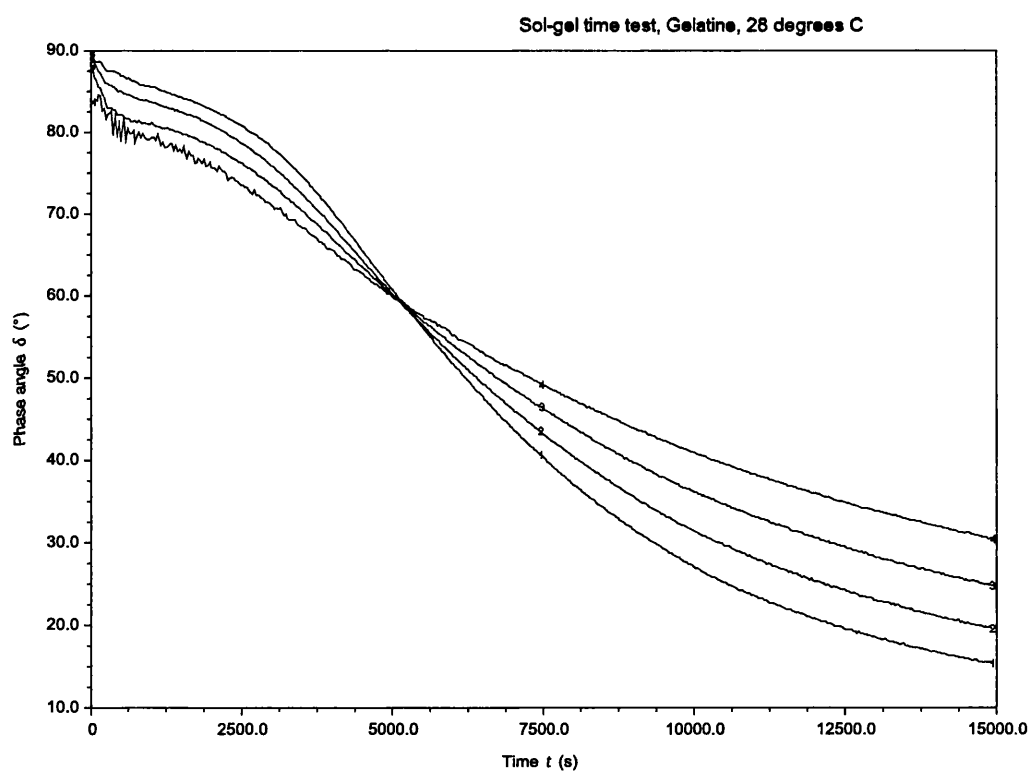


**Figure 2.4.2** - Figure showing the sol- gel transition of gelatine at 28°C



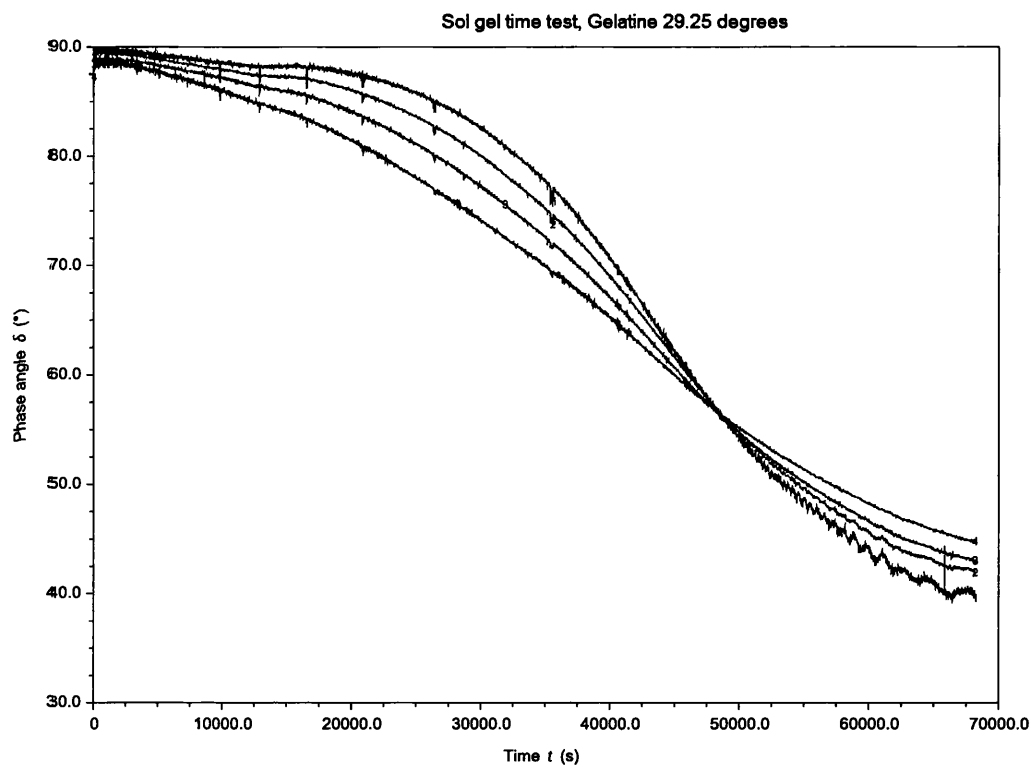


**Figure 2.4.3** - Figure showing the sol- gel transition of gelatine at 29.25°C

The Frequency independent sol-gel transition is readily available from this data, the time at which this occurs being noted as the gel time. The rate at which gelatine undergoes a transition from sol to gel becomes exponentially slower as temperature increases until it reaches such a point where it will not gel (see figure 2.4.4) – at the maximum gel temperature. This important parameter (from a manufacturing/process control viewpoint) is considered in detail in Chapter 3.

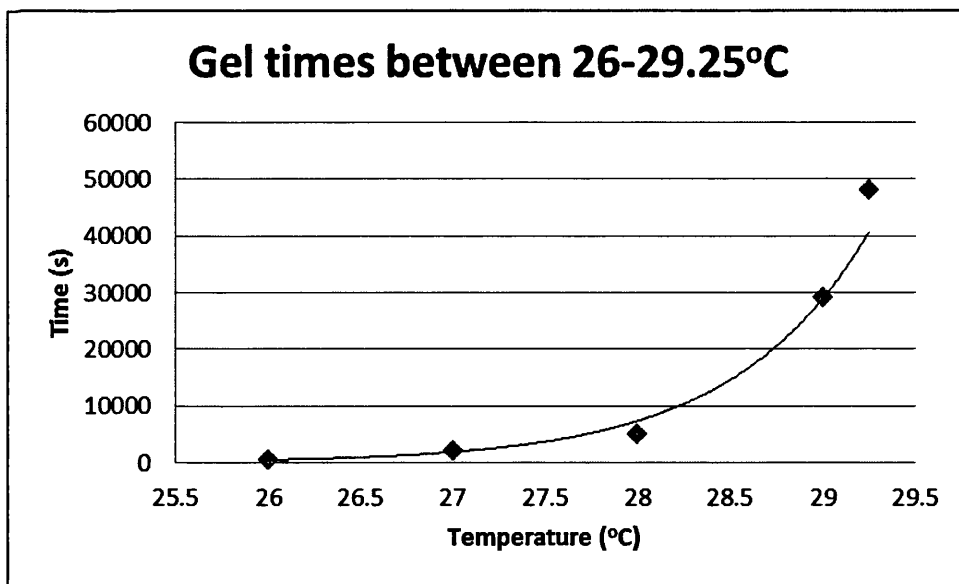


**Figure 2.4.4** - Figure showing the relationship between gel time and temperature for

10%wt gelatine

This is more clearly seen on a logarithmic scale as below in figure 2.4.5:

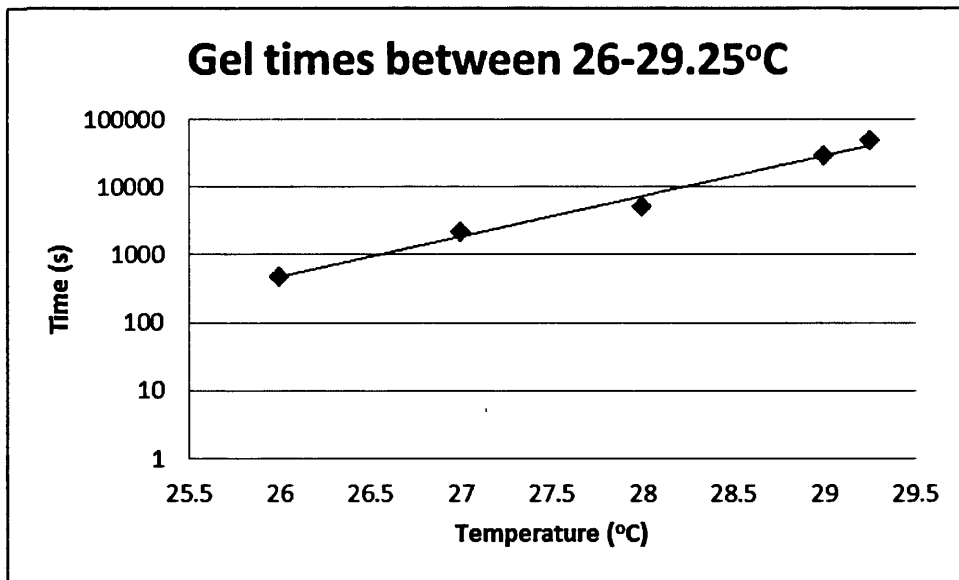


**Figure 2.4.5** - logarithmic scaled figure showing the relationship between gel time and

temperature for 10%wt gelatine

The main purpose these tests serve is to illustrate what temperature is suitable for a particular test length. Ideally this would be a temperature where sample mutation at low frequencies is as limited as possible, however also where the time is not so long that sample drying and test length hinder progress.

#### 2.4.1 - Experiment 2 – harmonic linearity criterion determination of gelatine

The result of the oscillatory sweep of gelatine at the gel point can be seen below in figure 2.4.6:

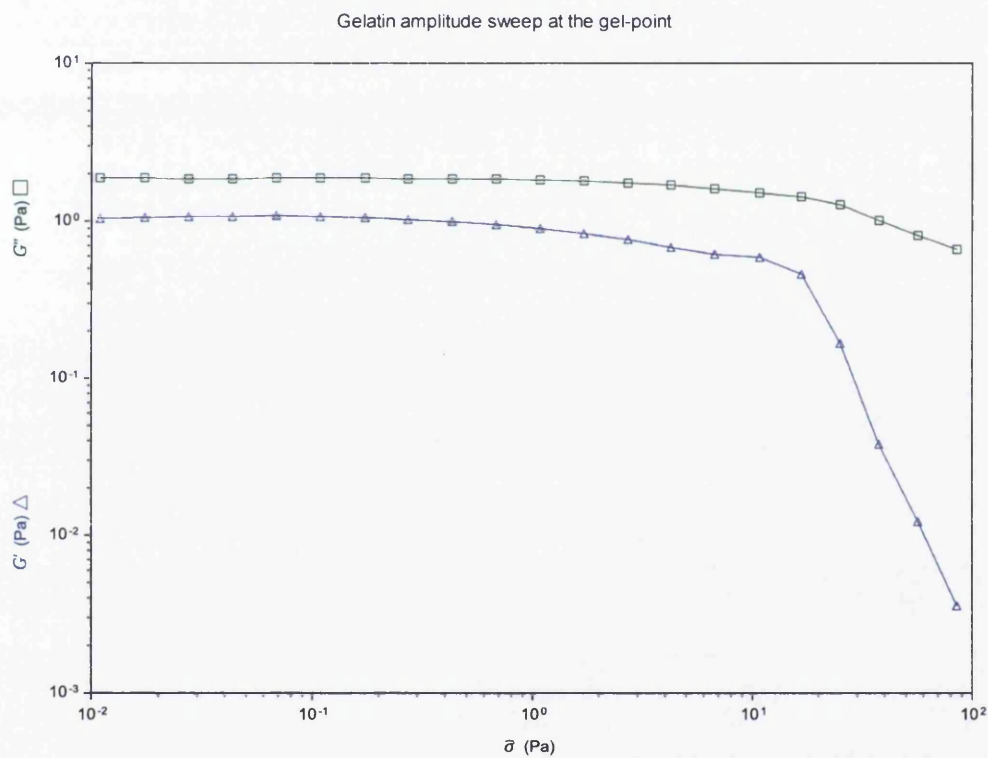


**Figure 2.4.6** - Figure showing an amplitude sweep carried out on 10% gelatine at the gel point

A standard test of linearity, it can be seen that at the gel point oscillatory strains past 0.18Pa begin to alter the value of storage modulus slightly, but it is still well within the limits of what could be ascribed to a mutation change. As oscillatory torque passes 0.7Pa the

linearity change is more prominent, past 2.5Pa and there is a deviation from the linear range significant enough to label a non-linear result.

It is readily identifiable what torque is required to remain in the linear region. The real challenge is to determine what combination of superposed and oscillatory stress is linear and which is not. To solve this, the third harmonic ratio is analysed. Where oscillatory torque reaches the point of non-linearity, that same level for the third harmonic ratio is the point where higher values invoke non linearity. This value for the third harmonic ratio is shown in table 2.4.1 below:

<i>Oscillation stress</i>	<i>Disp. 3rd Harm.</i>	<i>Oscillation disp.</i>	<i>Phase angle</i>	<i>Ratio of interest</i>	
Pa	rad ( $10^{-7}$ )	rad ( $10^{-2}$ )	°	( $10^{-2}$ )	
0.011	3.893	0.0118	62.19	0.3289	Near Instrument Limits
0.017	3.239	0.0199	62.17	0.1624	
0.027	3.879	0.0332	62.14	0.1167	
0.043	3.141	0.0562	61.86	0.0559	
0.069	5.362	0.0941	62.02	0.057	
0.109	15.453	0.159	62.16	0.0972	
0.172	19.951	0.27	62.49	0.0739	End of linearity to a small degree
0.272	30.324	0.4591	63.19	0.0661	
0.431	70.934	0.7876	64.03	0.0901	↓
0.681	229.23	1.3501	65.28	0.1698	End of linearity to a moderate degree
1.078	698.99	2.3415	67.01	0.2985	
1.702	2289	4.1305	69.01	0.5543	↓
2.685	7869	7.4311	69.94	1.0589	End of linearity to a great degree
4.234	20208	13.4587	70.18	1.5015	
6.7	25369	24.2069	76.87	1.048	
10.661	41428	46.3977	86.31	0.8929	
16.638	9915	92.7925	88.81	1.0685	
24.845	152255	182.206	89.64	0.8356	
37.297	228526	349.33	89.95	0.6542	
56.499	340407	622.001	90.01	0.5473	
84.783	333859	627.501	90.02	0.532	

**Table 2.4.1** –Table showing non linearity test data at the gel point

Using this table it can be determined how to maintain linearity while testing gelatine, a sample where both moduli and the linearity criterion change with time. The third harmonic ratio, labelled above as the ratio of interest must remain less than 0.001. Further work can now be carried out on optimising oscillatory and superposed tests through third harmonic ratio analysis.

#### ***2.4.2 - Investigation of unidirectional to oscillatory amplitude ratio***

The third harmonic ratio was plotted against a time relative to the gel point to see what linearity changes (if any) occur during the structural change of gelatine. As can be seen below in figure 2.4.7 the changes in linearity through the structural change of gelatine are relatively small, with an increase towards gelation as structure increases. A power law fit is shown below also as an illustration of this increase, although the fit is imperfect and merely serves to show the small increase.

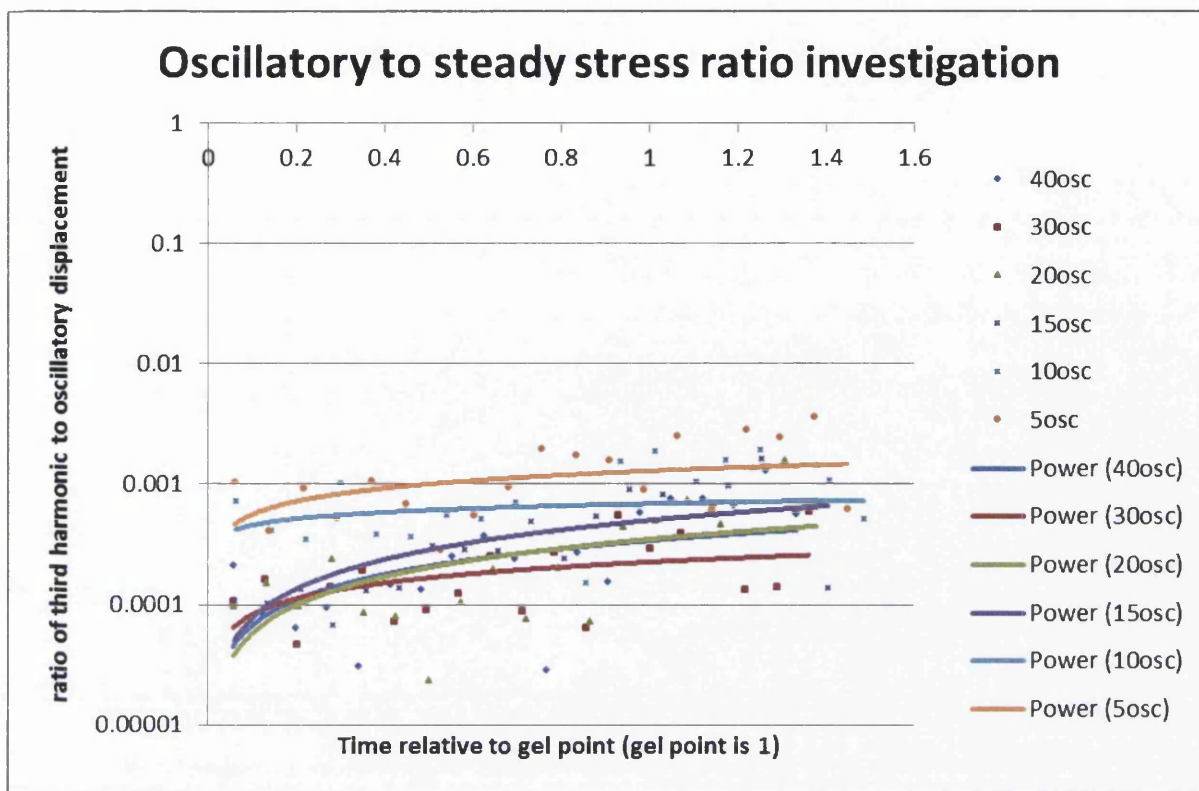


**Figure 2.4.7** - Figure showing the changes in linearity for all tests with time relative to the gel point

More interesting to note is how the ratio of oscillatory torque to steady stress does appear to be related to the linearity criterion as shown below where the ratio is defined as  $\sigma_s/\sigma_o$  (shear stress divided by oscillatory stress) and a specific time period (the gel point) is chosen as a reference (figure 2.4.8 below):

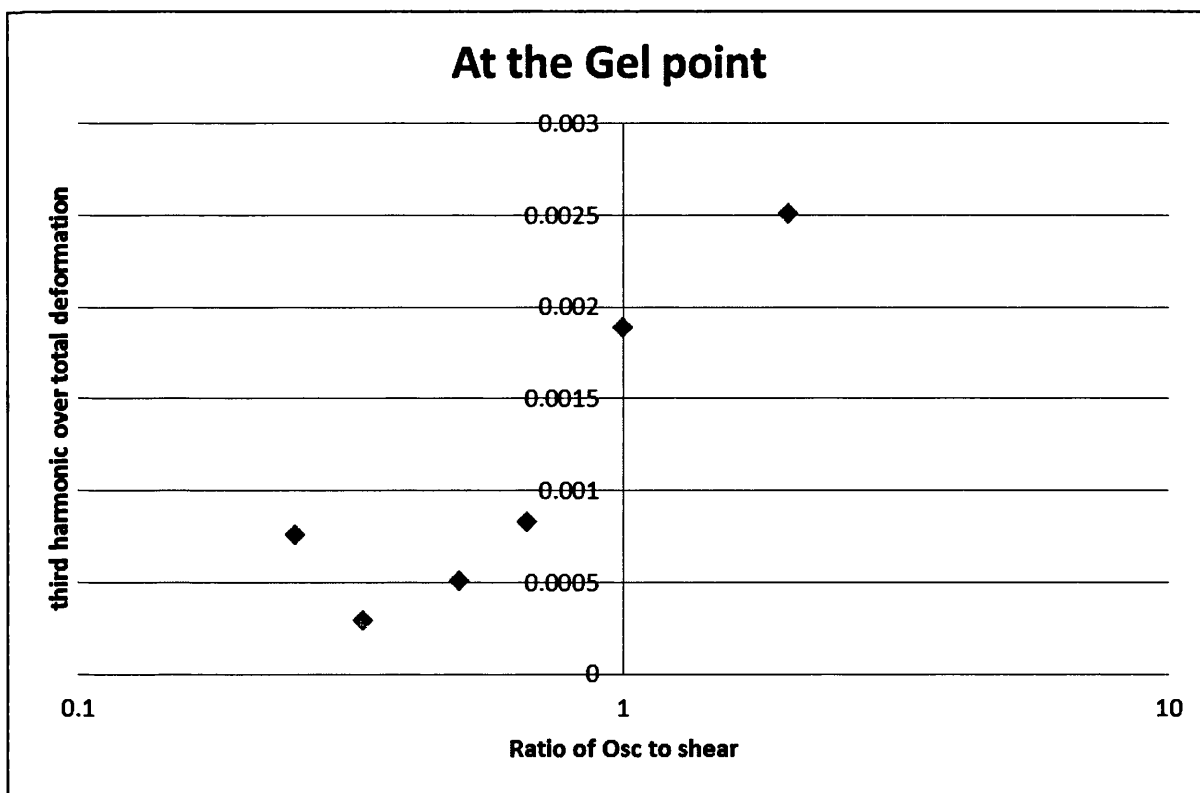


**Figure 2.4.8** - Figure showing the third harmonic linearity criterion at the gel point at varying ratios of oscillatory torque to oscillatory shear

It should be made clear that ratios lower than one indicate oscillatory torques higher than the steady applied torque and above 1 the opposite. It would appear then that from this figure there is an optimum ratio range at which the linearity is at its lowest. As a general rule it would appear that keeping oscillatory amplitude higher than that of the steady stress improves results greatly. This could be because if shear stress is higher than the oscillatory amplitude the response waveform could be less prominent within the constant stress.

From these results it is possible to establish the ideal ratio (0.5) where oscillatory amplitude is twice that of the shear stress. Further conclusions can be drawn from the results of the experiments reported below (2.4.4).

### ***2.4.3 - Parallel superposition linearity determination***

The linearity conditions at the gel point are plotted with colour indicating the linearity criterion met. Green shows that neither point mutation nor third harmonic criterion are too high to create a non-linear result, red illustrates a non-linearity in the harmonic ratio whereas orange indicates non-linearity in both the harmonic ratio and point mutation, every test is then plotted and shown on figure 2.5.9 below:



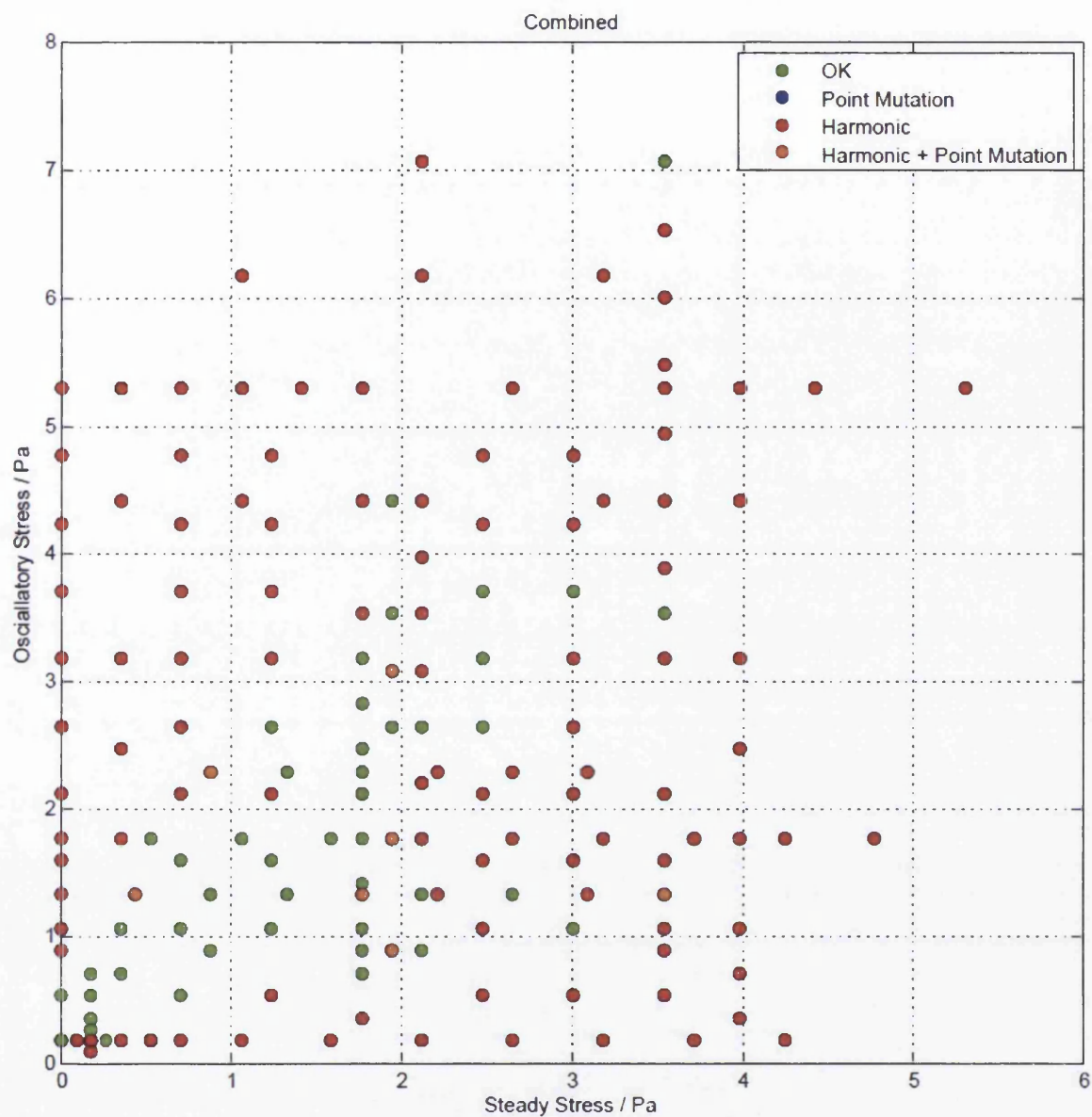


**Figure 2.4.9** - Figure showing the linearity conditions for several gel points at varying levels of oscillatory and parallel superposed shear

It can be seen that a linear 'region' opens up where oscillatory stress is marginally higher than shear stress. It would appear that to maintain linearity at the gel point tests can be performed with a steady stress of up to 2Pa while oscillatory stress can be increased to up to 3Pa. Beyond this it would most likely be a non-linear test. This however, only answers the

question at the gel point and not beyond it. Regional linearity is investigated further in experiment 5.

#### 2.4.4 - Regions of linear response in superposition experiments

From the data reported above it may be seen that the critical gel (at the gel point) is the most sensitive stage of the gelation process in terms of producing a non-linear response. This may simply be due to the large rate of change of rheological process around the gel point affecting the measurement of the oscillatory response through mutation. Figure 3.2.10 illustrates this point as well as the regions involved, region 1 is pre gel, region 2 the gel point and region 3 the post gel stage.

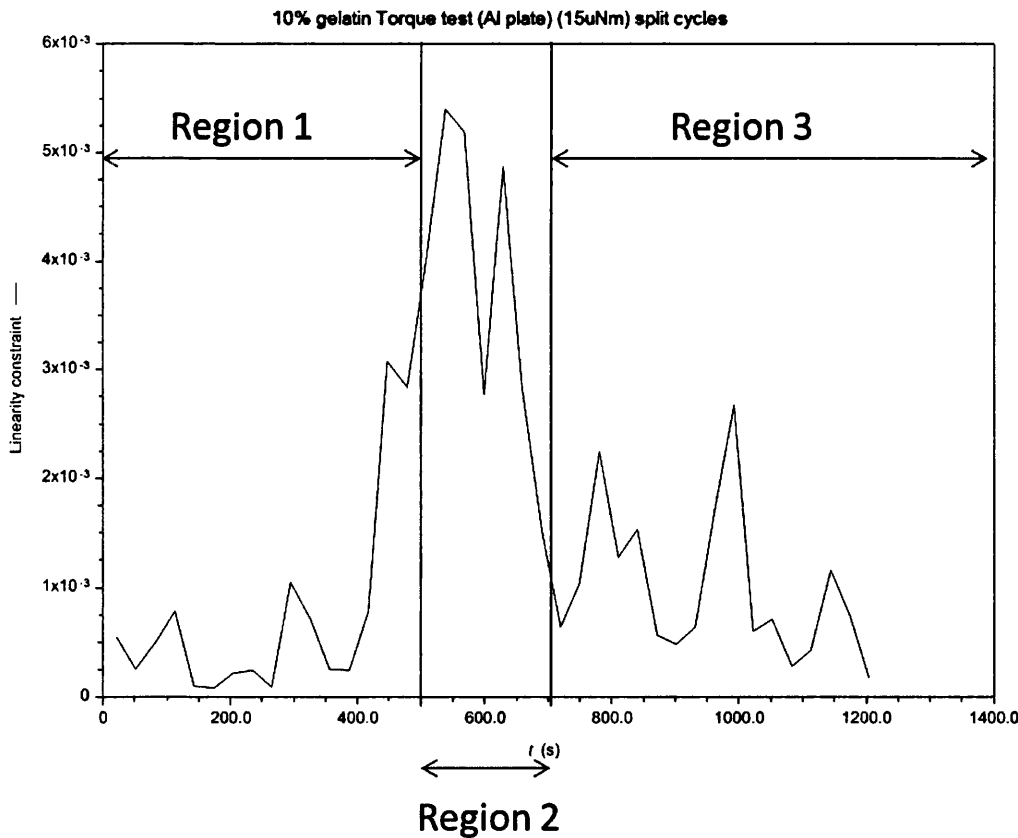


**Figure 2.4.10** - Figure showing the region definition and non linearity in those regions for 15 $\mu$ Nm torque on 10%wt gelatine

When all the data was analysed it could be put on a 3D plot of region by region showing the linearity constraints with the change in frequency and oscillatory torque. Figures 2.4.11-2.4.13 illustrate these change in linearity where blue is a linear region, red is a moderately non linear region. At no point do these results reach beyond the moderately non linear (considered linear).

It should be pointed out that this experiment was designed to simplify changes in linearity, through such a small time scale of gelation and through use of a wide band of frequencies. This has the effect of increasing mutation. The torques themselves as solely oscillatory are also relatively high and designed to illustrate what circumstances non linearity is most prominent.

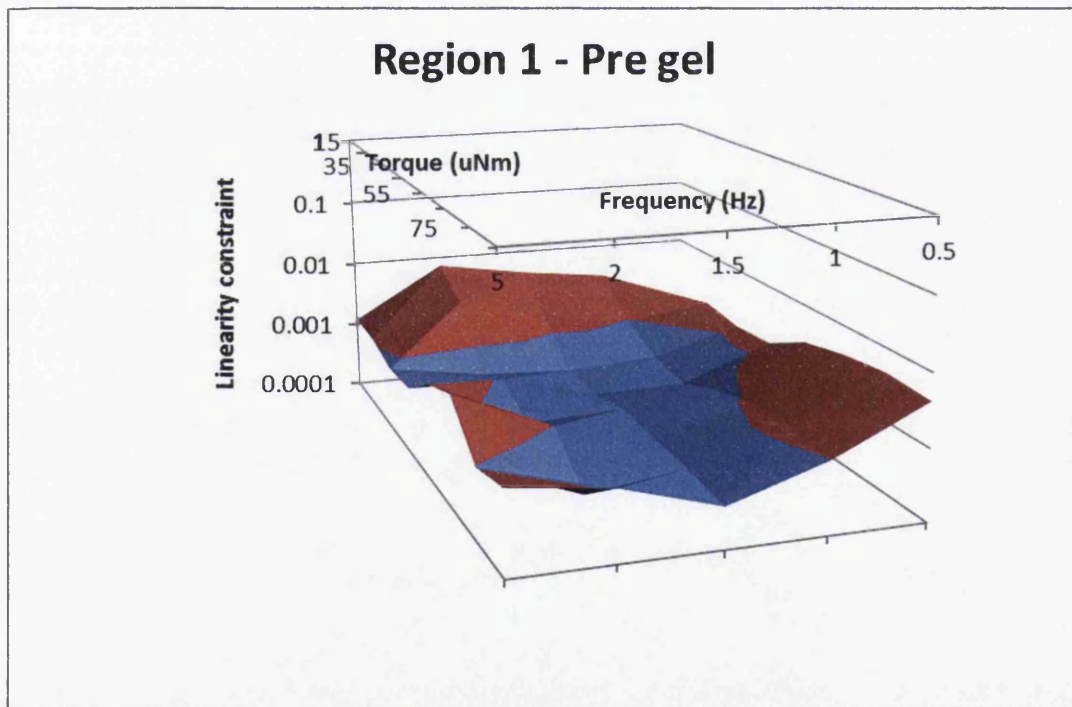


**Figure 2.4.11** - Figure showing the Pre gel values of linearity at varying torques and frequencies

The above 3D graph shows that pre-gel even at deliberately extreme conditions is vastly linear. It is however moderately linear at low values of torque this is reasonably close to the instruments limits and could be because the amplitude of the oscillation isnt high enough to garner an accurate response wave. This could be heightened by the fact that at the pre gel, gelatine is nearly perfectly viscous in its response, which could allow for significant relaxation systems to interfere with the wave form response, perhaps significantly while the oscillatory amplitude is low.

The linearity constraint also appears to increase at the extremities of the frequencies. At low frequencies this could be because of a heightened mutation effect, with one cycle taking two seconds and three complete cycles being needed to make a measurement. At high frequencies the problem could be the short times allow for quite rapid strains on the material, causing a poor response waveform.

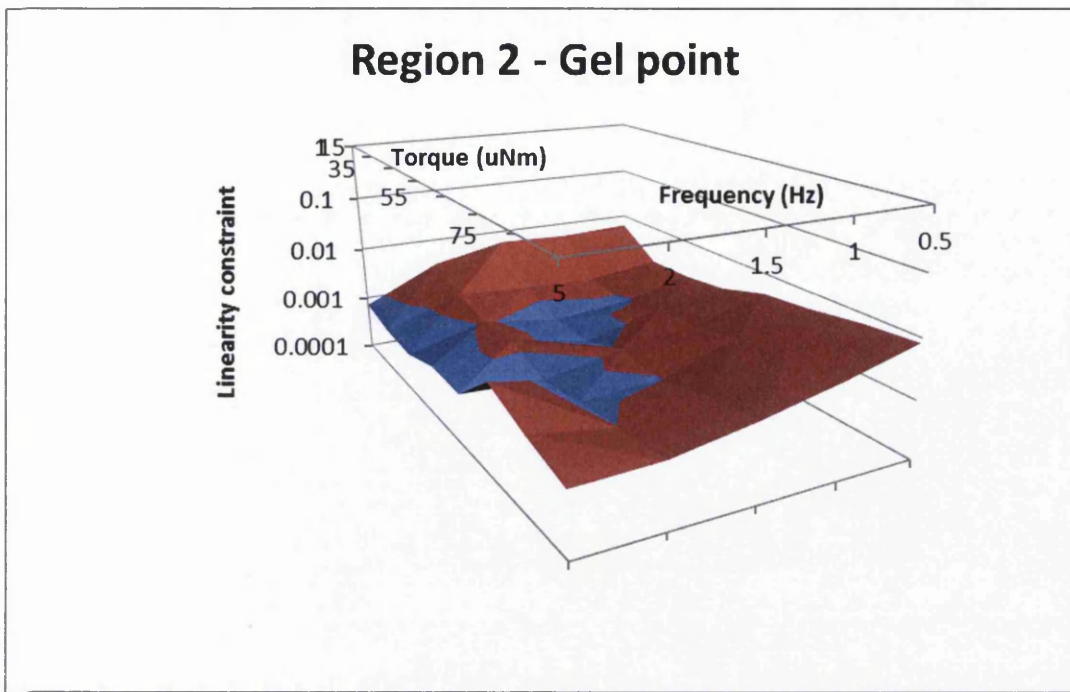


**Figure 2.4.12** - Figure showing the Gel point values of linearity at varying torques and frequencies

At the gel point the linearity constraints are expectedly higher. The great change in structure gelatine passes through during the gel point region cause greater problems with mutation, especially at lower frequencies, this would explain why at lower frequencies linearity constraints are significantly higher. As torque increases expectedly the linearity criterion rises, as well as this at the highest frequency 5Hz linearity remains perhaps due to a more elastic response from the gelatine while a low chance for mutation.

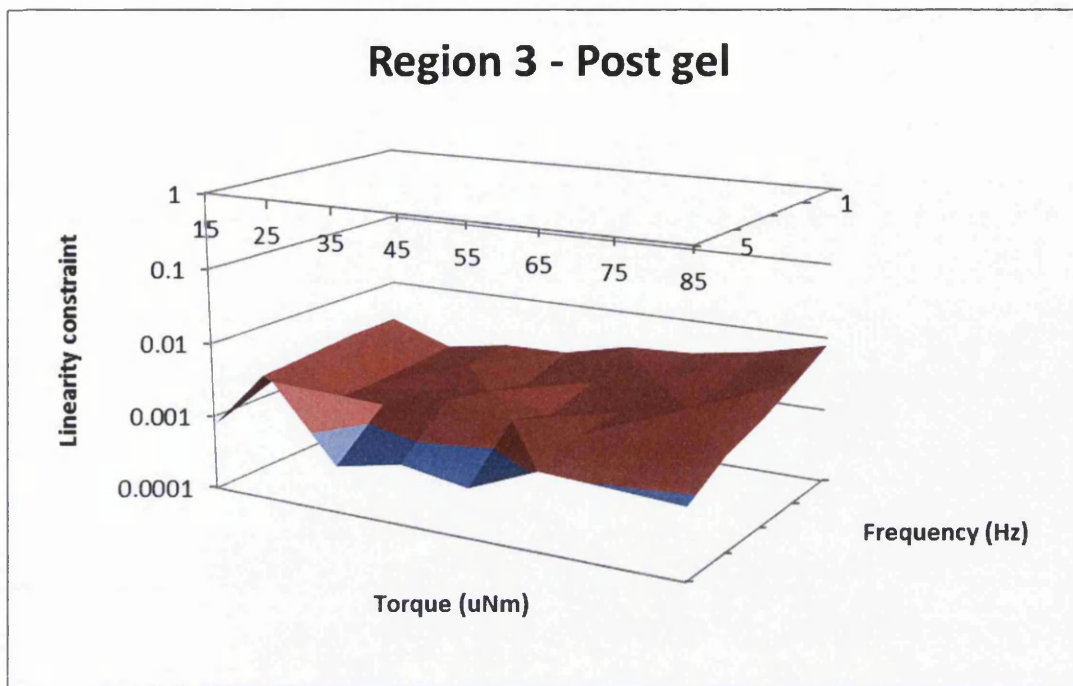


**Figure 2.4.13** - Figure showing the post gel values of linearity at varying torques and frequencies

Post gel appears to be seemingly more non-linear still, however this seems more attributed to mutation than either pre gel or gel point regions. As frequency increases to 5Hz testing becomes more linear at much higher torques than previously seen. This could be because the much more elastic response from the gelatine causes a smoother oscillation response. The stronger bonds formed within the gelatine post gel also allow it to withstand higher oscillatory torques in general.

**Summary:** Having established the appropriate operating criteria for conducting parallel superposition measurements under controlled stress, a series of critical validation experiments were devised where gelation of gelatine under CSPA was performed both within and beyond the established operating criteria. **Chapter 3** reports on the validation exercise, the validation criteria are and the subsequent results.



### ***3 - Chapter 3 – Assessment and validation of the controlled stress parallel superposition technique using the thermoreversible gelation and de-gelation characteristics of gelatine gels.***

The work reported in Chapter 2 provided an assessment of the LVR requirements for work involving SAOS and CSPA on a model sol-gel transition system – gelatine gels formed through cooling aqueous gelatine solutions.

The progressive decrease in the unidirectional shear field in the approach to the GP under constant stress in the controlled stress parallel superposition experiment (see Chapter 2) suggests that the interpretation of CSPA measurements might allow accurate GP determination given sufficiently small amplitudes of the unidirectional flow shear rate. In the present work this assumption was tested by comparing GP data obtained under SAOS and CSPA for gelatine systems. In addition, a series of experiments were devised in order to test whether CSPA could yield valid data for systems undergoing rheological change involving a progressive *increase* in the amplitudes of both the unidirectional shear field and the oscillatory shear strain under constant stress. In the work reported in this Chapter that rheological change was represented by a transition from a previously gelled viscoelastic solid (VES) state back to its precursor viscoelastic liquid (VEL) state. These experiments involved exploiting the thermoreversible gelation of aqueous gelatine solutions by inducing a rapid temperature increase to a value above the maximum gelation temperature in the post-GP regime.

In the work reported herein the biopolymer gel system was employed as a model gelling material to confirm the ability of CSPA to characterise the stress relaxation characteristics of critical gels in the presence of a) progressively decreasing and b) progressively increasing unidirectional and oscillatory strain rate amplitudes. In addition to confirming the validity of the CSPA technique in gelation studies, the latter feature of the experiments involved CSPA being used to record the thermally induced VES to VEL transition. In previous work on gelatine Michon et al. (Michon, Cuvelier et al. 1993) conducted SAOS frequency sweeps on gels which had previously formed at a fixed/aging temperature (for a specified aging period) then subsequently 'melted' ('de-gelled') by incrementally increasing the temperature and performing measurements on the material following a 1-hour period of equilibration at each temperature. These authors plotted values of  $\tan\delta(\omega)$  versus temperature and, by a process of extrapolation between data points obtained at each temperature, estimated the location of an apparent gel-sol transition from which estimates of the stress relaxation exponent  $\alpha$  and a "critical melting temperature" (maximum gel temperature) were derived. They recognised that the material was not at a thermal equilibrium following an hour at each test temperature as indicated by the increasing values of  $G'$  with time, and that this could lead to an overestimate of the critical melting temperature. However, no comment was made on the validity of the values of  $\alpha$  which were found to range from 0.47 to 0.81, and were found to be dependent on concentration, aging time and aging temperature. In the work reported in this Chapter no reliance was made on the reconstruction of  $\tan\delta(\omega)$  versus temperature data. Instead, the gel-sol transition was measured directly, for the first time, using both SAOS and CSPA (Curtis et al 2015).



### ***3.1 - Materials and Methods***

#### ***3.1.1 - Experiment 1 – Gelation and de-gel using SAOS***

Gelatine was loaded onto the AR-G2 rheometer as in chapter 2, however the experimental set up is quite different. First the gelatine sample underwent a gelation procedure, the temperature was set at 27°C for 4000 seconds while gelation occurred. The gel point was measured at the frequencies of 0.2, 0.43, 0.93 and 2Hz over this time period with an oscillatory stress of 0.4Pa. After the chosen time period had elapsed the measurement of viscoelastic properties through oscillation was maintained while the temperature was increased by 0.05°C/min from 27°C to 33°C (above the previously published critical temperature) to initiate de-gelling of the system.

The above test was done over frequency ranges and in conditions known to be linear from previous experiments. Another experiment was then done using the same method however increasing the range of frequencies to 0.04Hz-4Hz with two points per decade logarithmically spaced. The temperature was also increased to 27.5°C to counter increased mutation effects caused by lower frequencies.

#### ***3.1.2 - Experiment 2 – Gelation and de-gel during parallel superposition***

Gelatine was to be further tested as before, both gelling and de-gelling through the sol gel transition of gelatine. 10wt% sample of gelatine was prepared as before and placed under identical cone and plate geometry as before. The temperature was set at 27°C for 4000 seconds while gelation occurred. The gel point was measured at the frequencies of 0.2, 0.43, 0.93 and 2Hz over this time period with varying oscillatory and steady stress torques such that an increased stress was imposed on the gelatine. After the time period had elapsed the measurement of oscillatory torque through superposed stress was

maintained. The temperature was then increased by 0.05°C/min from 27°C to 33°C.

Through this way the sol gel transition from gel to liquid under flow was measured.

The values of oscillatory and unidirectional stresses were chosen as:

Oscillatory stress (Pa)	Unidirectional stress (Pa)
0.4	0
0.4	0.4
0.8	0.8
1.2	1.2
1.6	1.6
2	2
2.4	2.4

**Table 3.1.1– Table of CSPS parameters selected for experiment 2**

A further series of experiments was subsequently conducted involving a larger number of test frequencies between 0.2 and 2Hz (at seven frequencies) followed by a series which increased the range to 0.04Hz to 4Hz with two points per decade logarithmically spaced, the gelation temperature being increased to 27.5°C during the latter measurements.

## **3.2 – Results and Discussion**

### **3.2.1 – Gelation and de-gelation using SAOS**

After the gel point the sample was subjected to a rapid rise in temperature to a set value, the oscillatory measurements being continued throughout this process. The variable in this experiment is that of the temperature rise after gelation, such that a temperature range at

which gelatine melts and gels can be found. Temperatures used varied from 28.9-29.5°C in these experiments. The results shown below in figure 3.2.1 show the gelation under SAOS only within the previously determined LVR.

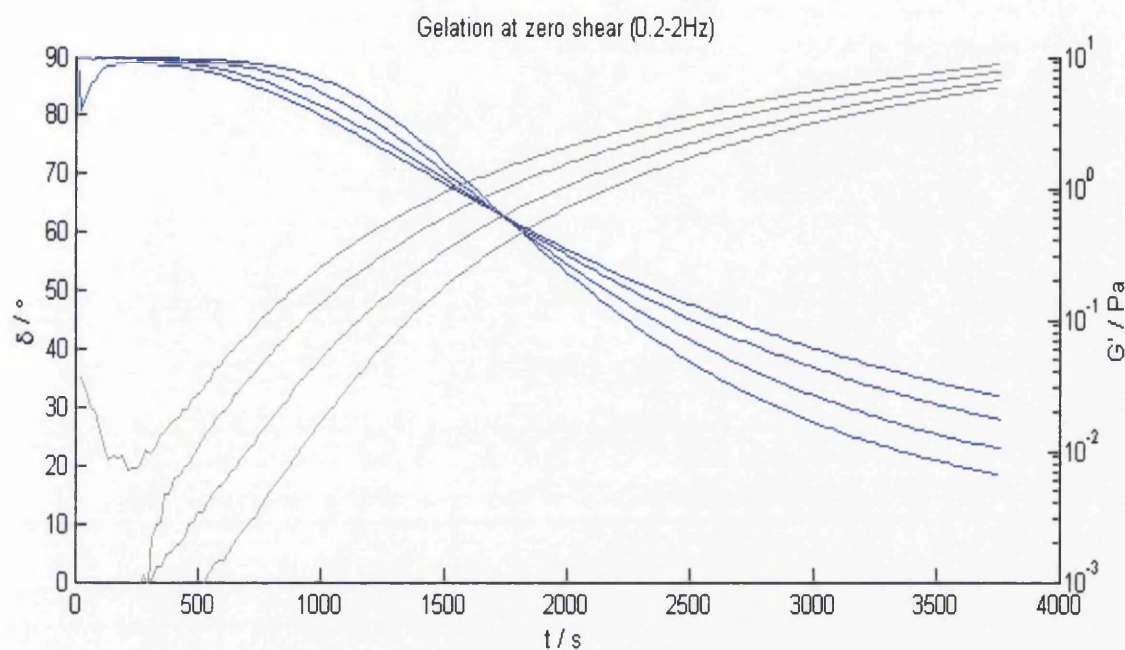


**Figure 3.2.1** - Figure showing Gelation of gelatine under SAOS within the LVR. The results show the frequency dependence of  $\delta$  and  $G'$  with the Gel Point marked by frequency independence of the loss tangent in accordance with the Winter-Chambon criterion.

The frequency independent value of  $\delta$  found is 62.49° ( $\alpha = 0.69$ ), in excellent agreement with established literature data for this system (Michon, Cuvelier et al. 1993, K. Hawkins 2008). This gel was then subsequently heated such that it underwent a gel-sol transition, the SAOS results being shown below in figure 3.2.2:

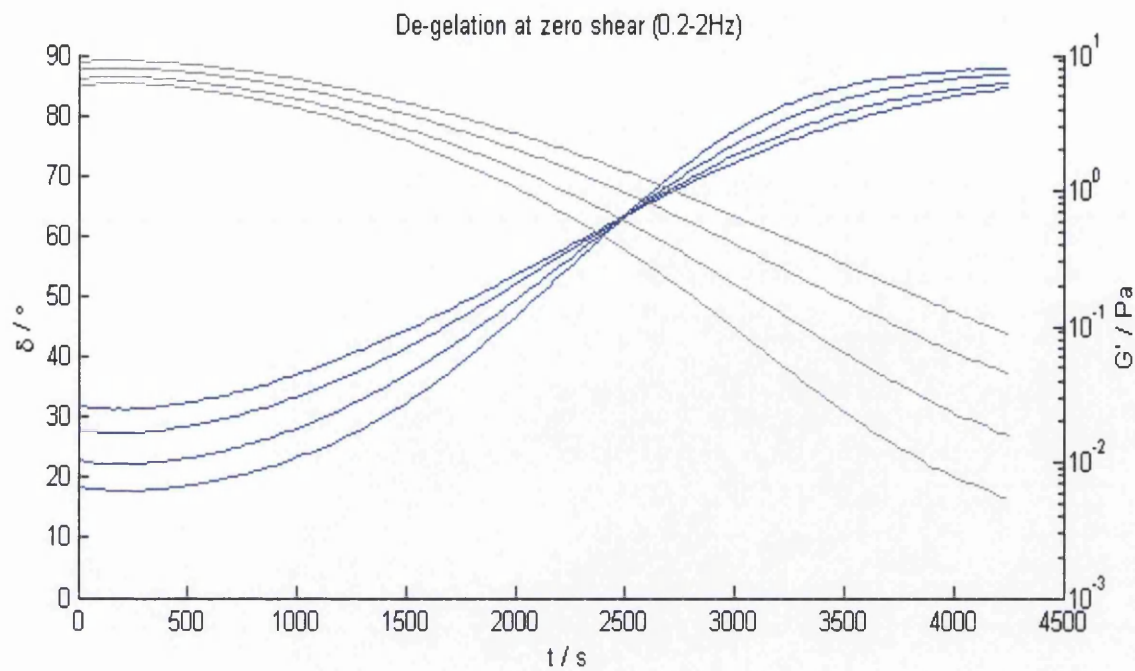


**Figure 3.2.2** - Figure showing de-gelation of gelatine under SAOS within the LVR. The results show the frequency dependence of  $\delta$  and  $G'$  with the Gel Point marked by frequency independence of the loss tangent in accordance with the Winter-Chambon criterion.

The figures 3.2.1-3.1.2 show the results of FS (SAOS) experiments in which the initial values of  $\delta$  (approximately  $90^\circ$  at all test frequencies) reflect the near-Newtonian fluid response of the material, this being followed at later times by the development of a frequency dependence of  $\delta$  characteristic of a viscoelastic liquid (VEL), with the recorded values of  $\delta$  declining with increasing oscillatory frequency. The frequency dependence of  $\delta$  declines progressively as the GP is approached, the GP being marked by frequency independence of the loss tangent, as previously reported for this system. The post-GP phase is marked by development of a viscoelastic solid-like response with the recorded values of  $\delta$  increasing with increasing oscillatory frequency  $\omega$ .

The transition from solid (VES) to (VEL) liquid occurs at a frequency independent value of  $\delta$  of  $62.45^\circ$  ( $\alpha = 0.69$ ), essentially indistinguishable from the result obtained at the GP during the gelation phase of the experiment. It is useful to plot both sets of data together (see figure 3.2.3 below). For the first time, these experiments establish that the de-gel phenomena in gelatine is indistinguishable from the rheological transition representing the Gel Point.

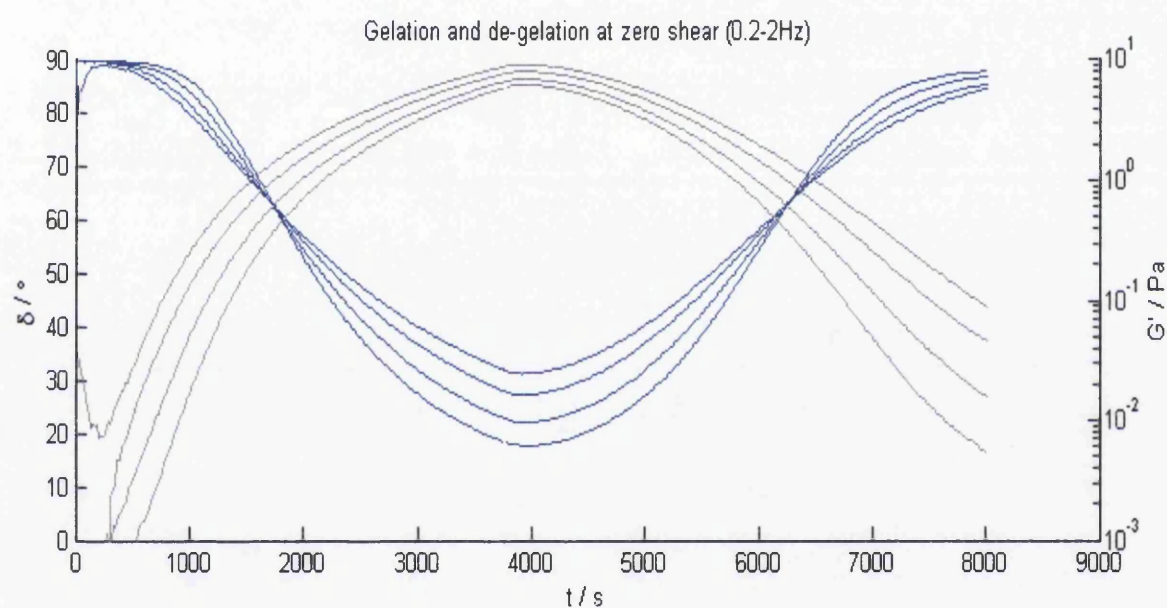


**Figure 3.2.3** - Figure showing the rheological transitions (VEL to VES and VES to VEL) for gelatine samples studied under SAOS.

To provide further confirmation, a series of additional experiments was conducted using a larger number (7) of frequencies within the same range (0.2-2Hz), see figure 3.2.4 below:



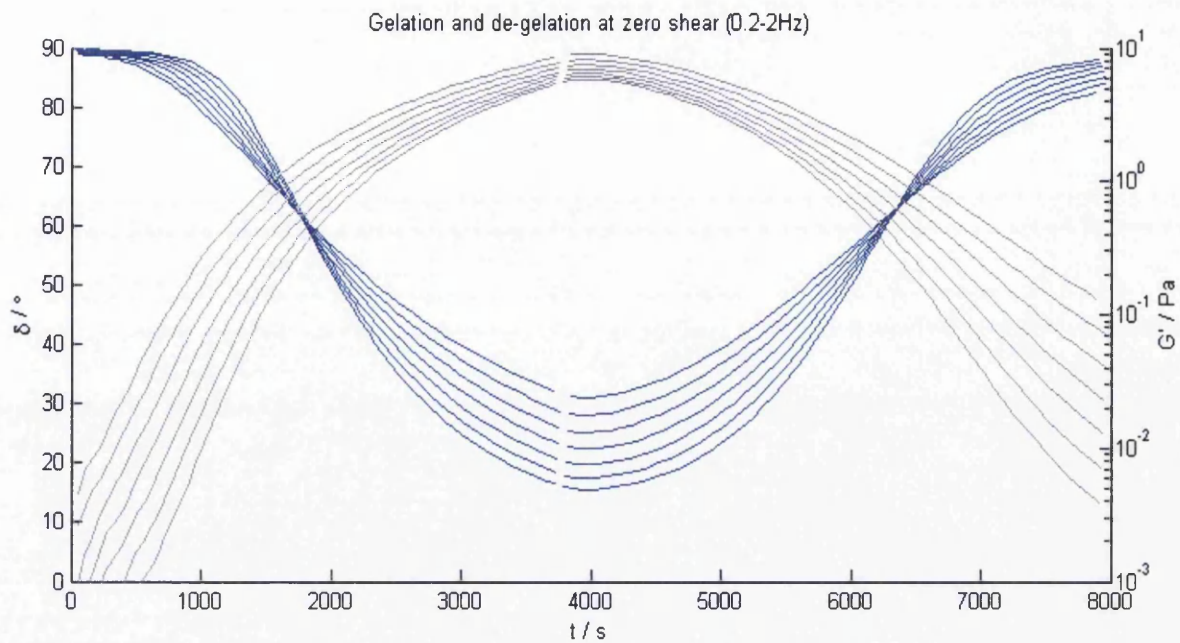


**Figure 3.2.4** - Figure showing the gelation and subsequent de-gelation of gelatine at zero shear under known linear conditions at seven frequencies within the range 0.2-2Hz.

The enhanced precision afforded by the increased number of frequencies gave a value of  $\delta = 61.73^\circ$  ( $\alpha = 0.686$ ). The corresponding value at the subsequent gel-sol transition is  $\delta = 62.18^\circ$  ( $\alpha = 0.690$ ) – again essentially indistinguishable and in excellent agreement with published GP data. Further validation was conducted using the same procedure at a wider frequency range (0.04 to 4 Hz) as seen in 3.2.5 below:

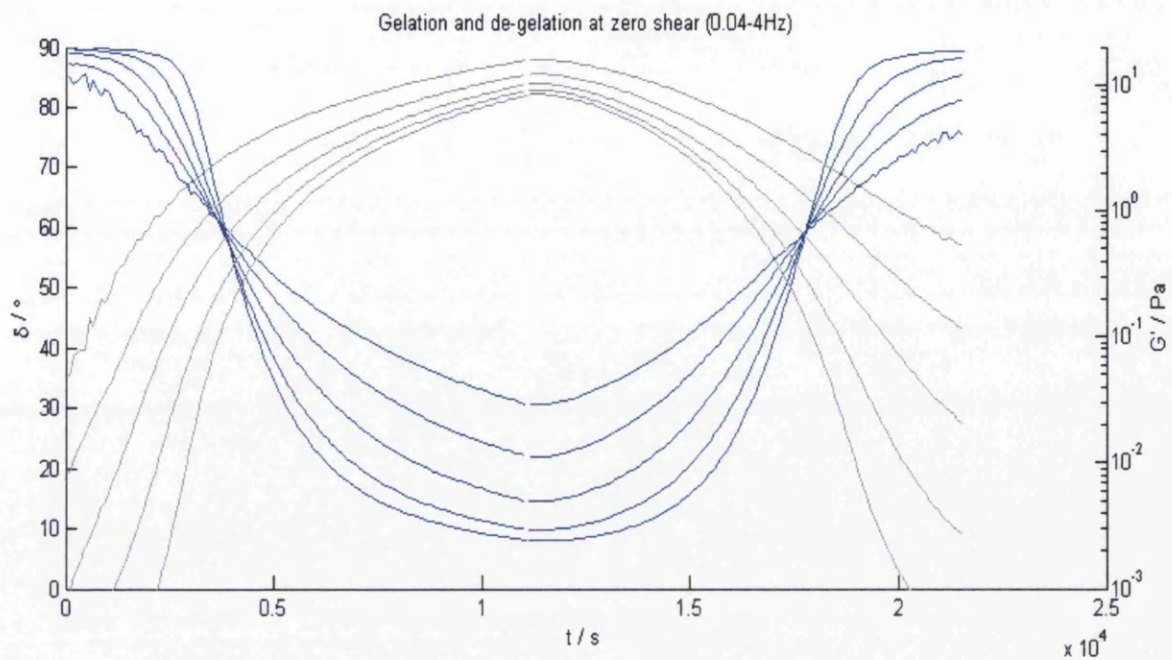


**Figure 3.2.5** - Figure showing the gelation and subsequent de-gelation of gelatine at zero shear under known linear conditions, for a wider frequency range (0.04 to 4 Hz)

The values obtained for  $\delta$  in this wider (and hence more accurate) range at the GP and the VES to VEL transition are  $60.3^\circ$  and  $60.4^\circ$  respectively, again in excellent agreement and sufficiently close to the literature data to validate the results (the corresponding values of  $\alpha$  being  $\alpha = 0.67$ ). The value of  $G'$  at 4Hz is also strikingly similar although marginally higher in the melt curve. The values are 2.49 Pa in the gel phase and 2.66Pa in the melt phase.

Having used the gel/de-gel transitions to show that the system behaved as a suitable model viscoelastic transition material, the process was studied using the CSPS technique in order to compare its ability to record the formation and destruction of the gel network in the presence of a unidirectional (though unsteady) shear flow.

### 3.2.2 – Gelation and melt during parallel superposition

The results for CSPS with four logarithmic frequency points from 0.2-2Hz are shown in figures 3.2.7-3.2.22 below. Oscillatory measurement without superposition is not included here as the results replicated the previous SAOS experiments (see above). All measurements were conducted under conditions (i.e. ratios and amplitudes of oscillatory and unidirectional shear stresses) within the previously established 'region of linearity' which is shown in figure 3.2.6. Note that on the basis of this data four of the five measurements made under CSPS were expected to conform to LVR requirements, while one measurement (at 120 $\mu$ Nm oscillatory torque [2.4Pa oscillatory stress], 120 $\mu$ Nm shear stress [2.4Pa superposed shear stress]) exceeded the LVR in order to exemplify the non-linear response.



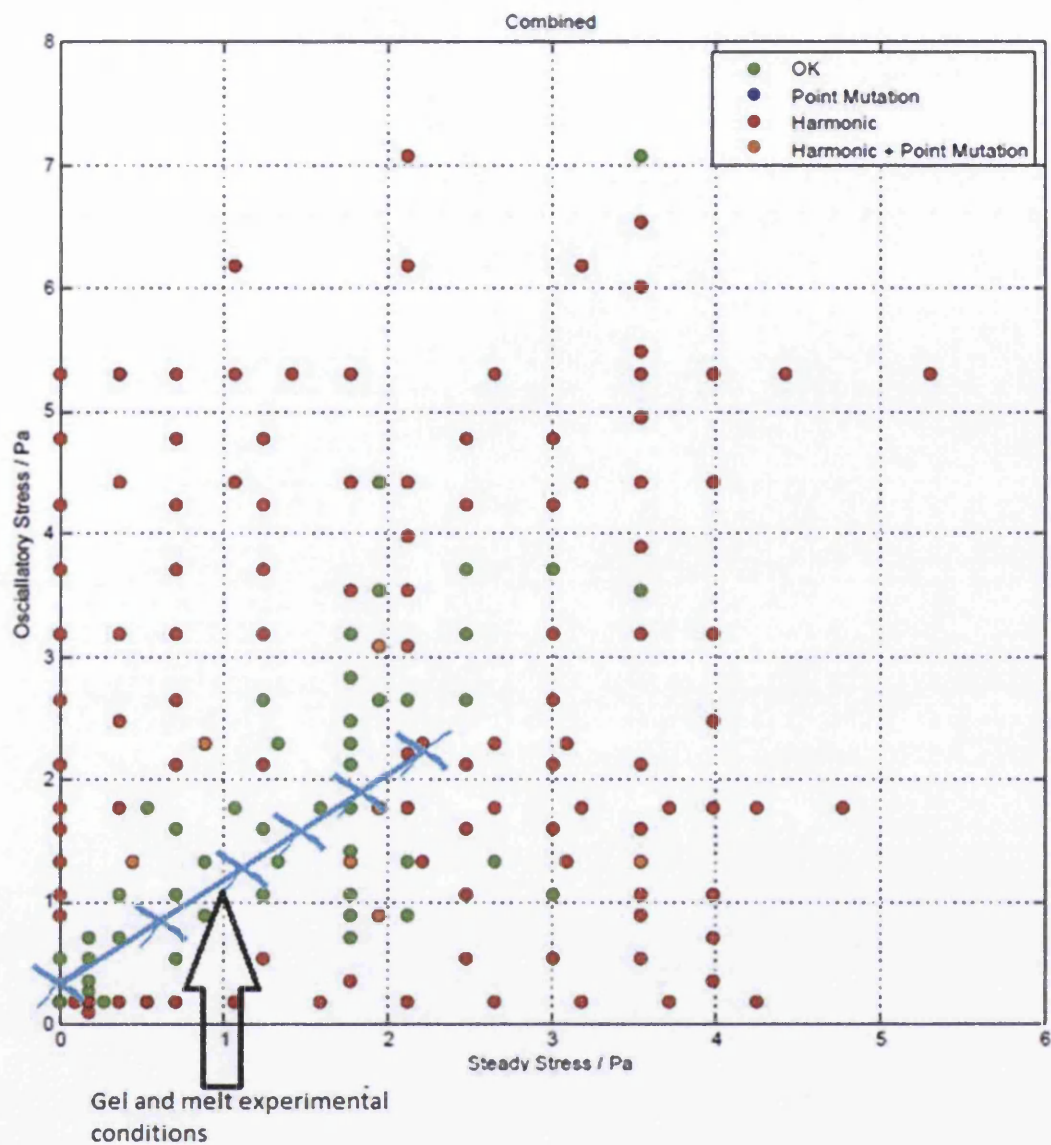


**Figure 3.2.6** - Figure showing where the test parameters fall in terms of expected linearity – a combination of oscillatory and parallel shear of 2.4Pa in previous investigations have shown non-linear results.

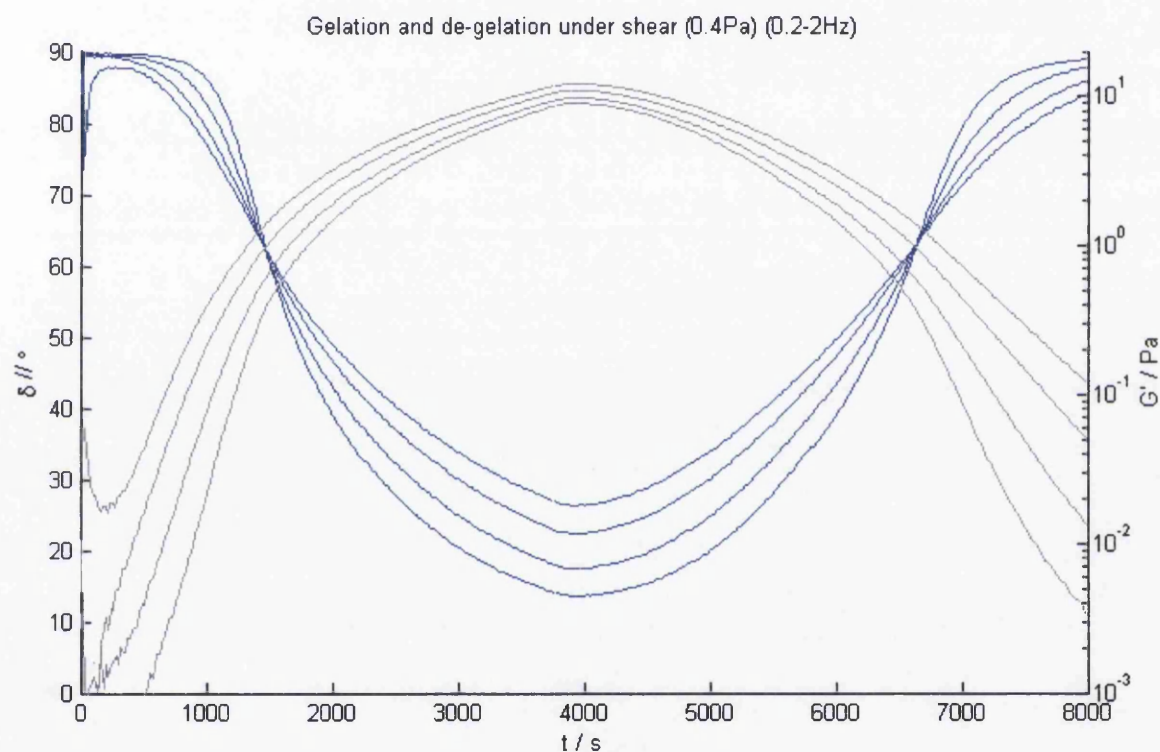


**Figure 3.2.7** - Figure showing the gelation and subsequent de-gelation of gelatine at  $20\mu\text{Nm}$  oscillatory torque and  $20\mu\text{Nm}$  controlled flow – this equates to an oscillatory stress and a superposed shear stress of  $0.4\text{Pa}$ .

Rheological transitions (VEL to VES and VES to VEL) for gelatine samples studied under CSPS.

GP marks the Gel Point which in CSPS is measured under conditions of progressively

decreasing unidirectional strain rate and oscillatory strain amplitude whilst SLT marks the solid-liquid (VES to VEL) transition. Note that under CSPA the latter is approached under conditions of increasing unidirectional strain rate and oscillatory strain amplitude.

As in SAOS the initial values of  $d$  (approximately  $90^\circ$  at all test frequencies) recorded during the CSPA experiments reflect the near-Newtonian fluid response of the material, this being followed at later times by the development of a frequency dependence of  $\delta//$  characteristic of a viscoelastic liquid (VEL), with the recorded values of  $\delta//$  declining with increasing oscillatory frequency. The frequency dependence of  $\delta//$  declines progressively as the GP is approached, the GP being marked by frequency independence of the loss tangent, as previously reported for this system. The post-GP phase is marked by development of a viscoelastic solid-like response with the recorded values of  $\delta//$  increasing with increasing oscillatory frequency.

It is emphasised that the results obtained by CSPA reveal the same rheological features as SAOS in terms of the frequency dependence of  $\delta$ . The value of  $d$  recorded at the GP by FS (SAOS) is approximately  $\delta = 62^\circ$ , the corresponding frequency independent value of  $\delta//$  recorded by CSPA being also  $62^\circ$ , in excellent agreement with published data. We now consider the results obtained on these systems following a rapid increase of the test temperature to a constant value above  $T_{crit}$ . These results are obtained during the resulting transition from a previously gelled viscoelastic solid state, back to the precursor viscoelastic fluid state. This increase in temperature to a value above the maximum gelation temperature causes a marked and progressive decrease in  $G'$  with a corresponding increase in  $\delta$  and  $\delta//$  the significant point being that their VEL-like frequency dependence is initially preserved.

A striking feature of the ensuing rheological change is that both  $d$  and  $\delta//$  subsequently pass through a second frequency independent point as the system loses its solid-like characteristics, this being accompanied by a rapid decline in the value of both  $G'$  (FS) and  $G'//$  (CSPS). It is noteworthy that the frequency independent values of  $\delta$  and  $\delta//$  at SLT are also indistinguishable at this 'de-gelling' (VES to VEL) transition; and are identical to those recorded during the initial gel formation (GP) experiments. Thereafter, the frequency dependence of  $\delta$  and  $\delta//$  change, becoming characteristic of a VEL, the values of  $\delta$  and  $\delta//$  both increasing progressively towards  $90^\circ$  as the temperature is maintained above  $T_{crit}$ .

A significant feature of these results is the increase in the frequency dependence of  $G'//$  (CSPS) in the pre-gel region compared with that of  $G'$  (FS) in the same region. This phenomena is consistent with previously reported findings that the presence of a unidirectional shear component has greatest effect on measurements performed at frequencies corresponding to shear rates lower than those associated with the background unidirectional shear flow. Hence, decreasing frequency is expected to generate larger differences between  $G'//$  and resulting in a more pronounced frequency dependence where the unidirectional shear rate is significant (i.e. only in the pre-gel region).

The experiments reported above established that when conducted under appropriate conditions (in terms of linearity and mutation number criteria) the results of FS and CSPS experiments on a system undergoing rheological transition (from VEL to VES, or *vice versa*) may be taken as indistinguishable. This conclusion is drawn on the basis that, during gelation, attainment of frequency independence of  $\delta//$  indicates the same rheological significance (in terms of the GP) as frequency independence of  $d$ .



A further (and hitherto unreported) feature of the present experiments is revealed during the transition from a previously gelled VES state back to the precursor VEL state. The significant feature of the latter CSPA results is that they are obtained from experiments in which both the oscillatory strain amplitude and the unidirectional shear field increase progressively during the approach to the rheological transition (SLT).

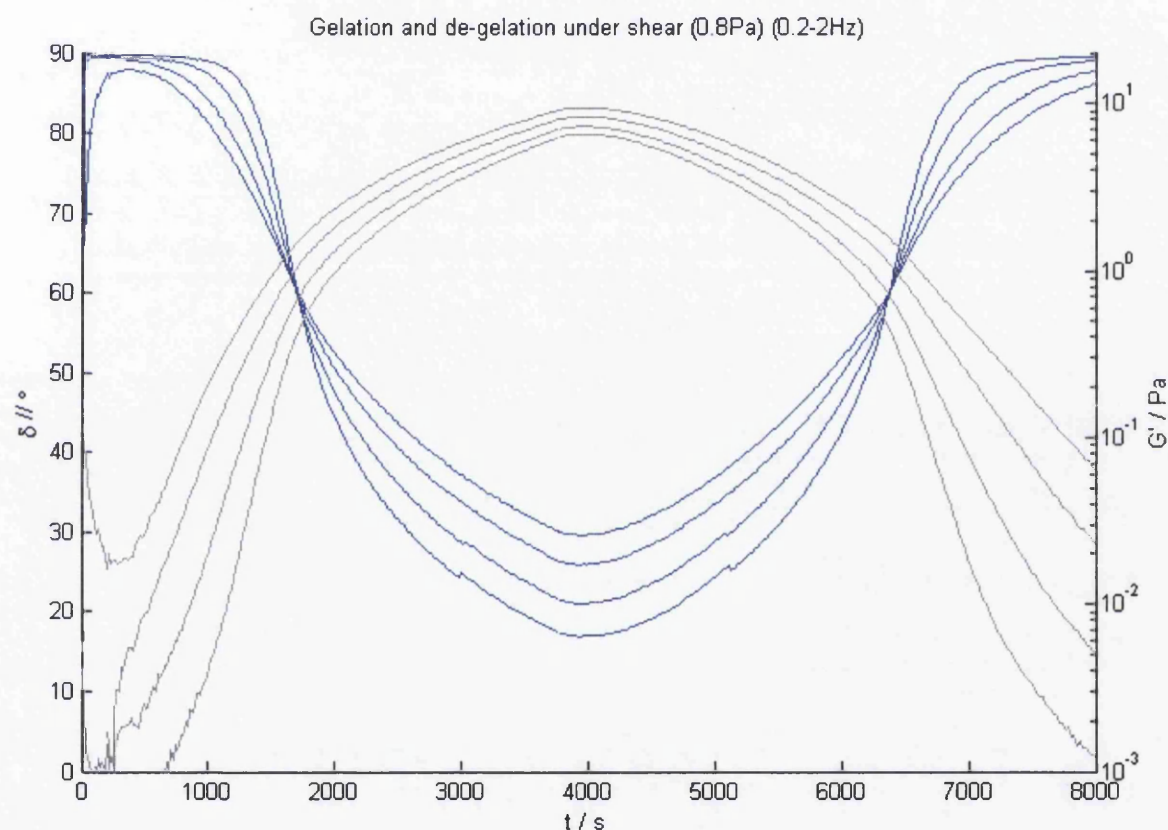


**Figure 3.2.8** - Figure showing the gelation and subsequent de-gelation of gelatine at  $40\mu Nm$  oscillatory torque and  $40\mu Nm$  controlled flow – this equates to an oscillatory stress and a superposed shear stress of  $0.8Pa$ .

The  $\delta$  (SAOS) and  $\delta//$  (CSPS) values here are  $60.3^\circ$  and  $59.95^\circ$ , the corresponding values of the stress relaxation exponent being 0.670 and 0.666, respectively. The value of the storage modulus  $G'$  at the gel point is 1.47 Pa and at the de-gel VES to VEL transition the value of  $G'//$  is 1.47Pa at 2Hz.

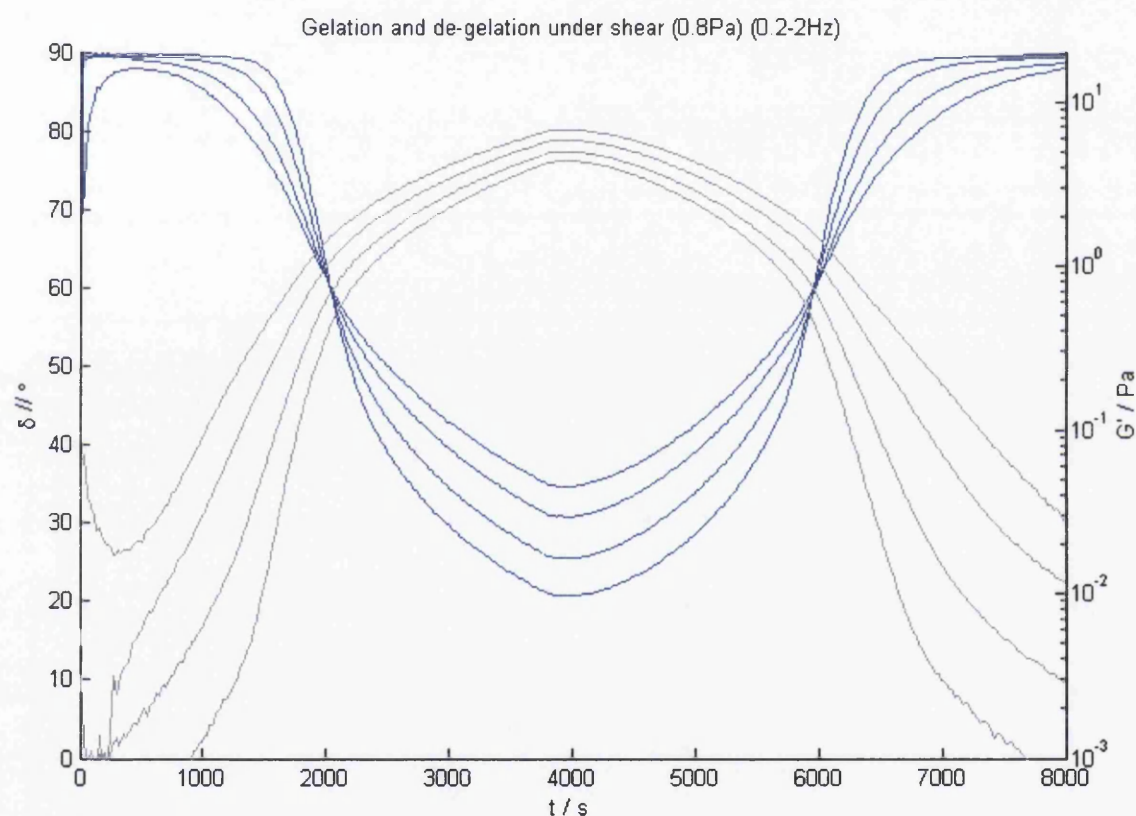


**Figure 3.2.9** - Figure showing the gelation and subsequent de-gelation of gelatine at  $60\mu Nm$  oscillatory torque and  $60\mu Nm$  controlled flow – this equates to an oscillatory stress and a superposed shear stress of 1.2Pa.



The  $\delta$  (SAOS) and  $\delta//$  (CSPS) values here are  $59.83^\circ$  and  $59.81^\circ$ , the corresponding values of the stress relaxation exponent being 0.665. The value of the storage modulus  $G'$  at the gel point is 1.53 Pa and at the de-gel VES to VEL transition the value of  $G'//$  is 1.52 Pa at 2Hz.

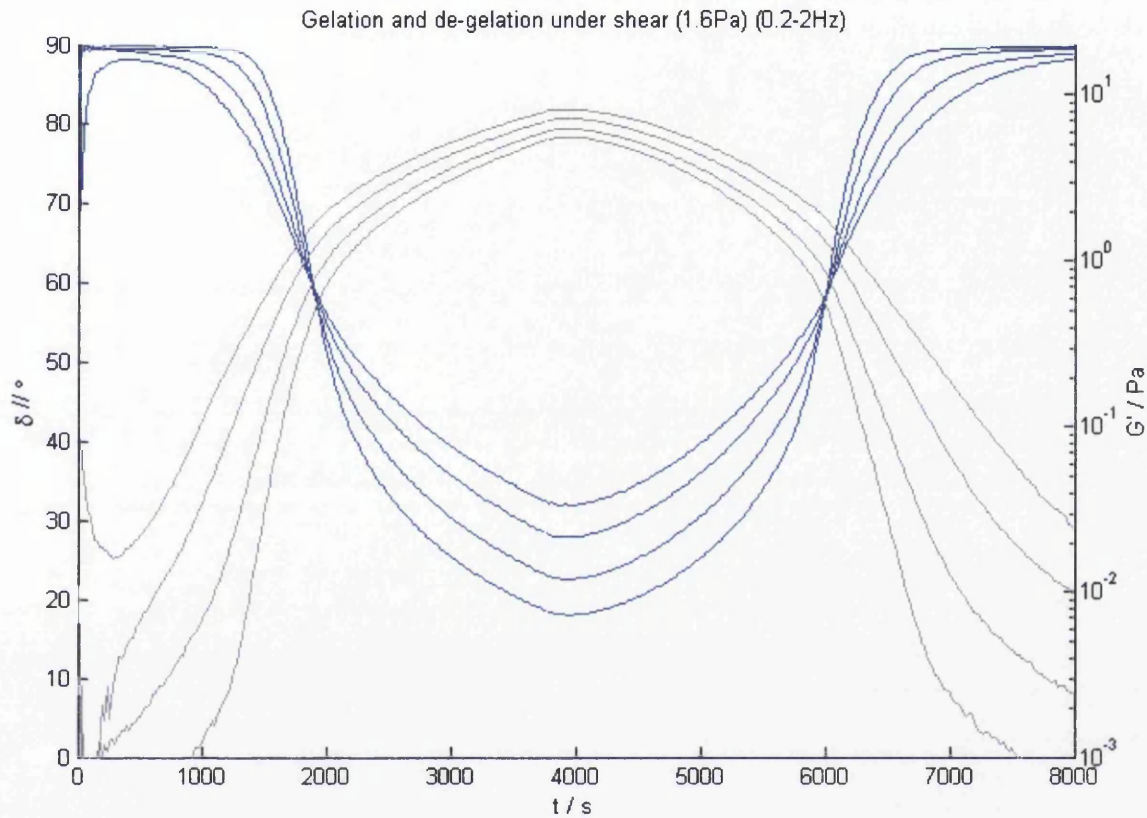


**Figure 3.2.10** - Figure showing the gelation and subsequent de-gelation of gelatine at  $80\mu\text{Nm}$  oscillatory torque and  $80\mu\text{Nm}$  controlled flow – this equates to an oscillatory stress and a superposed shear stress of 1.6Pa.

The  $\delta$  (SAOS) and  $\delta//$  (CSPS) values here are  $59.89^\circ$  and  $59.67^\circ$ , the corresponding values of the stress relaxation exponent being 0.65. The value of the storage modulus  $G'$  at the gel point is 1.72 Pa and at the de-gel VES to VEL transition the value of  $G'//$  is 1.78 Pa at 2 Hz.

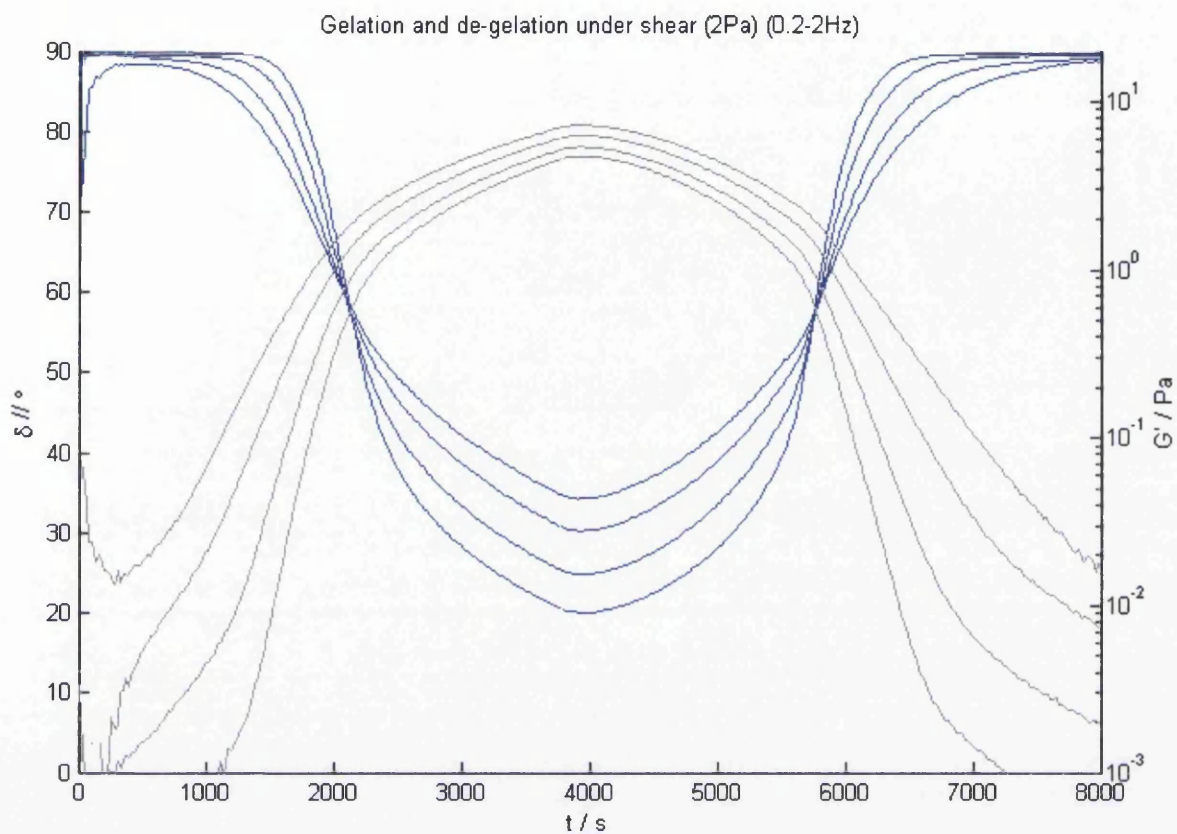


**Figure 3.2.11** - Figure showing the gelation and subsequent de-gelation of gelatine at  $100\mu\text{Nm}$  oscillatory torque and  $100\mu\text{Nm}$  controlled flow – this equates to an oscillatory stress and a superposed shear stress of  $2\text{Pa}$ .

The  $\delta$  (SAOS) and  $\delta//$  (CSPS) values here are  $57.95^\circ$  and  $57.87^\circ$ , the corresponding values of the stress relaxation exponent being 0.64. The value of the storage modulus  $G'$  at the gel point is  $1.87\text{ Pa}$  and at the de-gel VES to VEL transition the value of  $G'//$  is  $1.84\text{ Pa}$  at  $2\text{ Hz}$ .



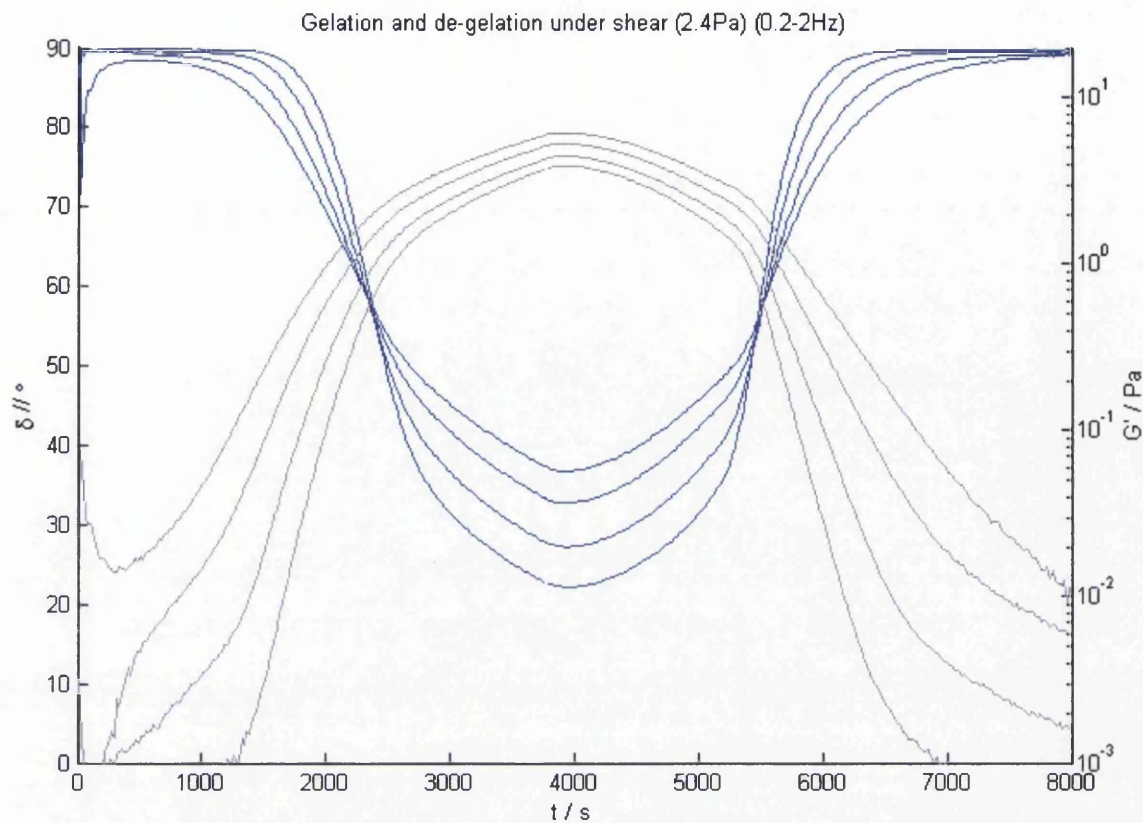


**Figure 3.2.12** - Figure showing the gelation and subsequent de-gelation of gelatine at  $120\mu\text{Nm}$  oscillatory torque and  $120\mu\text{Nm}$  controlled flow – this equates to an oscillatory stress and a superposed shear stress of 2.4Pa.

The  $\delta$  (SAOS) and  $\delta //$  (CSPS) values here are  $57.63^\circ$  and  $55.75^\circ$ , the corresponding values of the stress relaxation exponent being 0.64 and 0.62, respectively. The value of the storage modulus  $G'$  at the gel point is 2.0 Pa and at the de-gel VES to VEL transition the value of  $G' //$  is 2.18 Pa at 2Hz.

The latter results in particular illustrate the expected deviation from linearity above a 2Pa stress as the value at which the sol gel transition clearly differs ore substantially from

the other results. It can be clearly observed that it is not a mutation error as a frequency independent point is still found by every frequency, however the values are different. The increase in number of frequencies is shown to have little change on the values retrieved as shown below (figure 3.2.13).

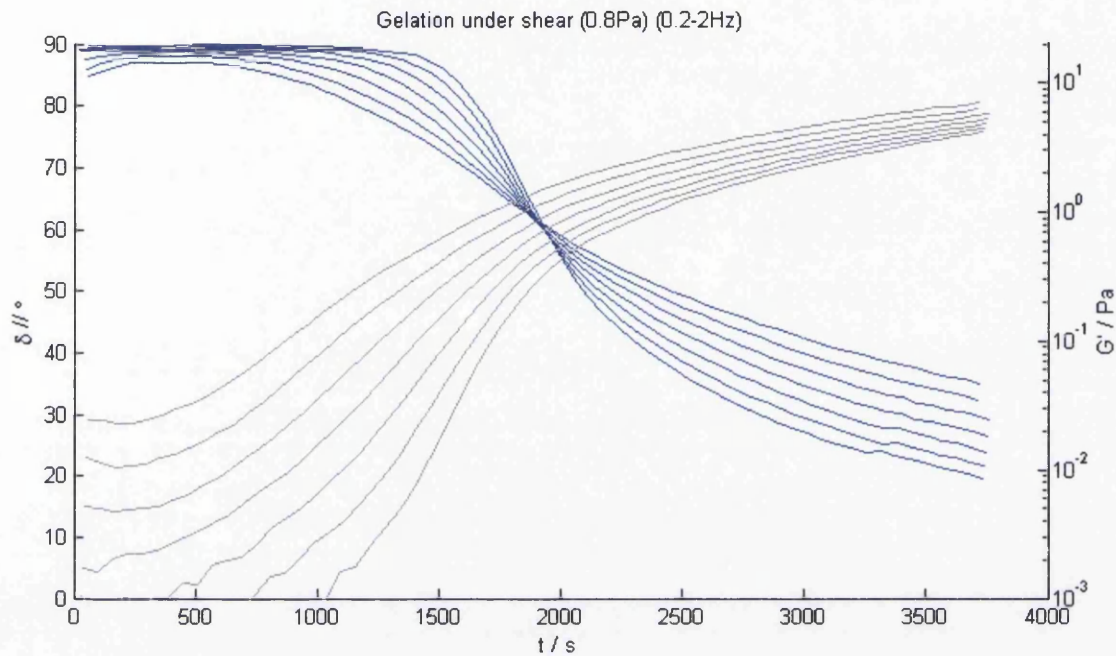


**Figure 3.2.13** - Figure showing the gelation of gelatine at  $40\mu\text{Nm}$  oscillatory torque and  $40\mu\text{Nm}$  controlled flow at seven known linear frequencies between  $0.2\text{-}2\text{Hz}$  – this equates to an oscillatory stress and a superposed shear stress of  $0.8\text{Pa}$ .

With the sol-gel transition occurring at a value of  $60.84^\circ$  which gives a relaxation exponent of  $0.676$ , the result is in agreement with the above set of data at the same conditions. The subsequent de-gelation is shown in figure 3.2.14 below:

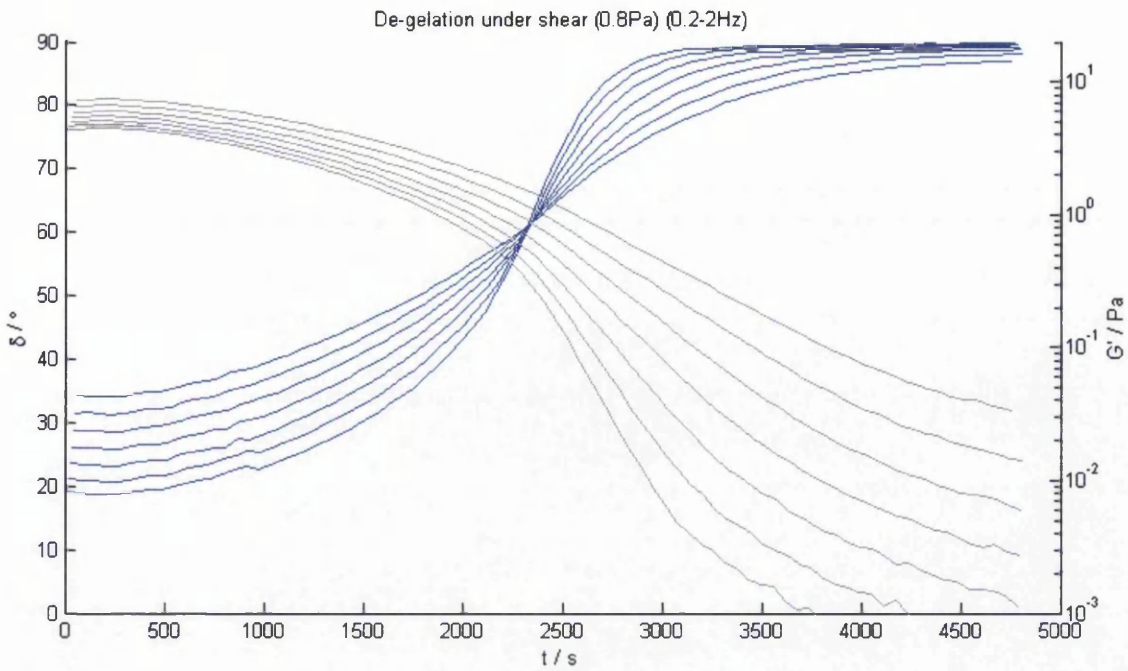


**Figure 3.2.14** - Figure showing the de-gelation of gelatine at  $40\mu\text{Nm}$  oscillatory torque and  $40\mu\text{Nm}$  controlled flow at seven known linear frequencies between  $0.2\text{-}2\text{Hz}$  – this equates to an oscillatory stress and a superposed shear stress of  $0.8\text{Pa}$ .

The transition from gel to sol occurs at  $60.91^\circ$  which gives a relaxation exponent of  $0.677$ , when both gelation and de-gelation are plotted on the same axis the similarities are more apparent. As seen below in figure 3.2.15.

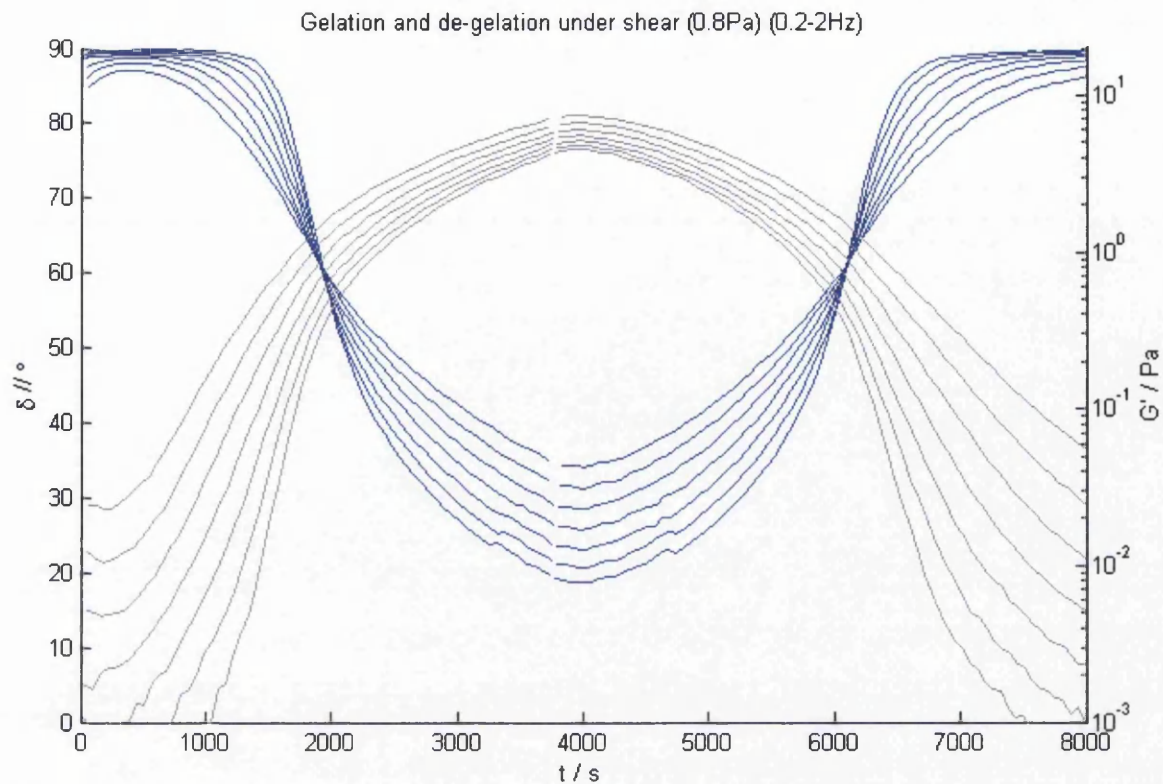


**Figure 3.2.15** - Figure showing the gelation and subsequent de-gelation of gelatine at  $40\mu\text{Nm}$  oscillatory torque and  $40\mu\text{Nm}$  controlled flow at seven known linear frequencies between 0.2-2Hz – this equates to an oscillatory stress and a superposed shear stress of 0.8Pa.

The difference between these values of delta as a percentage is 0.11%. The values for  $G'$  at the gel and de-gel point at 2Hz can be seen in the tabulated data below, first in table 3.2.2 for the data set with four frequencies used and then secondly in table 3.2.3 for the data set with seven frequencies used.

2Hz	G' (Pa) Gel	G'// (Pa) Melt	$\delta$ (°) Gel	$\delta$ /(°) Melt	Time (s) Gel	Time (s) Melt
No shear	1.446	1.442	62.49	62.45	1742.44	6233.69
0.4Pa	1.416	1.387	62.66	62.88	1466.11	6632.73
0.8Pa	1.474	1.467	60.3	59.95	1701.48	6376.86
1.2Pa	1.532	1.518	59.84	59.81	2035.85	5964.11
1.6Pa	1.72	1.784	58.94	58.81	1913.85	6008.73
2Pa	1.869	1.844	57.94	57.87	2120.47	5770.26
2.4Pa	2.001	2.184	57.64	55.75	2371.08	5471.13

**Table 3.2.1** - Table of CSPS gelation and de-gelation of 10% gelatine data between 0.2-

2Hz at four known linear frequencies – values of  $G'$  and  $G''$  are taken at 2Hz

Second set of data:

2Hz	G' (Pa) Gel	G'// (Pa) Melt	$\delta$ (°) Gel	$\delta$ /(°) Melt	Time (s) Gel	Time (s) Melt
No shear	1.386	1.357	61.73	62.18	1732.43	6342.75
0.4Pa	1.331	1.368	62.17	62.13	1793.8	6239.81
0.8Pa	1.503	1.472	60.84	60.91	1916.94	6093.59
1.2Pa	1.586	1.663	59.19	59.29	1578.69	6455.71
1.6Pa	1.589	1.691	58.89	58.67	1520.19	6592.15
2Pa	1.812	2.041	57.26	56.01	1802.13	6190.23
2.4Pa	2.078	2.445	54.77	51.33	2183.91	5733.91

**Table 3.2.2** - Table of CSPS gelation and de-gelation of 10% gelatine data between 0.2-

2Hz at seven known linear frequencies – values of  $G'$  and  $G''$  are taken at 2Hz

In both sets of data  $\delta$  and  $G'$  data are similar enough to be considered the identical during gelation as well as de-gelation during the linear regions. The value of  $G'$  appears to increase steadily with the increase of steady stress.  $\delta$  at the gel point appears to decrease with the increase of steady stress. Gel time appears to increase with the increase of stress, and melt time appears to decrease with the addition of stress, it should be noted that the values of melt time include the gelation phase in their total.

The relationship between loss and storage modulus both through gelation and through melting of gelatine can be compared to highlight similarities or differences in the process of gelation and de-gelation. By way of example, under zero shear conditions the properties of the storage and loss modulus at various set process times are shown below in figure 3.2.24:



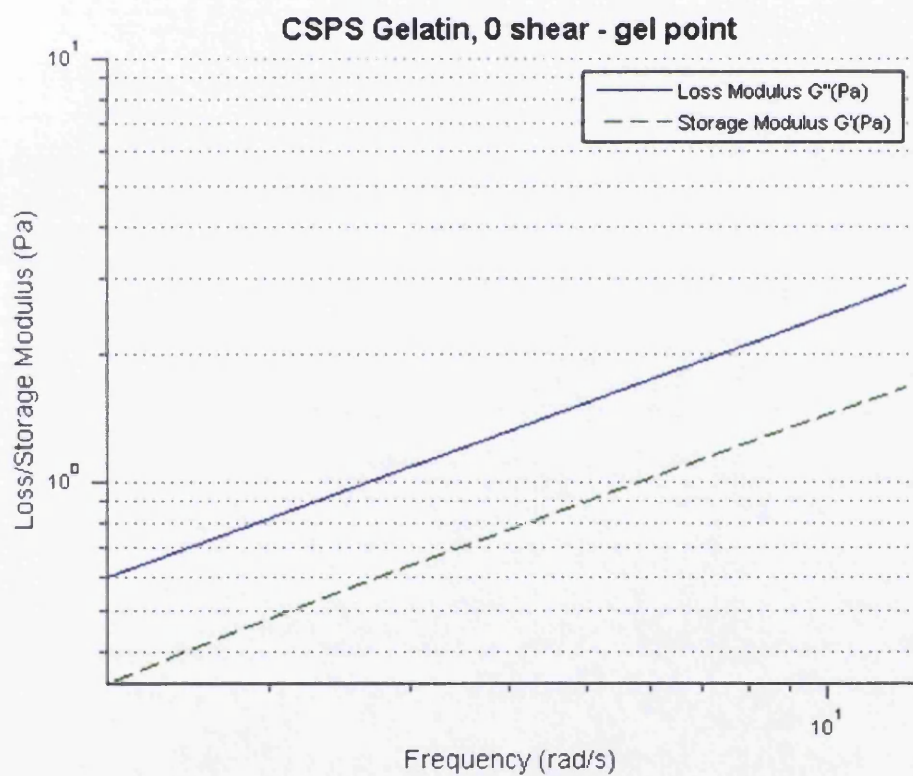
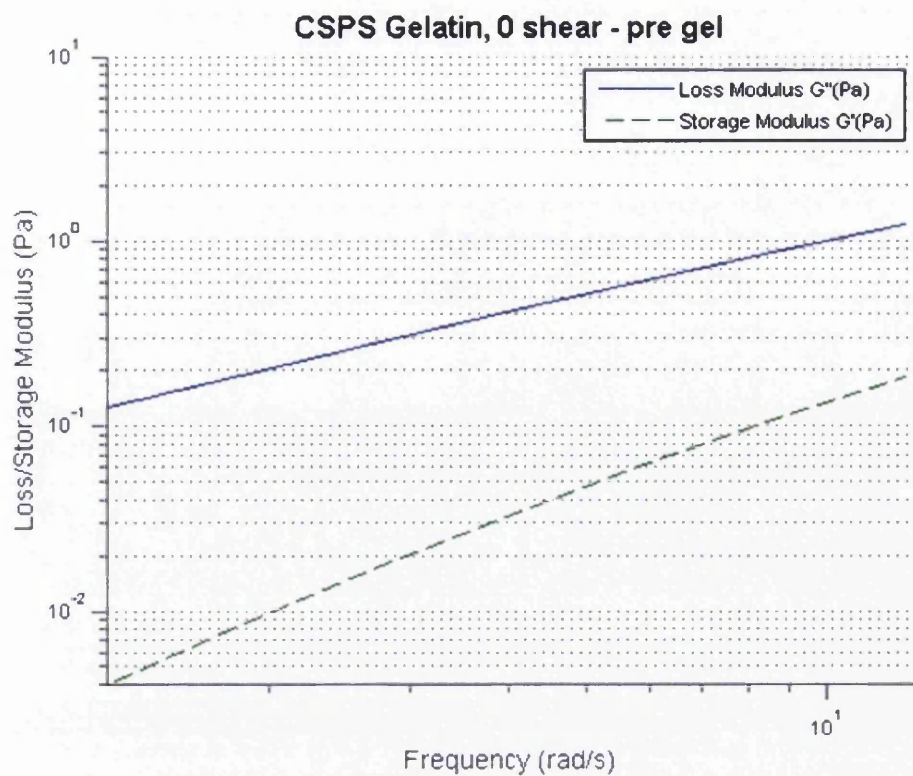


**Figure 3.2.16** - Figure showing the storage and loss modulus through the pre-gel and gel point under no shear plotted against frequency at which it was measured.

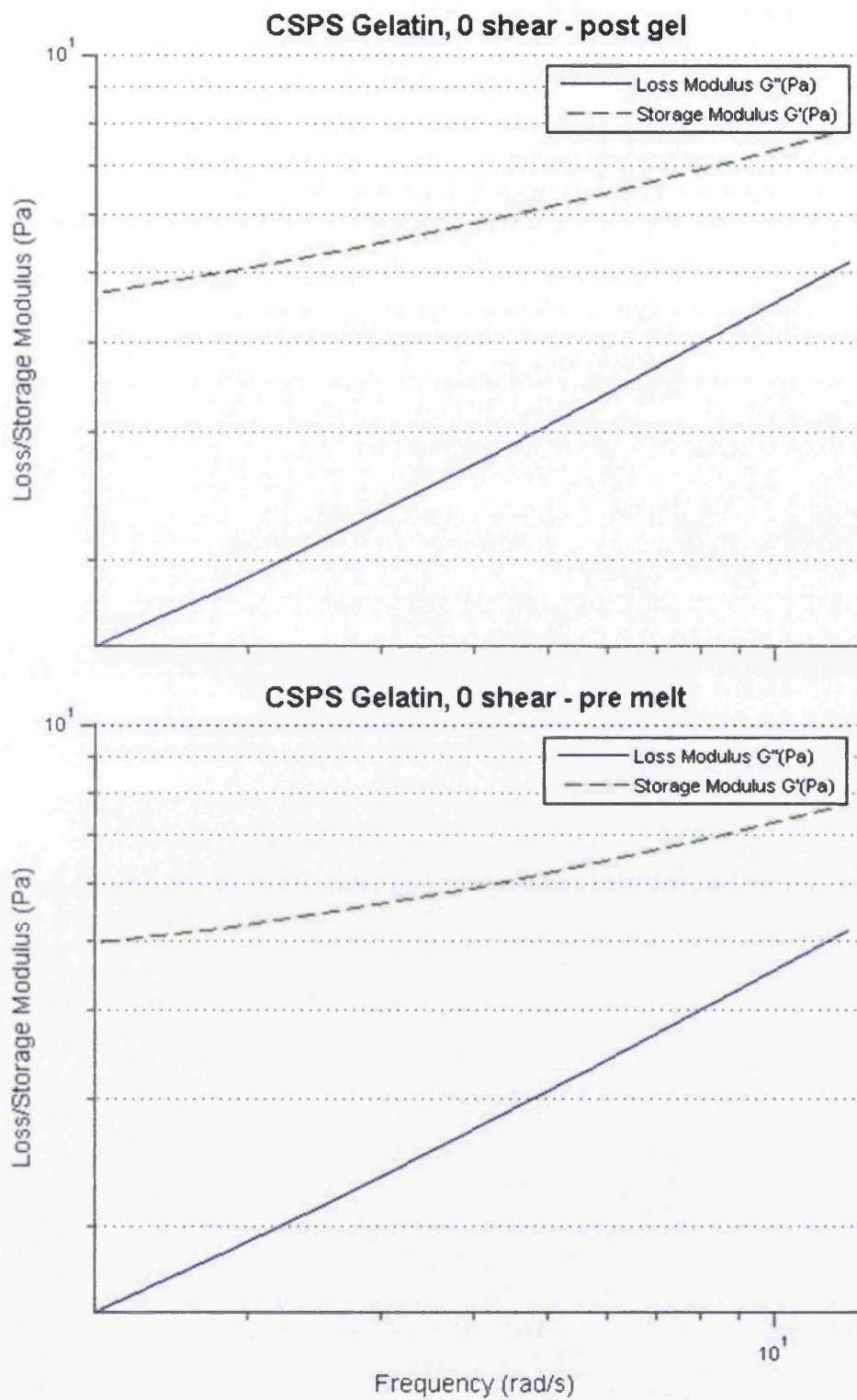


**Figure 3.2.17** - Figure showing the storage and loss modulus through the post-gel and pre-melt under no shear plotted against frequency at which it was measured.



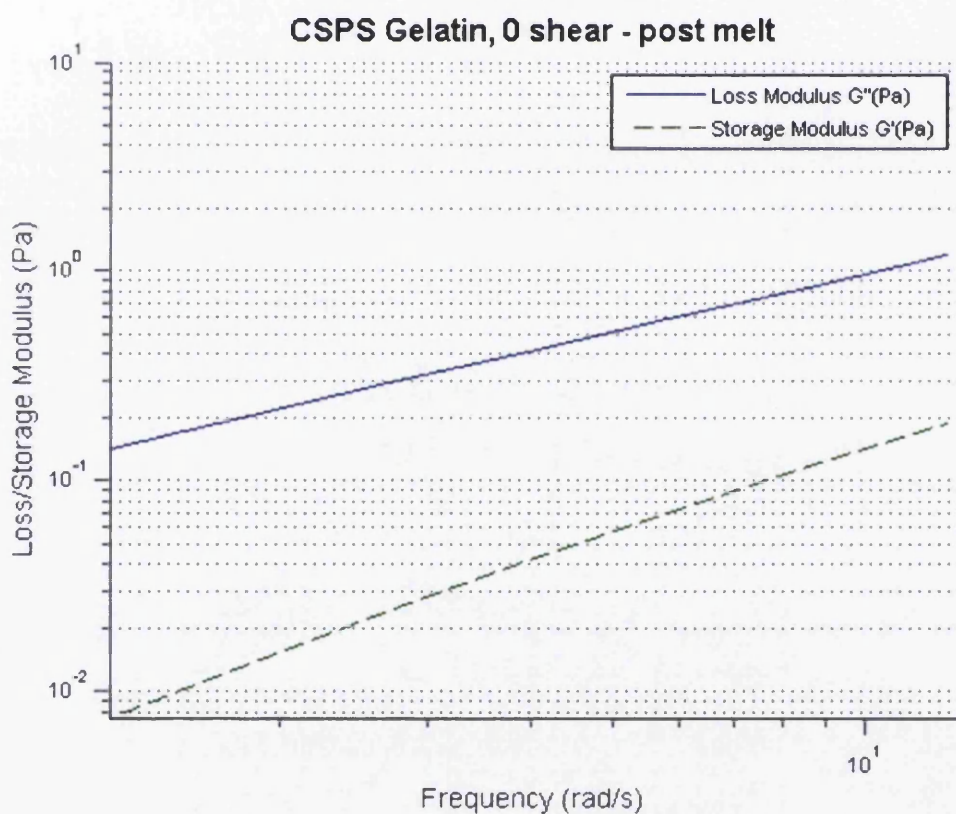
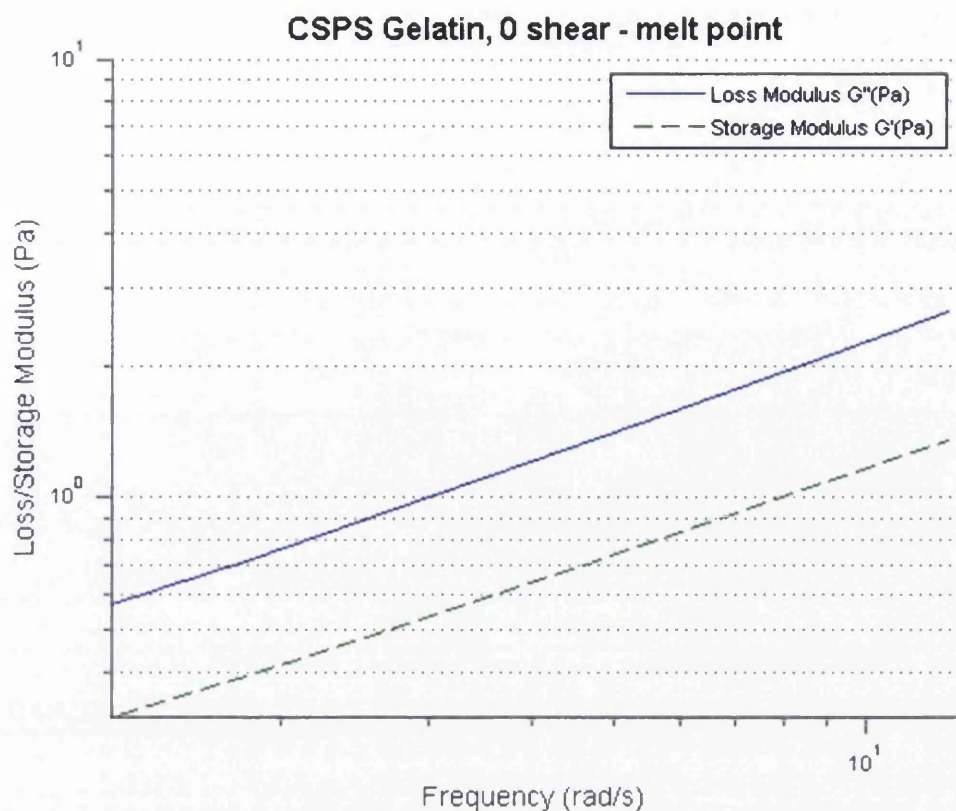


**Figure 3.2.18** - Figure showing the storage and loss modulus through the melt point and post melt under no shear plotted against frequency at which it was measured.

For the purposes of these results, pre gel is defined as 800 seconds before the gel point and the gel point is defined by a sol gel transition. Post gel is 800 seconds post sol gel transition and pre melt is 800 seconds before the melt point. A further 800 seconds after the melt point is defined as post melt.

It is clear from the figure above that the pre gel, gel point and post gel phases of gelation have almost identical viscoelastic corollaries with post melt, melt point and pre melt respectively. This is less apparent with values of pre and post gel and melt as the timings are not perfect mirrors of the process of gelation and de-gelation, however there is strong evidence to imply that there is a point at which these properties will mirror each other precisely. These three corollaries are plotted on the same axis in figure 3.2.19-20 below:

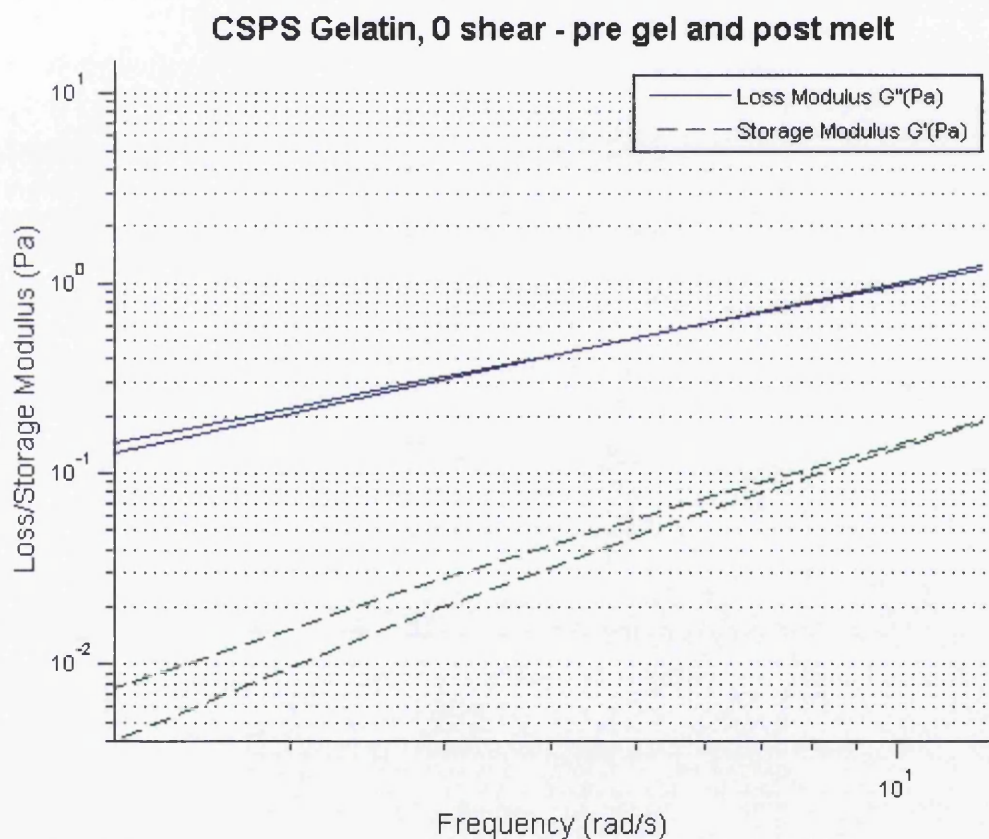
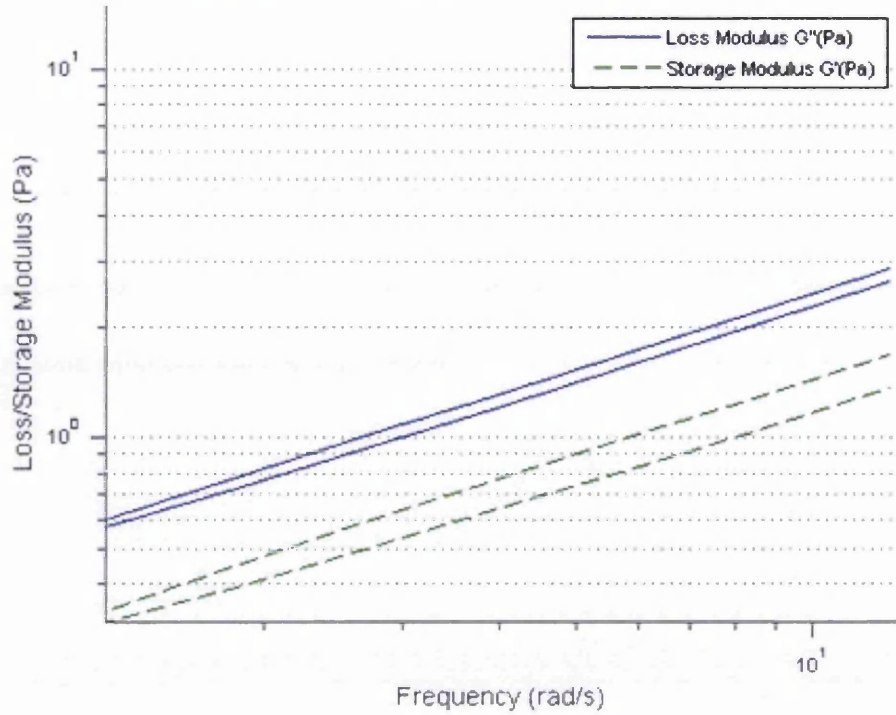


**Figure 3.2.19** - Figure showing the storage and loss modulus for pre gel and post melt under no shear plotted against frequency at which it was measured, on the same axis.

### CSPS Gelatin, 0 shear - gel point and melt point



### CSPS Gelatin, 0 shear - post gel and pre melt

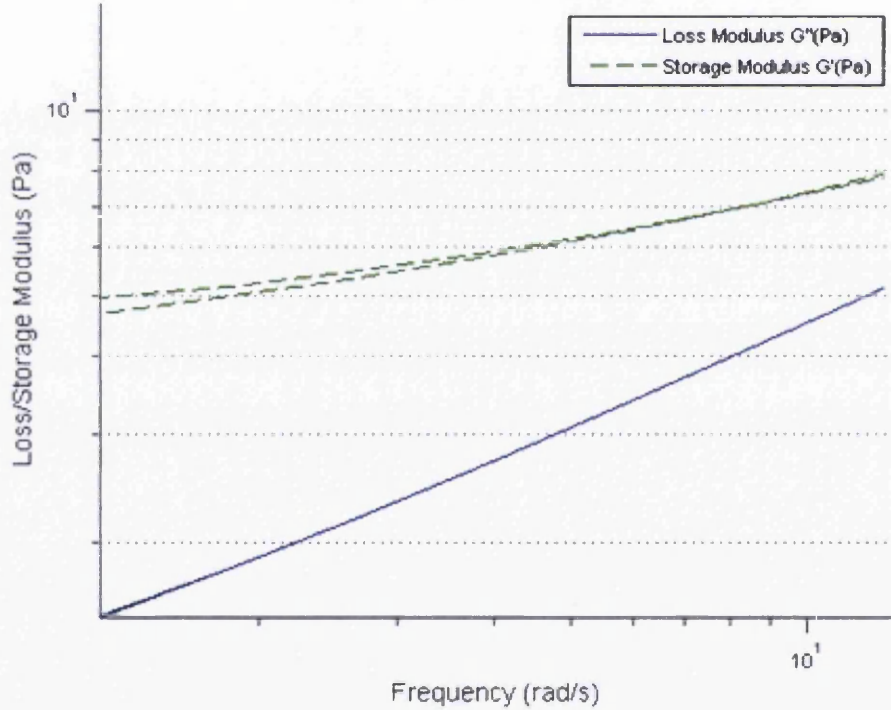


**Figure 3.2.20** - Figure showing the storage and loss modulus from the gel point and through the melting of gelatine under no shear plotted against frequency at which it was measured, on the same axis.

Interestingly, these viscoelastic profiles suggest that the process of gelation is exactly mirrored in the process of de-gelation i.e. the last structure that forms during gelation is the first structure that breaks down during de-gelation. Using these profiles it is also possible to investigate the effect of superposition on the gelation and de-gelation of gelatine. Figures 3.2.21-25 below show the viscoelastic profiles under 40 $\mu$ Nm superposed shear and those profiles with their corollaries respectively.



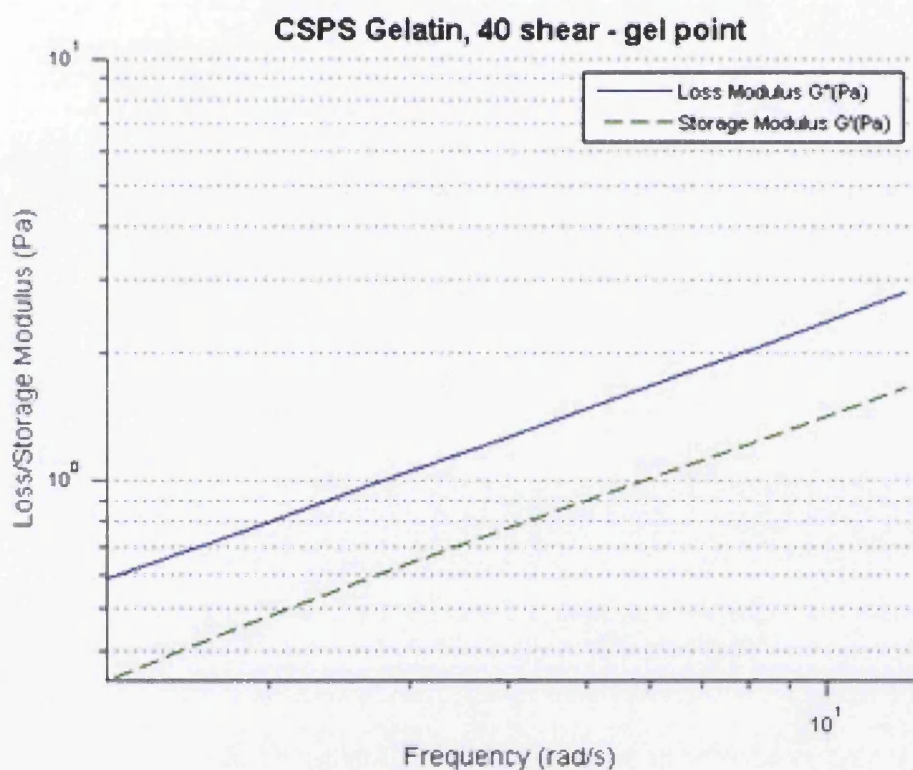
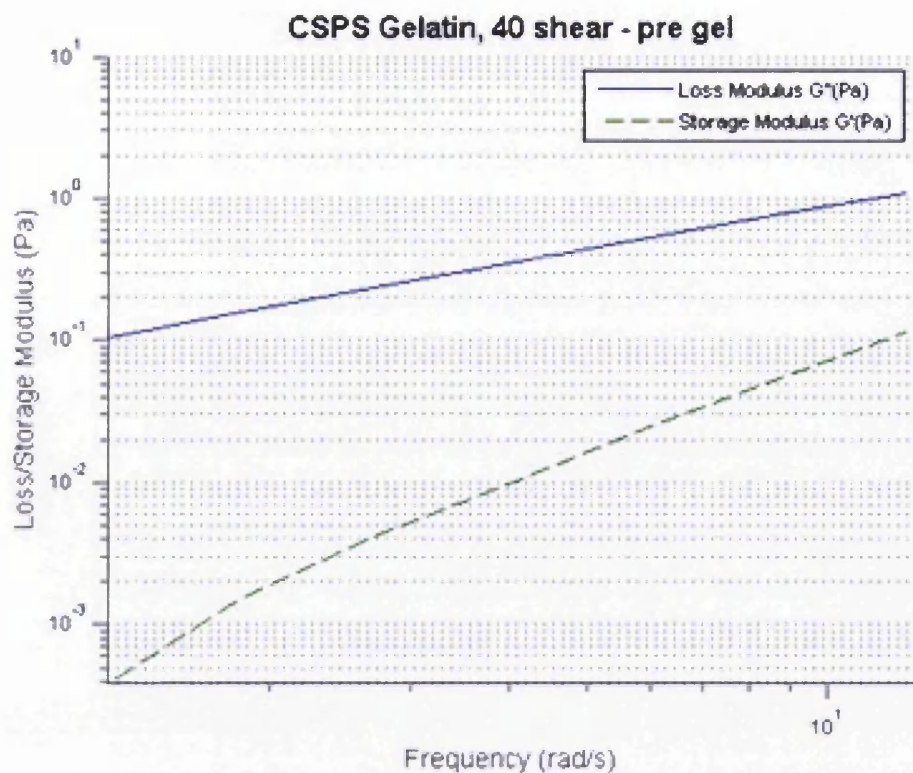


**Figure 3.2.21** - Figure showing the storage and loss modulus through the pre-gel and gel-point of gelatine under  $40\mu\text{Nm}$  constant torque ( $0.8\text{Pa}$  shear stress) plotted against frequency at which it was measured.

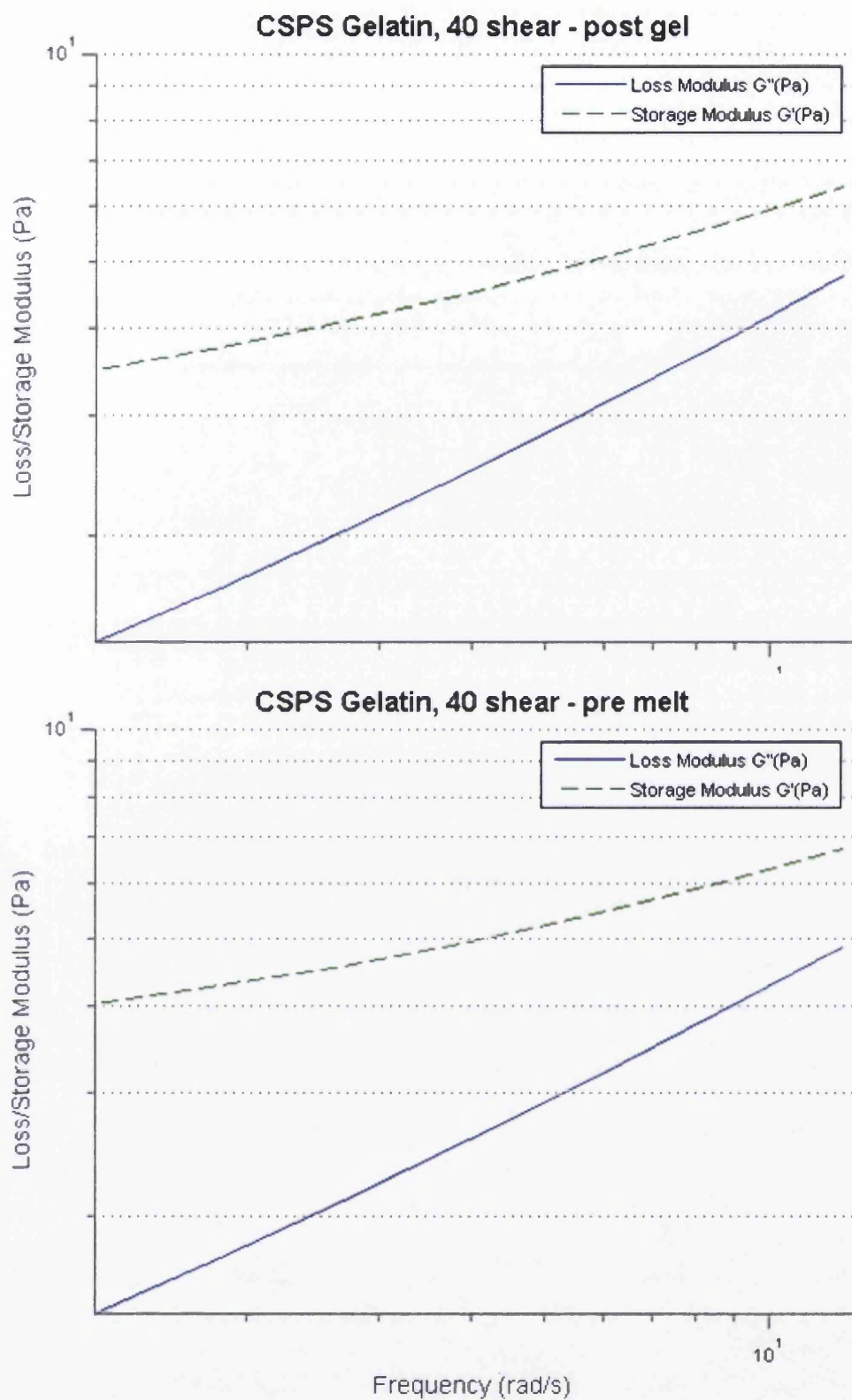


**Figure 3.2.22** - Figure showing the storage and loss modulus through the post-gel and pre-melt of gelatine under  $40\mu\text{Nm}$  constant torque ( $0.8\text{Pa}$  shear stress) plotted against frequency at which it was measured.

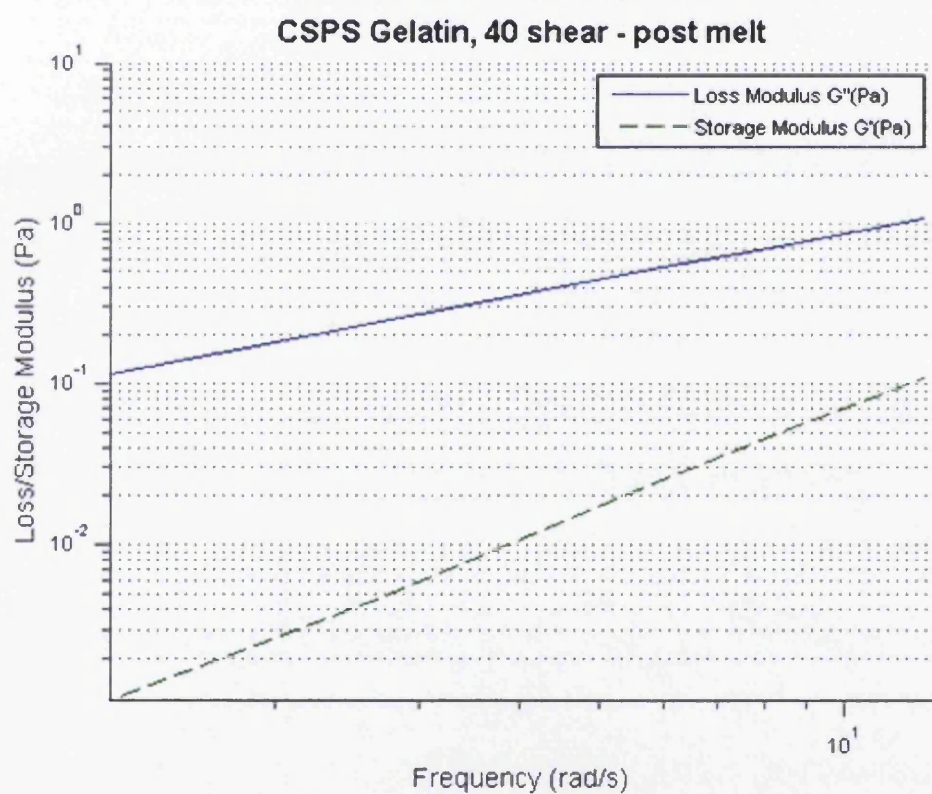
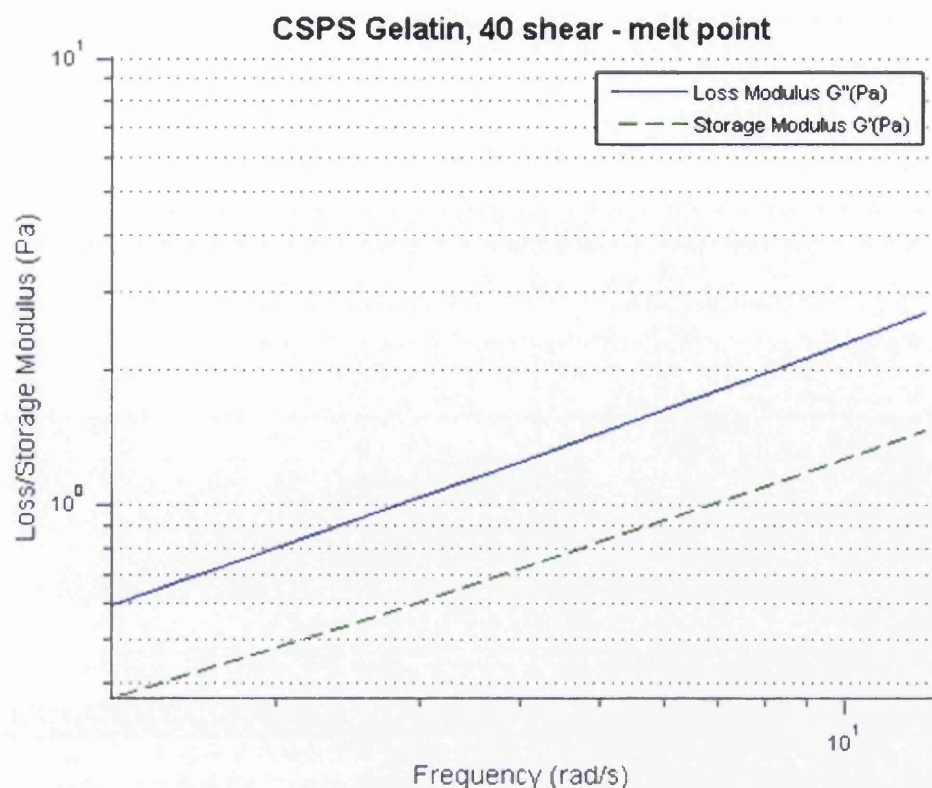


**Figure 3.2.23** - Figure showing the storage and loss modulus through the melt point and post-melt of gelatine under 40 $\mu$ Nm constant torque (0.8Pa shear stress) plotted against frequency at which it was measured.



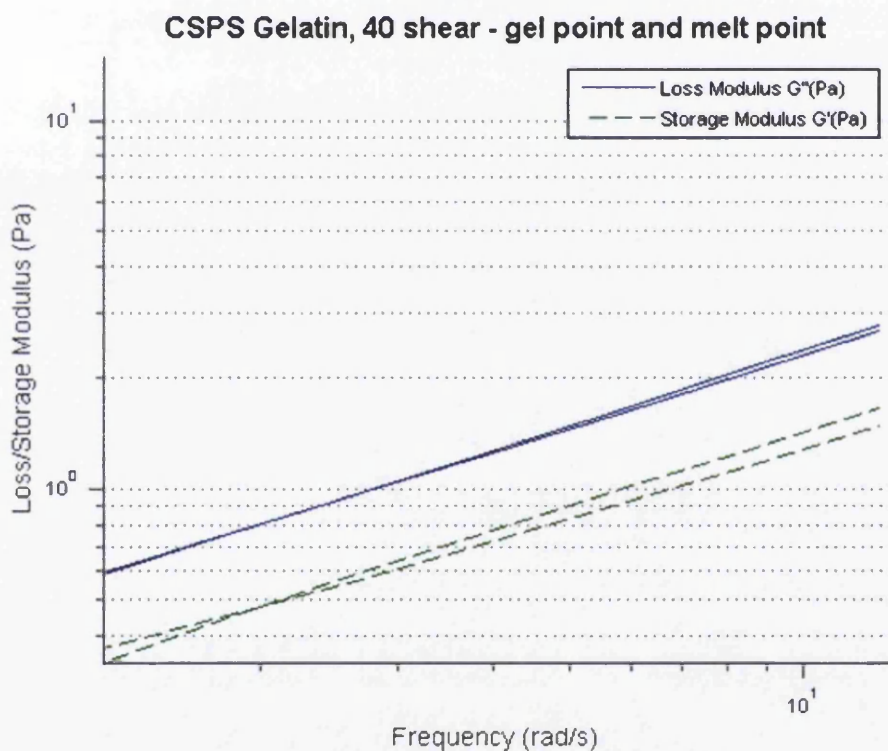
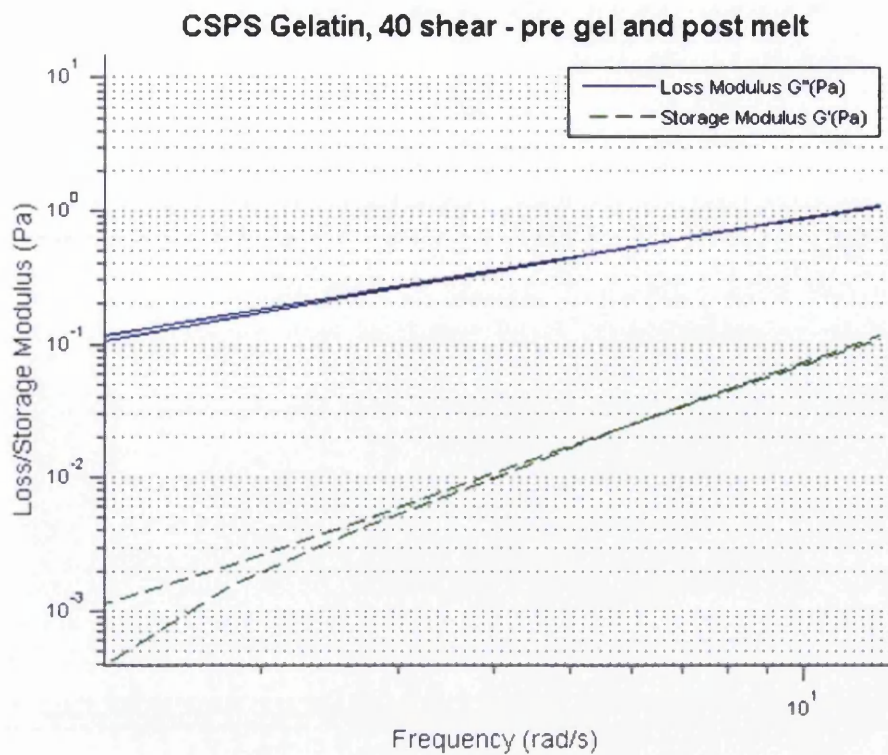


**Figure 3.2.24** - Figure showing the storage and loss modulus for pre/post gel and gel/melt point of gelatine under 40 $\mu$ Nm constant torque (0.8Pa shear stress) plotted against frequency at which it was measured, on the same axis.



### CSPS Gelatin, 40 shear - post gel and pre melt

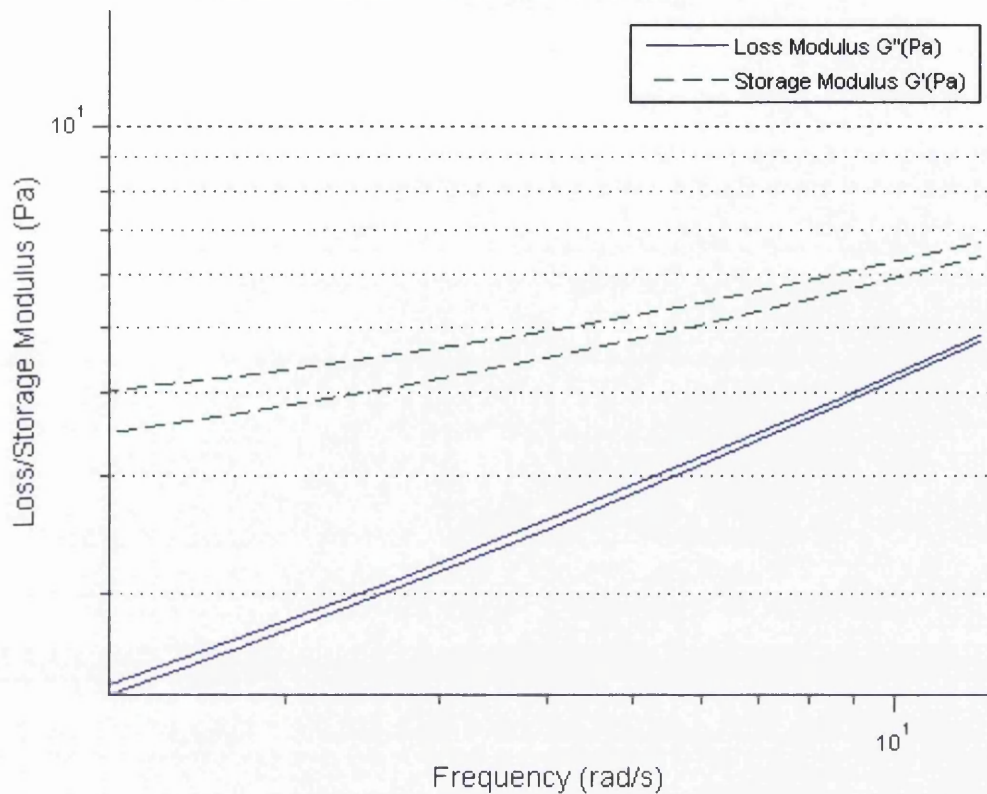


**Figure 3.2.25** - Figure showing the storage and loss modulus for the post gel and pre melting of gelatine under 40 $\mu$ Nm constant torque (0.8Pa shear stress) plotted against frequency at which it was measured, on the same axis.

Under these low shear rates, the viscoelastic profile of gelatine appears to be very similar, However through direct comparison the gradients of the storage modulus  $G'$  both in the pre gel/post melt and the post gel/pre melt phase are steeper, and over the same range of frequencies cover a wider range of Pascals. This could be interpreted such that under shear, the elastic response of gelatine is more time dependent than when at rest. A clearer picture can be assessed by looking at gelation under higher shear rates such as 80 and 120 $\mu$ Nm.

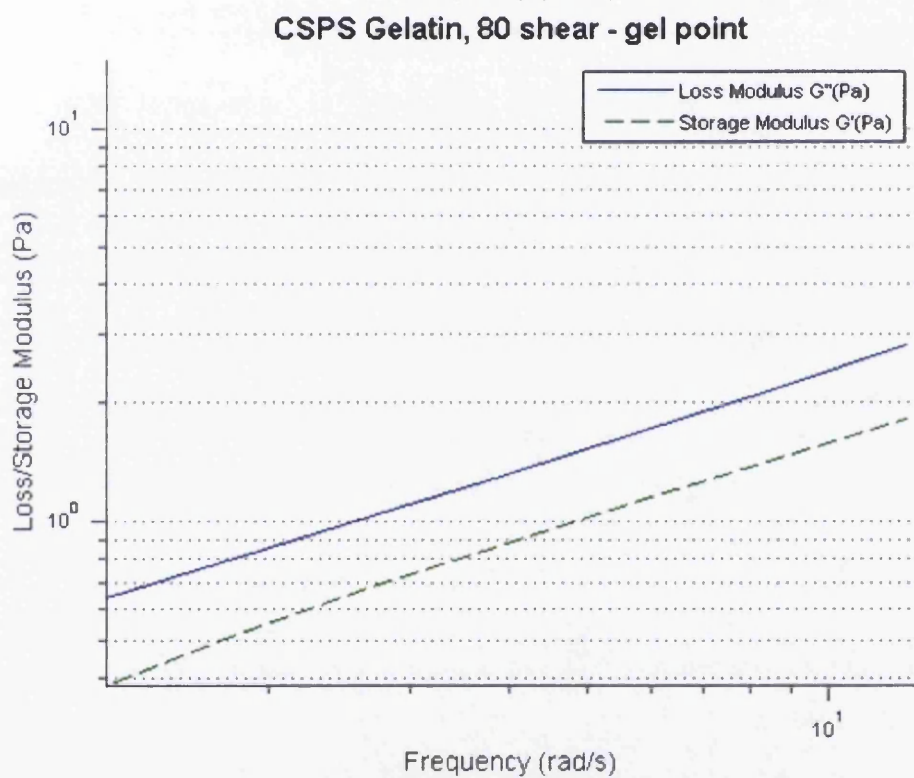
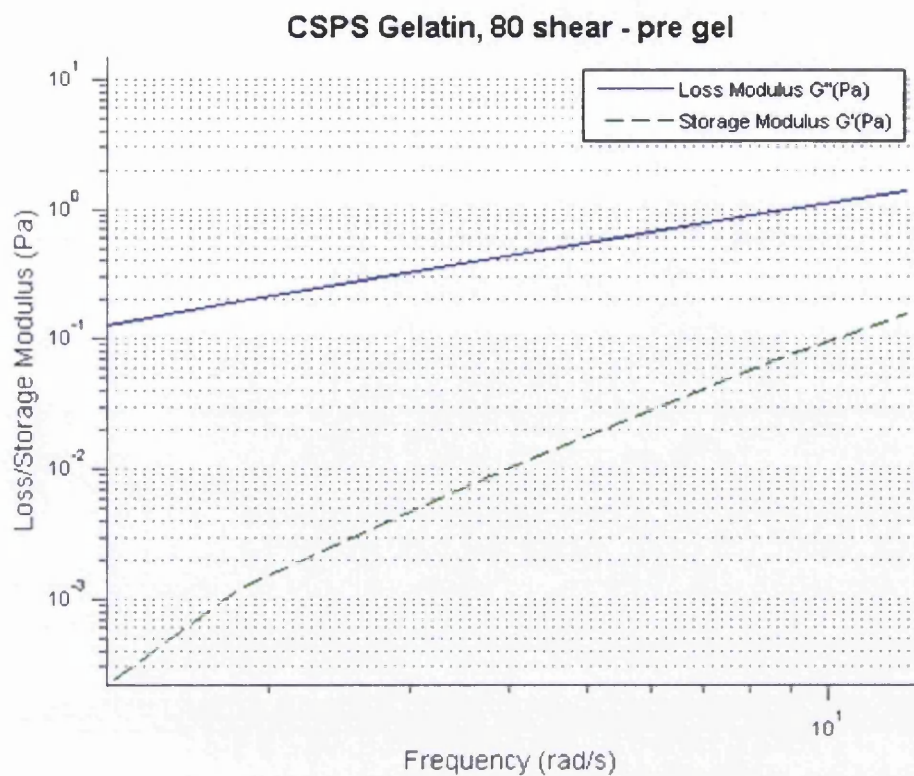


**Figure 3.2.26** - Figure showing the storage and loss modulus through the pre-gel and gel point of gelatine under 80 $\mu$ Nm constant torque (1.6Pa shear stress) plotted against frequency at which it was measured.

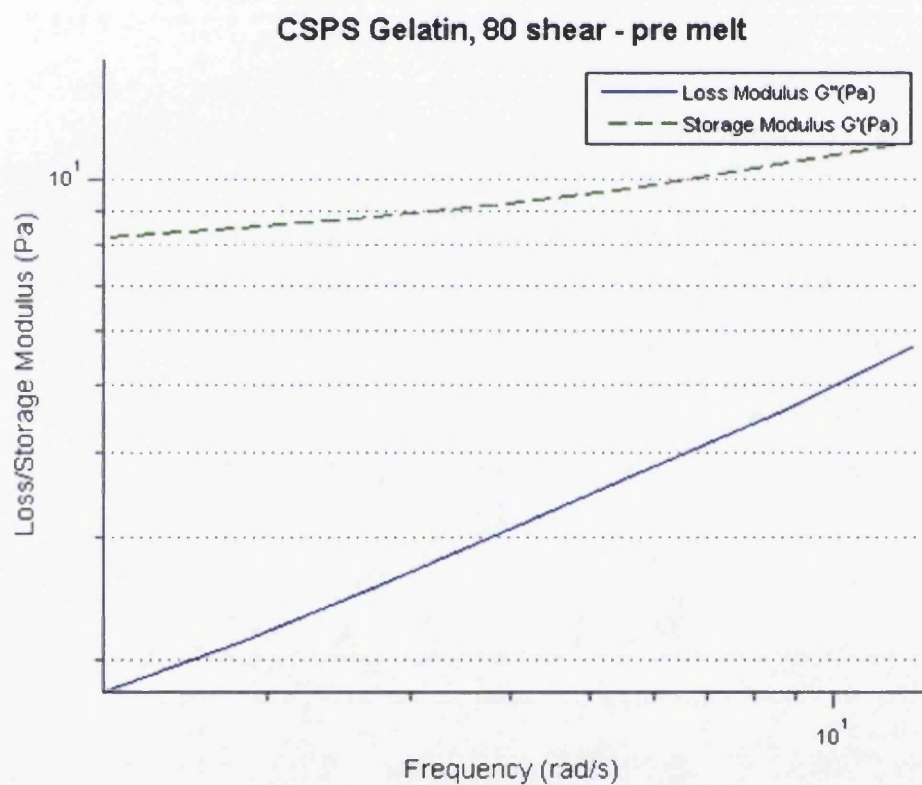
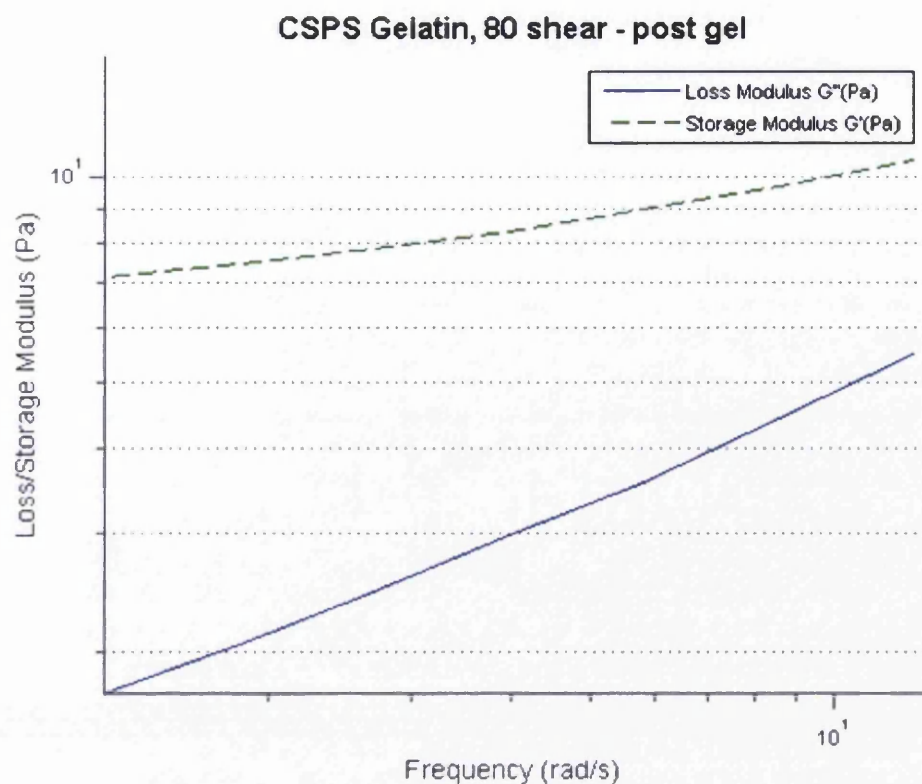


**Figure 3.2.27** - Figure showing the storage and loss modulus through the post gel and pre melt of gelatine under  $80\mu\text{Nm}$  constant torque ( $1.6\text{Pa}$  shear stress) plotted against frequency at which it was measured.

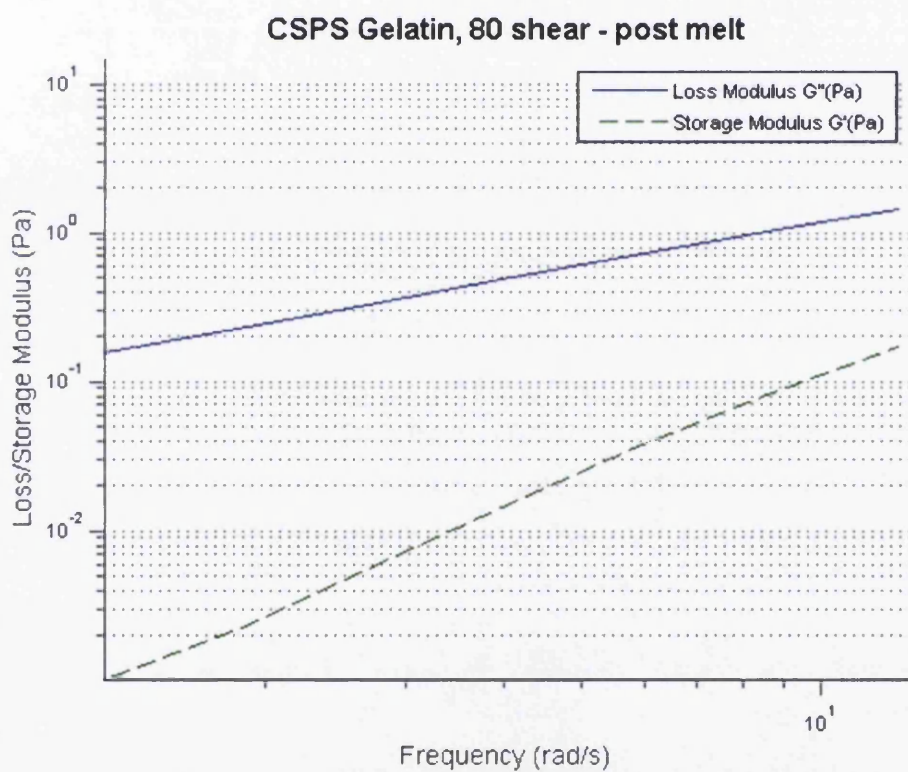
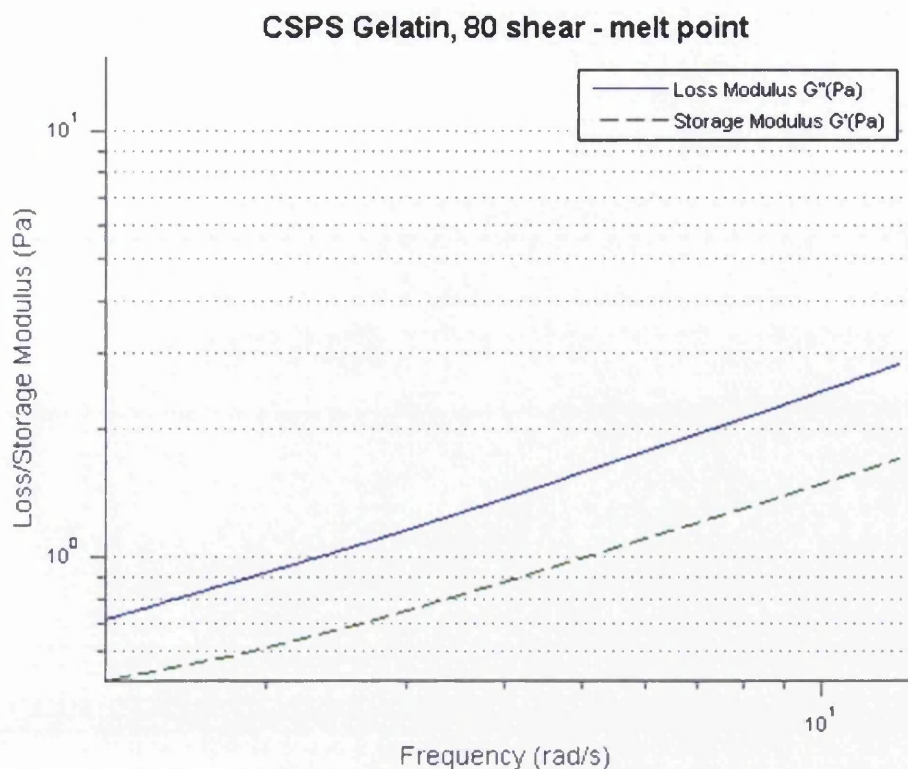


**Figure 3.2.28** - Figure showing the storage and loss modulus through the melt point and post melt of gelatine under 80 $\mu$ Nm constant torque (1.6Pa shear stress) plotted against frequency at which it was measured.



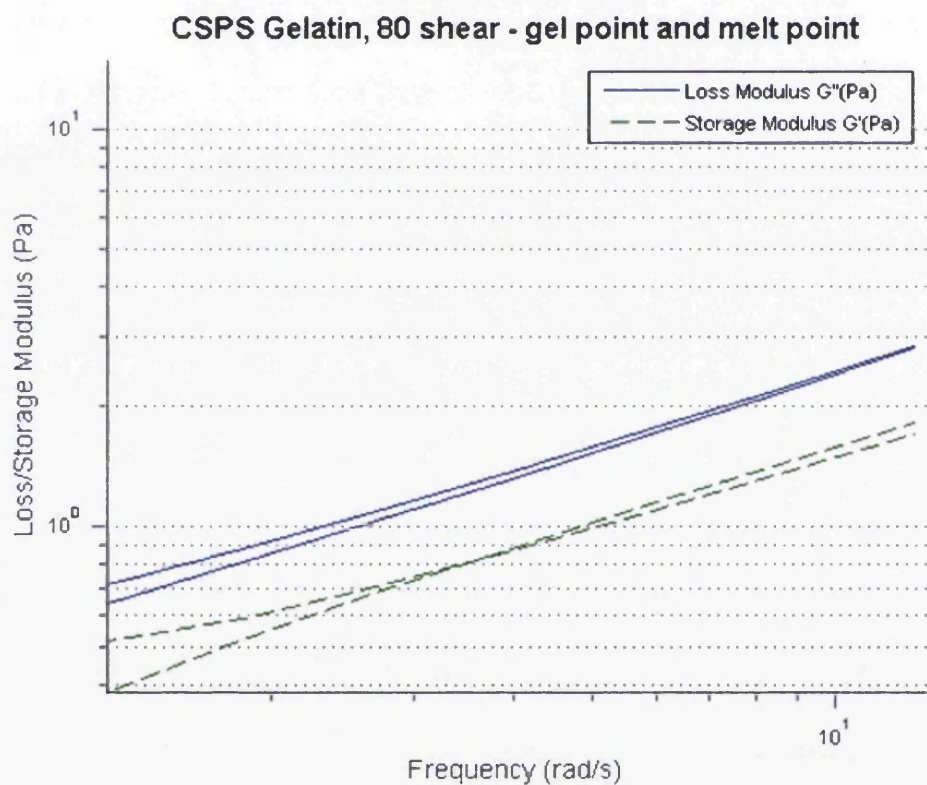
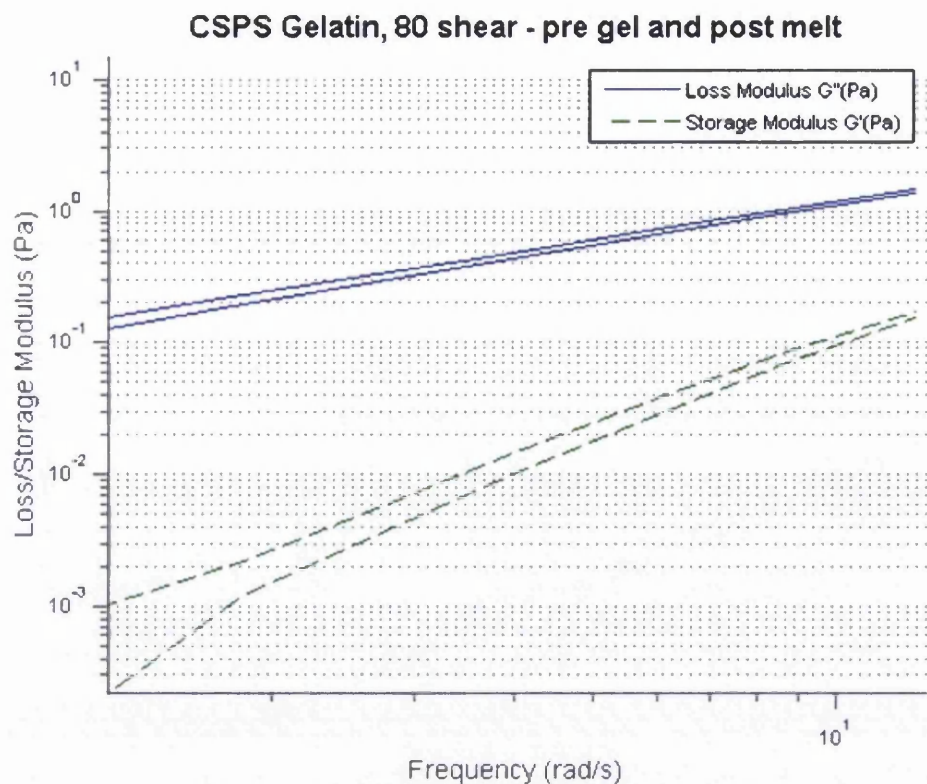


**Figure 3.2.29** - Figure showing the storage and loss modulus through for pre/post gel and gel/melt point of gelatine under  $80\mu\text{Nm}$  constant torque ( $1.6\text{Pa}$  shear stress) plotted against frequency at which it was measured, on the same axis.

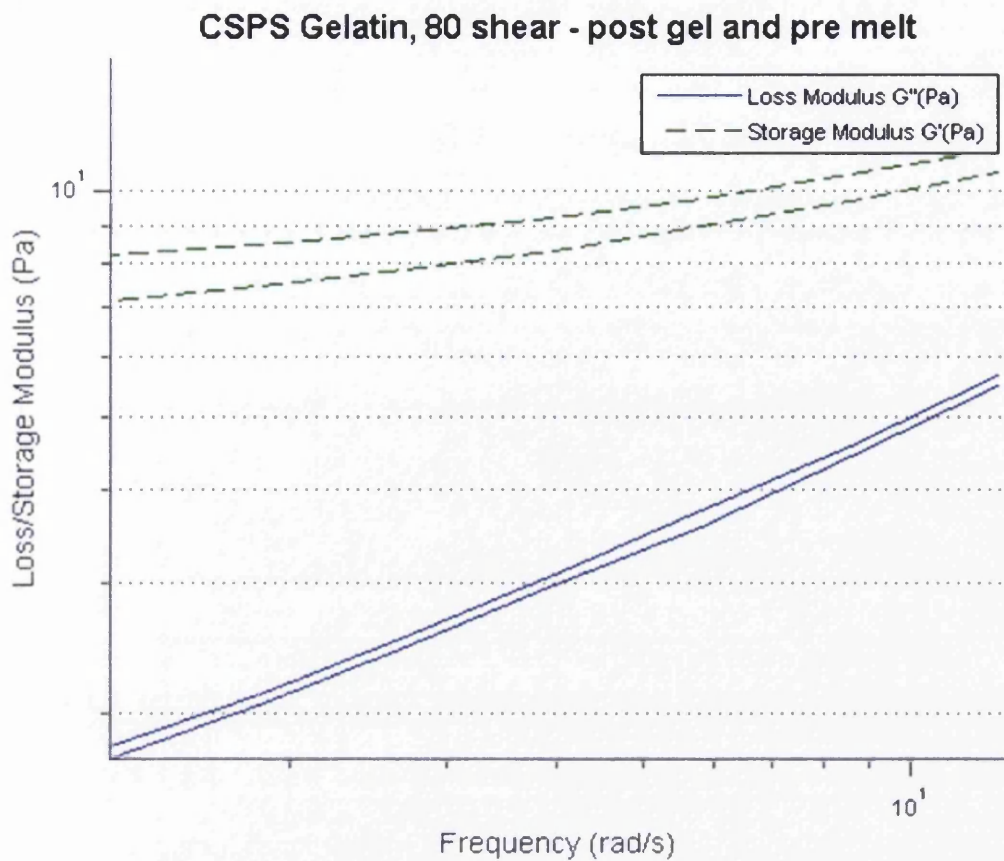


**Figure 3.2.30** - Figure showing the storage and loss modulus through for post gel and pre melt point of gelatine under  $80\mu\text{Nm}$  constant torque ( $1.6\text{Pa}$  shear stress) plotted against frequency at which it was measured, on the same axis.

Figures 3.2.26 to 3.2.30 above begin to suggest an issue with mutation within the sample. The mutation error is evident as the storage and loss moduli are further apart from each other at lower frequencies and closer at higher. This is caused by the positive gradient for gelation and negative gradient for melting and its effect is a greater difference in values at lower frequencies. The mean of both gelation and melting still highlight a change in viscoelastic properties under shear however. Moreover this increasing effect of mutation illustrates that the rate at which  $G'$  and  $G''$  change increases with shear and as this shear

increases its effect is more prominent. This is illustrated further at even higher shears shown overleaf in figures 3.2.31 to 3.2.35.

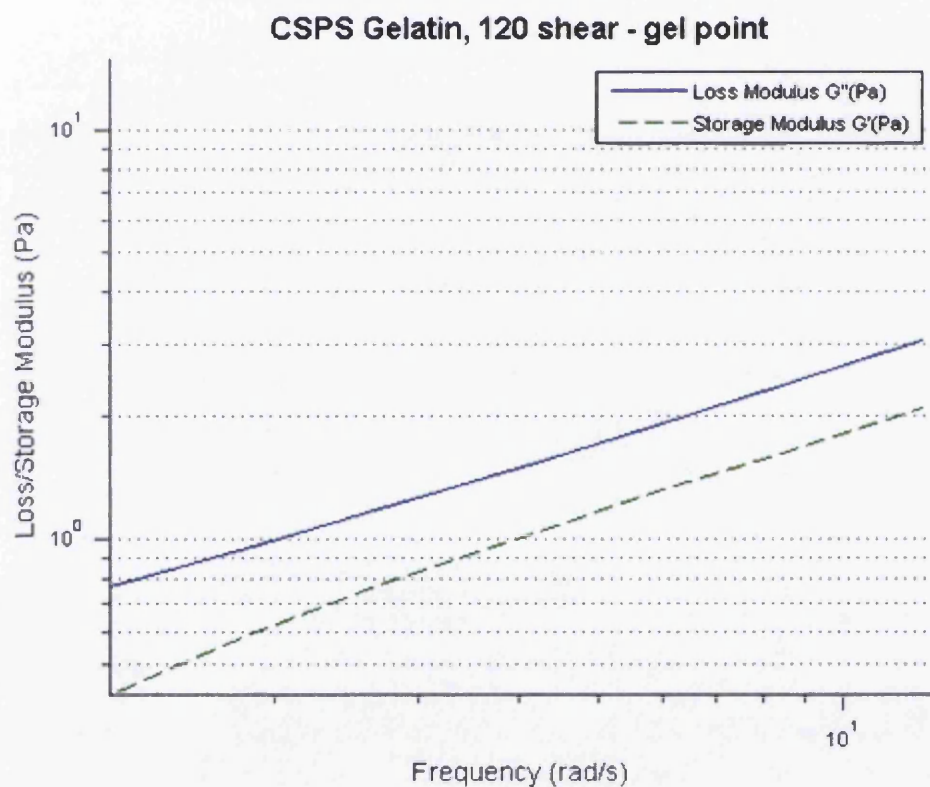
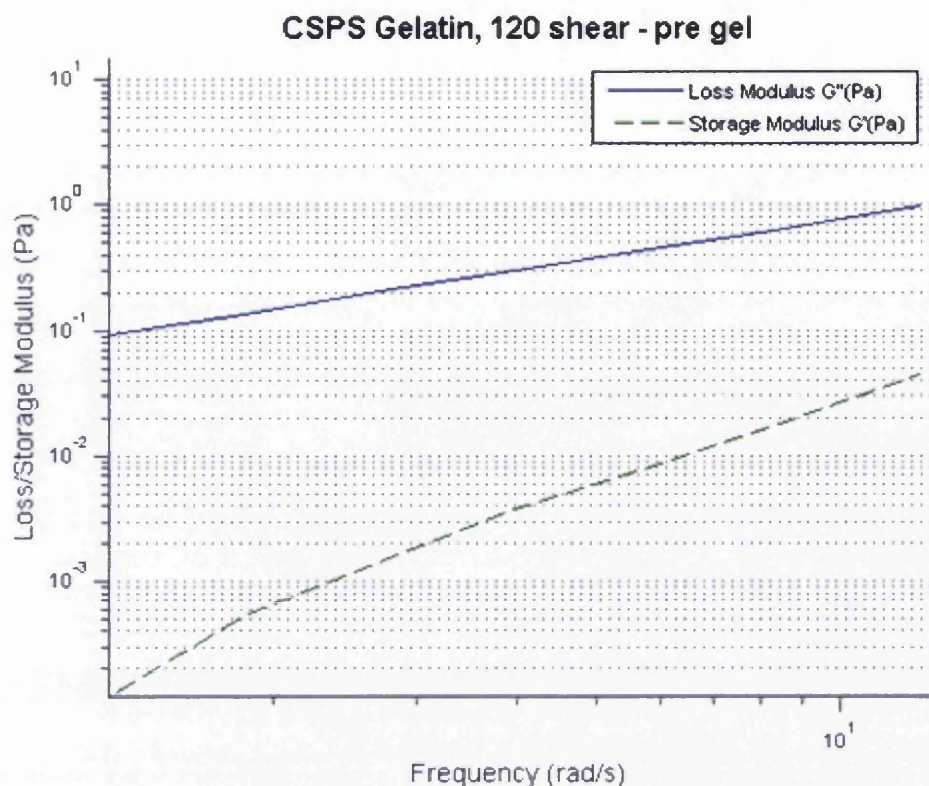


**Figure 3.2.31** - Figure showing the storage and loss modulus through the pre-gel and gel point of gelatine under 120 $\mu$ Nm constant torque (2.4Pa shear stress) plotted against frequency at which it was measured.



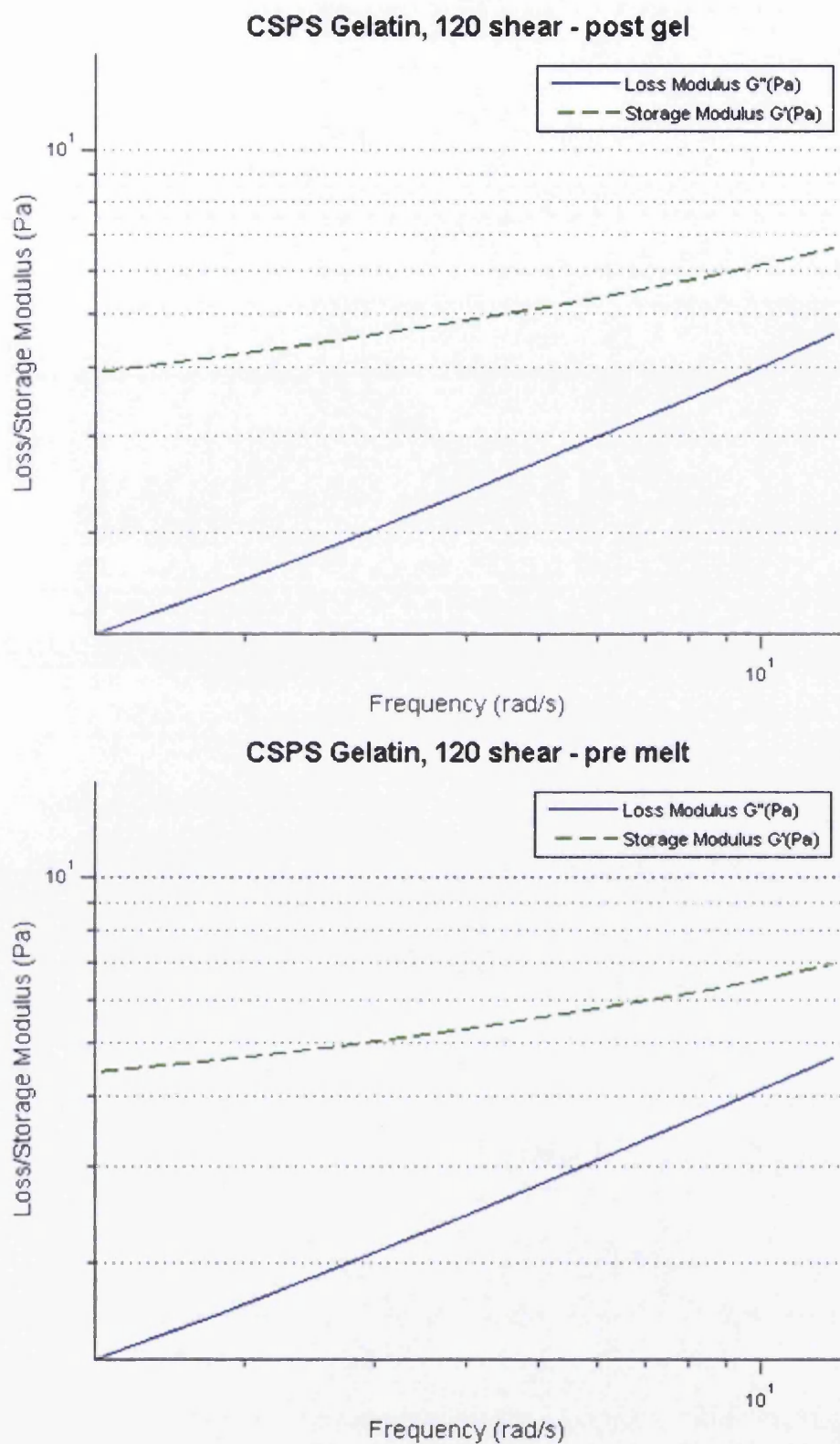


**Figure 3.2.32** - Figure showing the storage and loss modulus through the post gel and pre melt of gelatine under 120  $\mu\text{Nm}$  constant torque (2.4 Pa shear stress) plotted against frequency at which it was measured.

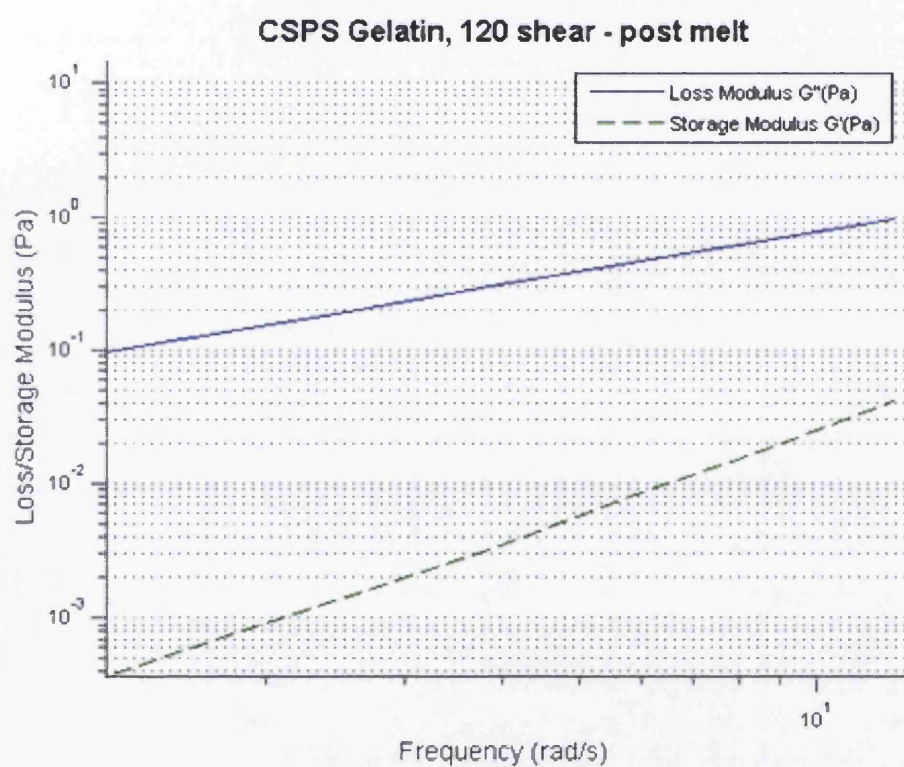
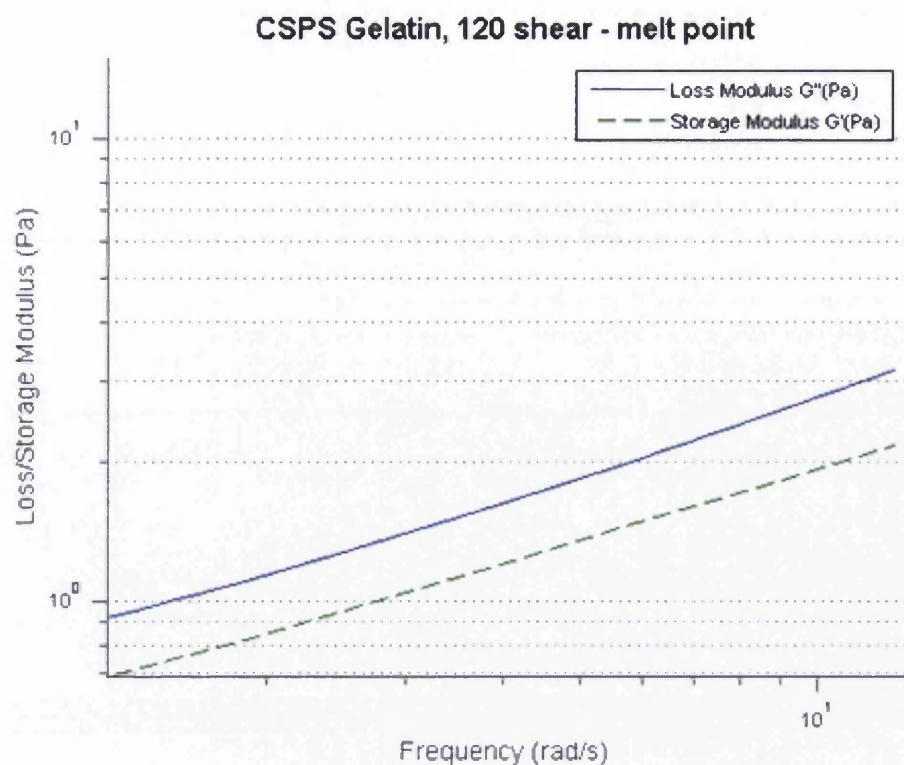


**Figure 3.2.33** - Figure showing the storage and loss modulus through the melt point and post melt of gelatine under 120 $\mu$ Nm constant torque (2.4Pa shear stress) plotted against frequency at which it was measured.

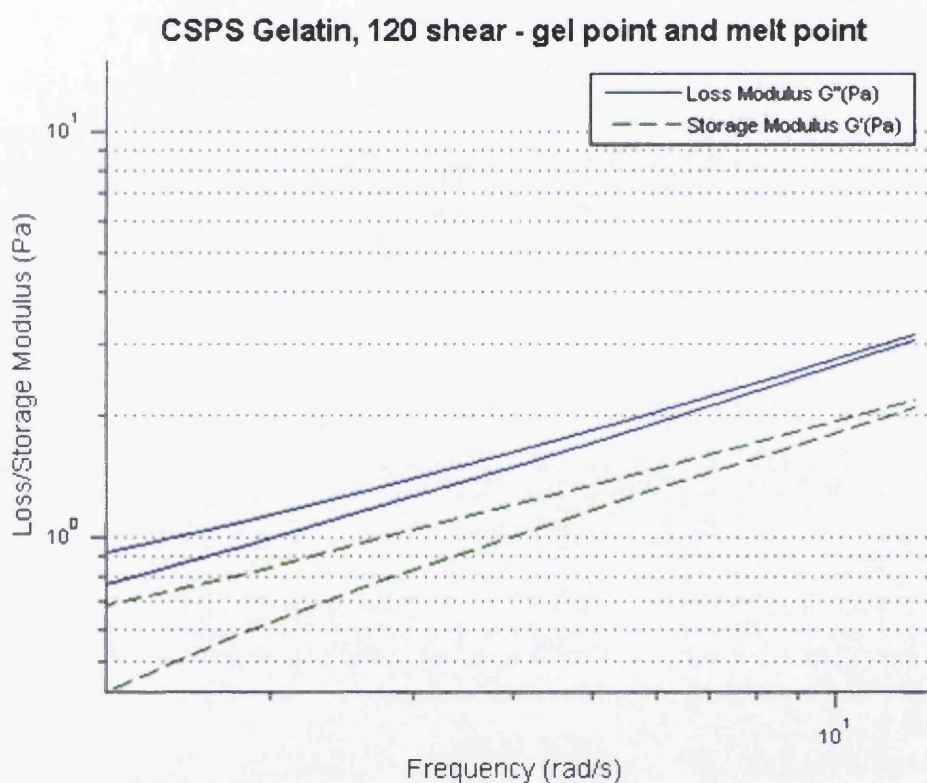
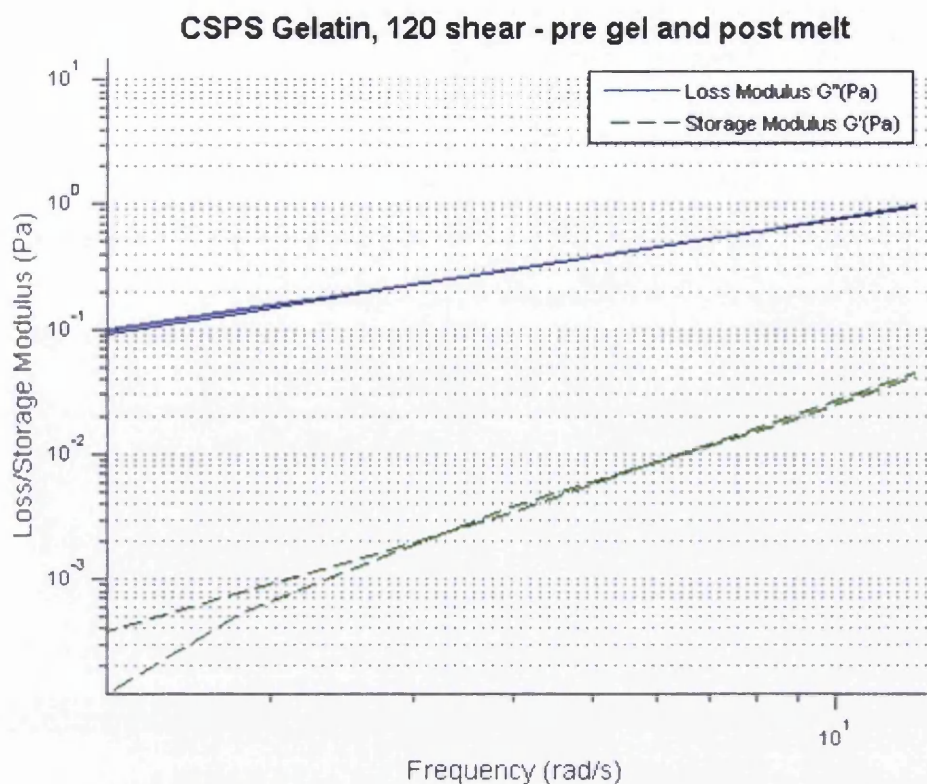


**Figure 3.2.34** - Figure showing the storage and loss modulus through for pre/post gel and gel/melt point of gelatine under  $120\mu\text{Nm}$  constant torque ( $2.4\text{Pa}$  shear stress) plotted against frequency at which it was measured, on the same axis.



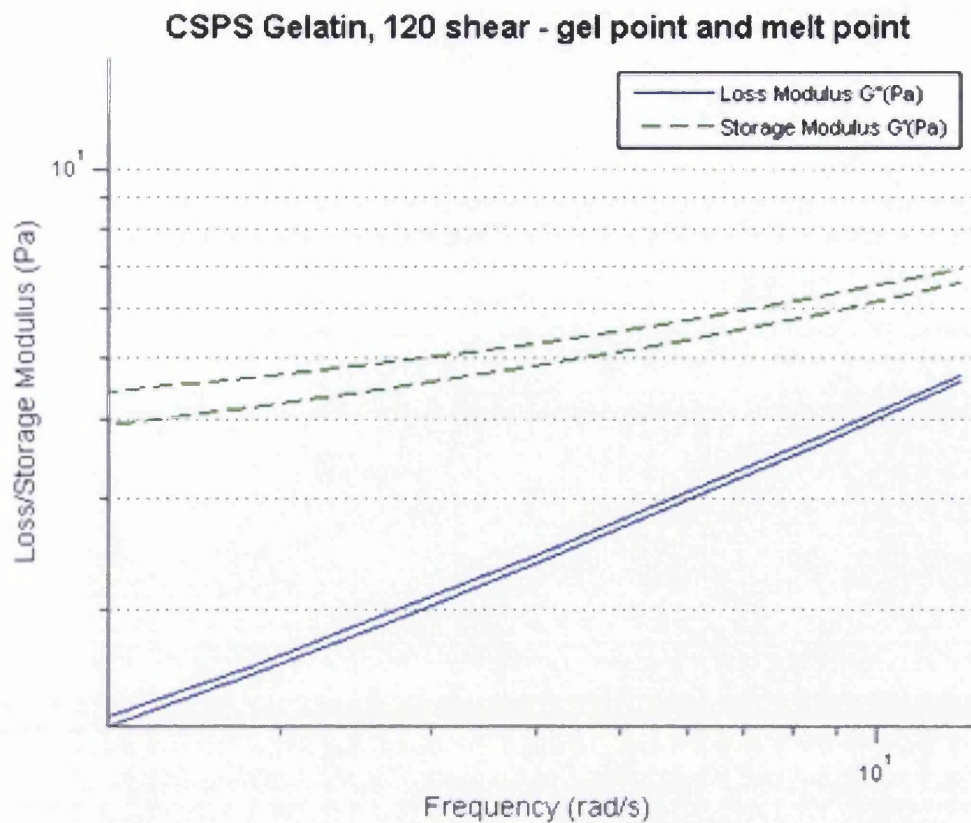


**Figure 3.2.35** - Figure showing the storage and loss modulus through for post gel and pre melt point of gelatine under 120 $\mu$ Nm constant torque (2.4Pa shear stress) plotted against frequency at which it was measured, on the same axis.

Harmonic analysis suggests that for parallel shear stresses above 2.4Pa (120 $\mu$ Nm) there are non-linear effects on the results as well as an increasing mutation issue with the quickening gradient of the moduli. It is clear from the results above that a power law relationship between the storage and loss moduli at the gel and melt point is more difficult to determine and as such a true sol gel transition cannot be established. This greater variance between melt and gel points serve to reinforce that these results are not within the linear viscoelastic range of the sample.

The results for the superposed stress tests with a wider frequency range further illustrate some changes in the gelation and de-gelation of gelatine as shear stress increases. Three exemplar results are illustrated in figures 3.2.37-3.2.39 below, with tabulated data found in table below.

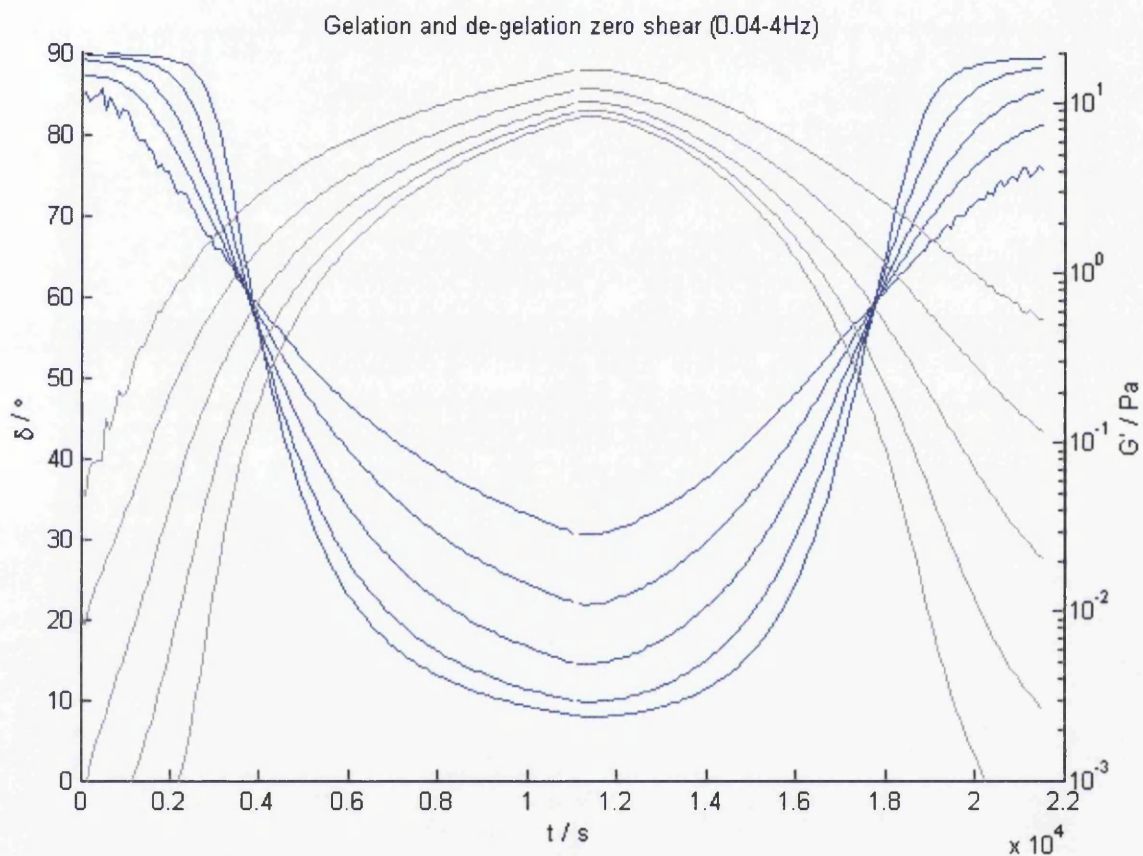


**Figure 3.2.36** - Figure showing the gelation and subsequent de-gelation of gelatine at  $20\mu\text{Nm}$  oscillatory torque and zero controlled flow at five known linear frequencies between 0.04-4Hz – this equates to an oscillatory stress of 0.4Pa.

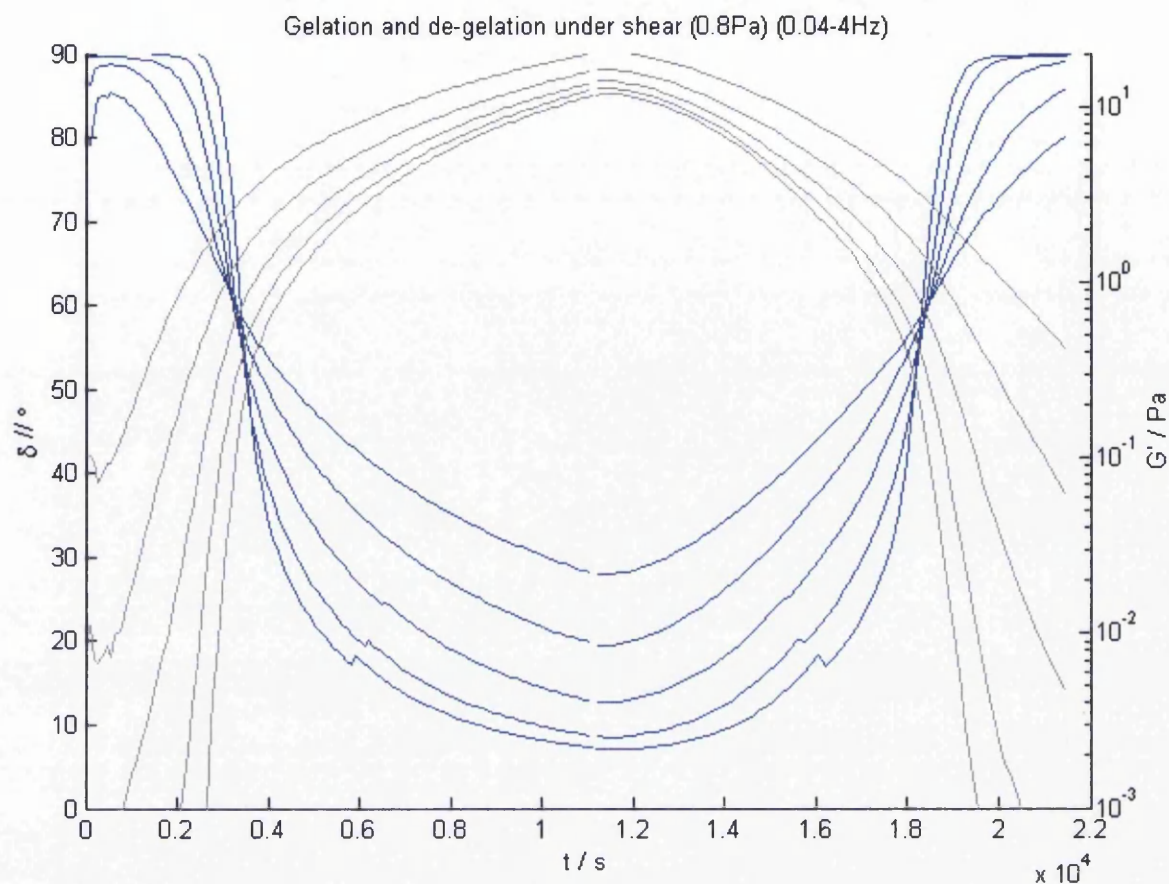


**Figure 3.2.37** - Figure showing the gelation and subsequent de-gelation of gelatine at 40 $\mu$ Nm oscillatory torque and 40 $\mu$ Nm controlled flow at five known linear frequencies between 0.04-4Hz – this equates to an oscillatory stress and a superposed shear stress of 0.8Pa.

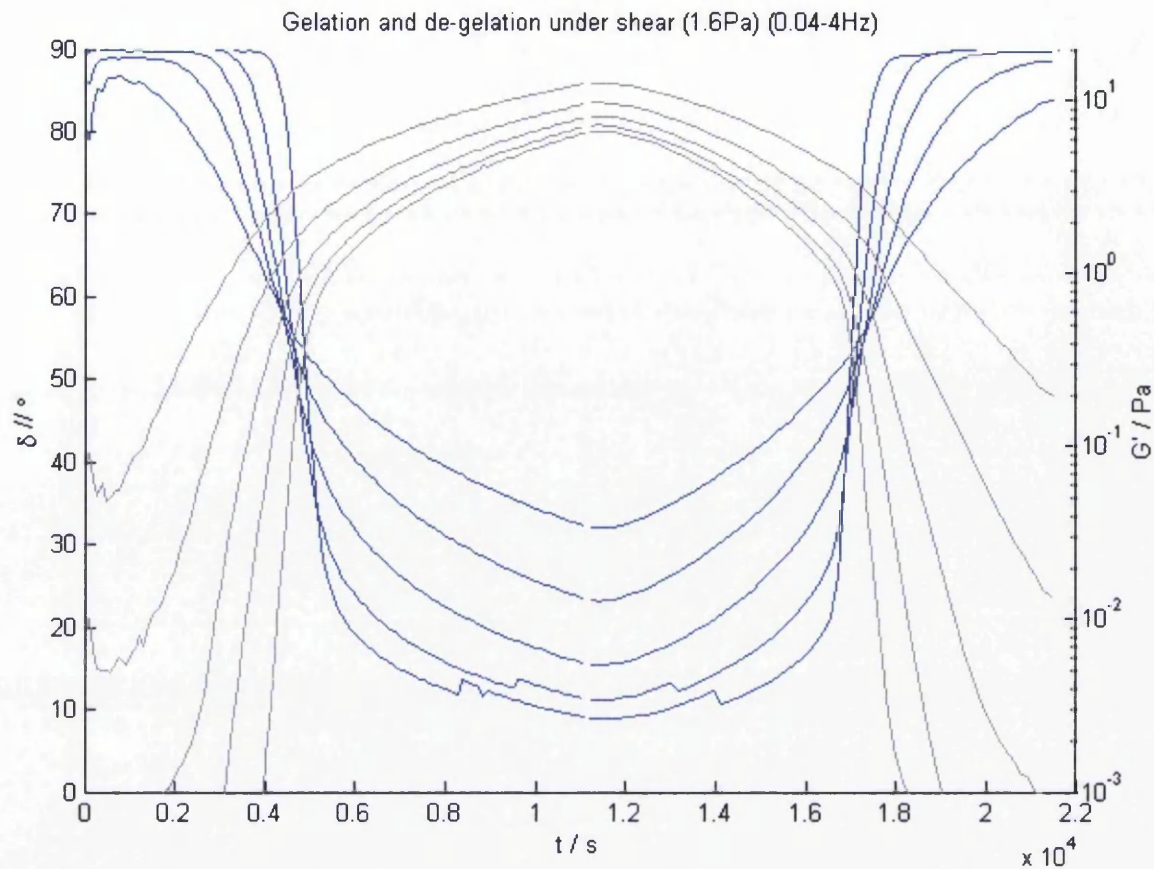


**Figure 3.2.38** - Figure showing the gelation and subsequent de-gelation of gelatine at  $80\mu Nm$  oscillatory torque and  $80\mu Nm$  controlled flow at five known linear frequencies between 0.04-4Hz – this equates to an oscillatory stress and a superposed shear stress of 1.6Pa.

The results appear non-linear above a shear torque of  $60\mu Nm$  (1.2Pa shear stress) as the sol-gel transitional point no longer appears frequency independent. The results are suffering from two noticeable problems:

- The lower frequencies naturally have a steeper gradient going through the gel point transition. As well as this the lower frequencies take longer to measure so the results suffer from an increased mutation effect.



- This problem is amplified when increasing shear – an increase in shear causes an even steeper gradient through the gel point, and lessens the gel time- increasing mutation number further.

So it is not an issue of linearity, moreover an issue of combating the issues brought about by the natural behaviour of gelatine under increased shear, and the increased length of measurement time caused by measuring at a lower frequency. It can be deduced then that at lower frequencies the linearity of gelatine is more sensitive to superposition than at higher frequencies.

The tabulated data is below:

4Hz	G' (Pa) Gel	G'' (Pa) Melt	$\delta$ (°) Gel	$\delta$ (°) Melt	Time (s) Gel	Time (s) Melt
No shear	2.492	2.660	60.39	60.23	3741.19	17811.5
0.4Pa	2.194	2.365	62.77	62.00	3016.59	18370
0.8Pa	2.756	3.011	59.86	59.15	3309.06	18367.9
1.2Pa	2.503	2.648	58.61	57.99	4984.37	16815.4
1.6Pa	2.756	2.895	56.90	57.20	4436.21	17405.3
2Pa	3.326	3.508	56.10	56.62	3297.5	18049.5

**Table 3.2.3** - Table of CSPA gelation and de-gelation of 10% gelatine data between 0.04-

4Hz at five known linear frequencies – values of G' and G'' are taken at 4Hz

In summary we remark on a significant feature of the foregoing experiments which is the increase in the frequency dependence of  $\delta$  (CSPA) in the pre-gel region (VEL) compared with that of  $\delta$  (FS SAOS) in the same region. This phenomena is consistent with previously reported findings that the presence of a unidirectional shear component has greatest effect on measurements performed at frequencies corresponding to shear rates lower than those associated with the background unidirectional shear flow. Hence, decreasing frequency is



expected to generate larger differences between  $\delta$  and  $\delta/\omega$  resulting in a more pronounced frequency dependence of  $\delta/\omega$  than  $\delta$  where the unidirectional shear rate is significant (i.e. only in the pre-gel region).

The most noteworthy outcome of the experiments reported above is that they establish that when conducted under appropriate conditions (in terms of linearity and mutation number criteria) the results of FS (SAOS) and CSPA experiments on a system undergoing rheological transition (from VEL to VES, or *vice versa*) may be taken as indistinguishable. This significant conclusion is drawn on the basis that, during gelation, attainment of frequency independence of  $\delta/\omega$  indicates the same rheological significance (in terms of the GP) as frequency independence of  $\delta$ .

A further (and hitherto unreported) feature of the present experiments is revealed during the transition from a previously gelled VES state back to the precursor VEL state. The significant feature of the latter CSPA results is that they are obtained from experiments in which both the oscillatory strain amplitude and the unidirectional shear field increase progressively during the approach to the rheological transition (SLT).

### ***3.2.3 - The critical gel temperature***

The critical gelation temperature  $T_{crit}$  is of great importance in many process applications as the gelation of gelatine may be indefinitely delayed by maintaining the temperature above this critical value (the gel formation time is then infinitely large). But its accurate determination is not complicated by the fact that the gel time increases exponentially as the temperature  $T$  approaches  $T_{crit}$  (Ferry 1948). The concentration of

gelatine also has a significant effect on the value of  $T_{crit}$  with a quasi-linear relationship between concentration and  $T_{crit}$  (J.E. Eldrige 1954). Several methods have been developed in an attempt to determine  $T_{crit}$  at different concentrations. The simplest (but least accurate) of these involves nonlinear regression of a set of gel times calculated over a range of  $T$  and fitted to an exponential curve. The value of critical gel time is then estimated based on the fit line, beyond the range of the experimental data.

An alternative method requiring a similar data set is also based on extrapolation, however in this method  $t_{gel}$  is plotted with a fractional negative exponent ( $t_{gel}^{-\frac{1}{2}}$ ). When plotted against temperature this forms a straight line that when fit will intersect at the  $T$  axis. This crossover is where  $t_{gel}$  tends to infinity and thus provides an estimate of  $T_{crit}$  (Michon, Cuvelier et al. 1993). Another methodology is to simply cool gelatine using a very shallow temperature gradient such that when the gelatine reaches the gel point it can be assumed that  $T_{crit}$  has been reached. Although it is clear that gelatine will not gel before reaching  $T_{crit}$  there will inherently be a delay between the sample reaching  $T_{crit}$  and the helical gel structure forming thus this method also involves an uncertain estimate.

Tosh and Marangoni (Marangoni and Tosh 2005) have proposed several methods of calculating  $T_{crit}$ , the most accurate of which calculates the absolute value, independent of concentration. By extrapolating  $t_{gel}$  over a range of temperatures and concentrations, with  $T$  on the x axis and  $\log t$  on the y, an intersection of the different extrapolations is found. The authors deem the temperature value at this intersection to be the most accurate estimate of  $T_{crit}$  (Liang Guo 2003).

Given the various uncertainties inherent in, and the *ad hoc* nature of these previously reported procedures for the determination of  $T_{crit}$ , a new and more rigorous approach was developed in the present work. This new method, described below, exploits the use of both FTMS and the newly discovered de-gel frequency independent  $\delta$  behaviour of gelatine during its thermoreversible gel-sol (solid to liquid) SLT transition. Its use in the direct determination of  $T_{crit}$  is reported herein for the first time and is explained below. The key point in the use of this new approach is that de-gelling may be recorded unequivocally on the basis of the previously identified frequency independent loss tangent at the SLT – hence the assessment of successful de-gelling does not require (or rely upon) an operational definition involving the attainment of an arbitrary level of  $G'$ ,  $G''$  or both.

### ***3.2.4 - Gelation and melt using stepwise temperature increase***

As discussed above, the gelation of gelatine at a temperature in excess of 29.25°C takes an inconveniently long time in terms of rheometric experiments and is essentially impractical as drying effects on the gelatine sample become unavoidable. As a novel alternative to this experiment a new approach was proposed which involved recording the de-gelling of gelatine over a range of temperatures close to previous estimates of  $T_{crit}$ . The data presented in Figures 3.2.40-3.2.44 below illustrate the results found through by this new method.

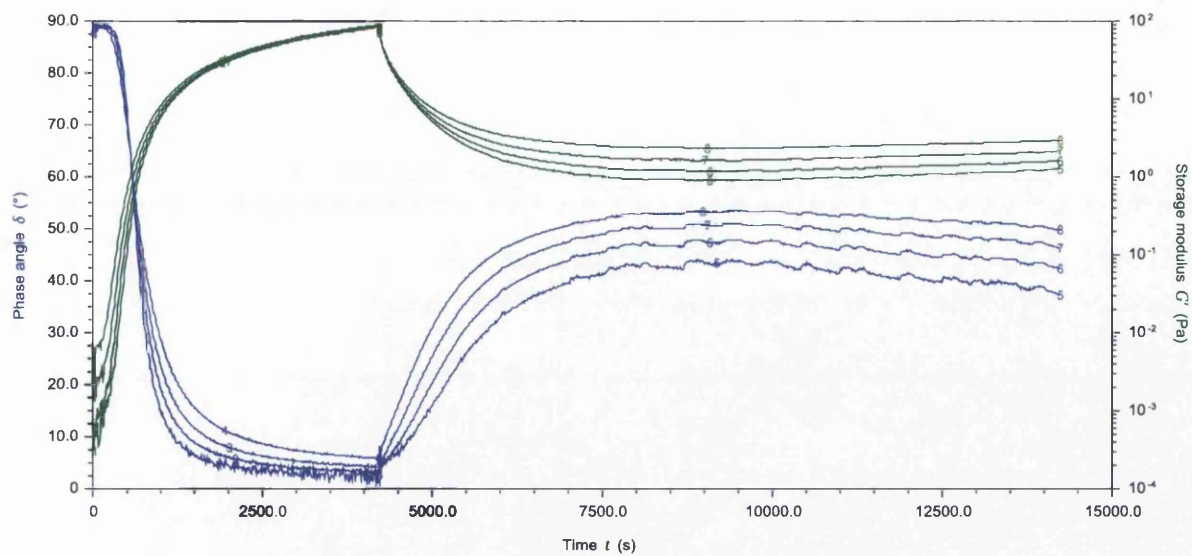


**Figure 3.2.39** - Figure showing the gelation and subsequent stepwise increase in temperature to 28.9°C

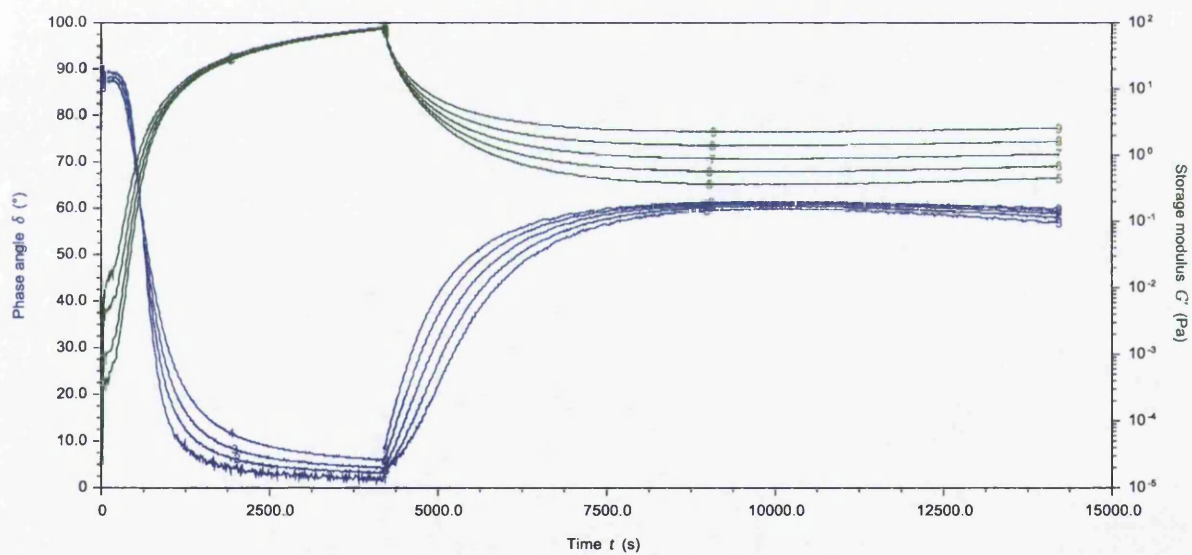


**Figure 3.2.40** - Figure showing the gelation and subsequent stepwise increase in temperature to 29°C

The experiments revealed *no evidence of de-gelation* of the system (from the previously formed gel state) up to a temperature of 29°C. The SAOS frequency sweep shows clearly that over the prolonged experimental time of observation (several hours), the sample maintains its viscoelastic solid-like characteristics (seen clearly in the VES frequency dependence of  $\delta$ ) at this temperature and does not pass through the SLT (solid to liquid transition) which was recorded in previous experiments (see above) at higher imposed post-GP temperatures.

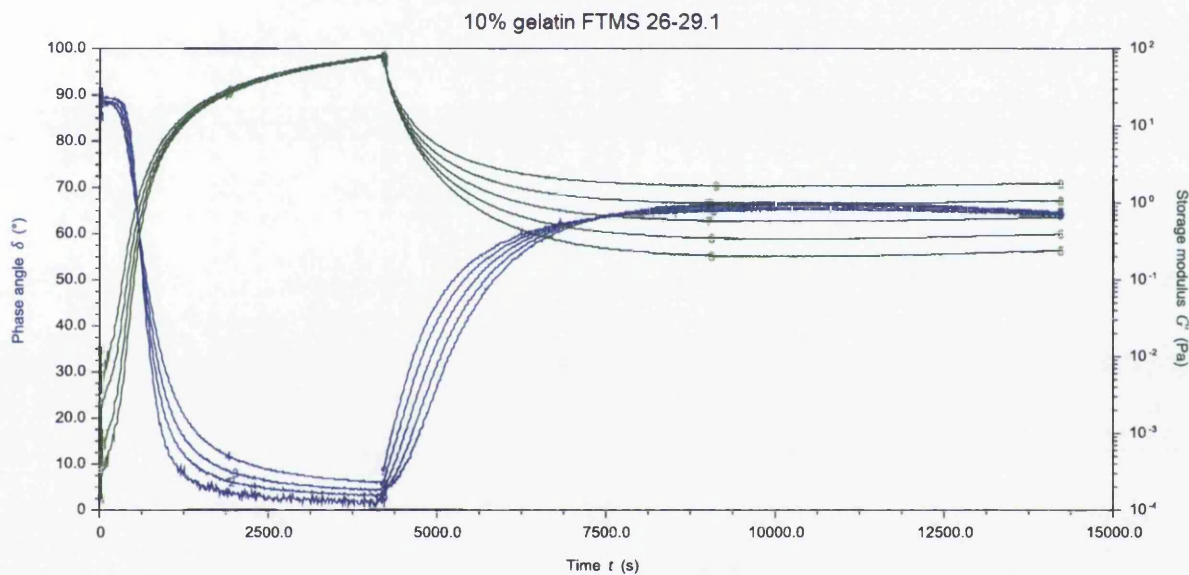


**Figure 3.2.41** - Figure showing the gelation and subsequent stepwise increase in temperature to 29.1°C

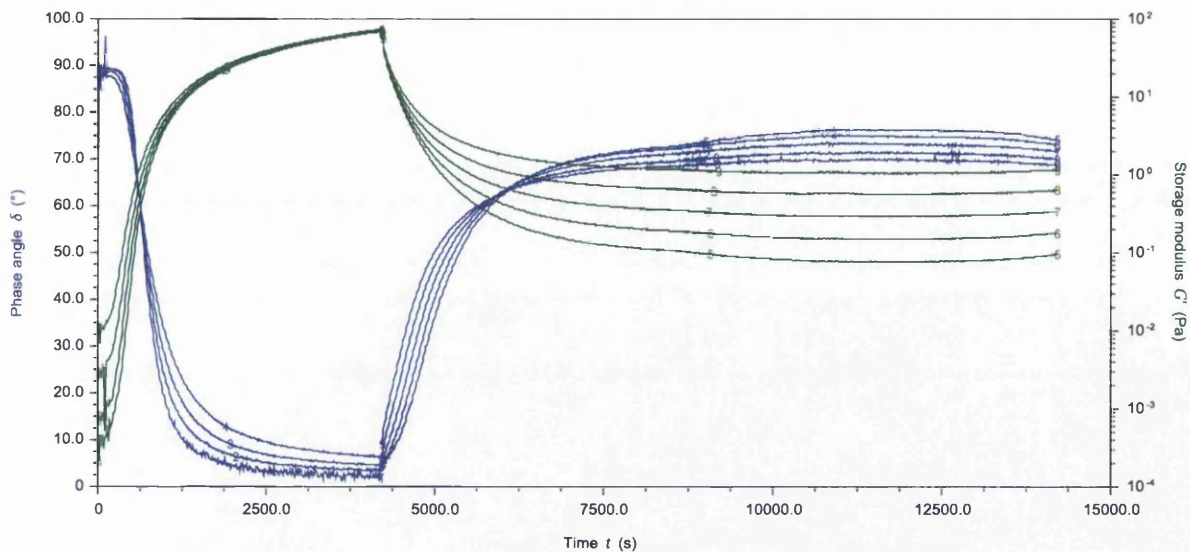


**Figure 3.2.42** - Figure showing the gelation and subsequent stepwise increase in temperature to 29.2°C

Further experiments were conducted at a series of incrementally higher temperatures.

These experiments were carefully conducted with increased values of the gel equilibration time ('soak' time) to ensure the maximum development of the gel's VES characteristics prior to the attempt to induce thermal de-gelling of the system. It is important to note that trial experiments showed that spurious results leading to incorrect assessments of  $T_{crit}$  may be obtained if the soak time is insufficiently long. As an example, the data presented in the figure below appears to show de-gelling at a temperature of 29.1°C. However, previous SAOS results confirm that the GP is attained at this temperature.



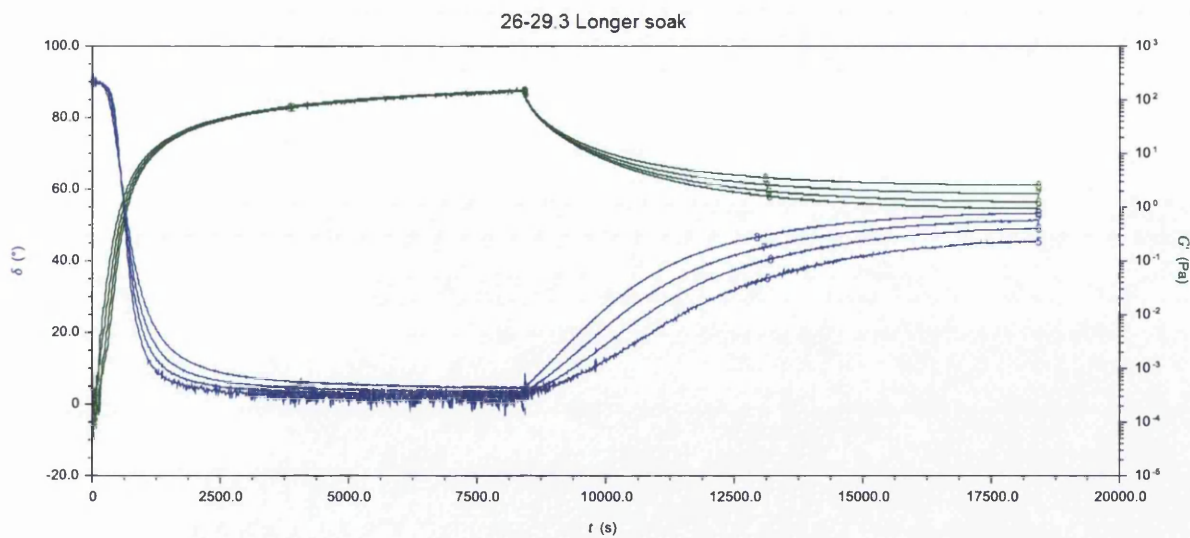


**Figure 3.2.43** - Figure showing the gelation and subsequent stepwise increase in temperature to 29.3°C

The results reveal definitively that at a temperature above 29.4 °C degrees gelatine will exhibit de-gelling. This estimate of  $T_{crit}$  is believed to be the most accurate presently available and is based on the fact that de-gelling may be recorded unequivocally on the basis of the previously identified frequency independent loss tangent at the SLT. This phenomenon is clearly evident in the data presented below in figure 3.2.45, the corresponding time being nearly 5 hours after the imposed temperature increase.

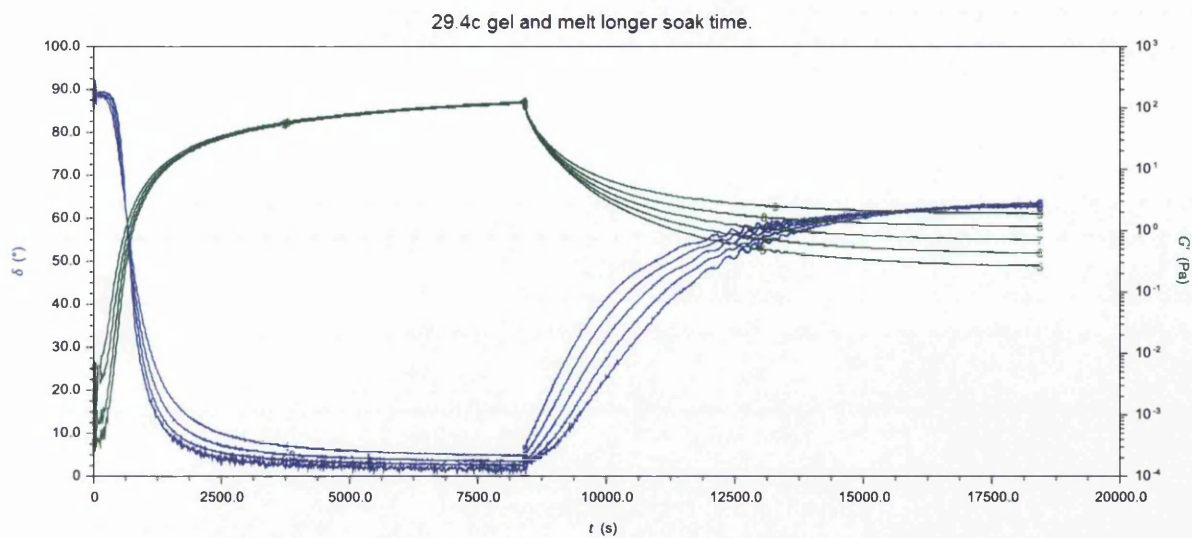


**Figure 3.2.44** - Figure showing the gelation and subsequent stepwise increase in temperature to 29.4°C

Further experiments involved the attempt to form a gel at 29.5°C but this was unsuccessful, with the eventual onset of artefacts due to drying of the sample being encountered. The experiments were terminated after a measurement time of approximately 22 hours (see figure 3.2.46).

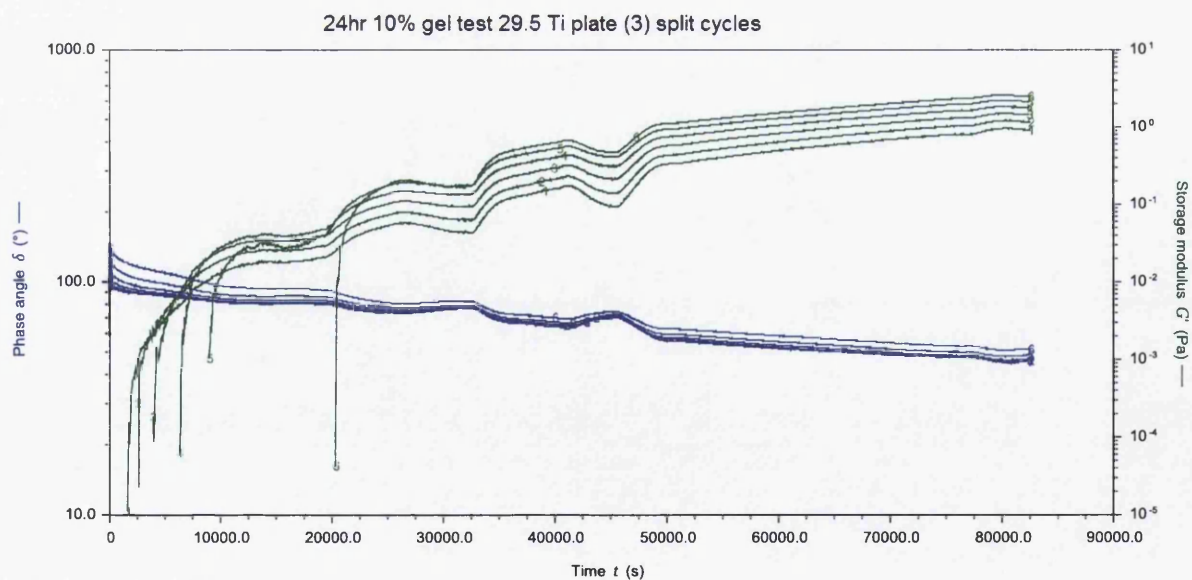


**Figure 3.2.45** - Figure showing an attempted gelation of 10%wt gelatine at 29.5°C



the dynamic shear moduli for a given lowest frequency and presents an optimal signal to noise ratio in the Fourier space. By comparison with the established 'MultiWave' (or FTMS) method, OFR has been shown to be (typically) five-times faster for the same fundamental frequency while giving quasi continuous spectra instead of a few data points. Furthermore, it has been reported that OFR does not present the linear viscoelastic domain problem of the FTMS technique as it avoids the 'additive' strain amplitude problem inherent in the latter technique. The paper on OFR by Ghirninghelli *et al* (Etienne Ghiringhelli 2012) does appear to be based on two serious misinterpretations of previous work. Firstly, the authors use the sample mutation criterion of Winter to assess artefacts as a consequence of changing material properties as the material gels. Such considerations are essential for gelling systems, however, the authors incorrectly apply a critical mutation number of  $N_{mu} = 1$ . The work by Winter identified a critical mutation number of  $N_{mu} = 0.15$  and work by Hawkins *et al.* on gelatine systems identified artefacts where  $N_{mu} < 0.15$ . Hence, the presence of mutation artefacts was not correctly addressed in the OFR study by Ghiringhelli *et al.* Further, the authors include in their manuscript a plot of  $N_{mu}$  as a function of time for several frequencies, but application of the Winter criterion of  $N_{mu} = 0.15$  to this data clearly shows that the data suffers significant mutation artefacts and as such their determination of the GP is likely to be inaccurate. Whilst OFR is compared to FS and FTMS techniques for a PDMS sample, such a comparison is lacking for the alginate sample. Hence, no conclusion regarding the validity of OFR for gelling materials can be made. Moreover, the paper claims that a fractal microstructure was obtained after 60 seconds, but no supporting evidence is given. Further, it should be noted that if (as appears to be the case)

OFR waveforms with a duration of 10 seconds were used to obtain this data it would be significantly affected by mutation artefacts.

Secondly, Muthukumar's theory, which allows the calculation of the fractal dimension of an incipient network cluster from an accurate measurement of the stress relaxation exponent  $\alpha$  (denoted  $\Delta$ ) in the Ghiringhelli work), is applied in the entire post-GP region. The relation is only valid at the GP where both  $G'$  and  $G''$  scale in frequency with identical exponents,  $\alpha$ . The authors present plots of  $G'$  and  $G''$  as a function of frequency for pre-GP, approximate-GP and post-GP, with no evidence for identical scaling exponents being present in any of these plots. Consequently, there is no evidence of the rigorous assessment of the GP claimed by the authors in the paper. Finally, the authors claim that OFR is more accurate than FTMS and that  $G'$  and  $G''$  were determined over a larger frequency range. Presumably the authors mean that OFR has improved frequency content however the range of frequencies is no better than that offered by FTMS. The authors also claim that OFR is 5 times faster than FTMS and appear to have based this on a requirement of 5 periods of data in FTMS analysis.

These points notwithstanding, OFR is a particularly suitable technique for rapidly changing systems such as those in fast gelation systems due to the high amount of frequency information gathered in a relatively short space of time. The OFR waveform is also of particular use to systems that are strain sensitive and where other techniques such as FTMS apply additive strains, OFR does not, allowing operation within the linear viscoelastic range. Accordingly, a series of experiments was devised to assess the application of OFR to a commercially (and biologically) important rapidly gelling, highly strain sensitive system, namely collagen.

#### **4.1.1 – Collagen gels: a biopolymer test system**

Collagen is one of the most common proteins within the human body (A. Ensanya 2013). It provides the strength of structure necessary within human tissues such as muscles and bones. Forming a fibrous structure, collagen consists of a bundle of three parallel, left-handed polyproline II-type helices (Matthew D. Shoulders 2009). Its use outside of the human body is primarily within tissue engineering and 3D cell culture scaffolds due to its inherent biocompatibility (Laura Pastorino 2014). Collagen itself has a wide array of application within tissue culture, both as a bio-coating for surface design (A. Ensanya 2013) as well as a tissue scaffold for the growth and insertion of tissue cultures in structured environments (J. Glowacki 2008, M.W. Tibbitt 2009).

Collagen, like its biopolymer counterpart gelatine undergoes a sol-gel transition at the gel point (GP) in terms of the Winter-Chambon gel criterion (M. Muthukumar 1986, Chambon F 1987). What makes it such a useful tool in the creation of bio scaffolds also allows a rheologically characterisable structure. The only drawback with collagen is that at or near physiological temperatures (28-37°C) the biopolymer networks within collagen form so rapidly as to make rheological analysis challenging with mutation effects causing significant inaccuracy in gel point measurements.

Previous work which aimed to record the rapid gelation of collagen has been performed on pepsin-solubilised collagen (Y. Yang 2009) and does not readily identify a sol gel transition. Work has also been reported for non-pepsin solubilised collagen, however at much lower temperatures (10-12°C) (G. Forgacs 2003). A means of studying the sol gel transition of acetic acid stabilised type I collagen near physiological temperatures is

required. In the present work OFR was chosen as a potential means of meeting this requirement.

#### ***4.1.2 – The OFR technique - improving on FTMS***

In Chapter 1 the basic aspects of FTMS were described. We take this as a basis for the development of a methodology for assessing the validity of OFR in its application to determining the GP of rapidly changing systems. Multi wave tests such as FTMS combine sine waves and apply them to a sample over the time period of the lowest frequency. The stress 'response' of the sample is then also a multi-wave waveform. Both of these waveforms can be analysed using a Fourier transform function This processes use on linear viscoelastic materials is outlined by Holly EE (Holly EE 1988) to determine the complex modulus  $G^*$  through decomposed components of a multi-wave waveform, composed of a base frequency and additive constituent harmonics.

Using a Fourier transform function with phase data the frequencies and amplitudes of both the strain and the corresponding stress waveforms are calculated along with their respective phases. By comparing these phases the phase angle at each frequency can be calculated. Calculation of  $G'$  and  $G''$  is also possible, the methodology of this measurement through a Fourier transform of a multi-wave waveform being reported by Holly et al (Holly EE 1988). The main points are now explained below.

Performing a Fourier transform on stress waveform data for the harmonic integers ( $m$ ) the resultant frequencies are illustrated in equation 4.1.1 below:

$$\sigma = \sum_{i=1}^m \sigma(\omega_i) = \sum_{i=1}^m (A_i \sin \omega_i t + B_i \cos \omega_i t)$$

**Equation 4.1.1** – Expression of component frequency and amplitude from a multi wave waveform

Where  $A_i$  and  $B_i$  are Fourier constants. The loss tangent between the stress and strain component waveforms can then be given by equation 4.1.2 below:

$$\tan \delta(\omega_i) = \frac{B_i}{A_i}$$

**Equation 4.1.2** – An expression relating loss tangent with Fourier constants

The storage and loss modulus are then calculated using the expressions below, which are derivations of similar equations discussed in the SAOS section above.

$$G'(\omega_i) = K_\sigma(\omega_i) \cos \delta(\omega_i) / \gamma(\omega_i)$$

**Equation 4.1.3** - Storage modulus calculation from FTMS data

$$G''(\omega_i) = K_\sigma(\omega_i) \sin \delta(\omega_i) / \gamma(\omega_i)$$

**Equation 4.1.4** – loss modulus calculation from FTMS data

Where the value  $K$  is a scaling factor of the geometry for the rheometer, and is calculated experimentally.

At present the system in place on most rheometers is to use the harmonics of the lowest frequency as the additional waves in a multi wave test (ie when the lowest frequency is 0.4Hz the other waves added to form the multi wave will be 0.8Hz 1.2Hz etc). This however has a number of limitations.

One primary limitation is that when trying to apply a multi-wave to a sample over a specific frequency range there is a limitation of harmonics available. As an example for a frequency range of 0.4-2Hz there are 5 available harmonics, whereas there are theoretically limitless anharmonic frequencies.

Typically the more frequencies in a multi-wave waveform the higher the peak strain, this is caused by frequencies within the waveform having a positive or negative gradient simultaneously. As the waveforms have to be harmonics there are only a few ways to optimise the system to decrease the peak strain. A high peak strain may interfere with the structure of strain sensitive samples and give an inaccurate representation of the viscoelastic properties of the sample due to the composite test waveform exceeding the LVR. As this is undesirable, lowering the peak strain is critical. One method involving harmonic waveforms is to alter the phase of these harmonics manually, such that their gradients do not interfere over the time period resulting in a high peak strain. Hence, the resultant peak strain (or stress) can quickly exceed the linear viscoelastic range for strain sensitive biopolymer systems even where a modest number of harmonics are employed (P. Evans 2008).

#### ***4.1.3 - The OFR waveform***

The OFR technique was developed from the field of acoustics by Ghiringhelli et al (Etienne Ghiringhelli 2012). The principle of OFR is to apply a waveform that is exponentially increasing in frequency from low to high on a sample then to utilise Fourier analysis to extract the relevant viscoelastic information from the material. The input signal wave is characterised by:

$$\gamma(t) = \gamma_0 \sin \left( K \left( e^{\frac{t}{L}} - 1 \right) \right)$$

*Equation 4.1.5– input wave equation for OFR*

$$\text{Where } K = \frac{T\omega_2}{\ln\left(\frac{\omega_2}{\omega_1}\right)} \text{ and } L = \frac{T}{\ln\left(\frac{\omega_2}{\omega_1}\right)}$$

The lowest and highest limit of frequency within the waveform are  $\omega_1$  and  $\omega_2$  respectively and T is the duration of the waveform. The waveform begins oscillating at  $\omega_1$  and cycles exponentially to  $\omega_2$  such that more of the wavelength time is spent on lower frequencies (that have less amplitude and therefore harder distinguish peaks within a fourier transform). An example of an OFR input wave can be seen in figure 4.3.1 below:

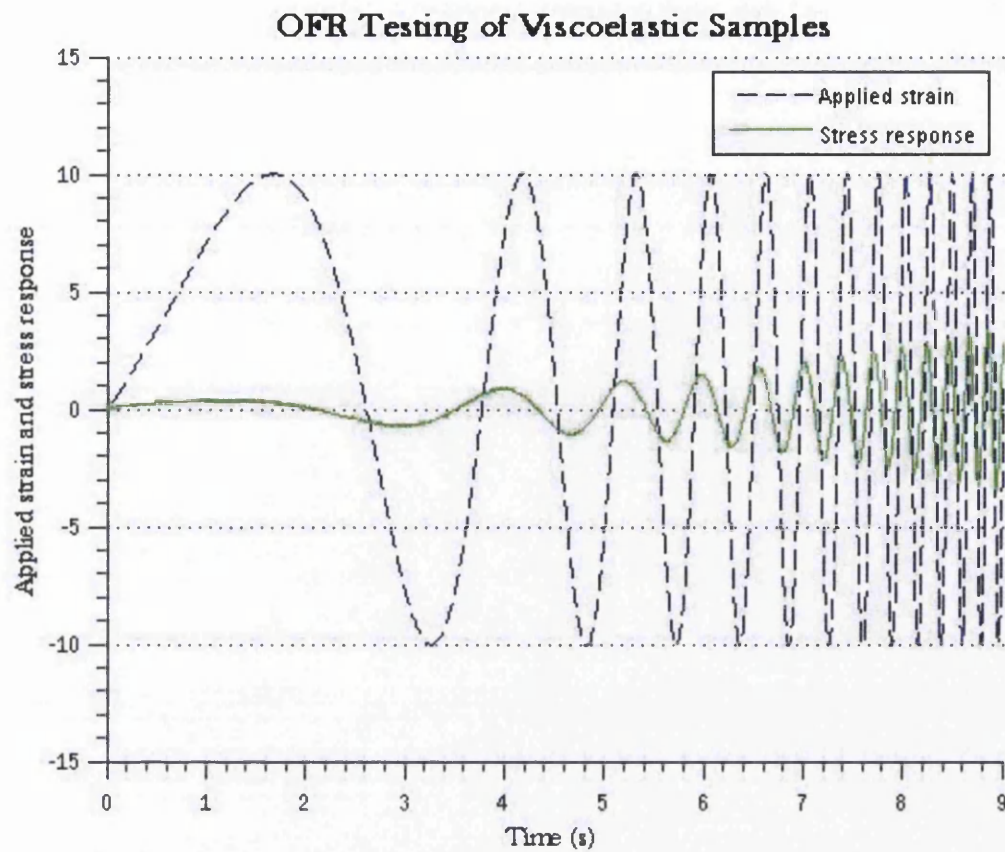


**Figure 4.1.1** - Figure showing a typical applied OFR strain waveform and its subsequent stress response against time

The duration of the waveform will affect the resolution of the Fourier analysis and as such a time period equal to that of the lowest frequency can effectively be used to create the shortest time with reasonable resolution. Operating within the linear range, a viscoelastic material is defined by Ferry (Ferry 1980) as:

$$\tau(t) = \int_{-\infty}^t G(t-t') \dot{\gamma}(t') dt' = (G * \dot{\gamma})(t)$$

Equation 4.1.6



where half space convolution is ' $\ast$ '. Using the convolution theorem:

$$\tilde{\tau} = i\omega \tilde{G}(\omega) \tilde{\gamma}(\omega)$$

Equation 4.1.7

Using Phan –Tien (Phan-Tien 2002)

$$\tilde{G}(\omega) = \int_0^{\infty} G(t) \cos(\omega t) dt - i \int_0^{\infty} G(t) \sin(\omega t) dt = \frac{G''(\omega)}{\omega} - i \frac{G'(\omega)}{\omega}$$

Equation 4.1.8

$$\text{Thus } \tilde{\tau}(\omega) = G^*(\omega) \tilde{\gamma}(\omega)$$

Equation 4.1.9

Where  $G^*$  is the complex modulus. This allows the complex moduli to be calculated using:

$$G'(\omega) = \text{Real} \left( \frac{\tilde{\tau}(\omega)}{\tilde{\gamma}(\omega)} \right) \quad G''(\omega) = \text{Imag} \left( \frac{\tilde{\tau}(\omega)}{\tilde{\gamma}(\omega)} \right)$$

Equation 4.1.10

Through the calculation of  $G'$  and  $G''$  (see figure 4.3.2), a value of delta over the entire range of frequencies can be calculated.

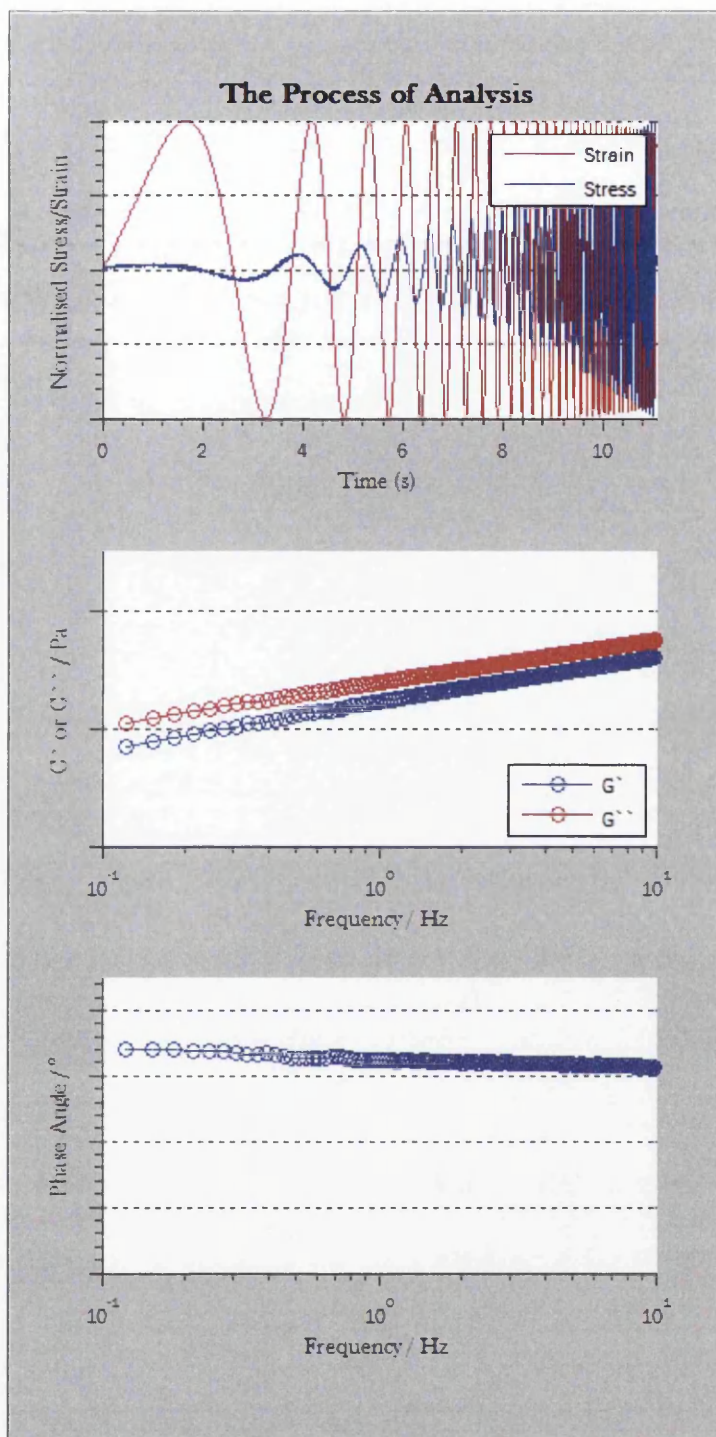


**Figure 4.1.2** – Figure showing the process of OFR analysis from experimentally gained strain/stress waveforms (top) through to storage/loss moduli calculation (middle) and finally phase angle calculation (bottom)

## **4.2 - Materials and Methods**

### **4.2.1 - Sample preparation**

#### **4.2.1.1 - Gelatine**

Gelatine was made up as a weight percentage from general purpose gelatine powder (supplied by Fisher). 30wt% gelatine was used as when using arbitrary waveforms it was necessary to ensure that there was a large stress response within a single waveform during the pre-gelation stage of measurement. Although lower concentrations could potentially have been measured, a high concentration was chosen to ensure the associated mutation issues with this method were negated.

The gelatine powder was mixed with distilled water to the correct concentration and heated in a water bath at 60°C under agitation for 5 minutes. The sample was left in the water bath for 45 minutes being agitated intermittently every 10 minutes to ensure a homogenous gelatine solution. This gelatine solution was then separated into single use aliquots and refrigerated. The aliquots were then heated in a water bath at 60°C for 45 minutes before being loaded onto the peltier base plate of the strain controlled ARES G2 (TA instruments) which was during loading/before test initiation set at 60°C also. The rheometer geometry was then lowered as the base plate was set to spin at 1rad/s to ensure an even loading of the sample. The geometry used was a 40mm titanium plate. Once the head was lowered the free surface of the sample was coated in low viscosity silicone oil (9.5 mPa.s) which prevented the sample drying at the high temperatures as well as having the added benefit of negating any surface tension effects of the gelatine solution with the air (the surface tension of gelatine solutions is significantly higher than that of low viscosity silicon oil and more comparable to that of water (James Hallewell Johnston 1925). The operating

gap was selected as 200 to minimise sample inertia effects while maintaining sufficient sample for the measurement of bulk flow properties. The sample was then lowered to the test temperature as the temperature began.

#### ***4.2.1.2 - Collagen***

High concentration type I rat tail collagen (RTC) (10 mg/ml, BD Bioscience) held in solution using acetic acid, distilled water and 1M NaOH (Fluka) was placed on ice. The high concentration collagen needed to be diluted to the required concentration and neutralised to a basic pH of 7.4 to allow the polymerisation to occur. 10x Phosphate Buffered Saline (Fluka) was used as a buffer and the required amount of distilled water (to create the correct concentration) and NaOH was added to neutralise the acetic acid within the RTC, allowing it to initiate gelation. The precise values depended on the concentration of collagen required and calculations based upon the manufacturer's instructions.

The rate at which collagen gels is highly affected by temperature (G.C. Wood 1960), with very low temperatures slowing the gelation process to a near standstill. The sample therefore is kept on ice briefly before loading and then loaded onto the peltier plate of the strain controlled ARES G2 (TA instruments) at a set temperature of 5°C. As before the rheometer geometry was then lowered as the base plate was set to spin at 1rad/s to ensure an even loading of the sample. The geometry used was a 40mm titanium plate. Once the head was lowered the free surface of the sample was coated in low viscosity silicone oil (9.5 mPa.s) to prevent evaporation and negate surface tension effects. The operating gap was selected as 200 to minimise sample inertia effects while maintaining sufficient sample for the measurement of bulk flow properties. For the collagen tests, viscoelastic properties

were monitored simultaneously to raising the temperature so that there was no delay in obtaining results for collagens very fast gelling system.

#### ***4.2.2 - Low frequency FTMS***

Fourier transform mechanical spectroscopy is a programmed feature in TA instruments rheometry software, TRIOS. Using TRIOS software to run FTMS waveforms on a sample, however, was not employed. This is because even when selecting one cycle and zero conditioning time for the sample, a 'processing time' delay occurs between two successive measurements. Although this delay is only approximately four seconds, when dealing with extremely fast gelling systems such as collagen or high concentration gelatine at low temperatures this delay can cause significant errors. It was necessary therefore to program the waveforms to be input consecutively, for a set time, using the instrument's TRIOS arbitrary waveform generator tool. This allowed the waveforms to be analysed off-line in the post experiment period without any delay caused by calculation.

The low frequency FTMS waveform consisted of four frequencies, the carrier of which was 0.2Hz. Its 4<sup>th</sup> 8<sup>th</sup> and 16<sup>th</sup> harmonic (0.8, 1.6 and 3.2Hz respectively) was added to the waveform. The carrier frequency had a strain of 10% whereas all the harmonics had a set additive strain of 5% each. Over the course of one waveform the peak strain of the low frequency FTMS wave totalled 21% which is within the LVR for 30wt% gelatine both as a liquid and as a gel (see figures 4.2.1 and 4.2.2 below).

This was tested on gelatine at a range of different temperatures to investigate both mutation effects and to compare FTMS techniques with OFR techniques that cover a similar frequency range.

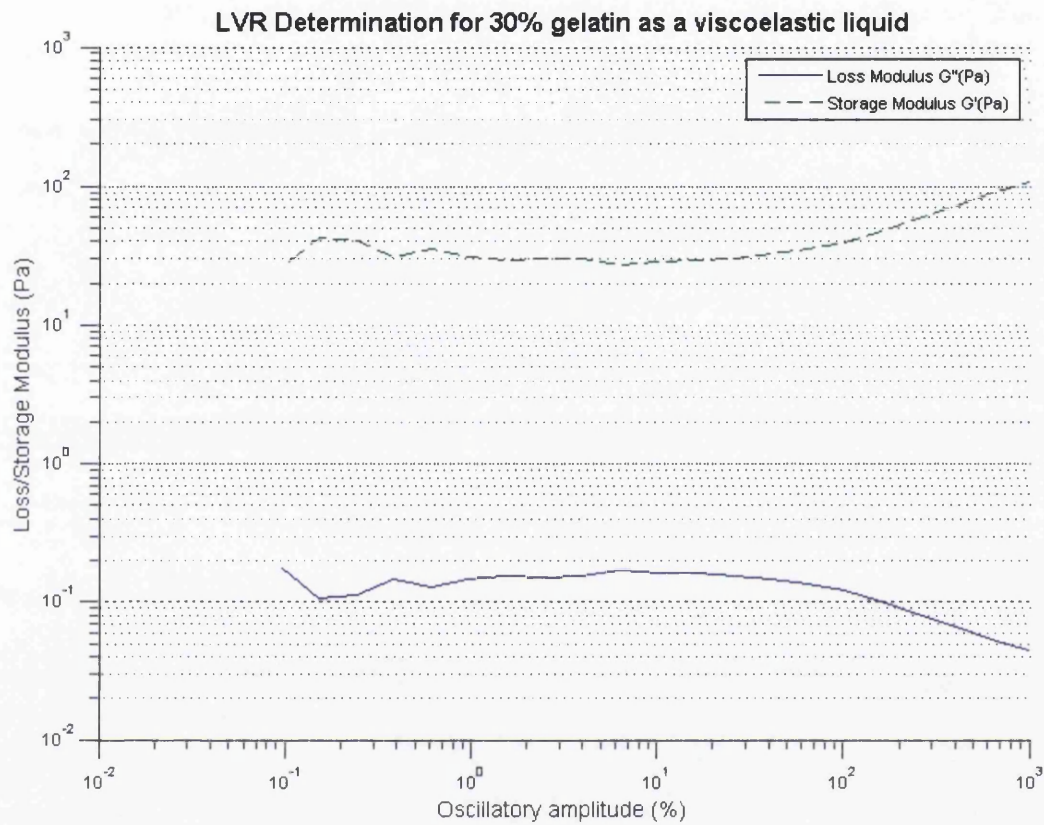


**Figure 4.2.1** - Figure showing the determination of the Linear viscoelastic range for molten 30%wt gelatine –It is evident that measurements deviate from the LVR after an oscillatory strain of 40%

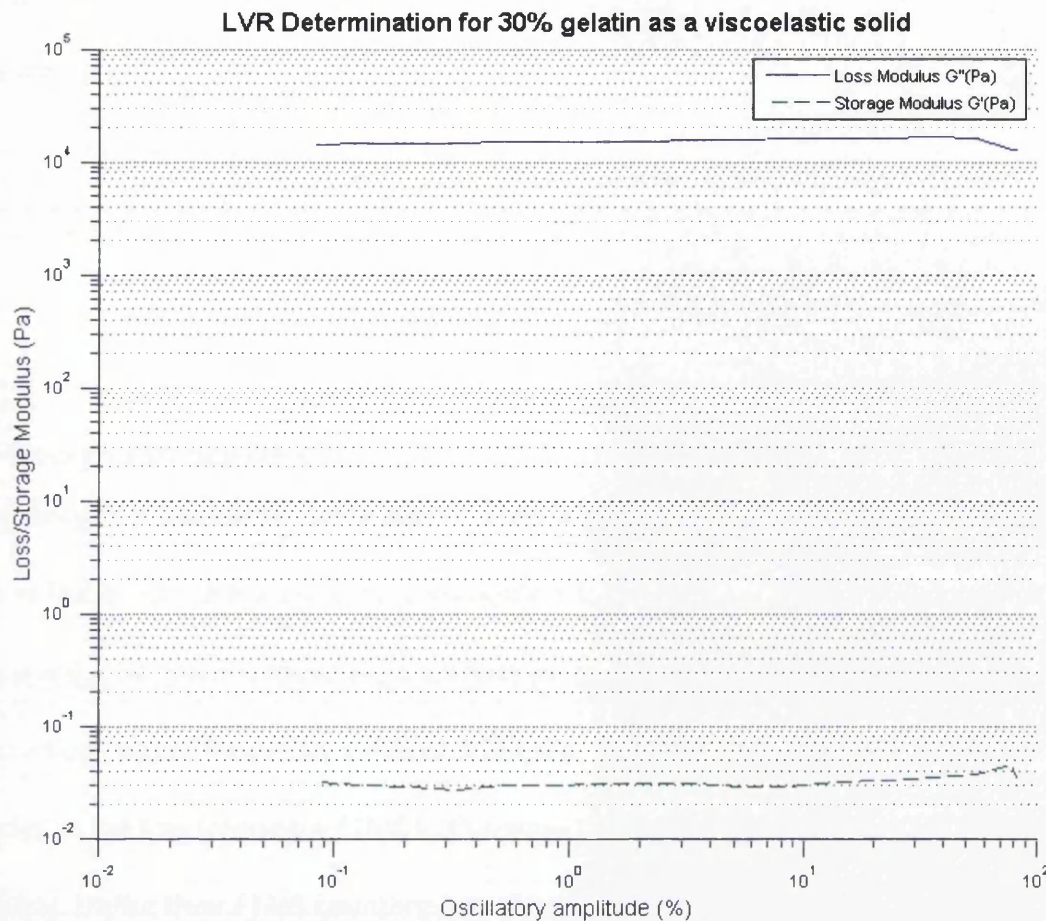


**Figure 4.2.2** - Figure showing the determination of the Linear viscoelastic range for solid

30%wt gelatine –It is evident that measurements deviate from the LVR after an oscillatory strain of 400%

### 4.2.3 - High Frequency FTMS

High frequency FTMS implemented through the standard TRIOS software suffers from a time delay which affects the results to a much greater degree than that of lower frequency runs (see above). Consequently the implementation of high frequency FTMS was also performed using the arbitrary waveform generating tool within TRIOS. A carrier frequency of 1Hz was selected with a strain of 10% and its 4<sup>th</sup>, 7<sup>th</sup> and 10<sup>th</sup> harmonic (4, 7 and 10Hz respectively) was added to the waveform each with a strain of 5% each. The total peak

strain of one cycle of this waveform was 24% which is again within the limit of the LVR for 30wt% gelatine as both a liquid and as a gel. The high frequency FTMS was used as a comparison for high frequency OFR and to investigate if both techniques suffer from mutation in the same way given their differing methodologies and analysis.

#### ***4.2.4 - Low frequency OFR***

Low frequency OFR waveforms were also created within the arbitrary waveform generator function in TRIOS. The OFR waveform (commonly referred to as a 'chirp' signal) began at a frequency of 0.2 Hz and increased exponentially in frequency over the successive 5 second period to a final, upper frequency value of 3.2Hz (i.e. covering the same range of frequencies as the low frequency FTMS in the same time period to allow for a direct comparison). Unlike their FTMS counterparts, the OFR waveforms could not be allowed to reach steady state as the waveform simply increases in frequency until the instrument's recording hardware fails due to buffering capacity. As such it was deemed prudent to specify the input of a conditioning time (of 5 seconds duration) between each successive application of the OFR waveforms to the sample. This step allowed the analysis of the OFR waveforms without the requirement for applying a windowing function to the signal. Avoiding this reduced the latency effect associated with the instrument's relatively low memory write capability, the instrument being found to be near the limit of how much data it could save and write simultaneously during the OFR tests. The strain of the waveform was set at 10%, significantly lower than that of FTMS, but sufficient for a response wave with adequate resolution for the high viscosity 30wt% gelatine samples. The inclusion of a conditioning time ensured that the OFR waveform was periodic and hence no discontinuity



errors (usually dealt with by including a windowing function) were present. As per FTMS analysis, the dynamic rheological parameters  $G'(\omega)$  and  $G''(\omega)$  were recorded as a function of time and frequency before being passed to the GP identification routine. OFR analysis was performed using Matlab (The MathWorks). No inertia correction was deemed necessary during the OFR analysis procedure.

#### ***4.2.5 - High frequency OFR***

As with all other waveforms the arbitrary waveform generator function of TRIOS was used to generate high frequency OFR waveforms. The chirp began at a frequency of 1Hz and cycled exponentially up in frequency to 10Hz over the course of 1 second so as to make it directly comparable to the high frequency FTMS waveform. The conditioning time was lowered to 1 second for the high frequency OFR so as to suit it towards faster gelling systems. Again the strain of the waveform was set at 10%. The FTMS and OFR waveforms were then analysed in MATLAB (The MathWorks) (see below for details).

#### ***4.3 - FTMS and OFR waveform analysis***

The arbitrary waveform gives a simple raw stress output wave to correlate with the applied strain input wave. For FTMS analysis the simple process of applying an FFT function in MATLAB on both the stress and strain will allow calculation of viscoelastic parameters  $G'$  and  $G''$ . The application of an FFT over the multi-wave for a length of time set at  $1/\text{carrier frequency (Hz)}$  yields both real and imaginary parts at varying frequencies and amplitudes.  $G'$  at any applied frequency is simply the value of the real part of the FFT of the stress

response at that same frequency over the FFT of the strain waveform also at that frequency.

$G''$  is the same process but for the imaginary part of the fourier transform see equations 4.3.1 and 4.3.2 below (G.C. Wood 1960). For the FTMS data a Bartlett windowing function was used to ensure that FFT peaks were well defined from each other.

$$G'(\omega) = \text{Re} \left[ \frac{\text{FFT}(\sigma(\omega))}{\text{FFT}(\gamma(\omega))} \right]$$

**Equation 4.3.1** - Storage modulus calculation from FTMS data

and

$$G''(\omega) = \text{Im} \left[ \frac{\text{FFT}(\sigma(\omega))}{\text{FFT}(\gamma(\omega))} \right]$$

**Equation 4.3.2** - Loss modulus calculation from FTMS data

These values of the storage and loss moduli can be converted to a phase angle and the sol-gel transition defined by eye from distinguishing a frequency independent point. The FTMS data was, however analysed using a gel point finder program created in MATLAB and described in section 4.3.2 below.

OFR waveform analysis utilised the same method as used by Ghiringhelli et al (Etienne Ghiringhelli 2012) in so far as to take the real and imaginary parts of the FFT (of both the

stress and strain data) and utilise them as above to quantify viscoelastic data. The crucial difference for OFR is that because the data is cycling through frequencies constantly, windowing would only serve to artificially increase or decrease the phase response of a fluid by artificially merging frequency data together. It was decided that no windowing function could be applied to the OFR waveforms. This was the second reason that a conditioning time was added to the OFR experiments – as this allowed both stress and strains to return to a zero point, ensuring the waveforms were periodic and no discontinuity errors could occur.

Once the viscoelastic properties of the sample were determined through the analysis of the OFR waveform, the data was processed in the gel point finder routine as with the FTMS data.

#### **4.3.1 - Gel point identification**

For each discrete frequency sweep or OFR measurement  $G'(\omega, t)$  and  $G''(\omega, t)$  were linearized using the relationships  $\ln G' = \alpha' \ln \omega + k'$  and  $\ln G'' = \alpha'' \ln \omega + k''$ , the scaling exponents,  $G'$  and  $G''$  were subsequently determined by linear regression with their corresponding residuals being summed to provide a single parameter, SSE, characterising the quality of the power-law fit. The GP was determined by identifying the intersection of cubic fits to  $\alpha'(t)$  and  $\alpha''(t)$  in the (manually identified) region of the intersection (see figure 4.3.1), i.e. the point at which  $G'(\omega)$  and  $G''(\omega)$  scale with identical exponents (see

panel B and E). For all GP data reported herein the parameter SSE was less than  $10^{-2}$ ,

indicating the expected power-law scaling of  $G'(\omega)$  and  $G''(\omega)$  at the GP. A measure of the

uncertainty of the value of  $\alpha$  (i.e.  $d\alpha$ ) was obtained using

$$d\alpha = \alpha \sqrt{\left(\frac{d\alpha'}{\alpha'}\right)^2 + \left(\frac{d\alpha''}{\alpha''}\right)^2}$$

**Equation 4.3.3** – calculation of a measure of the uncertainty of the value of  $\alpha$  - ( $d\alpha$ )

where  $d\alpha'$  and  $d\alpha''$  denote to the standard error of the linear regressions of  $\ln \alpha'$  and

$\ln \alpha''$  at the GP, respectively.

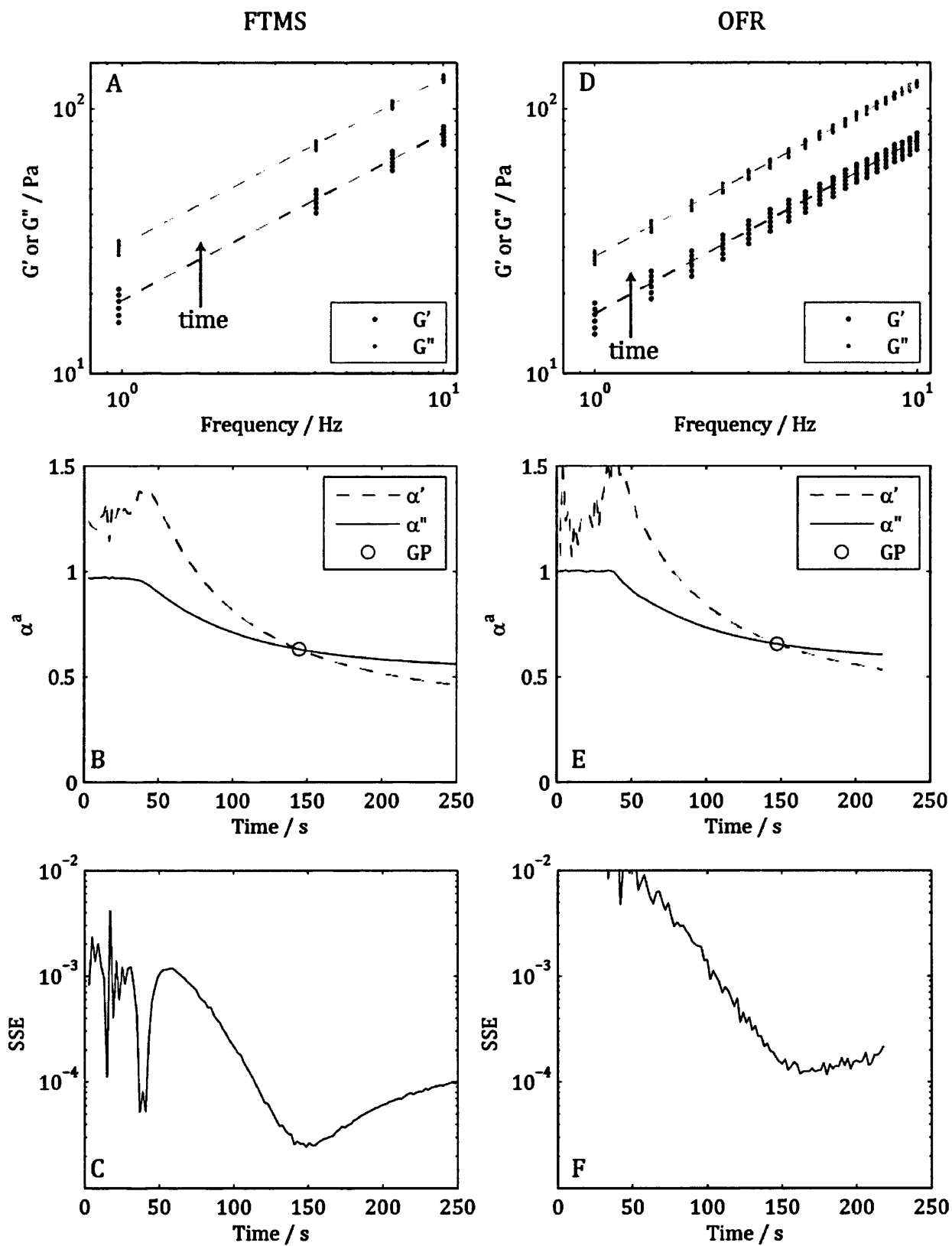


**Figure 4.3.1** – Figure showing the gel point identification process for 30wt% gelatine for

data gathered through FTMS (A-C) and through OFR (D-F)

## **4.4 - Results and discussion**

### **4.4.1 - Investigation of mutation artefacts in OFR**

A fundamental assumption underlying oscillatory shear experiments is that the rheological properties of the sample remain 'stable' (time-invariant) throughout the period  $t_{exp}$  of deformation. A criterion for this time-invariance has been established in terms of a mutation number,  $N_{mu}$ , which quantifies the change of a dynamic rheological property during an experiment and in a study of the gelation of model polyurethanes, Winter et al (Chambon F 1987) identified  $N_{mu} < 0.15$  as a cut-off point below which the sample could be assumed to be 'quasi-stable'. Figure 4.4.1 shows the apparent stress relaxation exponent,  $\alpha^a$  for gelatine systems undergoing increasingly rapid gelation as a function of a) gel time and b) mutation number. Rapid gelation appears to be associated with reduced values of  $\alpha^a$  for LF-FTMS and LF-OFR, however, the high frequency variants of these tests appear to show no such decrease in the value of  $\alpha^a$ . Figure 4b confirms that this apparent decrease in  $\alpha^a$  is a consequence of mutation artefacts apparent in LF-FTMS and LF-OFR procedures. Hence, OFR is subject the same mutation artefacts as FTMS. Further, the data presented in figure 4.4.1 shows that OFR and FTMS provide the same estimate of  $\alpha$  under valid rheometrical conditions.

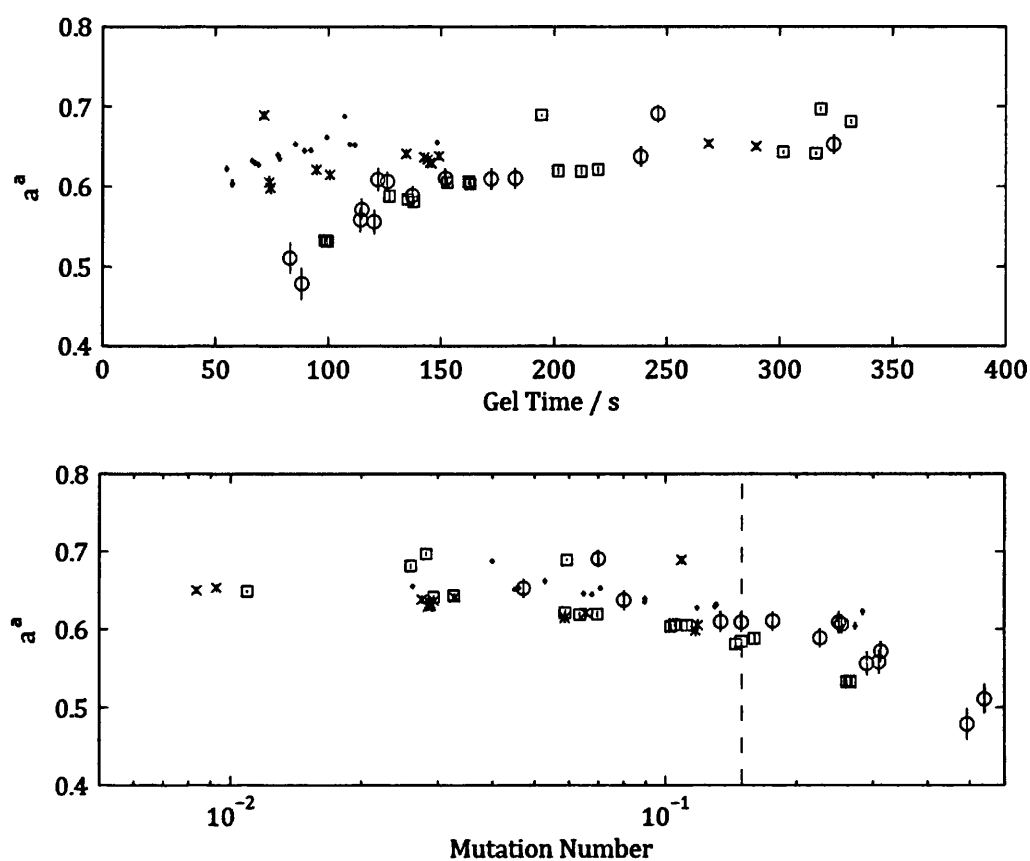


**Figure 4.4.1** – Figure showing a comparison of GP data obtained by 1) high frequency FTMS [x] 2) low frequency FTMS [o] 3) low frequency OFR [□] and 4) high frequency OFR (•). The dashed line in figure B shows Winter's mutation criterion of  $N_{mu} = 0.15$

The purpose of the investigation into mutation effects on OFR was to determine if it was limited by mutation in the same way as FTMS. It was plausible that as FTMS repeats certain frequencies over the course of the carrier frequency wave that it would be more affected by mutation errors than OFR. This is because OFR applies frequencies only once so in theory at least the sample time is always the length of time the waveform spends at any given frequency, which for OFR is a very short time.

The above results, however, illustrate that FTMS and OFR are equally affected by mutation artefacts and that both techniques suffer from deviation of the apparent relaxation exponent as the mutation number increases beyond an average value of 0.68. This is greater than the critical value established by Winter et al (Holly EE 1988) and is therefore in agreement with their findings.

Both high frequency waveforms performed adequately for fast gel times, significantly better than the lower frequency waveforms. It follows therefore that shifting frequency higher is the most effective way of avoiding mutation artefacts within systems where viscoelastic properties change with time.

#### ***4.4.2 - Direct comparison of OFR and FTMS techniques***

Figure 4.4.2 below shows the viscoelastic properties  $G'(\omega)$  and  $G''(\omega)$  for gelatine gels

before during and after the gel point. The pre gel stage is defined as half the gel time, the gel point stage is defined as the gel time (as identified by the gel point identifying routine) and the post gel stage is defined as twice the gel time. These viscoelastic properties were extracted from the high frequency results for OFR and FTMS such that they could be



compared directly. It is evident from the figure below that both techniques have near perfect agreement of the viscoelastic properties of gelatine during each important stage of gelation. This confirms that OFR is a valid technique for the measurement of gelling systems throughout the entirety of gelation.

It is important to note that while both techniques are in agreement of each other, OFR provides a significantly higher number of frequency data points over that of FTMS. Both waveforms were designed to be comparable with each other such that each wave took the same length of time and covered the same range of frequencies. This implies that OFR can achieve a greater value of frequency data points without sacrificing on increased mutation errors or required shear strains.

With more frequency data for the viscoelastic moduli the identification of the gel point can be performed with a greater degree of precision. This is due to a better fit of the power law to  $G'$  and  $G''$  data as there are more data points to fit to. Figure 4.4.3 below shows that the uncertainty of the calculated gel point as a function of sample mutation and illustrates clearly that OFR outperforms FTMS in the calculation of this uncertainty value.

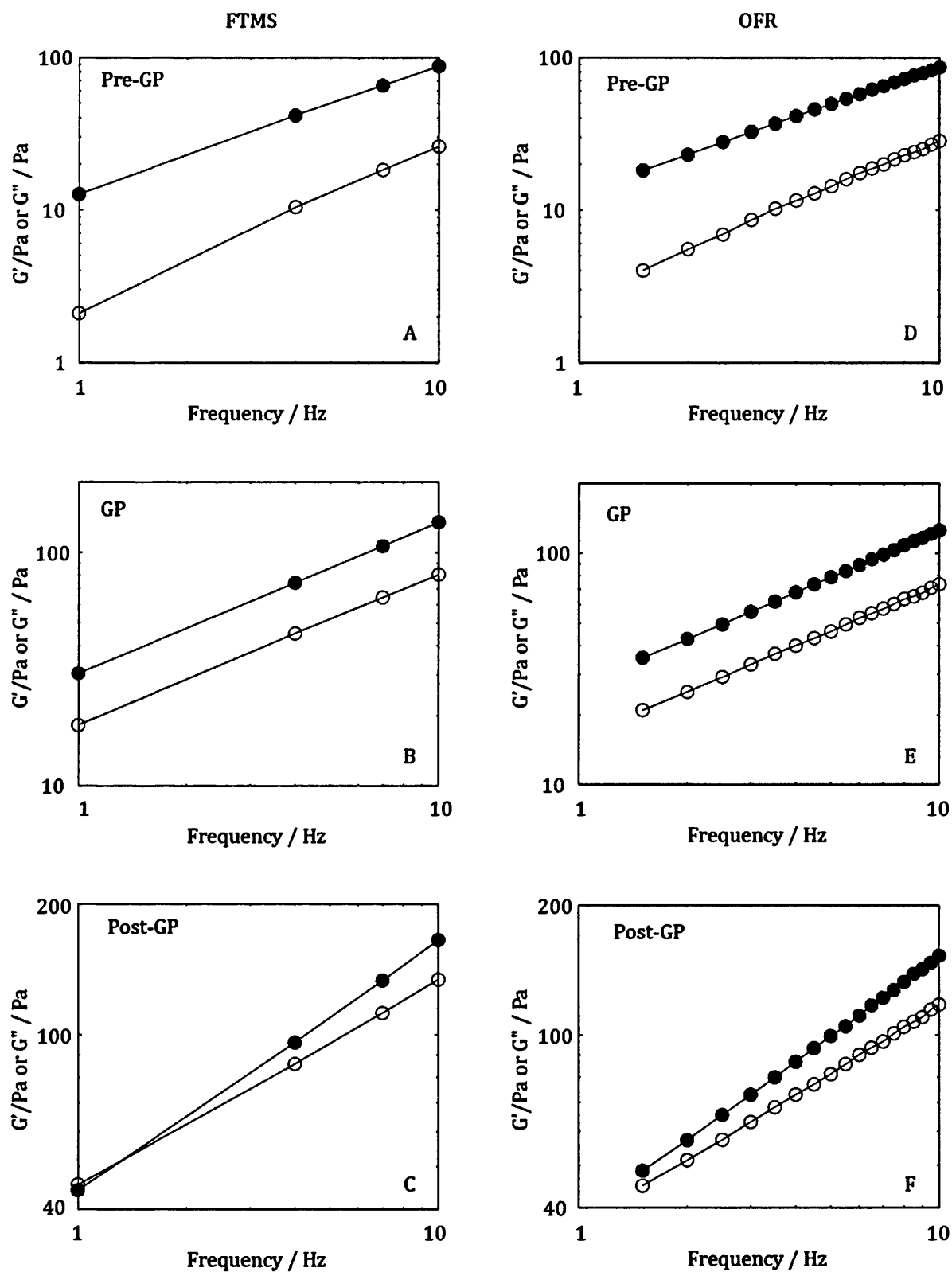


**Figure 4.4.2** - Figure showing a comparison of pre-GP, GP and post-GP rheological data

for 30 wt% gelatine obtained using FTMS and OFR

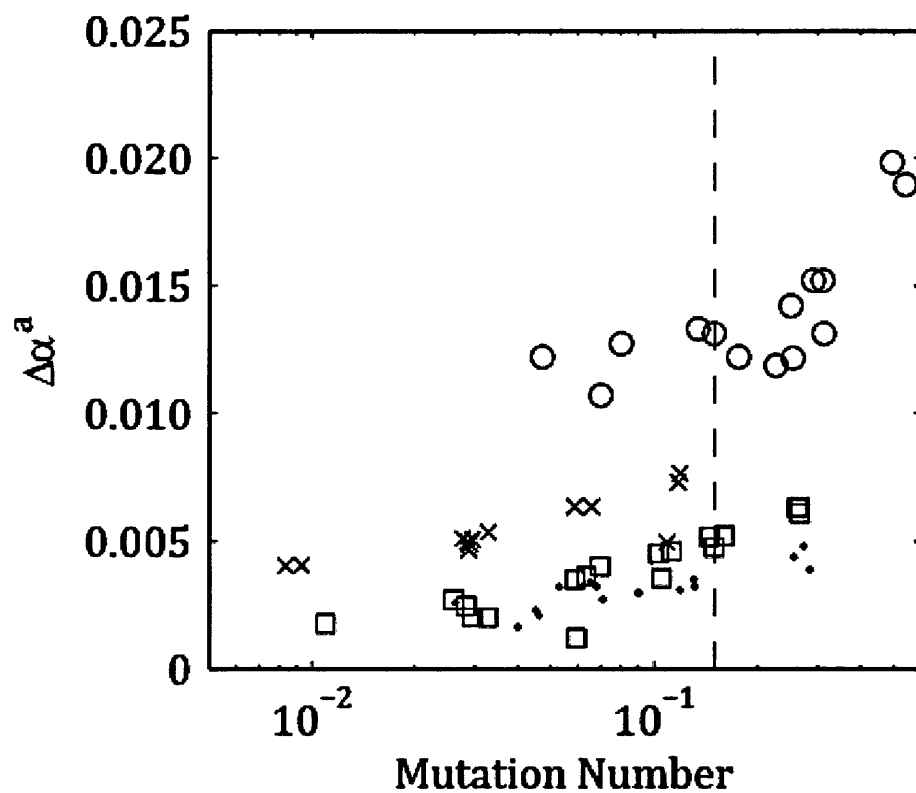


**Figure 4.4.3** - Figure showing a plot of uncertainty in  $\alpha^a$  as a function of mutation

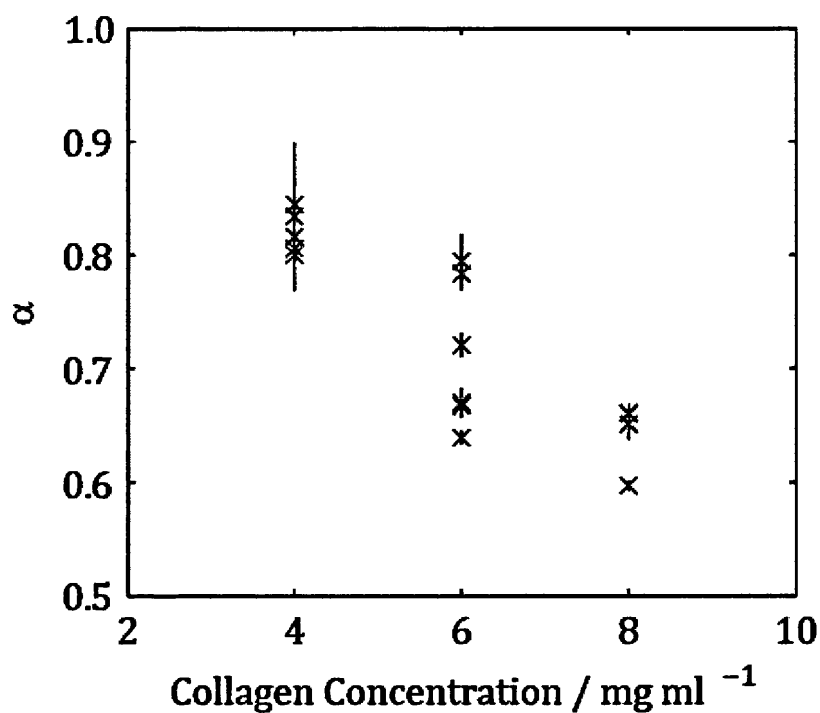
number for 1) HF-FTMS [x] 2) LF-FTMS [o] 3) LF-OFR [ $\square$ ] and 4) HF-OFR ( $\bullet$ )

It is clear then, from these results that the advantage of OFR over FTMS is the ability to produce a much greater number of accurate discrete frequency information in the same period of time. This allows a much more detailed picture of both the sol-gel transition (shown by the decrease of uncertainty in the relaxation exponent) but also shows that OFR would be an improved technique for any viscoelastic analysis desirable on transient systems (typically discrete and continuous relaxation spectra).

#### ***4.4.3 - Application of OFR to collagen gels***

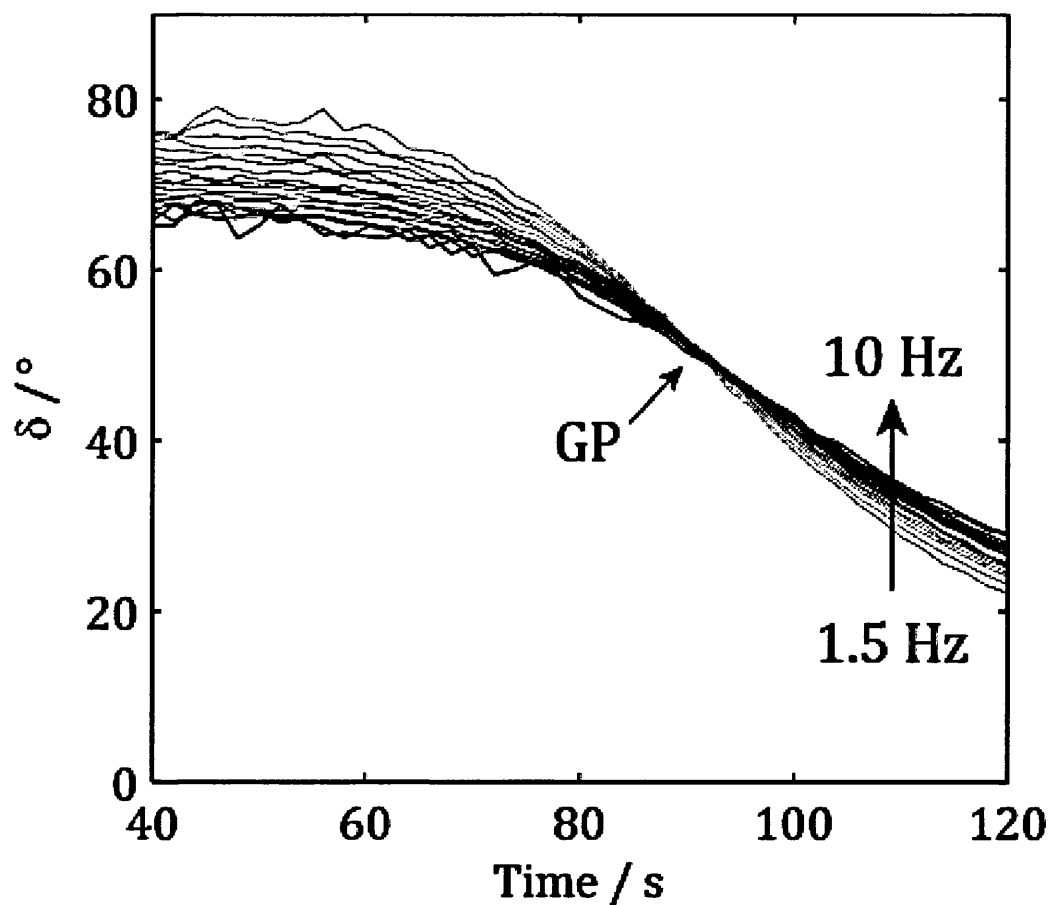
Through the application of both OFR and FTMS on 30wt% gelatine it has been shown that OFR is not only a valid method of measuring viscoelastic properties of transient materials, but also preferable for its greater level of frequency information. Following this work it appears (in principle) that OFR is a suitable candidate technique for measuring fast gelling systems such as acid solubilised type I collagen at, or near physiological temperatures where gelation is very rapid. To test this, high frequency OFR was used to measure rapidly gelling collagen solutions at varying concentrations.

Figure 4.4.4 below shows the results of OFR on a varied concentration of collagen gels. As concentration of collagen increased the relaxation exponent  $\alpha$  decreases. This illustrates that collagen concentration has an effect on the stress relaxation of collagen itself and that the relaxation characteristics are not limited to the values of 0.5 or 0.7 as it is suggested in the current literature (G. Forgacs 2003, Y. Yang 2009). This also explains why the literature on the value of the stress relaxation exponent of collagen has varying opinions on the absolute value.



**Figure 4.4.4** - Figure showing variation of the stress relaxation exponent for collagen gels over a range of concentration made using the HF-OFR routine at 28°C.

Figure 4.4.5 below shows a plot of phase angle,  $\delta$  as a function of time for 8 mg/ml collagen at 28°C obtained using the high frequency OFR technique. *For the first time* at this near-physiological temperature it successfully records the viscoelastic changes during collagen's transformation from a viscoelastic liquid, through the frequency independent sol-gel transition (GP) into a viscoelastic solid.



**Figure 4.4.5** - Figure showing collagen GP data in terms of frequency independence of  $\delta(t)$  for a 8 mg/ml collagen gel. Data was obtained using HF-OFR at 28°C.

The successful application of OFR to this biopolymer system is potentially of great significance. As discussed in section 4.1.2 collagen is very important in many applications for tissue engineering, more specifically as bio-scaffolds or biocompatible coatings. The microstructure of the triple helical polypeptide depends heavily on polymerisation conditions (G.C. Wood 1960, B.R. Williams 1978) such as pH and temperature. It follows therefore that a thorough investigation of the sol gel transition of collagen can provide a greater understanding of the gelation process and how the microstructure of the fibrillar

Optimal Tissue Architecture, Chapter 4

network forms can be achieved, potentially allowing a greater level of structural control within tissue engineering applications.

Rheological collagen gelation studies in the past have been unable to identify the sol gel transition through identification of a frequency independent point. Typical alternatives have been used, and previous studies have overlayed time courses of  $\tan \delta$  at different frequencies on discrete samples (G. Forgacs 2003, Y. Yang 2009). This is because collagen is such a complex biopolymer that relies on ionic strength and kinetic reactions around it, it is extremely sensitive to pH, temperature and concentration (G.C. Wood 1960, Williams 1999). It is this sensitivity that means that frequency independent determination is difficult and typically past estimations of gel point have been based on the intersection of  $\tan \delta(t)$  at the highest and lowest employed frequencies (G. Forgacs 2003, Y. Yang 2009).

The existence of possible mutation artefacts within fast gelling collagen systems has also not been investigated prior. Through the assessment of gelatine with similar changes in viscoelasticity as well as using OFR to determine a viscoelastic profile for collagen throughout the gelling process and identifying a frequency independent point it can be stated that no significant mutation artefacts occur on collagen using the high frequency OFR technique. A frequency independent point is clearly seen in figure 4.4.5.

Perhaps of more interest is the variation of the relaxation exponent as concentration of collagen was varied. Previous literature as stated that the relaxation exponent of collagen does not vary and is independent of concentration (G. Forgacs 2003). It is clear however through this study and measurements of the gel point at varying concentrations of collagen that the relaxation exponent is in fact dependent on the concentration of the collagen with

values decreasing as collagen concentration increases. This implies that a stronger network with a higher fractal dimension forms with an increase in concentration, which follows conventional logic.

Being able to readily identify a frequency independent point within strain sensitive collagen allows the determination of structure within the gel network at the gel point. Previous work on biopolymer gel networks indicates that the microstructure of the critical gel formed at the gel point provides a template for further microstructural growth (D.J. Curtis 2013). The implications of being able to determine under what conditions collagen forms certain microstructures have far reaching applications within tissue culture, more specifically using structural surroundings to encourage specific differentiation.

In summary the work reported herein establishes that OFR is currently the most effective way to measure rapidly gelling, strain-sensitive systems as it provides more viscoelastic information at the same high rate as FTMS while being able to operate at lower values of strain due to the lack of additive waveform phenomena. The application of OFR to the study of collagen has been able to uncover a relationship between the relaxation exponent (and therefore the microstructure) of collagen and concentration that was previously thought not to exist. OFR has also illustrated itself to be as effective as FTMS in negating mutation artefacts through the use of high frequency.



## ***5 Chapter 5 - Summary and Conclusions***

The work reported in this Thesis involves the development, validation and use of two rheometric techniques which have previously not been widely employed and whose validity has been questioned in terms of their application to gelling systems – specifically systems at the Gel Point (or sol-gel transition from viscoelastic liquid (VEL) to viscoelastic solid (VES)), the criterion used to identify the Gel Point being attainment of a frequency independent loss tangent in small amplitude oscillatory shear, SAOS.

The first technique considered (reported in Chapters 2 and 3) involves the parallel superposition of a steady (or unidirectional) shear flow on a small amplitude oscillatory shear (SAOS) flow under controlled stress conditions. The work reported in Chapter 2 successfully established the LVR requirements for work involving SAOS on a model sol-gel transition system (gelatine gels formed by the thermoreversible gelation of aqueous gelatine solutions). The progressive decrease in the unidirectional shear field in the approach to the GP under constant stress in the controlled stress parallel superposition CSPA experiment noted in Chapter 2 suggested that the interpretation of CSPA measurements might allow accurate GP determination given sufficiently small amplitudes of the unidirectional flow shear rate. This assumption was confirmed by comparing GP data obtained under SAOS and CSPA for gelatine systems.

In addition, a series of experiments were devised in order to test whether CSPA could yield valid data for systems undergoing rheological change involving a progressive increase in the amplitudes of both the unidirectional shear field and the oscillatory shear strain under constant stress. In the work reported in Chapter 2 that rheological change was

represented by a transition from a previously gelled viscoelastic solid (VES) state back to its precursor viscoelastic liquid (VEL) state. These experiments involved exploiting the thermoreversible gelation of aqueous gelatine solutions by inducing a rapid temperature increase to a value above the maximum gelation temperature in the post-GP regime. The biopolymer gel system was employed as a model gelling material to confirm the ability of CSPA to characterise the stress relaxation characteristics of critical gels in the presence of a) progressively decreasing and b) progressively increasing unidirectional and oscillatory strain rate amplitudes. In addition to confirming the validity of the CSPA technique in gelation studies, the latter feature of the experiments involved CSPA being used to record the thermally induced VES to VEL transition.

The experiments reported in Chapters 2 and 3 established that when conducted under appropriate conditions (in terms of linearity and mutation number criteria) the results of SAOS FS and CSPA experiments on a system undergoing rheological transition (from VEL to VES, or *vice versa*) may be taken as indistinguishable. This conclusion was drawn on the basis that, during gelation, attainment of frequency independence of  $\delta'$  indicates the same rheological significance (in terms of the GP) as frequency independence of  $\delta$ .

A further (and hitherto unreported) feature of the experiments reported in Chapter 3 involved the transition from a previously gelled VES state back to the precursor VEL state. The significant feature of the latter CSPA results is that they are obtained from experiments in which both the oscillatory strain amplitude and the unidirectional shear field increase progressively during the approach to the rheological transition (SLT).

Chapter 3 presented FS SAOS and CSPA results obtained on systems following a rapid increase of the test temperature to a constant value above the maximum gelation temperature  $T_{crit}$ . Results were obtained during the resulting transition from a previously

Summary and Conclusions Chapter 3  
gelled viscoelastic solid state, back to the precursor viscoelastic fluid state. The increase in temperature to a value above the maximum gelation temperature was found to cause a marked and progressive decrease in  $G'$  and  $G''$ , with a corresponding increase in  $\delta$  and  $\delta//$ , the significant point being that their VEL-like frequency dependence is initially preserved. A striking feature of the ensuing rheological change was that both  $\delta$  and  $\delta//$  subsequently pass through a *second* frequency independent point as the system loses its solid-like characteristics, this being accompanied by a rapid decline in the value of both  $G'$  (FS) and  $G''$  (CSPS).

A notable finding is that the frequency independent values of  $\delta$  and  $\delta//$  at SLT are also indistinguishable at this 'de-gelling' (VES to VEL) transition; and are identical to those recorded during the initial gel formation (GP) experiments. Thereafter, the frequency dependence of  $\delta$  and  $\delta//$  change, becoming characteristic of a VEL, the values of  $\delta$  and  $\delta//$  both increasing progressively towards  $90^\circ$  as the temperature is maintained above  $T_{crit}$ .

These findings presented a basis for developing a new method of assessing the maximum gelation temperature of the system. Given the various uncertainties inherent in, and the ad hoc nature of these previously reported procedures for the determination of  $T_{crit}$ , a new and more rigorous approach was required. This new method, described in Chapter 3, exploits the use of both FTMS and the newly discovered de-gel frequency independent  $\delta$  behaviour of gelatine during its thermoreversible gel-sol (solid to liquid) SLT transition. Its use in the direct determination of  $T_{crit}$  is reported herein for the first time, the key point in the use of this new approach being that de-gelling is recorded unequivocally on the basis of the previously identified frequency independent loss tangent at the viscoelastic solid to liquid transition – hence the assessment of successful de-gelling by this new procedure does

not require (or rely upon) an operational definition involving the attainment of an arbitrary level of  $G'$ ,  $G''$  or both.

The results of this novel approach to the estimate of  $T_{\text{crit}}$  reported in Chapter 3 reveal definitively that at a temperature above 29.4 °C gelatine will exhibit de-gelling. This estimate of  $T_{\text{crit}}$  is believed to be the most accurate presently available and it is emphasised that this is the result of direct measurements, rather than a dubious extrapolation procedure.

The second rheometric technique considered in this Thesis is *Optimal Fourier Rheometry*, OFR. In contrast to SAOS, the OFR waveform undergoes a continuous modulation between two defined frequency limits. The work reported herein confirms that OFR is a valid means of providing high densities of measurements of the complex shear modulus  $G^*(\omega)$ . This confirmation is based on validation studies of the OFR technique involving a comparison of OFR measurements with those obtained by established SAOS (FS and FTMS) multi-frequency oscillatory techniques.

This Thesis reports the first use of OFR in the study of rapidly gelling collagen gels formed at different collagen concentrations. The results (Chapter 4) are the first to identify the stress relaxation exponent  $\alpha$  of collagen gels in a single experiment and, contrary to previous reports in which no systematic variation in  $\alpha$  was observed upon variation of the collagen concentration, the OFR measurements reported herein establish that  $\alpha$  is dependent on the concentration of collagen, with  $\alpha$  decreasing with increasing collagen concentration. This is an important finding insofar that the gel network at the Gel Point provides a template for further microstructural growth and suggests that the measurement

of  $\alpha$  at the GP is potentially important in the fields of tissue engineering, for control and early evaluation of microstructure.

### ***5.1 Recommendations***

The study presented herein demonstrates the utility of OFR in the study of rapidly gelling systems such as those associated with collagen gelation at near-physiological temperatures. However, in order to measure the GP in even more rapidly forming gels, such as acid-solubilised collagen at physiological temperature, a further shift in to higher frequencies is likely to be necessary, the use of conventional oscillatory rheometry in such procedures will likely require consideration of artefacts such as those associated with sample inertia.

The present work confirms that OFR is currently the most effective way to measure rapidly gelling, strain-sensitive systems as it provides more viscoelastic information at the same high rate as FTMS while being able to operate at lower values of strain due to the lack of additive waveform phenomena.

The application of OFR to the study of a wider range of biopolymer gels – including fibrin thrombin systems may now be envisaged as a precursor to establishing the technique's use in haemorheology – in particular in the detection of incipient blood clot formation under a range of pathophysiological conditions.

OFR has also illustrated itself to be as effective as FTMS in negating mutation artefacts through the use of high frequencies. This, in conjunction with the high density of data it provides in rapid measurements suggests that combining OFR with CSPA may be a viable

and valuable further rheometric development. Further work is now required to establish the practicality of a combined OFR-CSPS instrument for the characterisation of a wide range of complex fluids.

## Nomenclature

$G$	The elastic modulus
$\sigma$	Shear stress
$\gamma$	Shear strain
$\dot{\gamma}$	Strain rate
$\eta$	Viscosity
$t$	Time
$\dot{\sigma}$	Stress rate
$\lambda$	Rate of relaxation
$J$	Creep compliance
$\tau$	Relaxation time
$G'$	Storage modulus
$G''$	Loss modulus
$\delta$	Phase lag/angle
$\omega$	Frequency
$G^*$	Complex modulus
$\sigma^*$	Complex shear stress
$\gamma^*$	Complex shear strain
$\dot{\gamma}^*$	Complex strain rate
$f$	Frequency (Hz)
$\sigma'$	Elastic stress
$\sigma''$	Viscous stress
$\tan \delta$	Loss tangent
$\alpha$	Relaxation exponent
$D_f$	Fractal dimension
$M$	Mass
$D$	Space dimension
$G_e$	Equilibrium modulus
$H$	Modulus density
$\square$	Angular displacement
$T_Q$	Applied torque

$R$	Radius
$D$	Gap distance
$Z^*_M$	Mechanical impedance
$F^*$	Complex force
$U$	Velocity
$R_M$	Sample friction
$X_M$	Mechanical resistance
$S_M$	Sample elastance
$S$	Relaxation modulus at the gel point
$t_{\text{gel}}$	Gel time
$H_3$	Third harmonic displacement
$H_1$	Fundamental frequency displacement
$N_{\text{mu}}$	Mutation number
$\delta//$	phase angle under shear
$T_{\text{crit}}$	Critical gel temperature
$G'//$	Storage modulus under shear
$d\alpha$	Uncertainty of alpha



## ***Bibliography***

Anderson V.J., Pearson J.R.A., Sherwood J.D (2006). "Oscillation superimposed on steady shearing: Measurements and predictions for wormlike micellar solutions." Journal of Rheology 50(5): 771-796.

Barnes, H. A. (2000). A Handbook of elementary rheology. University of Wales, Institute of Non-Newtonian Fluid Mechanics.

Baumgaertel M., Winter H.H., (1989). "Determination of discrete relaxation and retardation time spectra from dynamic mechanical data." Rheologica Acta 28: 511-519.

Baumgaertel M., Winter H.H., (1992). "Interrelation between continuous and discrete relaxation time spectra." J. Non-Newtonian Fluid Mechanics 44(1-2): 15-36.

Booij, H. (1966). "Importance of superimposed steady shear flow on the dynamic properties of non newtonian fluids (part I measurements on non newtonian solutions)." Rheologica Acta 7: 215-221.

Booij, H. (1966). "Importance of superimposed steady shear flow on the dynamic properties of non newtonian fluids (part II Theoretical approach based on the Oldroyd theory)." Rheologica Acta 7: 222-227.

Booij, H. (1968). "Importance of superimposed steady shear flow on the dynamic properties of non newtonian fluids (part III measurements on oscillatory normal stress components). ." Rheologica Acta 7: 202-209.

Bot A., van Amerongen I. A., Groot R. D., Hoekstra N. L., Agterof W.G.M. (1996). "Large deformation rheology of gelatin gels." Polymer Gels and Networks 4(3): 189-227.

Bulicek M., Malek J., Rajagopal K. R. (2012). "On Kelvin-Voigt model and its generalizations." Evolution Equations and Control Theory (EECT) 1(1): 17 - 42.

Carnali J. O., (1992). "Gelation in physically associating biopolymer systems." Rheologica Acta 31: 399-412.

Carvalho W., Djabourov. M. (1997). "Physical gelation under shear for gelatin gels." Rheologica Acta 36(6): 591-609.

Chambon F., Winter H.H. (1987). "Linear viscoelasticity at the gel point of a crosslinking PDMS with imbalances stoichiometry. ." J Rheology 31: 683-697.

Chawla K.K., Meyers M.A. (1999). Mechanical Behavior of Materials. Cambridge University Press; 2 edition

Conrad H., Li Y., Chen Y. (1995). "The temperature dependence of the electrorheology and related electrical properties of corn starch/corn oil suspensions." Journal of Rheology 39: 1041.

Curtis D.J., Williams P. R., Badiei N., Campbell A.I., Hawkins K., Evans P.A ., Brown M.R. (2013). "A study of microstructural templating in fibrin–thrombin gel networks by spectral and viscoelastic analysis." Soft Matter 9: 4883-4889.

Curtis D.J., Badiei N., Holder A., Claypole J., Deganello D., Brown M., Hawkins K.M., Williams P.R. (2015) "Assessment of the stress relaxation characteristics of critical gels formed under unidirectional shear flow by controlled stress parallel superposition rheometry." Journal of Non-Newtonian Fluid Mechanics, in press:  
DOI:10.1016/j.jnnfm.2014.12.004

Curtis D.J., Holder A., Badiei N., Claypole J., Brown M., Barrow M.S., Hawkins K.M., Williams P.R. (2015) "Validation of optimal Fourier rheometry for rapidly gelling materials and application to Collagen gelation". Journal of Non-Newtonian Fluid Mechanics, in press:  
DOI:10.1016/j.jnnfm.2015.01.003

Davies J. M., Jones T.E.R, Carter E.J. (1987). "A comparison between combined steady and oscillatory stress on a controlled stress rheometer and a pulsatile pipe-flow apparatus." Journal of Non-Newtonian Fluid Mechanics 23: 73-90.

De Rosa M.E., Muthukumar M., Winter H.H. (1997). "The Gel Point as Reference State: A Simple Kinetic Model for Crosslinking Polybutadiene via Hydrosilation." Polymer Gels and Networks 5: 69-94.

De Rosa M.E., Winter H. H. (1994). "The effect of entanglements on the rheological behaviour of polybutadiene critical gels." Rheologica Acta 33: 22-237.

Dealy J. M., (1984). "Official Nomenclature for Material Functions Describing the Response of a Viscoelastic Fluid to Various Shearing and Extensional Deformations." Journal of Rheology 28: 181-195.

- Dealy J., Wissbrun K. (1990). Melt Rheology and its Role in Plastics Processing, New York: Van Nostrand Reinhold.
- Deshpande A.P., Krishnan J.M., Kumar S. (2010). Rheology of Complex Fluids. Springer
- Eldridge J.E., Ferry J. D. (1954). "Studies of the Cross-linking Process in Gelatin Gels III. Dependence on Melting Point on Concentration and Molecular Weight." The Journal of Physical Chemistry 58(11): 992-995.
- Emri I., Tschoegl N. W. (1993). "Generating line spectra from experimental responses, Part I. Relaxation modulus and creep compliance." Rheologica Acta 32(3): 311-312.
- Ensanya A., Neel A., Laurent B., Knowles J.C., Syed O., Mudera V., Day R., Hyun J.K. (2013). "Collagen— Emerging collagen based therapies hit the patient." Advanced Drug Delivery Reviews 65(4): 429-456.
- Evans P., Hawkins K., Williams P.R., Williams R.L. (2008). "Rheometrical detection of incipient blood clot formation by Fourier transform mechanical spectroscopy. ." Journal of Non-Newtonian Fluid Mechanics 148(1-3): 122-126.
- Fernandez-Cara E., Guillen F., Ortega R.R. (1998). "Some theoretical results concerning non Newtonian fluids of the Oldroyd kind. ." Annali della Scuola Normale Superiore di Pisa-Classe di Scienze 26: 1-29.
- Ferry, J. D. (1948). "Mechanical Properties of Substances of High Molecular Weight. IV. Rigidities of Gelatin Gels; Dependence on Concentration, Temperature and Molecular Weight." Journal of the American Chemical Society 70(6): 2242-2249.
- Ferry, J. D. (1980). Viscoelastic properties of polymers. New York, Wiley.

Findley W.N., Lai J.S.L., Onaran K. (1976). CHAPTER 8 - Nonlinear Creep at Constant Stress and Relaxation at Constant Strain, Elsevier.

Forgacs G., Newman S. A., Hinner B., Maier C.W., Sackmann E., (2003). "Assembly of collagen matrices as a phase transition revealed by structural and rheologic studies." Biophys. J 84: 1272-1280.

Ghiringhelli E., Roux D., Bleses D., Galliard H., Caton F. (2012). "Optimal fourier rheometry Application to the gelation of an alginate " Rheologica Acta 51: 413-420.

Glowacki J., Mizuno S. (2008). "Collagen scaffolds for tissue engineering." Biopolymers 89: 338-344.

Groetsch C. (1985). "Uniform convergence of regularization methods for Fredholm equations of the first kind." Journal of the Australian Mathematical Society 39(2): 282-286.

Groetsch C. (1993). Inverse Problems in the Mathematical Sciences, Vieweg and Teubner Verlag.

Guerrero A., Partal P., Gallegos C. (1998). "Linear viscoelastic properties of sucrose ester-stabilized oil-in-water emulsions." Journal of Rheology 42: 1375.

Guo L., Colby R. H., Lusignan C. P., Howe A.M. (2003). "Physical Gelation of Gelatin Studied with Rheo-Optics." Macromolecules 36(26): 10009-10020.

Harman, P. (2003). The Oxford Companion to the History of Modern Science, Oxford University Press.

Harris, J. (1977). Rheology and non-Newtonian flow, Longman London Hermes & Fredrickson

Hawkins K., Lawrence M., Williams P.R., Williams R.L. (2008). "A study of gelatin gelation by Fourier transform mechanical spectroscopy." J Non Newtonian Fluid Mech 148(1-3): 127-133.

Holly .E.E., Ventkataraman S., Chambon F., Winter H.H. (1988). "Fourier Transform Mechanical Spectroscopy of Viscoelastic Materials with Transient Structure." J Non Newtonian Fluid Mech 27: 17-26.

Honerkamp J., Weese J. (1989). "Determination of the relaxation spectrum by a regularization method." Macromolecules 22(11): 4372-4377.

Isaacs A. (2009). Hooke's law. A Dictionary of Physics, Oxford University Press.

Johnston J.H., Peard G.T. (1925). "The Surface Tension of Gelatin Solutions." Biochem. J. 19(2): 281-289.

Joly M., Barbu E. (1949). "Etude par la birefringence d'écoulement de la denaturation thermique de la serumalbumine." Bull ste chim Biol 31: 1642.

Jomha, A. I., Woodcock L. V. (1990). "Effects of oscillatory shear on the steady-flow of shear thickening suspensions." Chemical Engineering Research & Design 68(6): 550-557.

Jones T.E.R., Davies J. M., Barnes H.A. (1984). "Dynamic flow properties of materials in a constant stress rheometer." Proc 8th International Congr Rheol 4(45).

M. Muthukumar, Winter H. H. (1986). "Fractal dimension of a crosslinking polymer at the gel point." Macromolecules 19(4): 1284-1285.

Marangoni A. G., Tosh S. M. (2005). "On the nature of the maximum gelation temperature in polymer gels." Biophysical Chemistry 113(3): 265-267.

Mezger, T. G. (2006). The rheology handbook: for users of rotational and oscillatory rheometers, Vincentz Network GmbH & Co.

Michon C., Cuvelier G., Launay B. (1993). "Concentration dependence of the critical viscoelastic properties of gelatin at the gel point." Rheologica Acta 32(1): 94-103.

Okuyama K., Xiaozhen. X., Iguchi M., Noguchi N. (2006). "Revision of collagen molecular structure." Biopolymers 84: 181-191.

Pal R. (1997). "Viscosity and storage/loss moduli for mixtures of fine and coarse emulsions." Chemical Engineering Journal 67: 37-44.

Pastorino L., Dellacasa E., Scaglione S., Giulianelli M., Sbrana F., Vassalli M., Ruggiero C. (2014). "Oriented collagen nanocoatings for tissue engineering, Colloids and Surfaces." B: Biointerfaces 114: 372-378.

Phan-Tien N. (2002). Understanding viscoelasticity basics of rheology, Springer.

Ren S.Z., Sorensen C. M. (1993). "Relaxations in gels: Analogies to  $\alpha$  and  $\beta$  relaxations in glasses." Physics Rev. Lett. 70: 1727.

Rodd A., Cooper-White J., Dunstan D., Boger D. (2001). "Gel point studies for chemically modified biopolymer networks using small amplitude oscillatory rheometry." Polymer 42: 185-198.

Roylance D. (2001). Engineering Viscoelasticity. Cambridge, Massachusetts Institute of Technology.

Rueb C.J., Zukoski C. F. (1997). "Viscoelastic properties of colloidal gels." Journal of Rheology 41: 197.

Shoulders M. D., Raines R. T. (2009). "Collagen Structure and Stability." Annual Review Biochem. 78(9): 29-58.

Simmons J. (1968). "Dynamic modulus of polyisobutylene solutions in superposed steady shear flow." Rheologica Acta 7: 184-188.

Somma E., Valentino O., Titomanilo G., Ianniruberto G. (2007). "Parallel superposition in entangled polydisperse polymer melts: Experiments and theory." Journal of Rheology 51: 987-1005.

Tanner, R. I. (1985). Engineering Rheology. Oxford University Press.

The MathWorks, I. MATLAB and Statistics Toolbox Release 2013b. Natick, Massachusetts, United States

Tibbitt M.W., Anseth K. S. (2009). "Hydrogels as extracellular matrix mimics." Biotechnology and Bioengineering 103: 655-663.



Tschoegl N. W. (1989). The Phenomenological Theory of Linear Viscoelastic Behavior, Springer Berlin Heidelberg.

van Wazer J.R., Lyons J.W., Kim K.Y. (1963). Viscosity and flow measurement: a laboratory handbook of rheology, Interscience publishers New York.

Vlastos G., Lerche D., Koch B., Samba O., Pohl M. (1997). "The effect of parallel combined steady and oscillatory shear flows on blood and polymer solutions." Rheologica Acta 36: 160-172.

Walters, K. (1975). Rheometry, London: Chapman and Hall.

Ward A.G., Courts A. (1977). The Science and Technology of Gelatin, New York: Academic Press.

Williams B.R., Gelman R. A., Poppke D.C. and Piez K.A. (1978). "Collagen fibrin formation." Journal of Biological Chemistry 253: 6578-6585.

Williams, P. R. (1999). Rheometry for non-Newtonian fluids, in: R.P.Chhabra and J.F. Richardson, Non-Newtonian Flow in the Process Industries, Butterworth-Heinemann, Oxford.

Winter H.H., Chambon F. (1986). "Analysis of linear viscoelasticity of a crosslinking polymer at the gel point." J Rheology 30: 367-382.

Wolf B. A. (1984). "Thermodynamic theory of flowing polymer solutions and its application to phase separation." Macromolecules 17: 615.

Wood G.C., Keech M. K. (1960). "The formation of fibrils from collagen solutions."

Biochem. J. 75: 588-598.

Yang Y., Kaufman L. J. (2009). "Rheology and Confocal Reflectance Microscopy as probes of mechanical properties and structure during collagen and collagen/hyaluronan self-assembly." Biophys. J 96: 1566-1585.

Zienkiewicz O.C. (1995). "Origins, Milestones and directions of the finite element method – a personal view." Archives of computational methods in engineering 2(1): 1-48.

Zienkiewicz O.C., Watson M., King I.P. (1968). "A numerical method of visco-elastic stress analysis." Int J Mech Sci(10): 807-827.